

A dissertation submitted in partial fulfilment of the requirements for the degree of  
Doctor of Philosophy in Chemical Processes Engineering

# **RISK ANALYSIS OF JET FIRES THERMAL EFFECTS**

**Vahid Foroughi**

Thesis supervisors:  
Prof. Joaquim Casal Fàbrega  
Prof. Elsa Pastor Ferrer

Centre for Technological Risk Studies  
Department of Chemical Engineering  
Universitat Politècnica de Catalunya

Barcelona, 2023



# Acknowledgements

Throughout my Ph.D. studies, I have had the privilege of benefiting from the knowledge and expertise of numerous individuals who have all made contributions to both this dissertation and my professional development in various ways. Now is the perfect time to express my gratitude to each and every one of them.

First and foremost, I would like to wholeheartedly thank my supervisor, Prof. Joaquim Casal who has been a constant source of support throughout my thesis. With his patience and extensive knowledge, he has allowed me the freedom to work uniquely. His encouragement and dedication have made completing this thesis possible, and I am incredibly grateful for his invaluable guidance on both academic and personal levels.

I sincerely thank Prof. Elsa Pastor for her invaluable guidance and support during my thesis. Her expertise and insightful feedback greatly shaped my research. I am grateful for her commitment to my academic journey.

Furthermore, I would like to convey my sincere respect and heartfelt appreciation to Prof. Eulalia Planas, head of CERTEC, for the support received during my stay at UPC.

I would like to extend my deepest respect and gratitude to Dr. Adriana Palacios. Over the course of the past five years, she has consistently offered exceptional guidance and support, demonstrated remarkable patience, and shared her extensive expertise. Despite our geographical separation, she has consistently made herself available to provide assistance and valuable insights whenever I needed them.

I am deeply appreciative of the funding sources that have made my Ph.D. work possible. I extend my gratitude to the Institut d'Estudis Catalans for their support during the years of my studies for their support through project PRO2018-SO3, and also to the Spanish Ministry of Economy and Competitiveness (project CTQ2017-85990, co-financed with FEDER funds).

Furthermore, I am immensely grateful to Dr. Alba Agueda and Alessia Cavini whose significant contributions have played a crucial role in the completion of this dissertation. Thank you sincerely for generously sharing your knowledge with me.

I want to express my sincere thanks and acknowledge the colleagues and friends in CERTEC at UPC. Your unwavering support throughout my time in Barcelona has been of immense importance. I also express my gratitude to Giulio Supporta, Marco Zappone, Sergio Martín, Pascale Vacca, Christian Mata and Kim Albo who provided exceptional assistance and support during my data collection efforts.

Last but certainly not least, I want to express my deepest gratitude to the most cherished blessings in my life: my parents Rahman Foroughi and Ozra Mohammadi. Their constant love, encouragement, and support have been instrumental in helping me achieve all my goals. I am also immensely thankful for my loving, supportive, and encouraging sister, Homa, who has been an invaluable gift from God. Thank you all from the bottom of my heart.

*To my dear late brother Hamid,*

*I dedicate this thesis to you. Your memory and unwavering support throughout my life have always been an inspiration to me. Though I am saddened by your physical absence, I proudly carry with me the experiences and memories we shared.*

*You have always been a source of love and belief in my abilities. This heartfelt dedication is a tribute to you. Your presence continues to reside in my heart, and your influence on my life remains restless. This thesis is a testament to the respect and admiration I hold for you. You will always be a guiding light in my life, and our memories will forever be cherished.*



# Index

1.	Introduction .....	1
1.1.	Risk and major accidents.....	1
1.2.	Fire accidents .....	3
1.3.	Jet fires and the domino effect .....	6
1.4.	The case of pipelines.....	10
1.5.	Objectives of the thesis.....	13
1.6.	Structure of the thesis.....	14
2.	Literature Review and Historical Analysis .....	15
2.1.	Introduction .....	15
2.2.	Domino accidents.....	15
2.3.	Elements of a domino accident.....	17
2.4.	Characteristics of accidents involving the domino effect .....	20
2.5.	Risk associated with pipeline systems .....	26
2.5.1	Parallel Pipelines .....	29
2.5.2	Jet Fires in Pipelines .....	32
2.5.3	Characteristics of domino accidents in pipeline systems.....	34
2.6.	Examples of domino accidents in pipeline systems.....	36
2.7.	Literature review on jet flames impingement .....	44
2.8.	Literature review on the study of jet flame geometrical features.....	48
2.9.	Tools for fire risk analysis in pipelines .....	53
3	Experimental Set-up and Test Methodology .....	55
3.1.	The experimental tests location.....	55
3.2.	The experimental set-up .....	56
3.2.1.	Jet fire generation section.....	57
3.2.2.	Target obstacle section .....	59
3.3.	Experimental tests methodology .....	60
3.4.	Components of the experimental setup .....	72
3.4.1.	Jet fire generation section.....	72
3.4.2.	Target pipe section.....	80
3.5.	Instrumentations.....	81
3.5.1.	Pressure measurement .....	81
3.5.2.	Temperature measurement.....	81
3.5.3.	Infrared Camera .....	86
3.5.4.	Visible camera .....	88
3.6.	Data collection system .....	88
3.6.1.	FireALL.....	89

3.6.2.	FieldPoint module .....	91
3.6.3.	PicoLog .....	94
3.6.4.	Optris PIXConnect .....	94
3.7.	Data acquisition system elements arrangement .....	96
3.8.	Test procedure .....	98
3.9.	Safety measures .....	101
4.	Geometric and thermal characteristics of horizontal jet fires .....	103
4.1.	Introduction .....	103
4.2.	Literature review on the study of jet flame geometrical features.....	107
4.1.1.	Jet Flame Lift-off correlations .....	109
4.3.	Experimental tests .....	110
4.3.1.	Flames temperature .....	111
4.3.2.	Flame geometry assessment .....	112
4.4.	Methodology of image processing.....	117
4.4.1.	Creation of a segmentation mask .....	119
4.4.2.	Calculation of the discretization areas.....	122
4.4.3.	Obtaining the main geometrical measurements .....	126
4.5.	Results and discussion .....	127
4.5.1.	Results of flame temperatures experiments.....	127
4.5.2.	IR image measurement results.....	130
4.6.	Analyzing the prediction of lift-off, flame reach and elevation .....	133
4.6.1.	Jet Flame Lift-off correlations .....	133
4.6.2.	Flame reach correlations.....	136
4.6.3.	Flames elevation .....	141
4.7.	Final remarks.....	143
5.	Thermal Effects of Jet Fire Impingement on a Pipe .....	145
5.1.	Introduction .....	145
5.2.	Impingement tests .....	145
5.3.	Results and Discussion of Group 1 Tests.....	152
5.3.1	Gas inside the pipe, sonic jet fire .....	152
5.3.2	Liquid inside the pipe, sonic jet fire .....	154
5.3.3	Liquid inside the pipe, subsonic jet fire.....	155
5.4.	Results and Discussions of Group 2 Tests .....	156
5.4.1	Operating condition of tests .....	156
5.4.2	Heat transfer fluxes and heat transfer coefficients .....	161
5.5.	Discussion.....	170
6.	CFD Simulation of Jet Fires.....	173
6.1.	Introduction .....	173
6.1.1.	Computational Fluid Dynamics (CFD) modelling.....	174



6.1.2.	CFD modeling of jet fire in literature .....	176
6.2.	Step-by-step modelling of jet fires using FLACS.....	177
6.2.1	Geometry .....	177
6.2.2	Computational grid .....	177
6.2.3	Scenario.....	179
6.3.	Jet fire results.....	183
6.3.1.	Radiation model .....	183
6.3.2.	Soot model .....	183
6.3.3.	Flame geometry .....	185
6.3.4.	Flame temperature .....	189
6.4.	Discussion.....	191
6.4.1.	Performance parameters .....	191
6.4.2.	Flame geometry .....	192
6.4.3.	Flame temperature .....	194
6.5.	Further studies: Jet Fire Impingement.....	196
6.5.1.	Experimental set up and impingement experiments.....	196
6.5.2.	CFD modeling and results.....	197
6.6.	Discussion.....	200
7.	Conclusions .....	203
	Nomenclature .....	206
	Acronyms.....	209
	References.....	211
A.	FLACS-Fire CFD .....	223
A.1.	Modeling approach.....	223
A.1.1.	Turbulence .....	224
A1.2.	Turbulence flow model .....	224
A1.3.	Combustion model.....	225
A1.4.	Radiation model.....	226
A1.5.	Soot formation model.....	226
A1.6.	Leak model.....	227
A2.	FLACS-CFD interfaces.....	227
A2.1.	CASD pre-processor .....	228
A2.2.	FLACS-CFD RunManager .....	231
A2.3.	Flowvis post-processor .....	233



# 1. Introduction

## 1.1. Risk and major accidents

It is obvious that the extraordinary increase of industrial activity in recent decades and, more specifically, the important growth undergone by the chemical one, including sectors such as petrochemical or pharmaceutical, has brought a notable improvement in the life of today's society as compared to the situation which existed one century ago. A clear indicator is the increase in the average life expectancy experienced by the population of industrialized countries.

Nevertheless, this rise in the industry has been associated with the unavoidable storage, transportation, and treatment of large amounts of hazardous materials. This has been associated with situations and operations that can imply a potential risk. And this can cause –and has caused– accidents that can have –and, in some cases have had– serious consequences on the environment and on the population.

To deal with these risks, it has been necessary to make an effort to analyze them, predict their probability of occurrence, and establish the safety measures necessary to reduce them to an acceptable value. A previous step in this analysis is the quantitative definition of the risk. The most appropriate and currently accepted is the one calculated by multiplying the frequency with which an event occurs (or will occur) by the magnitude of its probable consequences.

The aforementioned risks are associated with the so-called major accidents, defined (Council Directive, 1997) as “an occurrence such as a major emission, fire or explosion resulting from uncontrolled developments in the course of the operation of any establishment... and leading to serious danger to human health and/or the environment, immediate or delayed, inside or outside the establishment, and involving one or more dangerous substances”.

These major accidents are associated with one or more of the following phenomena:

- thermal: thermal flux (originated by fires)
- mechanical: pressure wave and ejection of fragments (originated by explosions)
- chemical: release of toxic materials (dispersion in air or water).

Major accidents are always associated with an unwanted event, usually an accidental release of hazardous material or energy. If there is the loss of containment of a hazardous (flammable, toxic) material, the evolution of the event will be a function of both the condition of this material (liquid, gas, or vapor, two-phase flow), the existence of safety barriers as for example a foam blanketing system, and in many cases also of the meteorological conditions.

The resulting accidents are essentially fires, explosions, and toxic releases. In each one of these categories, there may be several types depending on the involved material or on the event circumstances. The release itself can be a serious accident, as for example the explosion of a pressurized vessel or a dust explosion in a silo or in a dryer. Or the accident can correspond to a second step after the release, as in the case of the explosion of a flammable cloud that progressed and found an ignition source. And, of course, an accident may involve, as often happens, combinations of more than one of these phenomena such as, a release followed by a fire, an explosion plus a fire, the sequence of a release followed by a fire plus an explosion, etc.

The physical effects associated with these accidents are summarized in Table 1-1.

Table 1-1. Main effects of major accidents.

Major accident	Effects
Fire	Thermal radiation Possible flames impingement
Explosion	Overpressure wave Ejected fragments
Explosion/fireball	Overpressure wave Ejected fragment Thermal radiation
Gas cloud	Concentration, dose

Fires can have a strong action through radiation and, if there is impingement of the flames on equipment, also through convection. In the case of explosions there will be the effect of the pressure wave and, often, the ejection of fragments of the damaged equipment. And in the case of the dispersion of a toxic cloud, the consequences – essentially on people– will be those associated with the toxicity of the released material and will depend on the concentration and dose received by the affected population.

The damage associated with major accidents can affect people, the environment, equipment, and buildings; there can be also indirect damages or losses for the related companies (Figure 1-1).

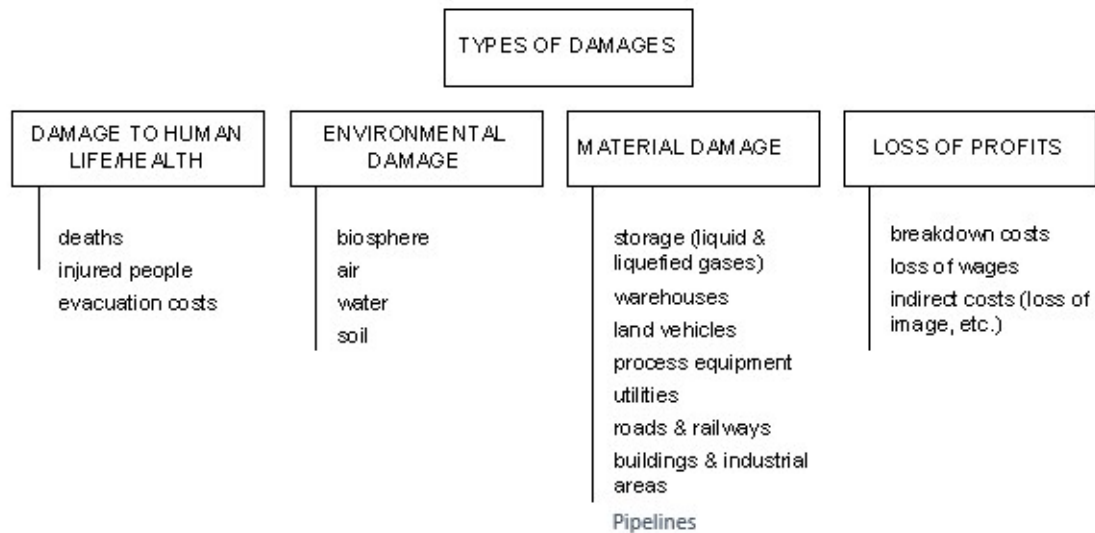


Figure 1-1. Potential damages originated from major accidents (modified from (Casal, 2018)).

## 1.2. Fire accidents

Among major accidents, those implying fire are important because of their frequency, their possible impact –which can be very important and destructive over a considerable area– and the possibility of triggering other accidents.

There can be different types of fires, depending on the involved material and the type and operating conditions of the equipment in which it takes place: pool and tank fires, jet fires, flash fires, and fireballs.

### Pool fires

A pool fire can occur when a loss of containment of a flammable liquid –often a hydrocarbon– originates a pool, often contained by a dike, and an ignition source exists. This source can be relatively far from the pool, and in most cases, it is the flammable cloud originated by the evaporation from the pool which reaches it, the flames moving very quickly through it to the pool. Then combustion is usually incomplete and large amounts of black smoke are formed; therefore, the fire envelope will be partly covered by this smoke, thus decreasing the average surface emissive power. The thermal radiation can be very strong up to a certain distance, depending on the pool and flame size. If there is contact of the flames with some equipment (a vessel, a pipe) the heat flux to it will significantly increase.

### Tank fires

When a tank containing a flammable liquid undergoes an explosion and its roof disappears, if the liquid contained in it is ignited a fire similar to a pool one will occur (Figure 1-2).



Figure 1-2. Fire in a crude oil tank.

### Boilover

This is an interesting accident that can occur in the case of a tank fire. In this type of fire, especially when they occur in large fuel tanks, containing for example crude oil, the fight to extinguish it can require large amounts of water and foam and also can last a long time. In such a situation, if the tank contains a layer of water in its bottom (which could be there already before the fire or can be originated from the water used by the

firefighters), a dangerous phenomenon can occur. Due to the existence of fire at the liquid surface, a heat wave will slowly propagate through the fuel contained in the tank, progressing toward its bottom. If, at a certain moment, this heat wave reaches the water, this will suddenly boil, generating a vaporization; this will cause the turbulent mixing of both layers with the explosive formation of steam. The result will be the ejection of burning fuel over a considerable distance. An example of a boilover phenomenon is the accident occurred in Tocoa, (Venezuela), in 1982, in which a fuel oil tank caught fire and experienced boilover resulting in 154 fatalities.

#### Jet fires

When a jet of a flammable gas/vapour or two-phase flow is released at high velocity from a hole, a flange, or a broken pipe is ignited, the turbulent flames originate a jet fire. Even though usually jet fires are much smaller than pool or tank fires, if they impinge on an equipment the heat transfer to it will be very high, implying a very dangerous situation.

#### Flash fires

When a flammable cloud, i.e., a mixture of air and a flammable gas with a concentration between the flammability limits, meets an ignition source and is ignited, bright flames will move very quickly through the cloud. As the possible contact with equipment will be very short, the effects on it are assumed to be negligible except for the case of floating roof tanks. Instead, the effects on people can be very strong. Usually, it is assumed that the people inside the zone covered by the cloud (i.e., the people engulfed by the flames) will die, while people outside this zone will undergo no consequences.

#### Fireballs

If a pressurized vessel containing a superheated flammable liquid explodes, the sudden release of a mixture of gas and liquid droplets originated by the flash vaporization of the liquid will form a flammable spherical cloud. If it is ignited, it will burn with a very bright flame (Figure 1-3).



Figure 1-3. Ethylene fireball during the Priolo accident, 1985 (DGPCSA, 1986).

As combustion is possible only at the surface of the cloud (inside the cloud the fuel concentration is higher than the upper flammability limit and combustion is not possible), this fireball will last a certain time which can vary from a few seconds up to approximately one minute, depending on the mass of fuel involved. Even if this time is relatively short, as the thermal radiation is very strong it can imply severe consequences for people over a large area.

Concerning the possible duration of an accidental fire, pool, and tank fires usually have a fairly steady state combustion and can last hours unless a quick extinguishing procedure acts, for example, covering the fire surface with foam. Jet fires show also a steady state combustion which can last a long time, even though often –but not always– they can be extinguished in a time much shorter than in the case of pool fires. Finally, fireballs have a much shorter duration (usually less than one minute), and flash fires last just a few seconds.

### **1.3. Jet fires and the domino effect**

If an accident occurs in a plant in which the density of equipment is high, as happens in a process plant or in an oil platform, its effects –overpressure, ejected fragments, thermal flux– can damage other equipment thus originating another release, fire or explosion, with the consequent escalation of the effects and consequences of the whole accident. This is called “domino effect”.



The domino effect has been defined (Delvosalle, 1996) as “a cascade of events in which the consequences of a previous accident are increased both spatially and temporally by the following ones, thus leading to a major accident”.

The primary event, the one that starts the domino sequence, can be a minor one, for example, a small fire. Among the major accidents that occur in the industry, diverse historical analyses have shown that fires are the most frequent ones, followed by explosions and gas clouds. Toxic clouds do not start domino effect sequences, while fires and explosions can do it. In the case of an explosion, both overpressure waves and ejected fragments can initiate it. Several authors have studied this, and a set of values have been proposed to set the thresholds and safety distances for estimating the blast values that can cause an accident escalation for the different types of equipment e.g. atmospheric or pressurized, spherical or horizontal tanks, etc. (Reniers & Cozzani, 2013). In the case of fire, the possibility of originating a domino effect is quite clear if there is flames impingement on an equipment, due to the high heat transfer flows that can be reached, which can cause a quick increase in the wall temperature (Figure 1-4). Historical analyses have revealed that approximately half of the domino effect accidents are initiated by a fire (Casal, 2018).

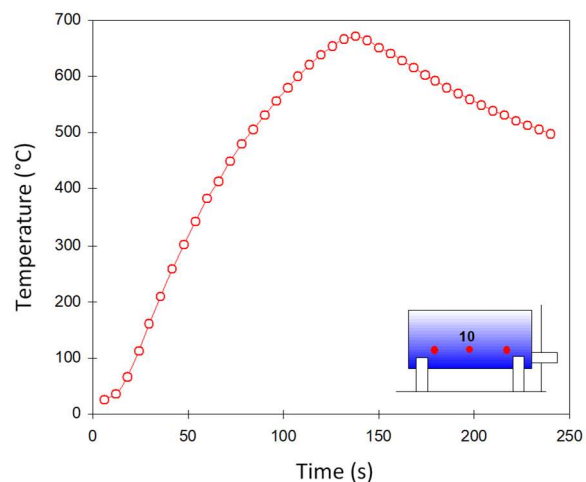


Figure 1-4. Temperature evolution as a function of time in a nonwetted wall of a vessel engulfed in a pool fire of kerosene (Planas et al., 1996).

Of course, the possible failure of equipment will depend on the circumstances; the most important ones are the heat flux value, the possible existence of passive (not damaged) or active protection, and the duration of the fire. Another fact that can have an influence

is the one related to the contents of the equipment: if a liquid is inside the zone receiving the heating action, the equipment wall will be cooled by it and possibly will avoid the equipment failure.

Jet fires are especially dangerous in case of flames impingement, due to the high heat transfer to the equipment originated by both the very good combustion and the high turbulence of the flames.

Jet fires are produced by the ignition of a fuel jet that comes out of a hole (or a flange, or a broken pipe) at a very high speed. In many cases, if the fuel comes out of a pressurized vessel or pipe, its speed at the exit will be sonic. This means that the fuel jet will be very turbulent and will entrain air, thus giving a very good combustion (much better than the one found in a pool fire) and, therefore, a very high heat release. A jet fire has very bright flames if the fuel is a two-phase flow (Figure 1-5), and an almost transparent flame if the fuel is gas. And, again due to the very good combustion, there is practically no smoke; this behavior is quite different from the one found in a pool or tank fire.



Figure 1-5. Left: Vertical propane jet fires. gas jet. Right: two-phase jet (Palacios, 2011).

The origin of jet fires can be due to different facts. In a historical analysis (Gómez-Mares et al., 2008) performed on 84 accidents in which the domino effect had been started by a jet fire, the causes were the ones shown in Table 1-2 (as the accidents could have one or more causes, the percentage sum is not equal to 100). This survey also showed that half of the registered jet fires originated in a domino effect sequence.

Nevertheless, when considering statistical data concerning the occurrence of jet fires in the industry the following should be taken into account: other types of accidents such as pool or tank fires and fireballs, and also explosions, are quite evident because of the large amount of smoke and because of the sound in the case of explosions; so, they are known and usually registered in the technical media or in accident databases. Instead, in the case of jet fires, they are not so evident: there is no smoke, no noise; so, if they do not originate a secondary accident and can be extinguished in a relatively short time (for example, by closing a valve), it is possible that they go unnoticed. So, it is probable that some of the jet fires that occur in industrial plants are not registered and therefore not included in the historical analyses. (Refer to Chapter 2 of this document for a detailed historical analysis of domino accidents).

Table 1-2. Main effects of major accidents.

Cause	Percentage %
Mechanical	37
Human	29
Impact	27
External	19
Unknown	17
Instrument	4
Violent reaction	2
Upset process conditions	1

Anyway, what is clear from the analysis of the accidents involving the domino effect is the fact that jet fires, even the small ones, can be –and have been– the first step of the accident sequence.

A good example is the serious accident that occurred in a petrochemical plant in Priolo, Italy, in 1985 (Figure 1-6). The failure of an instrument caused the increase of pressure in the reboiler of a distillation column and a safety relief valve was activated; the flammable gas released was ignited, forming a jet fire. This jet fire impinged on a pipe with a diameter of 600 mm containing ethylene at 18 bar that, after a relatively short time failed, originating a very large jet fire. This impinged on a set of cylindrical storage tanks located at a distance of 60 m; one of them underwent an explosion (BLEVE) followed by a fireball; the ejected fragments damaged other equipment, originating other fires. The plant had been evacuated, so there were no fatalities (one operator wounded), the plant was seriously damaged: a serious accident, started by a relatively small jet fire.

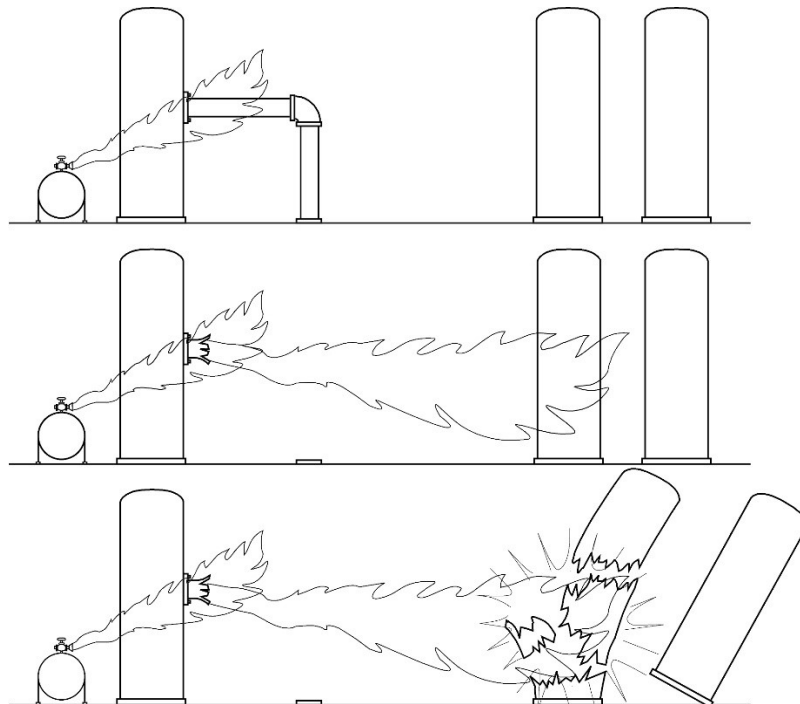


Figure 1-6. An example of a domino effect originated from a jet fire (Casal, 2018).

#### 1.4. The case of pipelines

The transportation of hazardous materials (for example, natural gas or ammonia) is an important aspect of the chemical and petrochemical industry and of the energy sector. Road, rail, and ship transportation modes are intensively used. However, for the transport of liquids and gases pipelines are essential: large amounts of natural gas are transported between regions of a country and between countries. It is a fact that the

length of pipelines is continuously increasing according to reports (e.g. European Gas Pipeline Incident Data Group, 2015) which shows the increase in the total length of the European gas transmission pipelines between 1970 and 2013

For the transportation of hazardous fluids pipelines are a fairly safe system as compared to other transportation modes, for diverse reasons. The most important one is the fact that pipeline is not a batch mode but a continuous one, this meaning that loading/unloading operations (rather dangerous operations, basically because human factor plays an important role in them) are not necessary. However, it is a fact that, due to the high number of pipelines that are being used for transporting flammable (such as natural gas) materials or, in much smaller amounts, toxic (such as ammonia) products, some accidents occur from time to time.

If there is a release in the transportation of flammable fluid, the accident sequence can follow diverse paths depending on the pipeline situation (aerial or underground), and the release characteristics (full bore rupture, a hole, immediate or delayed ignition) (Ramírez-Camacho et al., 2017). The possibility of immediate ignition is higher if the pipeline is aerial and near some human activity, although delayed ignition can also occur through the formation and evolution of a flammable cloud; ignition can also occur because of an electrostatic action. In the case of delayed ignition, a flash fire or a cloud explosion can also occur.

In the case of buried pipelines, the possibility of ignition still exists if the formation of a crater allows the exposition of the pipe to the air; a crater can be created by the energy of the pressurized fluid or by the explosion of a flammable mixture of gas and air in void spaces following a release.

If there is a crater, the situation is similar to the one found in the case of an aerial pipeline. Figure 1-7 shows a simplified scheme organized as an event tree of the diverse possible sequences following a release. The final accidental scenario can be a jet fire or a pool fire (depending on the condition of the release, gas or two-phase flow or liquid), a cloud explosion or a flash fire in the case of delayed explosion, followed by a jet or a pool fire, or environmental pollution if there is no ignition of the release.

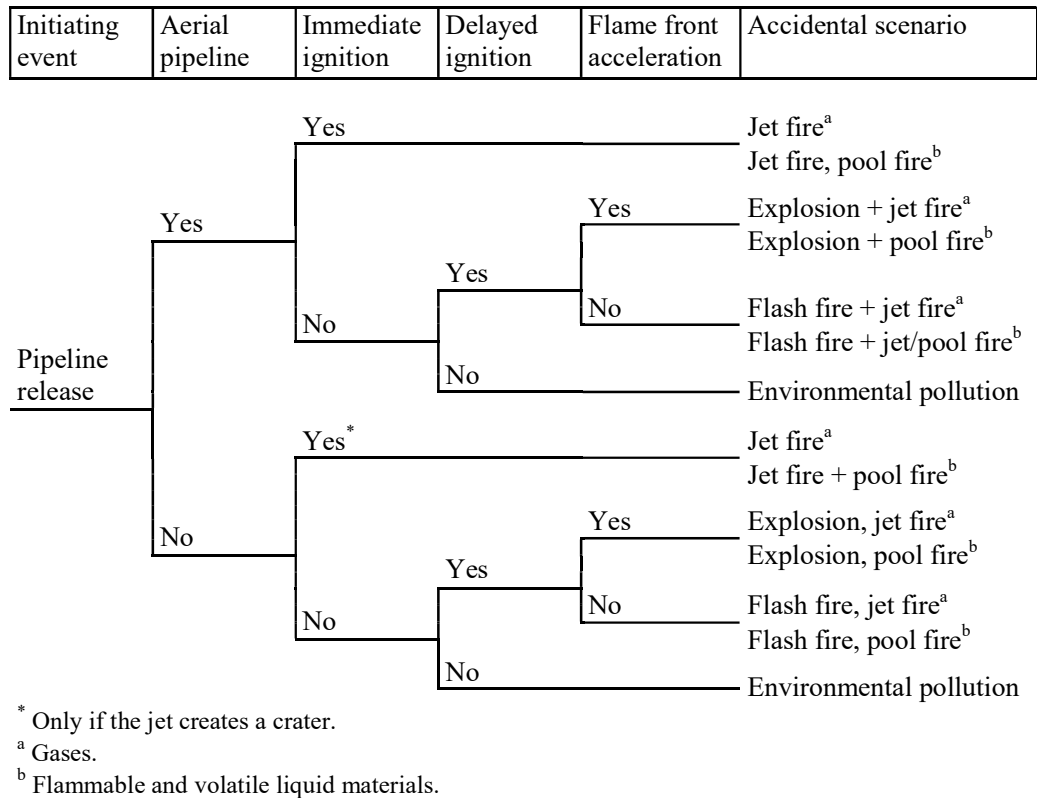


Figure 1-7. Possible consequences following a release from a pipeline (Ramírez-Camacho et al., 2017).

Looking at the different possibilities shown in this event tree, it is clear that the possibility of having a jet fire is considerable, both for aerial and buried pipelines.

And this is an important fact, because of two reasons. Often pipelines are exposed to external aggressions such as third-party activities (which, according to historical analysis cause approximately 40% of all releases) such as the action of excavating machinery. And also, due to the difficulty sometimes found in installing a corridor over large distances for the pipeline, often in the same corridor, more than one pipeline is installed (Figure 1-8).

When two or more pipelines are located in the same corridor, the distance between them is very short. This means that if there is a loss of containment in one of them and the gas or two-phase jet –often a sonic one, due to the high pressure existing inside the pipe– is ignited, the probability that the resulting jet fire impinges on another pipeline is very high. This means that probably a domino effect will occur, and the second pipeline will fail in a rather short time.



Figure 1-8. More than one pipeline in the same corridor  
([https://www.passuite.com/kbase/doc/start/WebHelp\\_en/pipesoil.htm](https://www.passuite.com/kbase/doc/start/WebHelp_en/pipesoil.htm)).

This accident has occurred several times. A well-known one is that occurred in Rapid City in 1995, in a corridor in which there were five buried pipelines transporting natural gas (TSBC, 1997). The failure of one of the pipes originated a crater that allowed the ignition of the released gas, with the formation of a jet fire. The flames impinged on a second pipeline, which after a short time ruptured.

This case is a good example of the potential destructive power of jet fires.

### 1.5. Objectives of the thesis

A certain number of authors have studied the main features of jet fires. Some of them have worked on vertical jet fires, proposing a model to predict the jet shape and dimensions; in this case, the length is the maximum possible for a given fuel flow rate. This allows the estimation of the maximum possible reach of a jet fire. And a few authors have studied horizontal and inclined jet fires, proposing models for estimating the shape and size of the flames.

Birk (2007) studied the effect of premixed flames from a burner on a vessel. However, there were no experimental data on the effect of the impingement of jet fire flames on equipment, a vessel, or a pipe.

Therefore, the objectives of this thesis were:

- Designing and building of an experimental setup to obtain and measure subsonic and sonic propane jet fires up to 3 m long.

- Obtaining and analysing the main geometrical parameters associated with the shape and size of horizontal propane jet fires. Propose adequate expressions to estimate these variables as a function of the jet pressure and flow rate.
- Measuring and analysing the behaviour and main features of the jet fire flames, as well as their temperature.
- Mathematical modelling of the jet fire characteristics mentioned earlier, obtaining a set of expressions allowing their approximate prediction.
- Studying the thermal effect of the jet flames (corresponding to each one of the jet fire sections) impingement on a steel pipe wall, both for the case of a wall in contact with air (internal surface) and with water.
- Studying the performance of Computational Fluid Dynamics (CFD) tools when simulating the aforementioned variables and jet fires behaviour.

### **1.6. Structure of the thesis**

The thesis has been organized into a series of chapters presenting the obtained results, as follows:

- Chapter 1. Introduction
- Chapter 2. Literature Review and Historical Analysis
- Chapter 3. Experimental Setup and Test Methodology
- Chapter 4. Geometrical Features of Horizontal Jet Fires
- Chapter 5. Thermal Effects of Jet Fire Impingement on a Pipe
- Chapter 6. CFD Simulations of Jet Fires
- Chapter 7. Conclusions
- Nomenclature
- References
- Appendices



## 2. Literature Review and Historical Analysis

### 2.1. Introduction

Major accidents, such as emissions, fires, or explosions can occur during the operation of any establishment. These accidents pose grave threats to both human health and the environment, both within and beyond the affected facility. Common accidents in the chemical industry involve the release of flammable or toxic substances in gas or liquid form, often resulting from pipeline ruptures, explosions of pressurized containers, or other factors. These accidents can lead to a range of consequences, including thermal radiation, pressure waves, fragment projection, and the release of toxic contaminants into the surrounding environment (Reniers & Cozzani, 2013).

### 2.2. Domino accidents

Accidents involving domino effects have been recognized as severe and efforts have been made to prevent them. In Europe, the hazard posed by domino effects was acknowledged in the first Seveso Directive, which mandated the evaluation of domino hazards in plants required to produce a safety report. The Seveso-III European Directive further addresses domino effects, requiring the assessment of scenarios where a primary accident can propagate to neighbouring plants. As a result, domino effects are officially acknowledged in the European Directive concerning major accident hazards.

The recognition of the risks associated with domino effect accidents has been established since the inception of process safety. The establishment of chemical clusters, where multiple active plants are concentrated, began in the 1960s to reduce costs and increase production capacity. However, this trend has led to complex and expansive industrial sites.

Petrochemical complexes, which handle significant quantities of various substances, are the primary hazardous installations. The presence of large amounts of flammable substances, coupled with high temperature and pressure conditions, renders these

systems potential sources of severe accidents. In the petrochemical plant sector, accidents are often not isolated incidents due to the intricate nature, congestion, and interdependence of subsystems. Consequently, there is a considerable risk of domino accidents occurring in these plants, whereby an initial accident triggers a series of subsequent accidents, exacerbating the overall consequences (Khan, 1998).

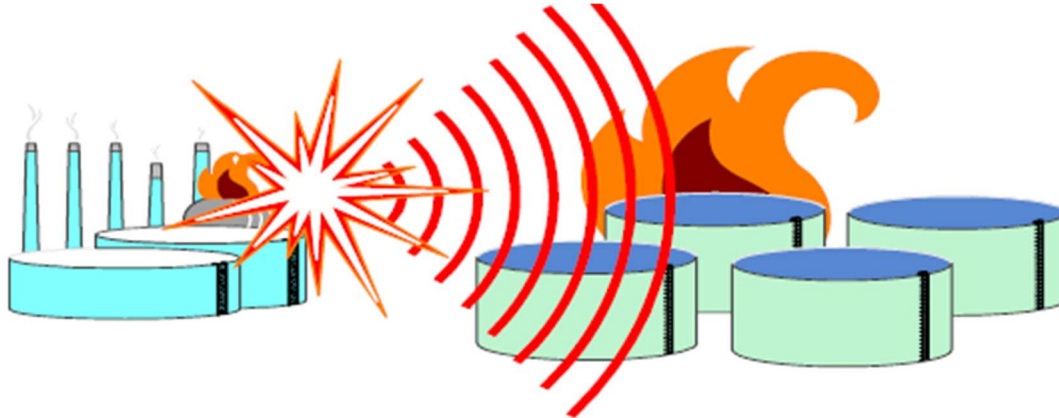


Figure 2-1. Example of a domino effect sequence between two industrial sites (Cozzani et al., 2007).

Defining a "domino accident" unambiguously is challenging due to its complex characteristics. Several definitions of a "domino effect" have been proposed, all of which hold scientific and technical validity as below ones:

- "An incident that originates in one component and can impact neighbouring components through thermal, blast, or fragment effects, leading to an escalation in severity of consequences or failure frequencies" (CCPS, 2000).
- Alternatively, it can be defined as "The propagation of a primary accidental event to nearby units, causing damage and further 'secondary' accidental events, resulting in a scenario that is more severe than the initial event that triggered the escalation" (Antonioni, 2009).
- Currently, the most commonly used definition is "an accident in which an undesired event propagates within an equipment ('temporally') and/or to neighbouring equipment ('spatially'), sequentially or simultaneously, triggering one or more subsequent undesired events, potentially leading to further higher-order undesired events and resulting in overall consequences more severe than those of the primary event" (Reniers & Cozzani, 2013).

### 2.3. Elements of a domino accident

There are some common elements that can be found in all definitions regarding the domino effect. In Table 2-1 some definitions are gathered concerning the common elements found every domino accident.

Table 2-1. Elements needed for a Domino Accident (Reniers & Cozzani, 2013).

Element	Definition
Primary scenario	An accidental scenario that starts a domino effect propagating and escalating to the other process or storage units, triggering one or several secondary accident scenarios.
Escalation	The intensification of the overall consequences of an undesired event.
Escalation vector	A vector of physical effects generated by the primary accident scenario.
Secondary scenario	An accidental scenario caused by the impact of an escalation vector generated by a primary accident scenario.
Propagation	In case of a spatial domino effect, the propagation indicates the involvement of other units or equipment items, present at different positions with respect to that of the primary accident. In the case of a temporal domino effect, there is propagation within the same unit or equipment item.

The main element that identifies scenarios where a domino effect takes place is the “propagation” effect. A domino effect sequence begins with a primary event (primary scenario) after which (and originated by it), through the escalation vectors, secondary events can take place. This development of the accident from a primary accident to one or more accidents is defined as propagation. Another important element is escalation, because the propagation alone cannot lead to a scenario as a domino effect. The primary events are only explosion (escalation vectors: overpressure, fragment projection) and

fire (escalation vectors: flame impingement, radiation). The gas cloud is not considered as a primary event, because this can develop as an explosion, fire, or toxic cloud, however, it does not cause secondary events that include escalation vectors. The potential escalation vectors associated with the different types of accidents that can occur are shown in Table 2.2.

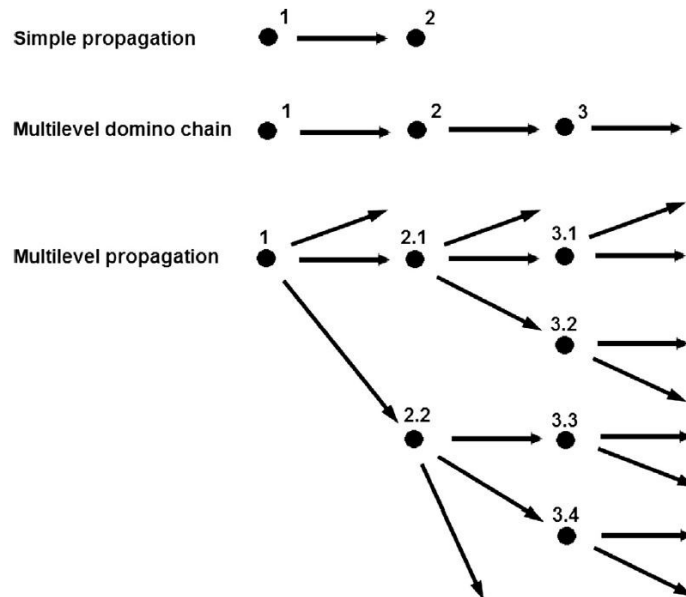


Figure 2-2. Examples of simple propagation, multiple-level domino chain, and multilevel (Reniers & Cozzani, 2013).

Figure 2-2 shows alternative propagation patterns that can be assumed in the domino scenario analysis. A "simple" propagation can be hypothesized by defining a "one-to-one" match, i.e. a single primary scenario triggering a single secondary scenario. Alternatively, second, third, and more generally multilevel one can hypothesize the propagation, defining a so-called "multi-level domino chain". Another important element is escalation because the propagation alone cannot result in a scenario as a domino effect. Two main patterns were identified for escalation: direct or indirect.

- Direct escalation is caused by the direct damage of target units due to the effect of radiation, blast waves, flame impingement and fragment projection.
- Indirect escalation scenarios may be triggered by the loss of control of units or plant sections due to the effect of the primary scenario. For example, the

damage of a control room by a blast wave or the flee of untrained operators due to a toxic dispersion or a fire may lead to the loss of control of a process.

Table 2-2. Escalation vectors and escalation criteria for the definition of escalation radius for different primary scenarios (Cozzani, et al., 2007).

Primary scenario	Escalation vector	Escalation Criterion	Escalation radius
Fireball	Heat radiation	Flame engulfment	Fireball radius
	Heat radiation	15 kW/m <sup>2</sup>	The distance at which heat radiation equals the threshold value
Jet Fire	Heat radiation	Flame impingement	Flame radius
	Heat radiation	15 kW/m <sup>2</sup>	The distance at which heat radiation equals the threshold value
Pool Fire	Heat radiation	Flame engulfment	Flame radius
	Overpressure	16 kPa	The distance at which peak pressure equals the threshold value
Vapour Cloud Explosion (VCE)	Overpressure	16 kPa	The distance at which peak pressure equals the threshold value
	Fragment projection	Fragment impact	Maximum projection distance
BLEVE	Overpressure	16 kPa	The distance at which peak pressure equals the threshold value
	Fragment projection	Fragment impact	Maximum projection distance
Mechanical and confined explosion	Overpressure	16 kPa	The distance at which peak pressure equals the threshold value
	Fragment projection	Fragment impact	Maximum projection distance

The occurrence of a domino effect is influenced by the type of escalation vector involved. Fires, for instance, can vary in their thermal power emissions, with some emitting high levels that can cause severe damage to nearby equipment. The duration of the phenomenon also plays a role, as certain accidents like flash fires have brief contact with equipment, while others may persist for longer periods. However, the most significant factor influencing the spread of an accident is the separation distance between the primary unit and potential targets. Escalation sequences involving

atmospheric and pressurized equipment are only possible when highly energetic primary scenarios occur. Table 2-2 provides an overview of primary scenarios and their corresponding escalation vectors based on the analysis of over 100 domino cases in a previous study. The primary scenarios represent events that can trigger escalation effects. The table also presents the physical effect data responsible for the identified escalation in each scenario, which are referred to as the escalation vectors.

The intensity of each escalation vector, also known as the escalation radius, is determined by the total amount of energy or substance that could potentially be released from the primary containment system, such as a reactor or storage tank. The escalation effects are considered plausible within the maximum distance defined by the escalation radius. To estimate the escalation radius, threshold values for escalation have been established based on investigations conducted by Cozzani et al.. (2006). These threshold values reflect the vulnerability of different groups of process equipment.

The duration of the incident is a crucial aspect to consider. Flash fires have brief contact with equipment, while pool and jet fires can endure for a longer duration. When it comes to explosions, although the overpressure can be reasonably estimated, accurately predicting the direction of ejected fragments remains a challenge. Regardless of the incident type, the separation distance between the primary unit and potential targets plays a pivotal role in determining the incident's propagation.

#### **2.4. Characteristics of accidents involving the domino effect**

The analysis of past incidents is a valuable approach to investigating the domino effect. Past incidents serve as important sources of experimental data, offering insights into various aspects of domino effects, such as common triggering events, frequent sequences, and substances involved.

Accidents involving domino effect can be found from the specialized literature, from reports of certain institutions and in certain databases. However, often the information thus obtained is not complete; this implies a reduction of the sample size when a statistical treatment must be performed, with the consequent loss of significance of the results obtained. Several historical surveys have been published on this subject.

Bagster and Pitblado (1991) studied the frequency and likelihood of domino accidents in a pioneering work. Kourniotis et al.. (2000) performed a survey on 207 accidents, of which 80 involved domino effect; their sequences (ratio of accidents with one or two domino effects) and their consequences on the population were analyzed. Ronza et al.. (2003) studied 108 accidents occurred in port areas which involved as well domino effect. With a much more specific approach, Gómez-Mares et al.. (2008) published a survey on accidents involving jet fires, 50% of which had been the primary event of a domino effect sequence.

Darbra et al.. (2010) performed a historical analysis on 225 accidents involving this effect. Shortly after, Abdolhamidzadehet al.. (2011) published another survey on 224 accidents also involving domino sequences. In these last two papers, the main features of the accidents were analyzed: substances involved, origin, primary events, consequences, etc. In Darbra et al.. (2010) the accident sequences were studied through the relative probability trees. In Abdolhamidzadeh et al.. (2011), a list of the accidents studied was included; this paper demonstrates that nearly three-fourths of all past domino events have been in fixed installations (Figure 2-3); of the 20% of analyzed accidents that occurred during transportation, the largest fraction happened on roads, closely followed by railroad events; and pipelines and shipping accounted for the rest (Figure 2-4).

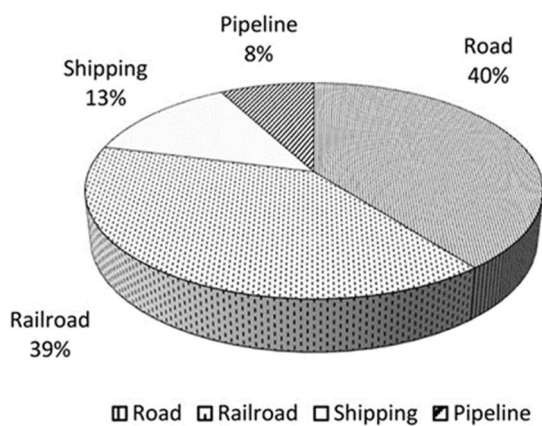


Figure 2-3. Domino events encountered during different modes of transportation

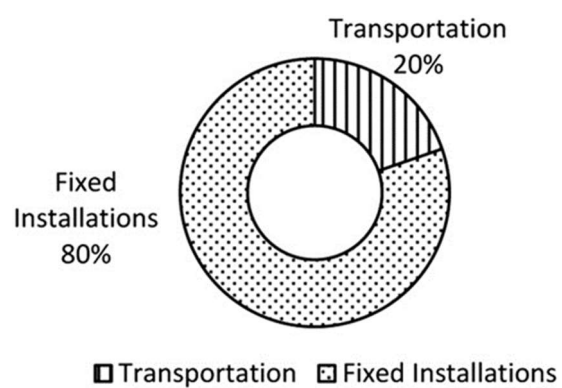


Figure 2-4. Domino events occurring in fixed installations and during transportation

The main features of domino accidents have been recently analyzed by diverse authors in Reniers & Cozzani (2013). However, although an increasing interest can be inferred from the publications found in the literature, this subject has been treated by a few number of authors. As a result, the main domino effect features and trends are still poorly known.

A historical survey was performed on 330 accidents involving domino effect, occurred in process/storage plants and in the transportation of hazardous materials, by Hemmatian et al. (2014), in which only accidents occurred after 1st-January-1961 were considered. The main features and studied parameters of this survey were similar to the previous ones in some aspects, although this later work dealt with a much larger number of accidents. In Hemmatian et al. (2014), it was highlighted that among the involved substances, LPG was the most frequent one, followed by liquid hydrocarbons.

Process plants (38.5% of cases) and storage areas (33%) were the most common settings; 10.6% of past domino accidents occurred in transfer operations. This study allowed the authors to perform a specific analysis of the accidents occurrence and features in developing countries (in which industry is developing quickly), as well as a comparison with the situation in the industrialized ones.

In addition, a specific analysis of accidents was also performed by these authors in the period 2000-2013. The graph shows that the highest percentage of accidents occurred in the 1970s, accounting for 23.9% of the incidents. After a decline in the 1990s, the frequency of accidents began to rise again in the early 21<sup>st</sup> century, approaching previous levels.



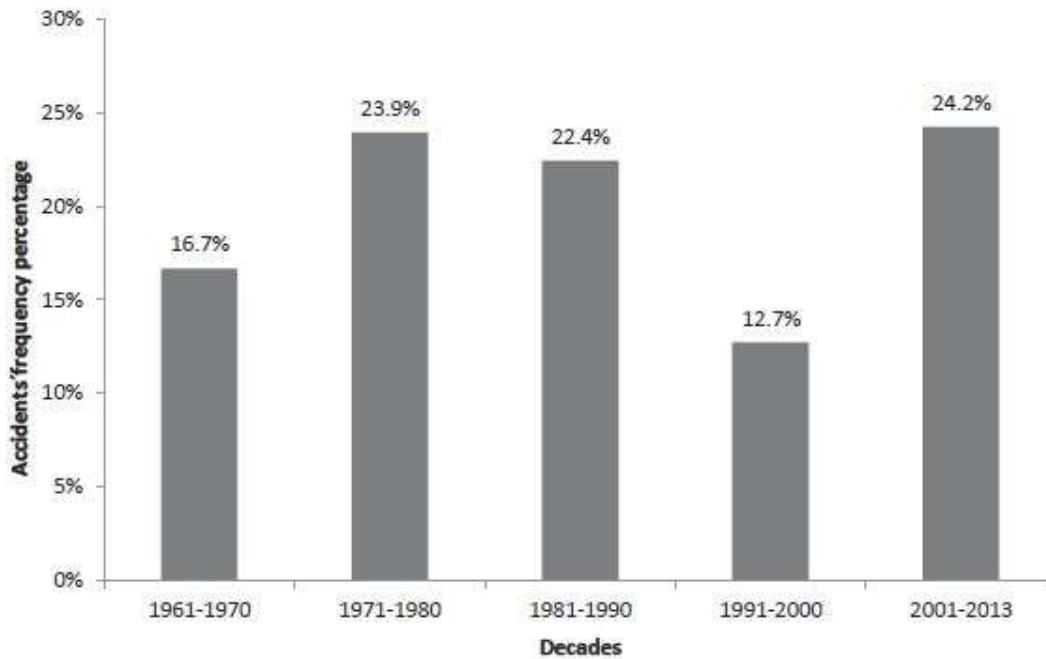


Figure 2-5. Distribution of domino accidents over time (Hemmatian, et al., 2014).

Multiple substances have been implicated in numerous accidents, with a total of 537 substances reported across 330 incidents. Table 2-3 provides insights into the most associated substances in domino accidents. LPG was the most frequently involved substance, accounting for 22% of the incidents. Gasoline followed at 10%, and oil at 9%. Other liquid hydrocarbons like gas oil/fuel oil and naphtha were also identified. Additionally, toxic substances such as chlorine and ammonia played a role in some accidents. It is important to note that the percentages in the table do not add up to 100 because many accidents involve multiple substances.

In terms of hazardousness, flammable substances were the most frequently involved, accounting for 83% of the domino accidents. Toxic substances followed at 27%, and corrosive substances made a smaller contribution at 7%. Once again, the percentages do not sum up to 100 due to the involvement of multiple types of materials in various accidents.

Table 2-3. Substances involved in domino accidents (Hemmatian, et al., 2014).

Substance	No. of accidents	Percentage
LPG	72	22
Gasoline	33	10
Oil	29	9
Gas oil/ fuel oil	20	6
Naphta	14	4
Vinyl chloride	13	4
Chlorine	11	3
Natural gas	11	3
Ammonia	10	3
Ethylene oxide	10	3
Other chemical substances	314	95
Total	537	162

Understanding the causes of accidents is crucial for preventing their recurrence. Table 2-4 provides an overview of the causes of primary accidents, using categories from the Major Hazardous Incident Data Service (MHIDAS) database to represent generic causes. The information sources may vary, but the categories used include external events, mechanical failures, human errors, impact failures, violent reactions (runaway reactions), instrument failures, disrupted processes, and service conditions. Understanding these causes can contribute to effective preventive measures.

Table 2-4. General causes of accidents (Hemmatian et al., 2014).

General cause	No. of accidents	Overall percentage
Mechanical failure	103	35.2%
External event	86	29.4%
Human factor	72	24.6%
Impact failure	49	16.7%
Violent reaction	25	8.5%
Instrument failure	13	4.4%
Upset process conditions	9	3.1%
Services failure	5	1.7%
Total	359	123.6

Mechanical failure was identified as the predominant cause, constituting 35.2% of the accidents and frequently associated with issues like overpressure and overheating. It is important to acknowledge that the total number of general causes listed in the table may exceed the overall number of domino accidents, as some incidents might have multiple causes occurring simultaneously.

Table 2-5 categorizes the origins of accidents using MHIDAS categories. It is important to note that the total number of general origins may exceed the overall number of domino incidents due to some incidents having dual origins. The primary origin of accidents, identified in 38.5% of cases, is process plants. This can be attributed to the inherent risks associated with operating such facilities. Storage areas were responsible for accidents in 33% of incidents, which can be attributed to the presence of tanks holding hazardous substances and the potential for containment breaches.

Interestingly, a significant percentage of accidents (10.6%) were attributed to "transfer". This highlights the ongoing contribution of accidents during loading and unloading

operations. Despite the well-known risks involved, preventive measures are often implemented to mitigate these types of accidents.

Table 2-5. General origin of accidents (Hemmatian, et al., 2014).

General origin	No. of accidents	Overall percentage
Process	127	38.5
Storage	109	33.0
Transport	53	16.1
Transfer	35	10.6
Warehouse	15	4.5
Domestic or commercial premises	11	3.3
Waste storage or disposal areas	1	0.3
Total	351	106.3

### 2.5. Risk associated with pipeline systems

Pipelines are the safest and most economical way to transport large amounts of substances over long distances, for this reason, the number of pipelines that are proposed or under construction is increasing year by year, connecting different regions of a country and, more and more, different countries (Casal, 2018). There are over 2.6 million kilometres of fuel pipelines in the United States and over 200.000 km in Europe.

Natural gas represents 23% of the primary energy consumption in the United States, and its distribution to customers relies on an extensive network of transmission and distribution pipelines spanning over 3.8 million kilometres (U.S. Energy Information Administration, 2011). Additionally, pipelines play a significant role in the transportation of liquid fuels. Hazardous liquid pipelines are responsible for transporting crude oil, diesel, gasoline, jet fuel, and kerosene. In 2008, hazardous liquid pipelines, covering 282,000 kilometres, accounted for 38% of crude oil transport and 62% of petroleum transport (Association of Oil Pipelines, 2011). Unfortunately, pipeline failures are not

uncommon, and their consequences can be catastrophic. For instance, a hazardous liquid pipeline rupture in Kalamazoo, Michigan, in July 2010 resulted in the spillage of one million barrels of oil. In September 2010, an explosion in a transmission pipeline in San Bruno, California, led to eight fatalities (Silver-Evans et al., 2014). Incidents like these have raised concerns about the safety of the nation's pipeline system. In assessing the severity of pipeline incidents, three metrics are commonly used: fatalities, injuries, and monetary property damage. For hazardous liquid pipelines, the volume of product spilled is also considered as a measure of accident severity. Figure 2-6 shows this increasing trend in the total length of European gas transmission pipelines (European Gas Pipeline Incident Data Group, 2015).

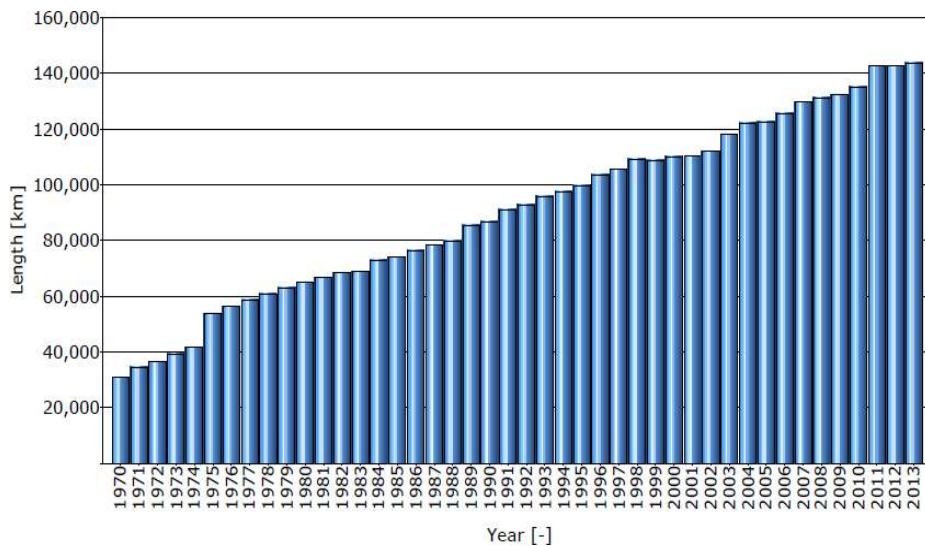


Figure 2-6. Variation of the total length of European gas transmission pipelines (EGIG, 2015).

Previous studies on pipeline accidents can be categorized into two groups: those focused solely on pipelines and those that compare risks across different energy supply chains, including natural gas and hazardous liquid pipelines. This highlights the potential risks associated with the interaction of these systems. In such situations, an accident in one pipeline could potentially impact nearby pipelines, introducing an additional level of risk.

Loss of containment events occur from time to time, for different reasons (Casal, 2018):

- The pipe: design, construction, ageing, corrosion, vibrations, etc.
- The fluid: erosion and chemical attack.
- Incorrect operation (overpressure).

- Third-party actions: excavating machinery, impacts (trucks), and sabotage.
- Other infrastructures: loads (roads and car parks), erosion from another pipe.
- Natural disasters: landslides, floods, and forest fires.

Two recent studies conducted on a database of pipeline incidents (Bubbico et al., 2016; Ramirez-Camacho et al., 2017) have provided evidence that third-party activities are the most common cause of pipeline damage, accounting for approximately 38% of incidents regardless of the substance involved or the severity of the release. Excavation activities were found to be responsible for the majority of damages, comprising approximately 30% of incidents. Corrosion ranked as the second most frequent cause of containment loss, accounting for 21% of cases, followed closely by mechanical failure at 20%. The studies also revealed that gasoline, natural gas, and crude oil were the materials most frequently involved, with proportions of approximately 29%, 27%, and 27% respectively. Other substances such as diesel fuel, jet fuel, and LPG were implicated in less than 5% of cases. Among all incidents, liquids were involved in the majority, accounting for 74% of occurrences. Flammable materials constituted 98.5% of the incidents, while 0.8% involved toxic substances, and 0.7% were attributed to corrosive materials.

Following the release of a hazardous substance from a pipeline, the subsequent sequence of events can vary depending on factors such as the material's properties (flammability, toxicity, volatility), pipeline location (underground or surface), release characteristics (full bore, hole, etc.), weather conditions, and environmental factors (urban or rural surroundings).

The nature of pipelines, whether they are aerial or underground, can significantly impact the consequences of an incident. In the case of aerial pipelines carrying flammable fluids, immediate ignition is possible, especially in areas with human activity. This can lead to a jet fire if the released material is a gas or a pool fire if it is a liquid. If there is no ignition, the spilled liquid can contaminate the soil and potentially reach nearby bodies of water, causing pollution. Volatile liquids may also disperse into the atmosphere. Delayed ignition is a possibility if the material released from an aerial pipeline is flammable. This can result in a flash fire or vapor cloud explosion, followed by a jet fire (for gas releases) or a pool fire (for liquid releases).

In the case of underground pipes, the presence or absence of a crater from the initial release will determine the scenario. Natural gas and highly volatile hydrocarbons pose a risk of fire and explosion, which can endanger the population. On the other hand, oil generally poses a risk to the environment.

If a crater is formed, similar to aerial pipelines, immediate ignition can occur, leading to a jet fire (for gas releases) or a pool fire (for liquid releases). Delayed ignition can result in a flash fire or vapor cloud explosions, followed by a jet fire or a pool fire. Without ignition, environmental pollution can occur. In the absence of a crater in underground pipelines, liquid may enter the soil and create a pool above the ground, while gas can seep through soil pores into the atmosphere. In any case, the potential final scenario can involve fires, pool fires, jet fires, vapor cloud explosions, or environmental pollution.

### **2.5.1 Parallel Pipelines**

Parallel pipelines are frequently installed near one another due to the challenges associated with creating and maintaining adequate space.

Establishing a dedicated corridor for these pipelines can be difficult and costly, often resulting in multiple pipes sharing the same corridor. As a result, it is common to find parallel pipelines transporting gas, oil, or water over long distances, sometimes with minimal separation between them. These corridors may contain a dense arrangement of parallel and intersecting pipelines and utilities, through which hazardous fluids are being conveyed. This configuration presents a certain level of risk associated with the potential interaction of these systems. In such scenarios, an accident occurring in one pipeline can have an impact on a nearby pipeline.

Various incidents have occurred where this has led to severe consequences for individuals or had adverse effects on the environment. In these situations, due to the relatively short separation distance between the pipelines, a loss of containment in one pipe, such as a hole caused by corrosion, can trigger a domino effect that affects another pipe. Erosion and thermal impact are potential escalation factors in such cases. The initial event involves the release of a jet through a hole in one of the pipes. The subsequent sequences of the domino effect will depend on factors such as whether the pipelines are aboveground or buried and whether the conveyed fluid is flammable.

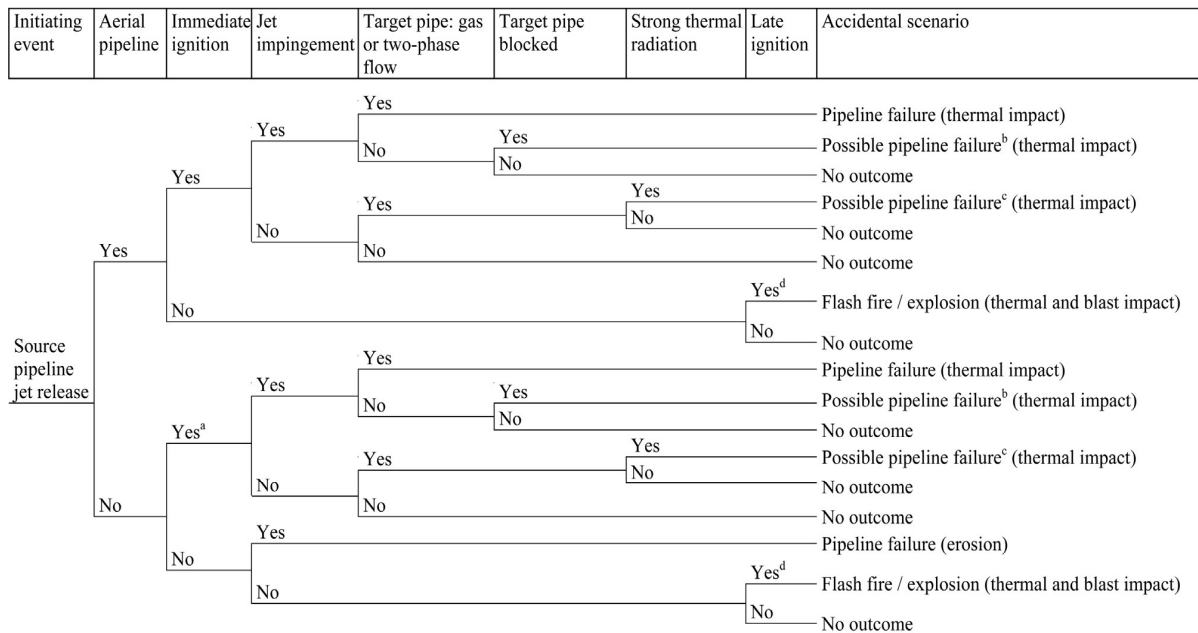


Figure 2-7. Domino effect sequences following a jet release from the source pipe (Ramírez-Camacho, et al., 2015).

In the case of aerial pipes, if the fluid being conveyed in the source pipe is flammable and ignites, there is a possibility of the flame impinging on the target pipe. If the target pipe carries gas and lacks adequate fireproofing measures, there is a high probability of failure within a relatively short period. However, if the target pipe carries a high-flow, high-pressure gas, the heat transfer coefficient to the internal fluid may be sufficient to prevent failure (Tugnoli et al., 2013).

On the other hand, if the target pipe carries a two-phase flow, the possibility of pipe failure due to the high temperature reached by the pipe wall should also be considered. If the target pipe carries a liquid, it helps cool the pipe wall and prevent failure. However, if the flow in the target pipe is interrupted due to the closure of shut-off valves, the pipe may fail once again. In the absence of a flame, the target pipe is unlikely to be affected. Nevertheless, even if it is subjected to intense heat radiation and carries a gas, it still has the potential to fail (Billota et al., 2016).

If the released fluid is flammable and experiences delayed ignition, there is still a risk of fire or explosion. In such a scenario, with the explosion of one pipe, both pipes could be damaged, or the fire jet following a flashback could impact the target pipe. However, if both pipes are buried, the situation is slightly different. If the released fluid is flammable,



there is a chance of ignition only if the jet or explosion creates a crater. The resulting scenarios are similar to those described earlier. In the case where there is no ignition but the jet impacts the target pipe, it may contain solid particles, resulting in a highly abrasive jet (Casal, 2018). Another important consideration is the duration of the release, as the loss of containment in aerial pipes is likely to be detected.

Conversely, if the source pipe is buried, detection becomes more challenging. If a small hole in the source pipe goes unnoticed, there is a high probability that it will eventually lead to another release into the target pipe. Even without direct impingement of the jet, the force of the fluid/solid blast can cause erosion, reducing the thickness of the pipe to a point where it cannot withstand the internal pressure, resulting in failure.

Furthermore, if there is no immediate ignition but the released fluid is flammable, there is still a risk of a subsequent fire and/or explosion (Casal, 2018). This can occur when a liquid saturates the ground and flows above the surface, evaporating into the atmosphere, or when a released gas flows through the soil and enters the air.

In such cases, if a crater is formed, the fire can propagate back to the fluid outlet, leading to a jet fire and potential damage to the target pipe. This investigation reinforces the understanding that when parallel pipelines are installed in the same corridor, the potential for a loss of containment in one pipeline affecting the others should not be underestimated. The domino effect can manifest through erosion caused by a fluid/abrasive soil jet in underground pipes or by thermal impact from a fire jet, particularly in overhead pipes when dealing with flammable substances. These factors significantly influence the frequency of system failures and should be duly considered in risk assessments (Reniers and Cozzani, 2016).

If a crater is formed in the case of a buried pipe, there is a possibility of ignition, and the potential sequences of events are similar to those mentioned previously. Additionally, when abrasive soil such as sand or gravel is present along with a high-velocity jet, it can result in significant erosion. Experimental tests conducted by Majid, et al.. (2008) demonstrated that a steel pipe exposed to the impact of a water-sand jet released from a 5-mm hole can experience considerable rates of wall thinning.

The duration of the release is also a crucial factor to consider. In the case of aerial pipelines, a loss of containment is likely to be detected promptly. However, if the pipelines are buried and the release is relatively small, it can persist for an extended period without immediate detection.

It is important to note that an explosion in one pipe, whether caused by a pressure increase or wall corrosion, can have an impact on other nearby pipes. In the context of parallel pipelines, it is possible to determine how a loss of containment in one pipe will affect the frequency of loss of containment in the other pipe, as these relationships can be precisely defined (Casal, 2018).

### **2.5.2 Jet Fires in Pipelines**

A comprehensive analysis of 1063 accidents in onshore pipelines have provided valuable insights into the development of detailed event trees for different categories of hazardous materials (Bubbico et al., 2016). These categories are classified based on their flash point ( $T_f$ ) and include compressed gases (consisting of 291 entries, predominantly natural gas), pressurized liquefied gases (with 50 entries, primarily LPG), volatile liquids with  $T_f \leq 21^\circ\text{C}$  (comprising 608 entries, mainly gasoline, and crude oil), and low-volatile liquids with  $T_f > 21^\circ\text{C}$  (accounting for 114 entries, primarily jet fuel and diesel oil). Through a quantitative analysis of the event trees, it was possible to determine the probabilities of occurrence for each type of post-release event (Table 2-6).

Clearly, the probabilities of occurrence for each category can exceed one since multiple accidents can happen simultaneously. Notably, jet fires generally have higher probabilities of occurrence compared to other potential events, making them particularly significant in pipeline risk analysis. Jet fires are typically smaller in size and emit relatively reduced thermal radiation compared to pool fires.

Table 2-6. Loss of containment probabilities in pipelines (Bubico et al., 2016).

Type of Fluid	Event	Probability
Compressed gases	Jet fire	0.410
	Fireball	0.111
	Flash fire	0.074
	Vapour cloud explosion	0.314
	No consequences	0.380
Pressurized liquefied gases	Jet fire + (pool fire)	0.465
	Fireball	0.047
	Flash fire	0.140
	Vapour cloud explosion	0.302
	No ignition	0.488
Volatile liquids	Jet fire	0.024
	Pool fire	0.057
	Flash fire	0.046
	Vapour cloud explosion	0.051
Low-volatility liquids	No fire/explosion	0.882
	Jet fire	0.009
	Pool fire	0.053
	No fire	0.938

Consequently, jet fires are primarily influential at short distances, as thermal radiation diminishes rapidly with increasing distance from the flames. Furthermore, there is a relatively high probability of a jet flame impinging on another pipeline, leading to a domino effect. When a jet fire occurs from one pipeline, the thermal flux reaching

another pipeline, especially with flame impingement, can be extremely high, resulting in damage to the secondary target and an escalation of the accident's severity.

### **2.5.3 Characteristics of domino accidents in pipeline systems**

Pipeline domino accidents due to jet fires refer to a sequence of incidents where a jet fire in one pipeline triggers a series of subsequent fires or explosions in neighbouring pipelines, leading to a cascading effect. These incidents can have severe consequences and pose significant challenges for emergency response and mitigation. This type of incident can have significant consequences and requires careful analysis and response.

Pipeline domino accidents resulting from jet fire impingement present significant risks in industrial environments. Jet fires, characterized by their intense heat release and flame projections, can cause thermal damage to adjacent pipelines, triggering a chain reaction of accidents. Understanding the dynamics of such domino accidents and their underlying mechanisms is crucial for designing effective safety measures and preventing catastrophic consequences.

This section focuses on investigating the occurred domino accidents in pipeline systems resulting from jet fire impingement. The study aims to assess the thermal effects of jet fires on pipelines and evaluate the potential for propagating thermal damage along a pipeline network. By analyzing the thermal behavior and structural response of pipelines, this research aims to provide valuable insights into the domino effect and aid in the development of proactive safety strategies.

Here are some key points to consider regarding pipeline domino accidents due to jet fires:

1. **Ignition Source:** The jet fire incident can be initiated by an ignition source, such as a spark, flame, or heat source, that ignites the flammable substances being transported in the parallel pipelines.
2. **Initial Jet Fire:** The domino effect begins with an initial jet fire in one pipeline, typically caused by an ignition source and a rupture in the pipeline system. The jet fire generates intense heat, flames, and pressure that can impact nearby pipelines.

3. **Heat Radiation and Flame Impingement:** The flame front can rapidly spread from one pipeline to another, increasing the scale and intensity of the incident. The heat radiation and flame front from the initial jet fire can impinge on neighboring pipelines. The intense heat can weaken the structural integrity of these pipelines and ignite the flammable substances they contain.
4. **Pressure Effects and Ruptures:** The domino effect can lead to increased pressure within the pipelines, potentially causing ruptures or leaks. The ruptured pipelines can release additional flammable substances, fueling the subsequent fires and explosions.
5. **Safety Systems and Containment Measures:** In pipeline systems, safety systems such as emergency shutdown valves, flame and gas detection systems, and fire suppression measures play a crucial role in mitigating the domino effect. Containment measures, such as blast walls or trenching, can help prevent the spread of fires and limit their impact on adjacent pipelines.
6. **Emergency Response and Evacuation:** Dealing with pipeline domino accidents requires a coordinated and swift emergency response. It involves activating emergency response plans, evacuating personnel from the affected area, establishing safe perimeters, and coordinating firefighting efforts to control and extinguish the fires.
7. **Risk Mitigation:** To prevent jet fire incidents in parallel pipeline systems, risk mitigation measures should be implemented. This includes regular inspection and maintenance of pipelines, installation of fire detection and suppression systems, implementation of safety protocols, and adherence to industry regulations and standards.
8. **Investigating Root Causes:** After a pipeline domino accident, a thorough investigation is necessary to determine the root causes and contributing factors. This investigation helps identify any deficiencies in pipeline design, maintenance, safety systems, or operating procedures to prevent similar incidents in the future.

Preventing pipeline domino accidents due to jet fires requires a comprehensive approach that includes rigorous inspection and maintenance programs, adherence to

safety regulations and standards, implementation of robust safety systems, and continuous training and awareness for personnel involved in the operation and maintenance of pipeline systems.

It is important to note that the specific response and mitigation strategies for a jet fire incident in a parallel pipeline system depend on various factors, such as the type of transported substances, pipeline design, available safety measures, and emergency response capabilities. Each incident should be evaluated on a case-by-case basis to ensure an effective and tailored approach to mitigate risks and minimize the impact of the incident.

## **2.6. Examples of domino accidents in pipeline systems**

There have been several notable incidents in industrial history involving pipeline domino accidents resulting from jet fire impingement. These incidents serve as reminders of the potential consequences of pipeline domino accidents caused by jet fire impingement. They underscore the importance of robust safety protocols, adequate risk assessments, and continuous monitoring and maintenance of pipeline systems to prevent such catastrophic events and safeguard lives, infrastructure, and the environment.

Table 2-7 provides information on several domino accidents in pipeline systems involving jet fire impingement, that occurred between 1971 to 2020, however, unfortunately, detailed information about some of these incidents were not available. The incidents described are for illustrative purposes and do not represent an exhaustive list of all such accidents.

These relatively high numbers of accidents involving jet fires and pipelines underscore the critical importance of including them in this discussion. These incidents serve as stark reminders that regardless of the initial trigger for an accident, be it corrosion, excavation activities, or an explosion, the moment a jet of flammable fluid is released and subsequently ignites while impinging on a pipeline, there is a substantial possibility of a chain reaction occurring. This domino effect can lead to a series of interconnected accidents, intensifying the overall impact and magnitude of the incident.

The inclusion of these examples emphasizes the need for heightened vigilance and thorough risk assessment in industrial settings where pipelines are present. It is crucial to recognize that a single ignition event can set off a sequence of events with potentially devastating consequences. The release of a flammable fluid can rapidly propagate along the pipeline, igniting further sections and amplifying the scale of the incident. Such scenarios demand proactive measures and comprehensive safety protocols to prevent and mitigate the escalation of accidents.

Considering the potential for a domino effect is imperative when designing, constructing, and maintaining pipelines. This broader perspective helps identify vulnerabilities and implement appropriate preventive measures. Factors such as pipeline materials, regular inspections, and effective monitoring systems are vital to detecting and addressing issues before they lead to catastrophic accidents. Additionally, establishing robust emergency response plans that account for the possibility of cascading incidents can help minimize the impact on personnel, communities, and the environment.

Table 2-7. Several cases of jet fire domino effect in parallel pipelines.

Location, year	System	Source pipe Material / Outer Diameter	Target pipe Material / Outer Diameter	Cause	Accident sequence	Brief description
Charleston USA, 1971	Ethanol/ Acetylene pipelines	Ethanol / Not available	Acetylene/ Not available	External event	Fire → Explosion	A railway wagon collided with an ethanol pipeline. An ethanol jet fire impinged on an acetylene pipeline, which later exploded (MHIDAS, 2007).
Las Piedras Venezuela, 1984	Refinery	Oil / 8 in	NG / 16 in	Welding failure	Fire → Fire→Failure	Oil pipeline failed; jet fire ruptured 16 in gas pipe: another jet fire led to further pipe ruptures (MHIDAS, 2007).
Colonial Pipeline USA, 1986	Gasoline transmission pipeline	Gasoline / 24 in	Oil / 18 in	External event	Fire → Explosion→ Fire	A ruptured gasoline pipeline led to a massive jet fire. The intense flames impinged on nearby pipelines, causing a domino effect of explosions. The incident resulted in multiple fatalities, injuries, and extensive damage to infrastructure (MHIDAS, 2007).
Gulf of Mexico, USA 1989	Natural gas transmission pipeline in the platform	NG / 18 in	Six nearby pipelines	External event	Explosion→Fire→ Rupture	18 in sales gas pipeline on the platform failed during installing a pig trap on it. Released hydrocarbons ignited. The explosion and fire burned the main structure and caused subsequent explosions when six other pipelines ruptured due to the intense heat (USDI, 1989).



Location, year	System	Source pipe Material / Outer Diameter	Target pipe Material / Outer Diameter	Cause	Accident sequence	Brief description
Das Island United Arab Emirates, 1991	Oil and gas processing facility	Oil / 24 in	NG / 36 in Oil/18 in	External event	Fire → Explosion → Fire	A major fire broke out on Das Island, which houses an oil and gas processing facility. The fire spread to nearby pipelines, causing a series of domino accidents. The incident resulted in casualties, extensive damage to infrastructure, and disruptions in oil and gas production (MHIDAS, 2007).
Victoria Australia, 1991	Natural Gas Plant	NG / Not available	NG nearby pipelines	External event	Fire → Explosion → Fire	A major fire broke out at the Esso Longford Gas Plant. The fire resulted in a jet fire that impinged adjacent pipelines, causing a series of domino accidents. The incident led to casualties, extensive damage to infrastructure, and disruptions in gas supply (MHIDAS, 2007).
Rapid City Canada, 1995	Natural gas transmission pipeline	NG / 42 in	NG / 36 in	Stress corrosion cracking	Fire → Fire → Failure	Corrosion ruptured a gas pipeline. The jet fire affected another gas pipeline: rupture; fire on a third 48 in gas pipe which did not fail (TSBC, 1995)
Al Khobar Saudi Arabia, 1996	Natural gas oil transmission pipeline	NG / Not available	NG nearby pipelines / Not available	Terrorist attack	Fire → Explosion → Fire	A terrorist attack targeted the U.S. military housing complex known as Khobar Towers. The attack involved a truck bomb that caused a massive explosion. The ensuing jet fire impinged on nearby pipelines, triggering a domino effect of fires and explosions. The incident resulted in significant casualties and infrastructure damage (MHIDAS, 2007).

Location, year	System	Source pipe Material / Outer Diameter	Target pipe Material / Outer Diameter	Cause	Accident sequence	Brief description
Victoria Australia, 1998	Natural Gas Plant	NG / Not available	NG nearby pipelines / Not available	External event	Fire → Explosion → Fire	The Longford Gas Plant explosion resulted in a major fire and jet fire impingement. The incident occurred due to a series of equipment failures, leading to a domino effect of explosions along the pipeline network. The incident caused multiple fatalities, injuries, and disruptions in gas supply (MHIDAS, 2007).
Uch Sharif Pakistan, 2004	Natural gas transmission pipeline	NG / 24 in	NG / 18 in	Sabotage	Explosion → Fire → Failure	Sabotage ruptured a gas pipeline. The jet fire affected an 18 in the gas pipeline, which failed (Hassan and Ahmed, 2007).
Buncefield United Kingdom, 2005	Oil storage facility	Oil / Not available	NG nearby pipelines / Not available	External event	Fire → Explosion → Fire	The incident occurred at an oil storage facility and the fire was triggered by a massive jet fire that engulfed the facility. The fire spread to nearby pipelines. The incident resulted in significant damage, with multiple storage tanks and pipelines being affected (MHIDAS, 2007).
Khavaran Iran, 2005	Natural gas transmission pipeline	NG / Not available	NG nearby pipelines / Not available	External event	Explosion → Fire → Explosion	A pipeline explosion occurred due to a leak, resulting in a jet fire that impinged adjacent pipelines. The subsequent domino effect caused a chain reaction of explosions. The incident resulted in casualties, widespread damage, and environmental contamination (MHIDAS, 2007).

Location, year	System	Source pipe Material / Outer Diameter	Target pipe Material / Outer Diameter	Cause	Accident sequence	Brief description
Lagos, Nigeria 2006	Oil transmission system	Oil / Not available	Oil / Not available	Sabotage	Fire → Explosion → Fire	A pipeline explosion occurred due to oil theft activities. The explosion resulted in a jet fire that affected nearby pipelines, causing a domino effect of explosions. The incident led to multiple fatalities, injuries, and significant damage to infrastructure (MHIDAS, 2007).
Varanus Island Australia, 2008	Natural gas transmission pipeline	NG / Not available	NG nearby pipelines / Not available	External corrosion	Explosion → Fire → Explosion	A gas pipeline on Varanus Island experienced an explosion. The incident caused a jet fire that impacted nearby pipelines, resulting in a domino effect of fires and explosions. The incident led to disruptions in gas supply, significant damage to infrastructure, and economic consequences.
San Bruno USA, (2010)	Natural gas transmission pipeline	NG / 30 in	NG nearby pipeline / Not available	External corrosion	Fire → Explosion → Fire	A natural gas pipeline ruptured due to high-pressure gas flow. The rupture led to a jet fire impingement on nearby pipelines, causing a chain reaction of explosions. The incident resulted in multiple fatalities, and extensive property damage (NTSB, 2011).
Ontario Canada, 2011	Natural gas transmission pipeline	NG / 46 in	NG / 36 in	Stress corrosion cracking	Explosion → Fire → Failure	Corrosion ruptured a gas pipeline. The explosion created a large crater → jet fire. The 36 inches pipeline was shut down due to leakage from the cross-over shut-off valve between both pipelines (TSBC, 2011)
Ontario Canada, 2011	Natural gas transmission pipeline	NG / 46 in	NG / 36 in	Stress corrosion cracking	Explosion → Fire → Failure	Corrosion ruptured a gas pipeline. The explosion created a large crater → jet fire. The 36 inches pipeline was shut down due to leakage from cross- over shut-off valve between both pipelines (TSBC, 2011).

Location, year	System	Source pipe Material / Outer Diameter	Target pipe Material / Outer Diameter	Cause	Accident sequence	Brief description
Alabama USA, 2011	Natural gas transmission pipeline	NG / 30 in	NG / 30 in	External corrosion	Explosion → Fire → Failure	A gas pipeline exploded, and the jet fire burned for hours and damaged a closed pipeline. (USDT, 2011)
Buick Canada, 2012	Sour gas gathering system pipeline	Sour gas / 16 in	Sour gas / 6.62 in	External corrosion	Explosion → Fire → Failure → Fire	A buried pipeline ruptured: crater, jet fire; in 25 min rupture/ignition of a 6.62 in a pipe in the same hallway (both pipes shut down before rupture) (TSBC, 2012)
Ain Amenas Algeria, 2013	Natural gas facility	NG / Not available	NG nearby pipelines / Not available	Terrorist attack	Fire → Explosion → Fire	A terrorist attack targeted a natural gas facility. The attackers ignited a jet fire, which impinged adjacent pipelines, causing a domino effect of fires and explosions. The incident resulted in multiple fatalities, extensive damage to infrastructure, and a temporary halt in gas production.
Kaohsiung Taiwan, (2014)	Natural gas transmission pipeline	NG / Not available	NG nearby pipelines / Not available	External event	Explosion → Fire → Explosion	A series of gas explosions occurred in a densely populated area. The explosions were triggered by a gas leak in an underground pipeline. The ensuing jet fires impinged on nearby pipelines, causing a domino effect of explosions.
Manitoba Canada, 2014	Natural gas transmission pipeline	NG/ 30 in	NG/ 36 in NG/ 48 in	Welding failure	Explosion → Failure → Fire	Natural gas released from the pipeline ignited, and the resulting fire burned for approx. 12 h. Two adjacent pipelines were shut down before rupture (TSBC, 2014).

Location, year	System	Source pipe Material / Outer Diameter	Target pipe Material / Outer Diameter	Cause	Accident sequence	Brief description
Kangan Iran, 2015	Gas processing plant	NG / Not available	NG nearby pipelines	Welding failure	Explosion → Fire → Explosion	An explosion occurred at a gas processing plant, leading to a jet fire that impacted nearby pipelines. The intense flames caused a domino effect, resulting in additional explosions along the pipelines network. The incident caused casualties, and extensive damage, and disrupted the gas supply.
Abadan Iran, 2016	Oil refinery	Oil / Not available	Oil and fuel nearby pipelines	External corrosion	Fire → Explosion → Fire	A massive fire broke out at the Abadan oil refinery, resulting in a jet fire that impacted nearby pipelines. The intense flames caused a domino effect of fires and explosions along the pipelines network. The incident led to casualties, significant damage to infrastructure, and disruptions in oil production.
San Jacinto USA, 2016	Natural gas transmission pipeline	NG / Not available	NG nearby pipelines	Welding failure	Fire → Explosion → Fire	A jet fire impingement on a natural gas transmission pipeline led to a domino effect of explosions along the pipelines network. The incident resulted in multiple injuries and substantial property damage.
Ilam Iran, 2020	Natural gas transmission pipeline	NG / Not available	NG nearby pipelines	Welding failure	Explosion → Fire → Explosion	An explosion occurred in a natural gas pipeline, leading to a jet fire impingement. The intense flames caused a domino effect, resulting in additional pipelines explosions. The incident caused casualties and significant damage to the pipelines network.
Norilsk Russia, 2020	Fuel Storage tank at a power plant	Diesel fuel pipe / Not available	nearby oil and fuel pipelines	External Event	Fire → Explosion → Fire	A major environmental disaster occurred when a fuel tank at a power plant owned by Norilsk Nickel collapsed, resulting in the release of diesel fuel. The spilled fuel caught fire, causing a jet fire that impacted nearby pipelines. The incident led to a domino effect of fires and explosions. It resulted in extensive environmental damage, including water and soil contamination.

## 2.7. Literature review on jet flames impingement

Most of the experimental works published over the last four decades were mainly undertaken in order to investigate the behaviour of pressurized vessels engulfed in flames, while scarce attention has been dedicated to the experimental analysis of other types of equipment such as atmospheric tanks and pipelines, which are commonly used in industries and in the transportation of certain fluids (Landucci et al., 2013). The target equipment usually consisted of small-scale cylindrical or spherical vessels filled up to different levels, and the fuels were propane or methane.

Table 2-8 summarizes some of the experimental studies found in the literature.

Wighus and Drangsholt (1993) studied the thermal features of horizontal sonic jet fires of propane (0.3 kg/s) impinging perpendicularly on a vertical surface. They observed that both the velocity and the temperature at the different points of the jet have an important influence on the heat transfer, with the highest velocities being associated to the lowest temperatures. Therefore, the highest values of convective heat flux density were found when the combustion products had reached a high temperature and the entrained air had not cooled yet the mixture. Maximum values of heat flux density (including both contributions, radiative and convective) of up to 340 kW/m<sup>2</sup> for a flat plate and 290 kW/m<sup>2</sup> for a pipe located in front of the flame were registered.

Somewhat different values were obtained by Bennet et al. (1991) from methane and propane jet fires impinging on a pipe (0.9 m diameter) and a 13 tons vessel. Their results varied significantly with the fuel flowrate and the distance between the jet source and the target; in the case of the pipe: propane: 240-250 kW/m<sup>2</sup>, methane: 200-325 kW/m<sup>2</sup>; and with the vessel: propane, 150-250 kW/m<sup>2</sup>; methane: 140-250 kW/m<sup>2</sup>.

Practically all of them were focussed on the analysis of the action of a jet fire impinging on a vertical surface or on a cylindrical vessel. In some cases (for example, Birk et al., 2006), the vessel contained both water and air.

Very few analyzed the impingement of jet flames on a pipe; Pattej and Durusel, 2007, with vertical jet fires and Hustad and Sonju, 1991, also with vertical jet fires.

Certainly, in some cases as for example Persaud et al.. (2001), the cylinder that was the target of jet flames, with a diameter of 1.2 m and a length of 4 m, could be considered to be equivalent to a pipe.

In any case, it is a fact that the value of the heat transfer coefficient resulting from the action of the flames impingement on the target wall was studied only in three cases, corresponding to different situations and with different results. And concerning the total heat flux ( $\text{kW/m}^2$ ), an important dispersion of the values obtained from the diverse authors is found, what can be partly attributed again to the different situations studied.

Taking all these results into consideration, it is clear that a study focussing on the effects of the flames impingement of an LPG sonic or subsonic jet fire on a pipe containing a liquid and/or a gas was still lacking and, without a doubt, will be quite interesting from the point of view of risk analysis.

Table 2-8: Experimental studies conducted on thermal effects by jet fire impingement.

Data source	Fuel	Mass flow rate (kg/s)	Release diameter (mm)	Release pressure (bar)	Gas exit velocity (m/s)	Convective heat transfer coefficient (kW/m <sup>2</sup> ·°C)	Total heat flux (kW/m <sup>2</sup> )	Heat rate (kW)	Flame direction	Type of target	Surface specifications	Exposure mode
Kuntikana and Prabhu, 2018	Methane	1.12×10 <sup>-5</sup>	13, 15, 17.25, 20.25	2	NA	7.8×10 <sup>-3</sup> - 1.1×10 <sup>-2</sup>	up to 6	NA	Vertical	Semi-cylindrical surfaces	quartz half-cut tube, d=100 mm, L=150 mm, thickness=2.5 mm	Direct
Morad et al., 2016	Methane	1 ×10 <sup>-6</sup> to 2.8 ×10 <sup>-6</sup>	3.5 mm × 25 mm	1	0.74 to 2.26	NA	up to 90	0.05-0.16	Vertical	Flat surface	Copper. 250 mm x 130 mm x 10 mm	Direct
Bradley, 2017	Propane	0.21 to 22	20 to 50	60-113	50-250	NA	50-250	NA	Vertical and Horizontal	Cylindrical/ Flat/Vessel	Copper plate (7 m x 10 m), Pipe (d=0.9 m), 13 tonne LPG tank, 2 tonne vessel (d=1.2 m x 15 m)	Direct. Engulfed
Virk, 2015	Propane	NA	70	NA	NA	0.048 -0.094	68-110	NA	Horizontal	Flat	Aluminium, 0.61 m x 0.61 m	Direct
Patej and Durussel, 2007	Propane	1.23 to 5.31	10.9	NA	11-47	NA	NA	62-296	Vertical	Cylindrical	Steel pipe, d= 22 mm, OD=34 mm,	Direct
Lowesmith et al., 2007	Propane	NA	NA	NA	NA	0.08	240	NA	Horizontal	Cylinder	NA	Engulfed
Birk et al., 2006a	Propane	NA	15	2.05	NA	NA	NA	NA	Horizontal	Cylindrical vessel	Steel, d=0.953 m, L=3.07 m	25% engulfed
Birk et al., 2006b	Propane	NA	15	2.07	NA	NA	NA	NA	Horizontal	Horizontal cylinder	Steel, d=0.953 m, L=3.07 m	25% engulfed



Data source	Fuel	Mass flow rate (kg/s)	Release diameter (mm)	Release pressure (bar)	Gas exit velocity (m/s)	Convective heat transfer coefficient (kW/m <sup>2</sup> ·°C)	Total heat flux (kW/m <sup>2</sup> )	Heat rate (kW)	Flame direction	Type of target	Surface specifications	Exposure mode
Birk and Vander Steen, 2006	Propane	NA	21	NA	NA	NA	NA	NA	Horizontal	Cylindrical vessel	Steel, d=0.96 m, L=3.07 m	Partially engulfed
Birk et al., 2006b	Propane	NA	15	2.07	NA	NA	NA	NA	Horizontal	Horizontal cylinder	Steel, d=0.953 m, L=3.07 m	25% engulfed
Birk and Vander Steen, 2006	Propane	NA	21	NA	NA	NA	NA	NA	Horizontal	Cylindrical vessel	Steel, d=0.96 m, L=3.07 m	Partially engulfed
Persaud et al., 2001	Propane	1.5	12.7	NA	NA	NA	180-200	NA	Horizontal	Horizontal cylinder	Steel, d=1.2 m, L=4 m	Fully engulfed
Malikov et al., 2001	Methane/ Natural gas	NA	4, 6	0.5	up to 230	NA	up to 500	NA	Vertical	Cylindrical	Water-cooled, cylindrical calorimeter (0.108 m in diameter)	Direct
Droste and Schoen, 1998	Propane	NA	NA	5.5-9.8	NA	NA	NA	NA	NA	Horizontal cylinder	Steel, d=1.25 m, L=4.3 m	Engulfed
Wighus and Drangsholt, 1993	Propane	0.3	17.8	1-2.3	40-150	NA	190-340	14000	Horizontal	Cylindrical/Flat (Box-like)	Steel	Direct
Hustad and Sonju, 1991	Propane	NA	5, 8.6, 10, 40	NA	5-200	NA	up to 200	33.3	Vertical	Cylindrical	Steel pipe, d= 50 mm	Fully engulfed
Hustad and Sonju, 1991	Methane	NA	5, 8.6, 10, 40	NA	10-125	NA	up to 125	37	Vertical	Cylindrical	Steel pipe, d= 50 mm	Fully engulfed

It can be observed from these examples that the published data on the heat flux density show an important scattering and uncertainty. One experimental campaign was performed by Patej and Durussel (2007) aiming at the analysis of heat transfer to a pipe impinged by a jet fire. Within this framework, the thermal impacts of fires on industrial pipes and tanks were studied. The measurements from the experiments made it possible to define the dimensions of jet fires, their surface emissive power, and the hot gas velocities for then deducing from them the heat received by the pipe; these authors analysed the response of a pipe as well as transporting water subjected to the jet fires, by monitoring the pipe with thermocouples.

## **2.8. Literature review on the study of jet flame geometrical features**

The jet flame geometry has been addressed by several authors through experimental and theoretical approaches.

In a study conducted by Hawthorne et al.. (1949), turbulent vertical flames of various fuels with lengths up to 1 m were examined. They proposed an inverted circular cone shape, with the apex near the orifice exit, to represent jet flames (Figure 2-8 (a)). This conical shape has also been suggested by subsequent researchers such as Odggard (1983), Turns (1991), Schefer et al.. (2004), and Schefer et al.. (2007).

Baron (1954) proposed a shape resembling a vertical ellipse for the jet flame surface of turbulent vertical flames without significant buoyant force (Figure 2-8 (b)). This suggested elliptical shape was compared to a photograph of a small-scale city-gas flame taken during experimental work on city-gas and butane flames up to 1.35 m in length by Whol et al.. (1949a). However, it is important to note that the characteristics of this flame differed considerably from those of real accidental jet fires, which are typically larger and associated with supersonic exit velocities.

A cylinder has also been proposed as a shape to define jet flames. Various authors, including Odggard (1983), Schuller et al.. (1983), Sonju and Hustad (1984), Hustad and Sonju (1986), Bagster, and Schubach (1996), have suggested this shape based on experimental and theoretical studies of subsonic jet fires.

Another proposed flame shape is a frustum of a cone (Figure 2-8 (c)), which has been suggested by Kalghatgi (1983), Chamberlain (1987), and Johnson et al. (1994). However, while this shape can describe a turbulent diffusion flame in a crosswind, a horizontally released jet fire influenced by wind, or a flare under wind conditions, it does not accurately represent the contour of a real accidental vertical jet fire in still air. Experimental data by Kalghatgi (1983) on flames of various fuels up to 2.7 m in length, obtained at crosswind speeds ranging from 2.7 to 8.1 m/s, indicate that at relatively high wind speeds, the frustum of a cone shape becomes nearly cylindrical (Mudan and Croce, 1990).

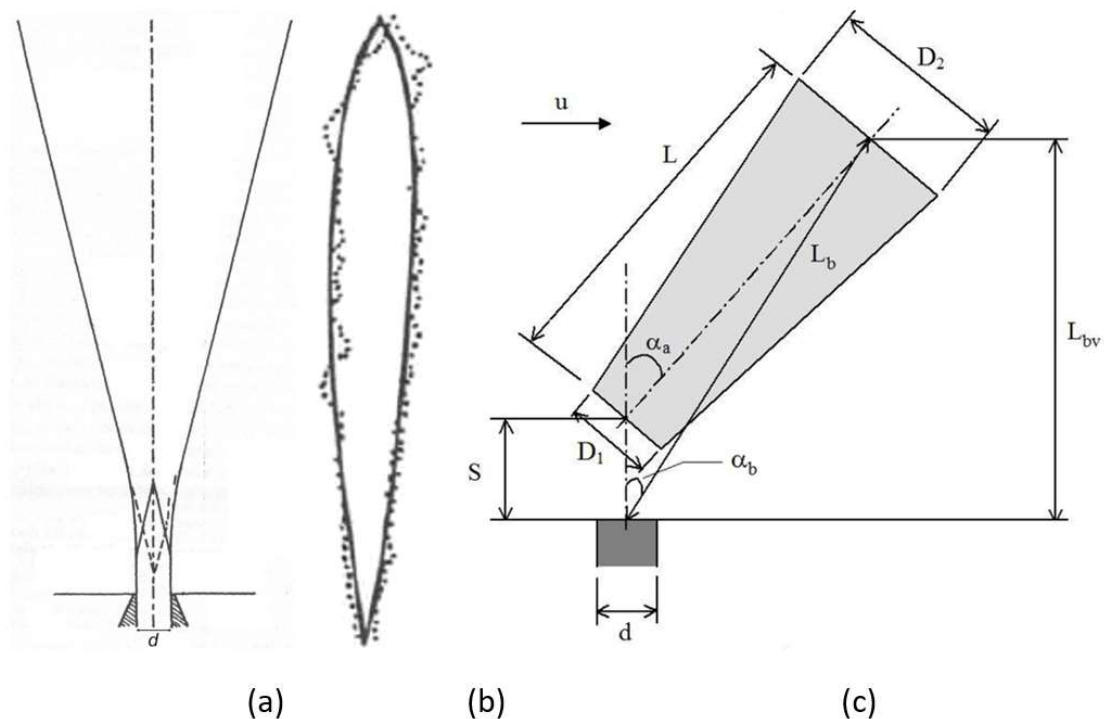


Figure 2-8. Suggested flame shapes: (a) The inverted circular cone shape, proposed by Hawthorne et al. (1949), Odggard (1983), Turns (1991), Schefer et al. (2004), and Schefer et al. (2007). (b) An elliptical shape, introduced by Baron (1954), with the full line representing the theoretical prediction and the dotted line corresponding to the tracing of a photograph by Wohl et al. (1949(a)). (c) The frustum of a cone shape, as described by Kalghatgi (1983), Chamberlain (1987), and Johnson et al. (1994), demonstrating the impact of cross-winds. (Palacios, 2011).

The majority of the investigations mentioned primarily focus on flares or subsonic jet fires, which have distinct conditions that differ considerably from accidental jet fires. Due to this limited research on the shape of large-scale supersonic hydrocarbon jet fires, our understanding of them remains inadequate.

The width of a jet flame is influenced by various factors, such as the mass flow rate (Imamura et al., 2008), the dimensionless heat released during combustion (Sugawa and Sakai, 1997), the stagnation pressure (Iwasaka et al., 1979; Imamura et al., 2008; Mogi and Horiguchi, 2009), and the Froude number (Iwasaka et al., 1979; Schuller et al., 1983; Sonju and Hustad, 1984; Hustad and Sonju, 1986; Bagster and Schubach, 1996).

Most of the existing models that describe flames based on their centerline trajectory do not include specific formulations to account for the width of the jet flame. Furthermore, the few proposed expressions for jet flame width are primarily focused on either hydrogen flames or jet fires with subsonic exit velocities.

Various formulations have been suggested to estimate the trajectory and both vertical and horizontal displacement of a jet flame. These studies have focused on different scenarios, including horizontal jet flames (Becker and Liang, 1981; Gore and Jian, 1991; Johnson et al., 1994), jet flames under crosswind conditions (Brzustowski et al., 1975; Gollahalli et al., 1975; Kalghatgi, 1983; Cook et al., 1990), and flares (Brzustowski et al., 1975; APIRP521, 1982; McMurray, 1982; Cook et al., 1987b; Cook et al., 1987c; Chamberlain, 1987; APIRP521, 1997).

Table 2-9 shows the experimental studies concerning jet flames at small and large scales. Most of these studies concern jet flames geometry and tried to develop methodologies to estimate the flame size and shape. From the literature survey, the interest of working with LPG was also shown; according to Gomez-Mares et al. (2008) and Palacios et al. (2011), most of the jet fire events registered in four European accident databases (60% of cases) had involved LPG as fuel.

Table 2-9. Experimental studies on small scale gas jet fires, focused on jet flame geometry.

Scale	Authors	Fuel	Orifice Diameter (mm)	Flame Length (m)	Flame Type
Small	Hawthorne et al.. (1949)	Acetylene, Carbon Monoxide, City Gas, Hydrogen, Propane, Mixture Of CO <sub>2</sub> -City Gas And H <sub>2</sub> -Propane	3-8	up to 1	Vertical
	Baev et al.. (1974)	Hydrogen	1-16.65	0.08-3.12	Vertical
	Backer and Liang (1981)	Acetylene, Carbon Monoxide, Ethane, Ethylene, Hydrogen, Methane, Propane	0.69-4.57	up to 1	Vertical/ Horizontally
	Kalaghatgi (1984)	Ethylene, Hydrogen, Methane and Propane	1.08-10.1	up to 1.7	Vertical
	Santos and Costa (2005)	Ethylene and Propane	5-8	up to 1.7	Vertical
	Imamura et al.. (2008)	Hydrogen	1-4	up to 1.8	Horizontal

Table 2-10. Experimental studies on large -scale gas jet fires, focused on jet flame geometry.

Scale	Authors	Fuel	Orifice Diameter (mm)	Flame Length (m)	Flame Type
Large	Gore et al.. (1974)	Natural Gas	1-16.65	up to 25	Vertical
	Sugawa and Sakai (1981)	Propane	6.5-27.6	up to 8	Vertical
	Sonju and Hustad (1984)	Methane/ Propane	10-80	up to 8	Vertical
	McCaffrey and Evans (1986)	Methane	38-102	up to 23.5	Vertical
	Schefer et al.. (2006)	Hydrogen	7.94	up to 5.6	Vertical
	Schefer et al.. (2007)	Hydrogen	5.08	up to 10.7	Vertical
	Mogi and Horiguchi (2009)	Hydrogen	0.1-4	up to 6.5	Horizontal
	Gómez-Mares et al.. (2009)	Propane	12.75-30	2.2-8.1	Vertical
	Palacios et al.. (2010)	Propane	10-43	up to 10	Vertical
	Gopaldaswami et al.. (2016)	Propane	191	1-6	Horizontal
Laboureur et al.. (2016)	Propane	191	1-10	Vertical /Horizontal	

### 2.9. Tools for fire risk analysis in pipelines

When considering the analysis of the effects and consequences of a situation in which a jet fire can affect a pipeline, a set of tools are certainly required to simulate and predict what can happen and also when can happen. And as usually occurs, different possible situations must be considered and studied, which will be a function of both the source term and also of the physical features of the system.

Considering the source term, diverse options should be considered, the most common ones being a release from a hole or from a flange. The corresponding release area and expected frequency of occurrence can be found from the specialized literature (as, for example, RIVM, 2009; Mannan and Lees, 2012).

With respect to the physical situation, diverse possibilities can exist: aerial pipelines and buried pipelines. In the case of buried pipelines the possibility of the formation of a crater should be considered (several authors have studied it). The existence of thermal protection could also be considered, especially in pipe systems located in industrial zones.

For these situations, the classical tool used in risk analysis is the use of the adequate mathematical expressions. These expressions, sometimes based on a theoretical approach and practically always adjusted from a set of experimental data, can be found in the specialized literature (Mannan and Lees, 2012; Casal, 2018). As a number of calculations must usually be performed when considering the diverse possibilities -for example, diverse values of source terms-, several calculation programs have been proposed and are available. This is a tool commonly used for professionals in this field. Computational Fluid Dynamics (CFD) models are an invaluable tool for analyzing the risk in pipeline systems. These models are highly complex mathematically and require significant computational resources and time to execute. They are based on solving the Navier-Stokes equations, which describe the balance of mass, energy, and momentum in a fluid system. CFD models also incorporate sub-models to account for physical changes and chemical reactions that occur within flames. Their applications are extensive, allowing for detailed assessments of fire effects, considering intricate geometries, and representing fires at various scales.

Validating simulation results by comparing them with experimental data is essential. This validation process enables the evaluation of the predictive capabilities of CFD models. By comparing simulated and experimental data, adjustments can be made to enhance the accuracy of the simulation results before their practical application in real-world scenarios (Rengel et al., 2018).



## 3 Experimental Set-up and Test Methodology

### 3.1. The experimental tests location

The experimental facility was purposefully designed and constructed within the framework of this thesis. It was installed in the indoor fire-testing laboratory of the Centre for Technological Risk Studies (CERTEC), in the Escola d'Enginyeria de Barcelona Est (EEBE) of Universitat Politècnica de Catalunya (UPC) in Catalonia, Spain.

The intention of these experimental tests was to investigate and analyze domino accidents due to impingement by jet fires on pipes and pipelines and to determine the geometrical features of the jet flames (lift-off distance, size, shape, reach, and elevation) of horizontal subsonic and sonic hydrocarbon jet fires.

For this purpose, a laboratory-scale experimental set-up was designed and fabricated to gather data concerning propane jet fires impinging on a pipe conveying gas or liquid and. The obtained data were used to study the thermal response of the pipe as a “secondary” object to the heat flux or thermal impact of direct flame contact in different possible situations (associated with the angle and surface of impingement, the zone of the jet fire in contact with the pipe).

Additionally, the results of the experimental tests on free jet fires (experimental tests without flames impingement conditions) were utilized to contribute to the knowledge and prediction of the main features of jet fires, focusing on their shape and size, and more specifically on the distance over which flame impingement can occur. Existing correlations have been reviewed, and new expressions are proposed to predict this distance for the case of horizontal subsonic and sonic hydrocarbon jet fires, from both experimental data and the mathematical and computational modelling of the main geometrical (size, reach, elevation) features of the flame.

The plan map of the experimental laboratory including a control room and the fire testing room is shown in Figure 3-1. The experimental setup was located in the fire

testing room. The control and monitoring devices were located in the control room section.

The dimensions of the laboratory are 10 m × 6.8 m × 4 m (length × width × height). The control room located on the right side is separated by a wall, which has an observation window, and a firebreak door, and it is equipped with a hole for electrical connections from the adjoining room. Both rooms of the laboratory are equipped with a ventilation system, water, compressed air supply connections, and portable fire extinguishers.

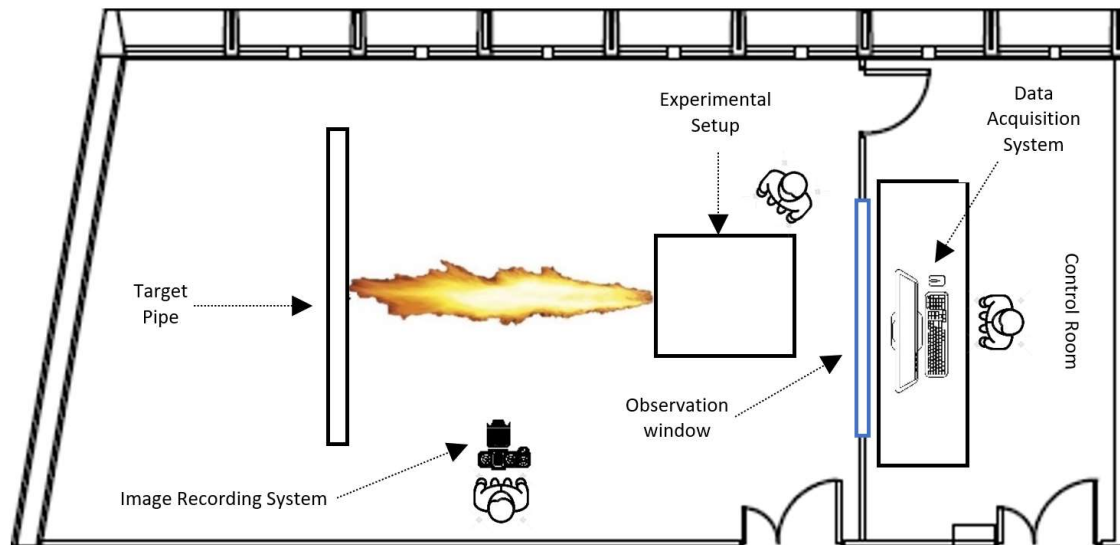


Figure 3-1. Plan map of the fire-testing laboratory at CERTEC.

The aim of the experimental tests was to investigate the shape and size of medium-sized jet fires –up to 3 m length of radiant flame–, as well as jet fire impingement impact on a target pipe, using propane gas as the fuel. The literature survey presented in the previous chapter showed that a few numbers of researchers had worked experimentally with sonic jet fires impinging on obstacles (pipes, vessels). Furthermore, some of those who had published experimental work had performed with rather small jet fires and/or at subsonic regime conditions.

### 3.2. The experimental set-up

The experimental set-up was designed with safety at the forefront. It comprises a fire generation section and a target obstacle section, allowing both the analysis of the behavior of the “free” jet fire flames and the analysis of the thermal response of the target section to jet fire impinging on it. The fire section allows for generating a jet fire capable of a partial or total fire engulfment of the pipe.

### 3.2.1. Jet fire generation section

This part is designed to reproduce an accidental loss of containment from a pressurized pipe or pipeline through a small bore or crack in it. In such events, the main consequence is a release of flammable hydrocarbon that could lead to a jet fire in the case of ignition (ignition can occur immediately due to, for example, an electrostatic spark, or with a certain delay once the flammable cloud originated by the leak meets an ignition source). A series of safety and control valves and measurement tools were installed on the fuel line in order to increase the operability of the operating conditions of the experimental setup. A 35 kg pressurized propane industrial cylinder was utilized as the source of fuel. For safety purposes, two safety valves were installed, to control the fuel flow in case of emergency conditions. A manual pressure regulating valve was installed to control the release pressure of propane from the nozzle with a wide range of gas release pressure. Downstream of the pressure regulating valve, a gas flow meter was installed to measure the fuel flow. At the gas release point, a series of changeable nozzles, with different orifice diameters (4 to 8 mm), were used to release the fuel. All devices were installed on a portable structure, equipped with five wheels allowing them to move off the structure to increase operational flexibility during the tests. A general scheme of the jet fire section is shown in Figure 3-2 and Figure 3-3. More details of the devices will be introduced in the following sections.

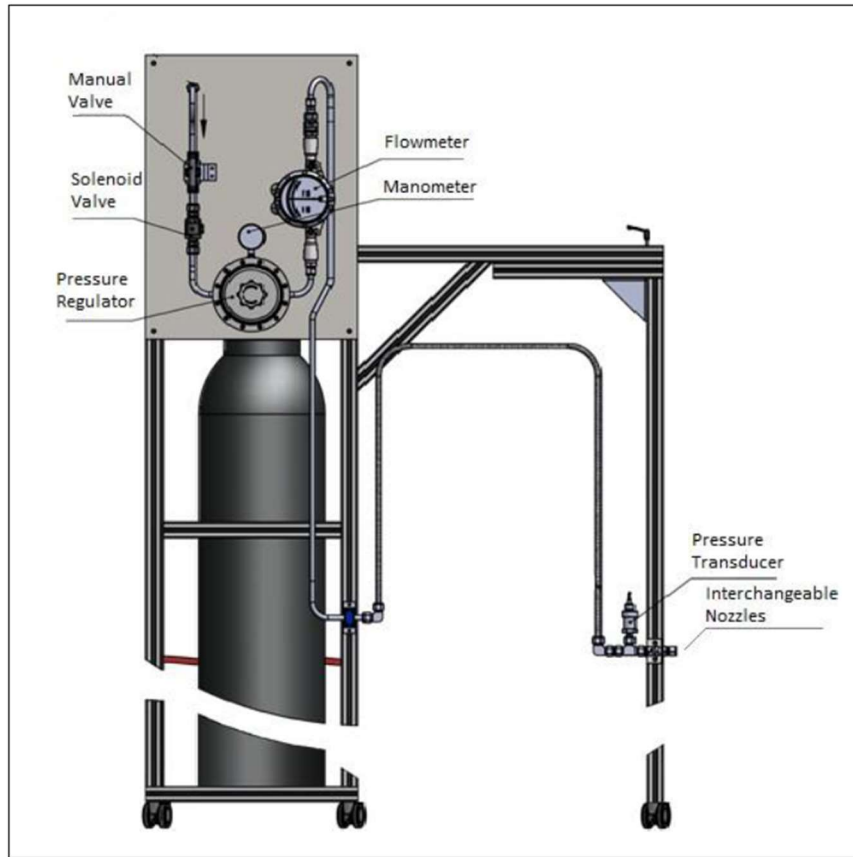
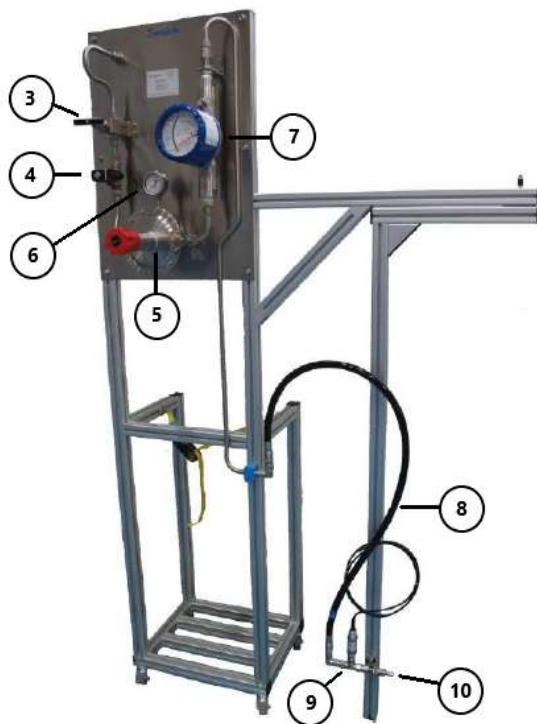


Figure 3-2. A scheme of the experimental set-up.



Number	Item	Reference
1	Flexible Hose	HS-01
2	Manual Valve (on bottle)	VLV-00
3	Manual Needle Valve	VLV-01
4	Electrical Solenoid Valve	ESV-01
5	Pressure Regulator Valve	PCV-01
6	Manometer	PG-01
7	Flowmeter	FM-01
8	Flexible Hose	HS-02
9	Pressure Transducer	PT-01
10	Interchangeable Nozzles (4, 6, 8 mm)	NZ-01

Figure 3-3. Assembled experimental set-up.

Aluminium material was used to construct the body of the setup because of its ductility, lower mass density, and its lower price compared to the other materials.

All the main tubing parts, valves, and fittings of the fuel system were sized and designed with a diameter of 12.7 mm (equivalent to ½ inch) to be capable of the maximum estimated flow rate of propane gas in the system.

### 3.2.2. Target obstacle section

The objective of this part is to allow the testing of an incident in which a neighbouring pipe or pipeline is impinged with a sonic or subsonic jet fire, originated from a release of hydrocarbon from hole or crack on another parallel pipeline. In real incidents, depending on the flow and the condition of the fluid inside the target pipe and the distance of two pipes, several situations may occur.

For this purpose, the jet flames impinged on a carbon steel pipe containing stagnant air or water (Figure 3-4). A set of K-type thermocouples located inside the pipe wall (4 mm inside pipe wall thickness) allowed the measurement of the wall temperature evolution at different positions during the tests. A summary of the tests has been included in Table 3-1.

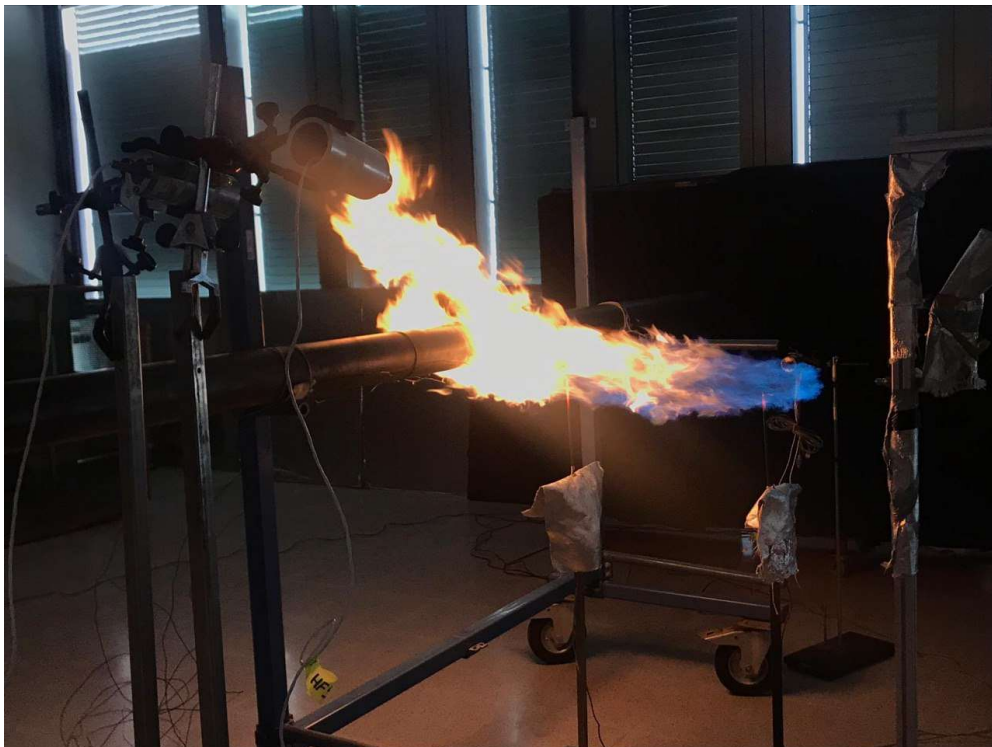


Figure 3-4. A jet fire impinging on the pipe.

### 3.3. Experimental tests methodology

Four experimental tests groups (1 to 4) were designed and conducted to investigate the thermal effects of the jet fire impingement and geometrical features of jet fires in different operating conditions. Every experimental test group consisted of a set of tests that were systematically named according to a standardized methodology, as outlined below:

JFT-YYMMDD-XX, in which

JFT stands for Jet Fire Test,

YY: the year of the test,

MM: the month of the test,

DD: date of the test,

XX: number of the test within the same date.

As an example, the identification number JFT-190401-2 corresponds to the second experimental test conducted on April 1st, 2019.

Experimental test groups 1 and 2 were focusing on the impacts of a jet flame impingement on a pipe. Additionally, experimental test groups 3 and 4 were performed in order to characterize the geometrical features of the jet fire flame.

Table 3-1. Description of the experimental Test Groups.

Test series ID	Purpose/Description	Investigated Parameters
Group 1	10 experimental tests were designed to study the thermal impacts of the pipe based on the operating fluid conditions.	<ul style="list-style-type: none"> <li>• Pipe wall temperature evolution</li> <li>• Flame temperature</li> <li>• Release gas flow, pressure, and temperature</li> </ul>
Group 2	25 experimental tests were designed to study the thermal impacts of the pipe based on the distance from the release point of the jet flame.	<ul style="list-style-type: none"> <li>• Pipe wall temperature evolution</li> <li>• Flame temperature</li> <li>• Release gas flow, pressure, and temperature</li> <li>• Heat flux and heat transfer coefficient</li> </ul>
Group 3	2 experimental tests were designed to measure and characterize the temperature profile of the flame with 6 mm and 8 mm nozzle diameters.	<ul style="list-style-type: none"> <li>• Flame temperature</li> </ul>
Group 4	10 experimental tests were designed to assess the impact of release pressure and divergent gas flow rates on the geometrical features of the flame (size, shape, area, etc.).	<ul style="list-style-type: none"> <li>• Flame temperature</li> <li>• Flame Shape</li> <li>• Flame area</li> <li>• Visible Flame length</li> <li>• Flame elevation</li> <li>• Lift off distance</li> </ul>

### **3.3.1. Group 1- Thermal effects on pipe performance: fluid condition study**

The objective of this set of tests was to allow the testing of different potential conditions in terms of the fluid conveyed by the target pipe that might happen during a flame impingement, originating from another parallel pipeline. Hence, three test conditions were defined, corresponding to the flow and the condition of the fluid inside the target pipe in two possible situations that can occur during the stationary operation of the pipe/pipeline or in the event of an emergency stop of the fluid flow:

- a) Stationary liquid: the liquid flow is stopped, and the liquid is blocked inside the pipe during the jet fire impingement.
- b) Continuous flow of gas: a continuous flow of gas inside the pipe during the jet fire impingement.

### **3.3.2. Group 2- Thermal effects on pipe performance: jet flame distance study**

The objective of this group of tests was to analyze the impact of distance from jet exit on the heat flux received by the pipe. Hence, three test conditions were defined depending on the distance of the pipe with the release point of the gas. Condition inside the pipe was a continuous gas flow during the jet fire impingement.

#### **Arrangement of tests Group 1 and 2**

To study the flames impingement, a steel pipe was added as the target for the flames, together with the adequate measurement devices. So, in these tests the jet flames impinged on a carbon steel pipe (API 5L X60, 11.5 cm outside diameter, 6 mm wall thickness, 3 m length) containing stagnant air or water (Figure 3-5).



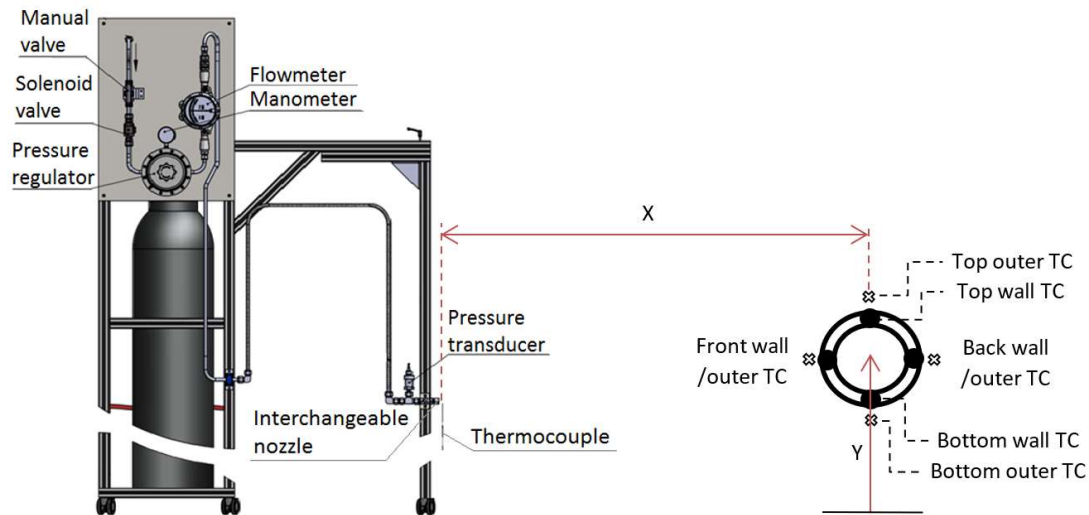


Figure 3-5. Scheme of the experimental set-up and cross-section of the pipe.

A set of K-type thermocouples (TC stands for thermocouples) located inside the pipe wall (4 mm inside pipe wall thickness) allowed the measurement of the wall temperature at different positions during the tests as shown in Figure 3-7, Figure 3-10 and Figure 3-12. Additionally, another set of four B-type thermocouples was located outside the pipe (at 1 cm distance from the pipe wall), to measure the flame temperature at the same above-mentioned positions. (Figure 3-6, Figure 3-9 and Figure 3-11).

In order to analyse the heat loss during the experiment through the air temperature inside the pipe, four type K thermocouples (TC stands for thermocouples) were installed on a metal support (Figure 3-8). They were placed next to the thermocouples on the wall, at a distance not exceeding 3 cm. Looking at heat loss was useful to understand how long the heating of the pipe wall was effectively influenced only by a convective mechanism, and not by others. The values of pressure, temperature, and release mass flow rate were continuously registered during the tests through a data acquisition system (Field Point) from the measuring devices. During these tests, the gas release nozzle was located 105 cm (horizontal distance) from the target pipe centre, and the pipe centre line was elevated 115 cm from the ground level. The position of the experimental test equipment is shown in Table 3-2.

Table 3-2. Position of experimental test equipment in the test group 1.

X: Horizontal distance from the nozzle to pipe centreline (cm)	Y: Elevation distance from level ground to pipe centre line (cm)	Location of thermocouples (cm)				
		Position	Front	Top	Back	Bottom
105	115	Wall TC	X: 100	X: 105	X: 110	X: 105
			Y: 115	Y: 120	Y: 115	Y: 110
		Flame TC	X: 99	X: 105	X: 111	X: 105
			Y: 115	Y: 121	Y: 115	Y: 109
		Internal TC	X: 101	X: 106	X: 109	X: 105
			Y: 115	Y: 119	Y: 115	Y: 108

The essential data concerning the operating conditions of test group 1 have been summarized in Table 3-3.

Table 3-3. Operating conditions of three tests in the test group 1.

Experiment Title	Release diameter [mm]	Condition of the fluid inside the pipe	Flow Regime	Distance Nozzle to pipe surface [cm]	Distance Nozzle to ground level [cm]
JFT-190308-1		stagnant air inside the pipe	Sonic	100	115
JFT-190311-1	6	stagnant liquid inside the pipe	Sonic	100	115
JFT-190311-2		stagnant liquid inside the pipe	Subsonic	100	115

The data concerning the operating conditions of test group 2 have been summarized in Table 3-4, Table 3-5, Table 3-6 and Table 3-7.

Looking at a jet fire, three clearly distinct zones are identified inside the flame. These zones are characterized by different color, shape and behavior (Figure 4-1).

- Blue zone: it is the closest zone to the nozzle, it has a blue color, the shape is cylindrical and orientation is mostly horizontal.
- Middle zone: color of the flame is orange and buoyancy forces start to smoothly change the shape and the orientation of the flame.

- Front Zone: it is the most distant from the nozzle, the color is bright yellow, higher buoyancy effects are present and shape is undefined.

Table 3-4. Test conditions of three zone Impingement tests for 8 mm nozzle (test group 2).

Experiment Title	Release diameter [mm]	Impingement Zone	Release pressure [bar abs]	Flow Regime	Distance of Nozzle to pipe surface [cm]	Distance of Nozzle to ground level [cm]
JFT-200225-1	8	Front Zone	1.83	Sonic	130	110
JFT-200227-1			1.83	Sonic	130	110
JFT-200226-1			1.66	Subsonic	130	110
JFT-200224-2		Middle Zone	1.81	Sonic	100	114
JFT-200227-2			1.62	Subsonic	100	114
JFT-200228-1			1.65	Subsonic	100	114
JFT-200207-1		Blue Zone	2.07	Sonic	35	116
JFT-200211-1			1.64	Subsonic	35	116

Table 3-5. Test conditions for 6 mm nozzle (pipe located in the front zone of the flame)

Experiment Title	Release diameter [mm]	Impingement Zone	Release pressure [bar abs]	Flow Regime	Distance of Nozzle to pipe surface [cm]	Distance of Nozzle to ground level [cm]
JFT-200221-1	6	Front Zone	1.75	Sonic	100	110
JFT-190409-1			1.74	Sonic	100	110
JFT-191203-3			1.70	Subsonic	100	110
JFT-200221-2			1.60	Subsonic	100	110
JFT-200224-1			1.40	Subsonic	100	110
JFT-191204-1			1.40	Subsonic	100	110
JFT-191204-2			1.20	Subsonic	100	110

Table 3-6. Test conditions for 6 mm nozzle (pipe located in the middle zone of the flame).

Experiment Title	Release diameter [mm]	Impingement Zone	Release pressure [bar abs]	Flow Regime	Distance Nozzle to pipe surface [cm]	Distance Nozzle to ground level [cm]
JFT-200130-2	6	Middle Zone	1.75	Sonic	70	114
JFT-200220-2			1.74	Sonic	70	114
JFT-200130-1			1.71	Subsonic	70	114
JFT-200130-3			1.60	Subsonic	70	114
JFT-200219-1			1.66	Subsonic	70	114
JFT-200219-2			1.59	Subsonic	70	114
JFT-200220-1			1.41	Subsonic	70	114
JFT-200129-1			1.30	Subsonic	70	114
JFT-200129-2			1.20	Subsonic	70	114

Table 3-7. Test conditions for 6 mm nozzle (pipe located in the blue zone of the flame).

Experiment Title	Release diameter [mm]	Impingement Zone	Release pressure [bar abs]	Flow Regime	Distance of Nozzle to pipe surface [cm]	Distance of Nozzle to ground level [cm]
JFT-200206-2	6	Blue Zone	1.81	Sonic	35	116
JFT-200206-1			1.77	Sonic	35	116
JFT-200211-2			1.77	Sonic	35	116
JFT-200214-1			1.71	Subsonic	35	116
JFT-200218-1			1.63	Subsonic	35	116
JFT-200205-1			1.60	Subsonic	35	116
JFT-200218-2			1.59	Subsonic	35	116
JFT-200205-2			1.42	Subsonic	35	116
JFT-200204-1			1.20	Subsonic	35	116

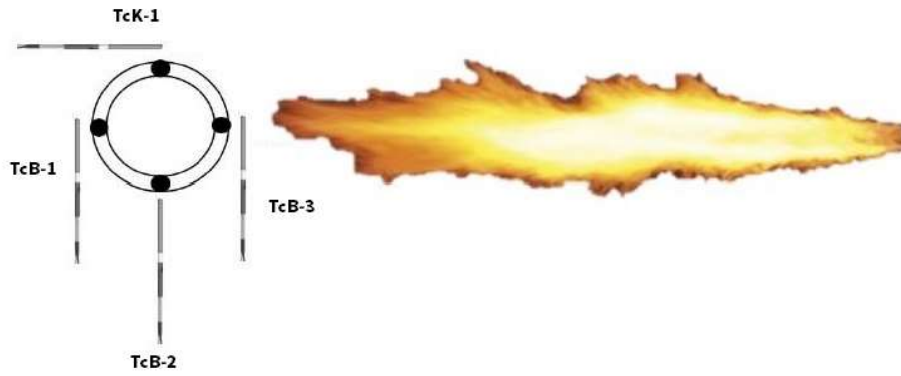


Figure 3-6. Scheme of the position of the external thermocouples.



Figure 3-7. Scheme of the position of wall thermocouples.



Figure 3-8. Scheme of the position of internal thermocouples.



Figure 3-9. The location of the two thermocouples (inside and outside the pipe wall) at the front position.



Figure 3-10. K-type thermocouple inside the pipe wall.

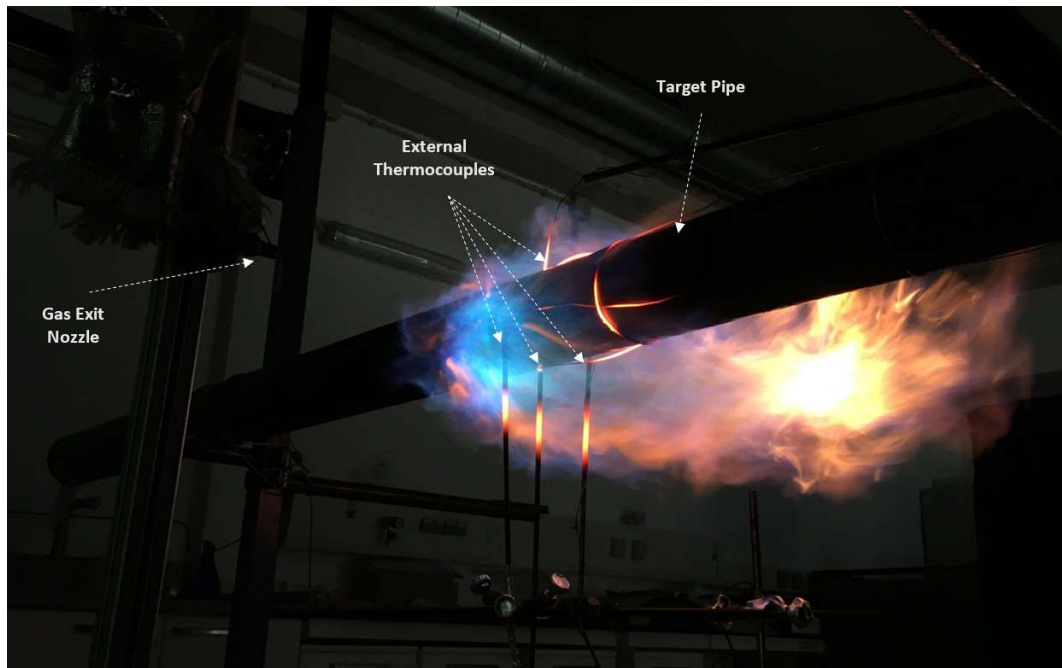


Figure 3-11. Flames impinging on pipe indicating the external thermocouples.



Figure 3-12. Preparing the position of a thermocouple inside the pipe wall.

**3.3.3. Group 3- Temperature profile tests:** These experimental tests were designed to measure and characterize the temperature profile of the flame with 6 mm and 8 mm nozzle diameters.

**3.3.4. Group 4- Geometrical features assessment by means of IR and visible image processing:** These experimental tests experiments were designed to assess the impact of release pressure and divergent gas flow rates on the geometrical features of the flame (size, shape, area, etc.).

#### **Arrangement of tests Groups 3 and 4**

In order to obtain data on the main features and effects of propane gas medium-size sonic and subsonic jet fires, an experimental set-up was designed and constructed.

The size, geometry and behavior of a jet fire depend on the exit velocity and the mass flow rate of the fuel. For most gases, in the event of a release from an equipment (at a pressure  $P_i$ ) to the atmosphere (at pressure  $P_a$ ), the exit velocity will increase with the pressure  $P_i$ . Sonic velocity (also called critical velocity) will be reached when the release occurs at  $P_i/P_a \geq 1.9$ . For propane, this situation happens when  $P_i/P_a \geq 1.73$  (Casal, 2018). Further increase in  $P_i$  will not imply a higher exit velocity, which will keep constant at the sonic value; however, the gas density will increase, this implying a higher density and, consequently, a higher mass flow rate.

Horizontal jet fires with different lengths and reach could be obtained by using different gas pressures and outlet orifice diameters. Nozzles with a diameter of 6 mm and 8 mm were utilized. The propane pressure was measured at a point located 12 cm upstream of the release point. The gas jet temperature at the release point was measured with a K-type thermocouple (Figure 3-13). The flame temperature was measure with nine B-type thermocouples along the flame as illustrated in Figure 3-14.

CCD and IR cameras were used to record the experiments. The Optris PI 640<sup>®</sup> IR used camera had a spectral range of 8–14  $\mu\text{m}$ . From observations of visible and infrared images, the flame boundary was defined as that corresponding to a temperature of 800 K (Palacios and Casal, 2011), and an emissivity value 0.35 was used (Palacios et al., 2012).

During the tests, the gas release nozzle was located 115 cm from the ground level. The position of thermocouples used during the experimental tests is shown in Table 3-9.



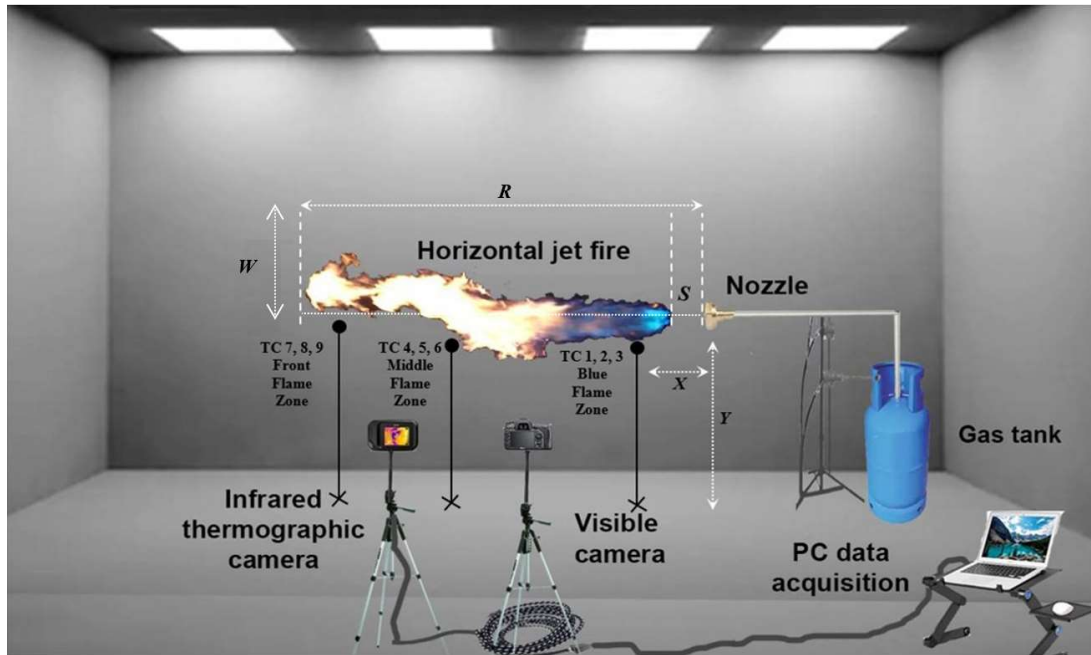


Figure 3-13. The arrangement of experimental setup for free jet.

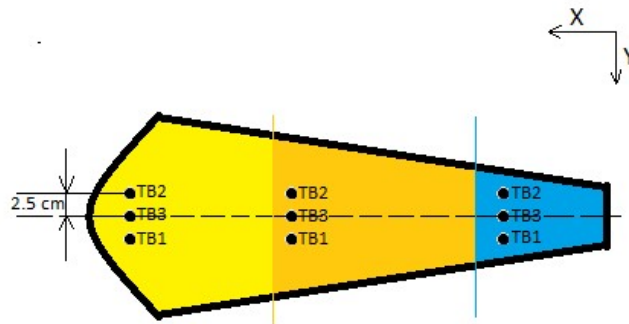


Figure 3-14. Thermocouples type-B positions along the hot flame (from top view). The release conditions for temperature profile test are shown in Table 3-8.

Table 3-8. Release conditions for flame temperature assessment tests.

Experiment Title	Exit Nozzle Diameter (mm)	Gas Release Pressure (barg)	Release Regime
JFT-191114-2-T6	6	0,546	Subsonic
JFT-191114-2-T8	8	0,790	Sonic

The position of thermocouples as shown in Figure 3-7 are summarized in Table 3-9. X represent distances of the thermocouple from the nozzle and Y of the thermocouple distance from the ground level.

Table 3-9. Location of the thermocouples along the jet flame during test group 3.

Experiment Title	TC Tag	Location of thermocouples (cm)		
		Blue Flame Zone	Middle Flame Zone	Front Flame Zone
JFT-191114-2-T6	TCB-1, 2 & 3	X: 46	X: 46	X: 46
		Y: 115	Y: 115	Y: 115
	TCB-4, 5 & 6	X: 80	X: 80	X: 80
		Y: 115	Y: 115	Y: 115
	TCB-7, 8 & 9	X: 138	X: 138	X: 138
		Y: 129	Y: 129	Y: 129
JFT-191114-2-T8	TCB-1, 2 & 3	X: 46	X: 46	X: 46
		Y: 115	Y: 115	Y: 115
	TCB-4, 5 & 6	X: 80	X: 80	X: 80
		Y: 115	Y: 115	Y: 115
	TCB-7, 8 & 9	X: 138	X: 138	X: 138
		Y: 129	Y: 129	Y: 129

### 3.4. Components of the experimental setup

#### 3.4.1. Jet fire generation section

The Swagelok Ibérica Company was employed to carry out the fabrication of the jet fire generation section and to provide all the parts of the setup facility. The jet fire section is divided into three main sections:

- ❖ Fuel storage section
- ❖ Flow/pressure regulation panel
- ❖ Release nozzle

#### Fuel storage section

An industrial size (35 kg) propane bottle containing pure propane at a pressure of approximately 9.5 bar was utilized as the fuel source for the experiments (Figure 3-16) The bottle was equipped with a manual valve on the gas outlet. Repsol company was chosen as the provider of propane bottles. A hose connection was installed with a diameter of 3/8-inch between the bottle and the inlet connection of setup with respect to the standard size of industrial propane cylinders. An adapter joint was placed to connect the 3/8-inch hose to the 1/2-inch setup inlet tube.

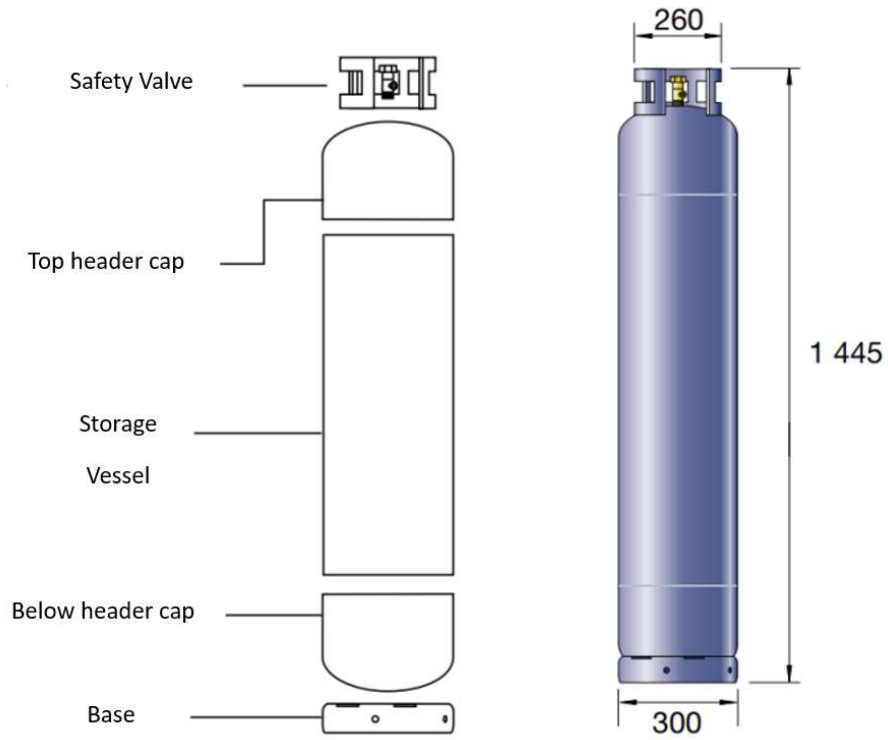


Figure 3-15. Image of the design of a propane cylinder (35 kg) and its dimensions (units in mm) (Cepsa, 2001).



Figure 3-16. Fuel storage.

### Flow/pressure regulation panel

This section was designed to control and supervise the operating condition of gas release to adjust the required jet fire length. A needle valve (VLV-01), an electrical solenoid valve (ESV-01), a pressure regulator valve (PCV-01) associated with the manometer (PG-01), and a variable area flowmeter (FM-01) are the main components of the regulation panel (Figure 3-17).

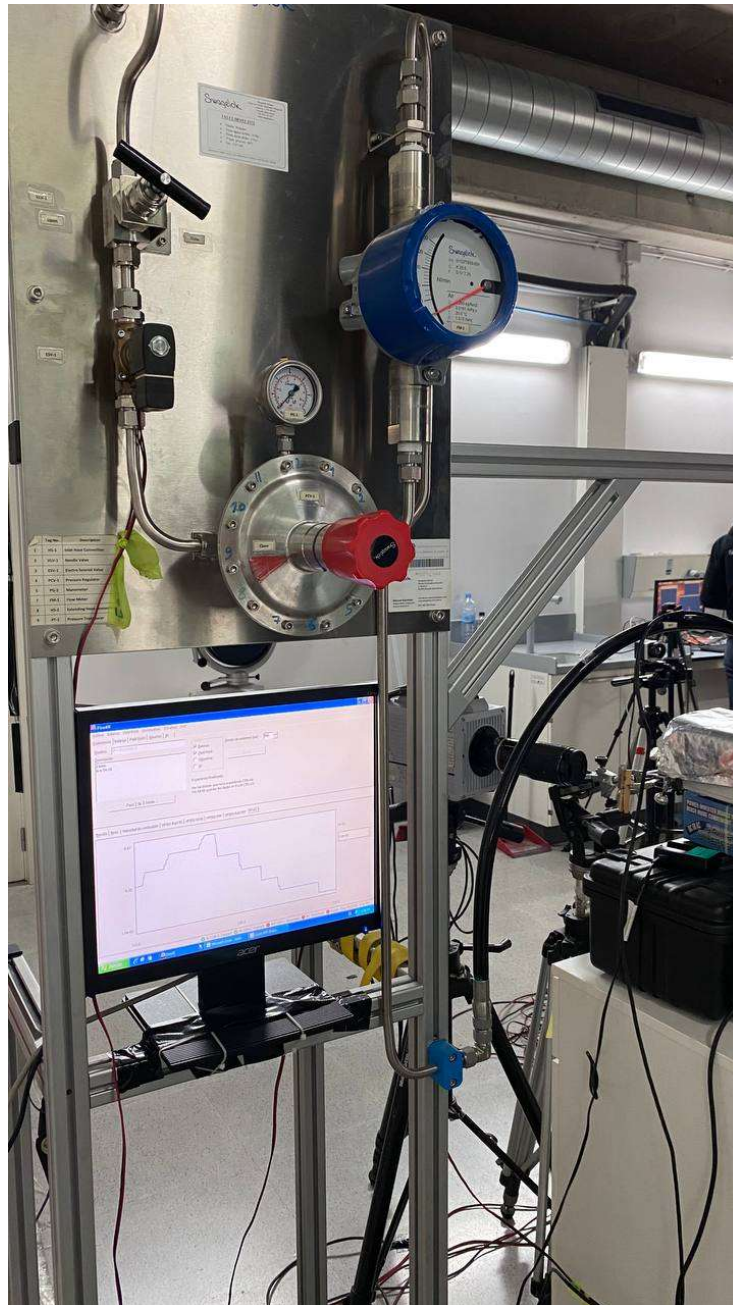


Figure 3-17. Control and measurement panel.

Each component is described in detail below:

**Manual needle valve (VLV-01):** the manual needle valve was provided for the opening and closing of the propane pass in the setup (Figure 3-18). This type of valve was chosen because it allows the control of the flow with a higher precision compared to another valve.



Figure 3-18. Manual needle valve.

**Electrical solenoid valve (ESV-01):** an electric solenoid valve (Figure 3-19) was located downstream of the needle valve. Thus, in case of emergency, the solenoid valve could be closed remotely to stop gas flow in the system. The selected valve is a 2/2-way membrane type with a servo control system connected to an electrical power supply required for the turn on/off operation of the valve. It was designed in a way that the source of electricity and the controlling operator remain protected behind the laboratory wall, remote from fire, allowing stronger safety measures. To ensure the safety of both the users and the installation, the normal state of the valve was considered as normally closed [NC], to bring the safest condition for the operation until the valve bobbin was de-energized. Energizing the bobbin by connecting the power source, ensures that the valve is left open and allows the fuel to pass through it. As in the case of the power supply failure, the electro valve would be closed automatically.



Figure 3-19. Electrical solenoid valve.

### Electrical Power supply

A fixed power supply (Figure 3-20) was chosen to keep the selected solenoid valve running. Based on the voltage and power required of the solenoid valve, a source of 24 V and 3 A is chosen.



Figure 3-20. Electrical power supply

The reason for generating a linear voltage was to keep the power supply voltage of the solenoid valve constant, ensuring that there was no way for an operator to make a mistake when starting up the installation.

**Pressure regulator valve (PCV-01):** a high-sensitivity spring type pressure regulator valve (Figure 3-21) was provided to break down the pressure from 9.5 bar (the pressure of the gas from the bottle up to the upstream of the regulator) to a lower pressure (downstream of the regulator) by means of a manual adjustable valve.



Figure 3-21. Pressure Regulator Valve.

**Pressure Gauge (PG-01):** the pressure gauge (Figure 3-22) was used in order to identify and adjust the relative pressure downstream of the pressure regulator, a manometer was mounted on top of the pressure regulator valve.



Figure 3-22. Pressure gauge.

**Variable area flowmeter (FM-01):** a rotameter type flowmeter (Figure 3-23) was selected to identify the flow of passing gas through the system. The position of the float inside the rotameter changes by the flow that passes through the device providing a direct visual indication of the value of the volumetric flow rate. The chosen model covers a flow rate ranging from 200 to 2000 NL/min. The flow range of this device was taken into consideration corresponding to the minimum and maximum potential flow of propane gas.



Figure 3-23. Variable area flowmeter.

**Flexible hose (HS-02):** a flexible hose (Figure 3-24) was used so that the length, height, and angle could be changed according to the purpose of the experiments. The adequate model and flame-retardant material were chosen taking into account the close distance of this part to the flames of the fire.





Figure 3-24. Flexible hose.

### Gas release nozzle

**Interchangeable nozzles (NZ-01; NZ-02; NZ-03):** the gas exit orifice was equipped with removable/changeable nozzles in order to generate different flame lengths. The nozzle sizes, ranging from 4 mm to 10 mm, were installed at the end of the section (Figure 3-25 and Figure 3-26).



Figure 3-25. Gas release nozzles.



Figure 3-26. Interchangeable nozzles.

### 3.4.2. Target pipe section

A carbon steel pipe with a diameter of 4 inches and a length of 3 m was picked as the target pipe to be impinged by the propane jet fire. The diameter of 4 inches for the target pipe was selected with respect to the maximum estimated diameter of the jet fire which allows testing partial fire engulfment and total fire engulfment condition of the pipe.

With respect to the indoor location of the experimental tests, flammable substances were not allowed to be used for the passing liquid through the pipe due to the risk of fire and explosion. Air and water were chosen as fluids more adapted by their easy accessibility and their safe condition.

In order to study the thermal effect of flame impinging on the target pipe an appropriate type and adequate number of thermocouples were installed. Four K-type thermocouples were inserted within the wall of the pipe.

To fix the thermocouples in the wall thickness of the pipe, four diagonal holes (on the top, bottom, behind, and front section) of 5 mm depth were formed in the pipe with fine drilling equipment. Thermocouples were positioned inside the holes and hammered to ensure that were held firmly in place.

### 3.5. Instrumentations

A set of instrumentation was installed and used on the fuel gas line and pipe wall in order to measure the main operating conditions of the tests, e.g., temperature, pressure and flow.

#### 3.5.1. Pressure measurement

The pressure of the fuel gas was measured in each test; the measurement was effectuated at 10 cm upstream of the outlet orifice, using an explosion-proof type electronic pressure transmitter (model). This was taken as the upstream stagnation pressure of the flow. Photographs of the electronic pressure transmitter equipment are shown in Figure 3-27.



Figure 3-27. Pressure transducer.

#### 3.5.2. Temperature measurement

The temperature at the exit orifice was continuously measured using an uncoated K-type thermocouple located at the jet outlet orifice. The jet velocity at the outlet orifice and the mass

flow rate for both sonic and subsonic regimes could then be calculated assuming isentropic expansion between the stagnation point and the orifice jet exit, by applying the appropriate thermodynamic relationships. A scheme of the nozzle's arrangement and the location of the pressure transmitter and the uncoated K-type thermocouple can be seen in Figure 3-28.

The jet flame axial temperature distribution was measured using a set of thermocouples along the jet flame centreline. Three B-type were used; higher temperatures (~ 1800 K) can be measured with this type of thermocouple (Table 3-10). The three thermocouples were arranged on a mast at different distances from the release point, in an attempt to cover all the flame regions, taking into account the lift-off of the jet flame (i.e., the centreline distance from the gas release point to the start of the detached and stabilized flame). The thermocouples were supported on a series of metallic bars and insulated with rock-wool. These bars showed excellent mechanical strength at high temperatures (up to 1900 K) and good resistance to thermal shock. During the tests, the positions of the thermocouples were changed as required according to flame length.

Some features of the diverse thermocouples used in the present study are shown in Table 3-10.

Table 3-10. Thermocouple features.

	Thermocouple	Thermocouple
Type	K	B
Composition	Nickel – Chromium vs. Nickel – Aluminium	Platinum-30% Rhodium vs. Platinum-6% Rhodium
Maximum temperature range	from -200 °C to 1250°C	from 0 °C to 1700 °C

### B-type thermocouples

B-type thermocouples are a type of temperature sensor commonly used in high-temperature applications. They are part of the thermocouple family, which consists of two different metal wires joined together to form a temperature-sensitive junction.

Specifically, B-type thermocouples are made by combining a platinum-rhodium alloy wire (typically 70% platinum and 30% rhodium) as the positive leg with a platinum wire as the negative leg. This combination of metals allows B-type thermocouples to measure temperatures within a wide range, typically from around 200°C to 1820°C.

Some key features and characteristics of B-type thermocouples include:

- **High Temperature Range:** B-type thermocouples are suitable for measuring temperatures in high-temperature environments, making them ideal for applications such as industrial furnaces, combustion processes, and certain laboratory settings.
- **High Accuracy:** B-type thermocouples offer good temperature accuracy, typically within a few degrees Celsius or Fahrenheit. However, the accuracy can be affected by factors such as aging, oxidation, and contamination of the thermocouple wires.
- **Oxidation Resistance:** B-type thermocouples are known for their resistance to oxidation at high temperatures, which helps maintain their accuracy and reliability over time.
- **Non-Magnetic:** The platinum-rhodium alloy used in B-type thermocouples is non-magnetic, making them suitable for applications in magnetic fields where other types of thermocouples may be affected.
- **Limited Chemical Compatibility:** While B-type thermocouples are robust at high temperatures, they may not be compatible with certain corrosive or reactive environments. It is important to consider the chemical compatibility of the materials being measured to ensure accurate and reliable temperature readings.
- B-type thermocouples require a specialized temperature measuring instrument or data acquisition system that can accurately read and interpret the small voltage generated by the thermocouple junction. These thermocouples are widely used in various industries where high-temperature measurements are critical for process control, safety, and research purposes.

### **K-type thermocouples**

K-type thermocouples are a popular type of temperature sensor widely used for measuring temperature in various applications. They belong to the thermocouple

family, which consists of two different metal wires joined together to form a temperature-sensitive junction.

- Specifically, K-type thermocouples are made by combining a positive leg made of a chromel alloy (typically nickel-chromium) with a negative leg made of an alumel alloy (typically nickel-aluminium). This combination of metals allows K-type thermocouples to measure temperatures within a wide range, typically from around  $-200^{\circ}\text{C}$  to  $1350^{\circ}\text{C}$ .
- Here are some key features and characteristics of K-type thermocouples:
  - **Wide Temperature Range:** K-type thermocouples are suitable for measuring temperatures across a broad range, making them versatile and widely used in various industries and applications.
  - **Good Accuracy:** K-type thermocouples offer reasonable temperature accuracy, typically within a few degrees Celsius or Fahrenheit. However, the accuracy can be affected by factors such as wire aging, oxidation, and contamination.
  - **High Sensitivity:** K-type thermocouples exhibit high sensitivity to temperature changes, allowing them to detect even small temperature variations.
  - **Compatibility:** K-type thermocouples are compatible with most metals, making them suitable for a wide range of applications in different industries, including HVAC systems, industrial processes, food industry, and laboratory settings.
  - **Cost-Effective:** K-type thermocouples are relatively inexpensive compared to other types of thermocouples, making them a cost-effective option for temperature measurement.
  - **Limited Corrosion Resistance:** While K-type thermocouples are generally robust and reliable, they may not be suitable for highly corrosive or reactive environments. In such cases, specialized thermocouples with higher corrosion resistance may be required.
  - K-type thermocouples generate a small voltage at the temperature junction, which is read and interpreted by a temperature measuring instrument or data acquisition system. These thermocouples are widely used due to their versatility, wide temperature range, and affordability, making them a popular choice for temperature measurement in various industries and applications.

The thermocouples were located in three different locations described as follows:

- **Exit of the nozzle**

A type K thermocouple was utilized to track the operating conditions of jet release at the outlet of the orifice. This thermocouple was named TCK-00, and its location is shown in Figure 3-28. At this point the temperature is around room temperature, sufficiently low to use a type K thermocouple. Combined with the pressure at the outlet of the orifice and assuming an isentropic expansion with the measurement of the temperature at the orifice, the density of propane could be calculated. With the value of the density at the orifice, the mass flow at this point could be determined and compared to theoretical values.

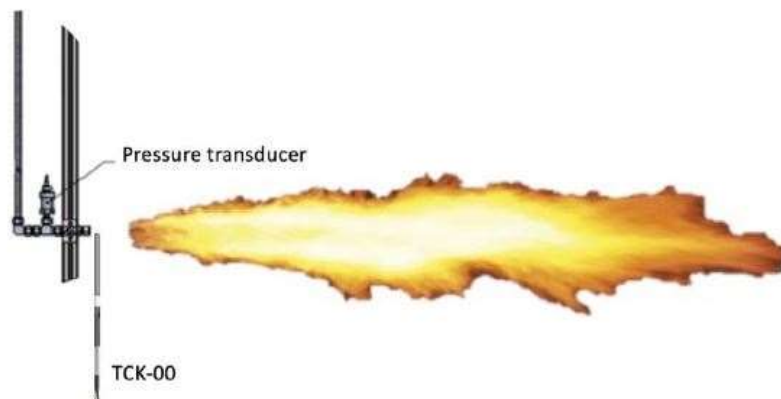


Figure 3-28. Scheme of the position of the thermocouple in the exit of the orifice.

- **Jet flames**

The flame temperature was continuously recorded along the outer circumference of the pipe, placing four thermocouples at the vertexes of an ideal rhombus circumscribed to the round section of the pipe. In this way it was possible to analyze the temperature in the front, bottom, back and top areas of the pipe. In this case, B-type thermocouples were used, because of the high temperatures of the flames, except for the top area, where there was a K-type. The thermocouples were placed no more than 2 cm away from the pipe, in order to have a direct measurement of the flame temperature that was going to impact on it. In Figure 3-6, Figure 3-9 and Figure 3-11 the positioning of the thermocouples is illustrated.

- **Target pipe**

To study the thermal effect of the flame impingement on the target tube, an appropriate type and an adequate number of thermocouples were installed. Four type K thermocouples were inserted into the pipe wall. To fix the thermocouples in the wall thickness of the pipe, four diagonal holes (top, bottom, back and front) 5 mm deep in the pipe were drilled with fine drilling equipment. The thermocouples were positioned inside the holes and hammered to ensure that they were held securely in place. The position of the thermocouple position is shown in Figure 3-7, Figure 3-9, Figure 3-10, Figure 3-11 and Figure 3-12.

### **Internal thermocouples**

In order to analyse the heat loss during the experiment through the air temperature inside the pipe, four type K thermocouples were installed through a metal support. They were placed next to the thermocouples on the wall, at a distance not exceeding 5 cm. The study of heat loss was useful to understand how long the heating of the pipe wall was effectively influenced only by a convective mechanism, and not by others. The position of each internal thermocouple is shown in Figure 3-8.

### **3.5.3. Infrared Camera**

The Optris PI 640<sup>®</sup> IR used camera had a spectral range of 8–14  $\mu\text{m}$ . From observations of visible and infrared images, the flame boundary was defined as that corresponding to a temperature of 800 K (Palacios and Casal, 2011), and an emissivity value of 0.35 was used (Palacios et al., 2012).

The thermographic camera works as a radiometer composed of a two-dimensional set of sensors. The signal of every sensor is proportional to the heat radiated by every small part of the object that the camera sees. The signal turns into temperature through the emissivity and the distance of the object. The output of the thermographic camera is an image that represents the distribution of the temperature of the objects that the thermographic camera sees. The speed of acquisition of data is high, the output of the camera is an image of the distribution of temperature of the object.

The Optris PI 640<sup>®</sup> IR is a high-resolution infrared camera manufactured by Optris GmbH, a company specializing in non-contact temperature measurement devices. The



PI 640® IR is designed for industrial and scientific applications that require accurate thermal imaging and temperature measurement. Table 3-11 describes key features and specifications of the Optris PI 640® IR:

Table 3-11 Features of Optris PI 640® IR camera.

Featrure	Description
Resolution	The camera offers a resolution of 640 x 480 pixels, providing high-definition thermal images with a high level of detail.
Temperature Measurement Range	The PI 640® IR has a wide temperature measurement range, typically from -20°C to 900°C (-4°F to 1652°F). This range can be extended with optional temperature ranges.
Thermal Sensitivity	The camera has a thermal sensitivity of 40 mK, enabling it to detect small temperature differences with high accuracy.
Optics and Field of View	The camera comes with a selection of different lenses, allowing users to choose the appropriate field of view for their application. The available field-of-view options range from 7° to 90°.
Frame Rate	It offers a fast frame rate of up to 120 Hz, allowing for real-time monitoring of dynamic processes.
Integration and Connectivity	The PI 640® IR supports various integration options, including GigE Vision and USB 2.0 interfaces. It can be easily connected to a computer or industrial control system for data transfer and analysis.
Software and Analysis:	Optris provides software tools, such as PI Connect, for configuring the camera settings, analyzing thermal images, and performing temperature measurements. The software offers features like line profiles, spot meters, and region of interest (ROI) analysis.
Detector	Focal plane array (FPA), uncooled microbolometer
Operating mode	Continuous recording (32 fps)
Resolution	The camera offers a resolution of 640 x 480 pixels, providing high-definition thermal images with a high level of detail.

#### **3.5.4. Visible camera**

The experiments were also filmed with a visible camera, in order to analyse the shape of the visible flame and compare it with the infrared camera images. For these purposes, the rear camera of an iPhone 11 (by Apple) device was used. The slow-motion mode were used to record a number of the experiments giving the possibility of handling the various moments of the tests in order to analyse the flame and impingement trends.

#### **3.6. Data collection system**

The experimental data were collected and registered in real-time by using a FieldPoint device hardware. It consisted of a FP-1001 communication module (RS-485, 115 kb·s<sup>-1</sup>), three connection terminals FP-TB-1 and three input/output (I/O) modules. An RS-485 communication port was used to connect the I/O modules to the FP-1001 module, which was connected to the computer and to the power supply. The FP-TB-1 terminal connection bases were used to support the I/O modules, to guarantee a constant power supply, and serve as an internal communication system between the I/O and FP-1001 modules. Two of the I/O modules were FP-TC-120 modules. The thermocouples and radiometers were connected to each one of these FP-TC-120 modules and the measurements were stored by the computer. The other I/O module was of type FP-AI-110 and was used to collect the information generated by the electronic pressure transmitter (Figure 3-29).

Two laptops were used to collect the data from the different equipment. They recorded the measurement and controlled the operation of the device. It is important to note that the instruments provided four measurements per second. The IR camera and the FieldPoint were connected to one of the computers, through RS-485 connections, respectively; the balance was connected to the second computer by a RS-232 connection. Furthermore, the two laptops were linked via a network in order to synchronize the data collection.

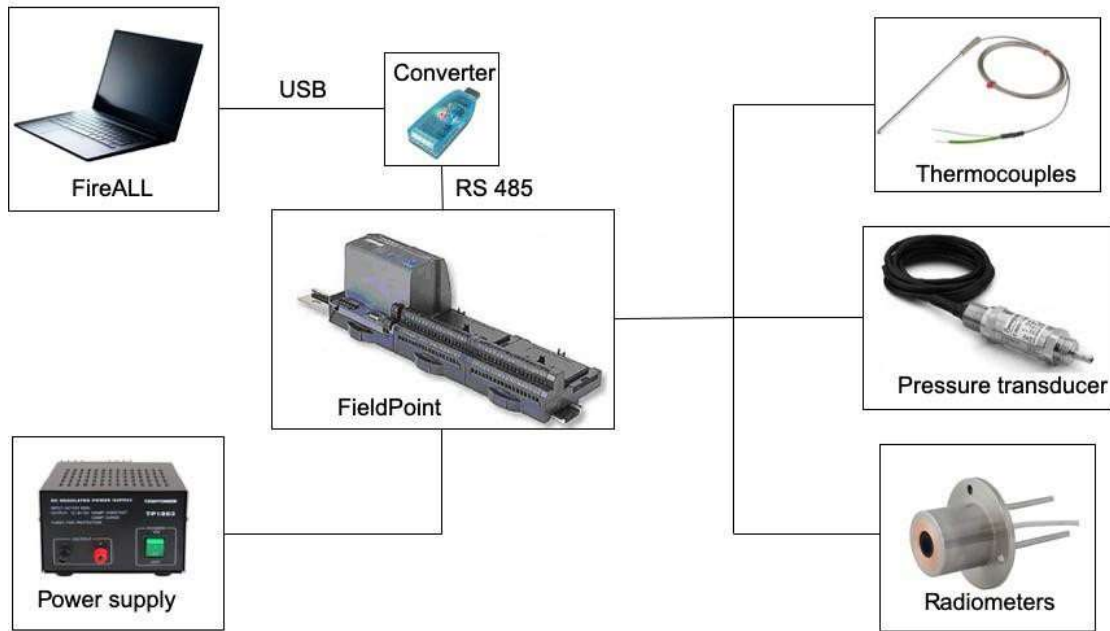


Figure 3-29. Scheme of the measurement devices and their communications interfaces.

### 3.6.1. FireALL

The FireALL software developed by Muñoz (2005) and subsequently modified by the CERTEC, was used to automatize the process of data management and the control of the devices from a common interface. Besides, the software allows to synchronize the acquisition of data of different nature.

This software runs connected to a data acquisition hardware module. In this case, an input/output modular system was used, called FieldPoint, which reads and converts in digital data all the data that are originated from thermocouple, radiometer and pressure transducer. FireALL is also able to synchronize the point at which the computers start recording the data. The principal window of the program is shown in Figure 3-30.

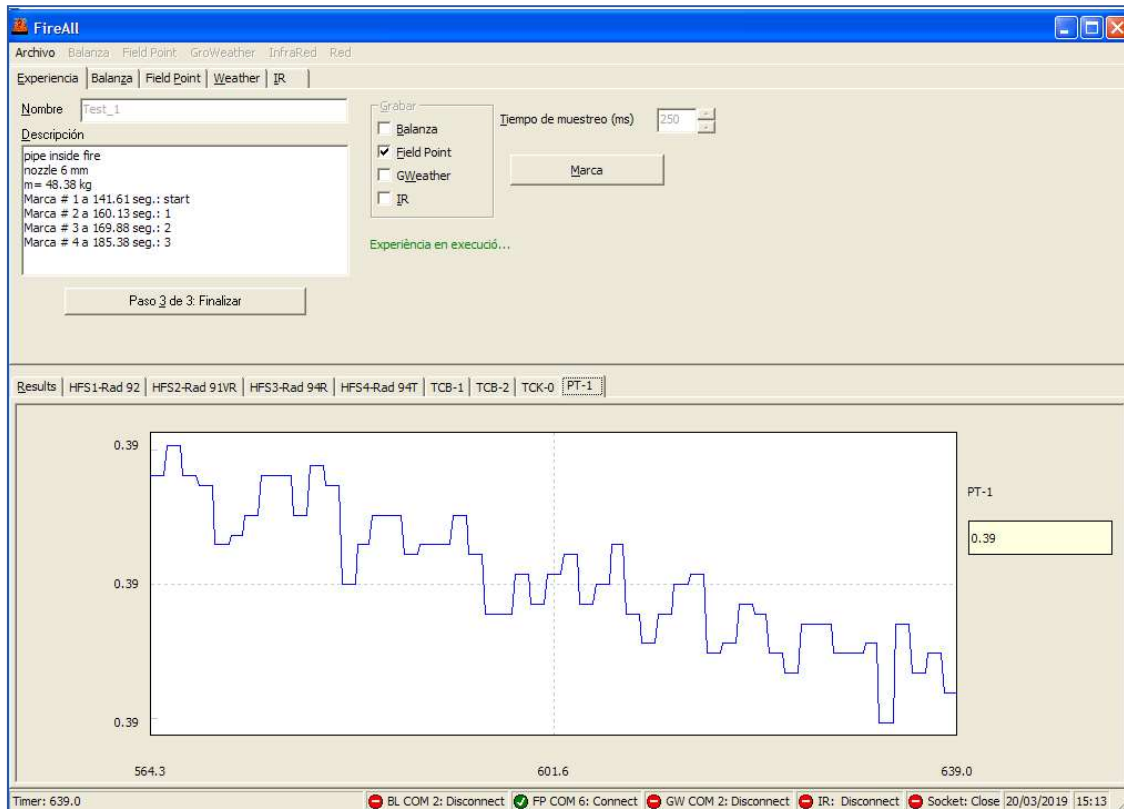


Figure 3-30. Principal window of the program FireALL.

In the principal window, two main sectors are present:

- “Devices and experiments” control part: in this tab it is possible to configure and control the several connected devices. Besides, it is possible to give a name to the experience and add notes. Finally, this section allows to manage the recording of the data coming from the devices.
- “Data” part: in this sector the evolution of the measure of the desired variables can be monitored in real time through automatically updated graphs. Subsequently these data are saved.

Before the start of the experiments the software is in the waiting mode, in this way all the devices can be connected though the net connection. First of all, before starting the collection of the data, the name of the folder where the data will be stored must be defined.

### 3.6.2. FieldPoint module

To collect the data coming from the tools of measurement the system FieldPoint, of the National Instruments, was used. It is a distributed modular system of Input/Output, both analogical and digital.

The FieldPoint is formed by these elements (Figure 3-31):

- Communication module;
- Input/Output module called I/O module;
- Terminal Base.

In Figure 3-31 an image of the FieldPoint with all its parts (modules and terminal base) is presented.

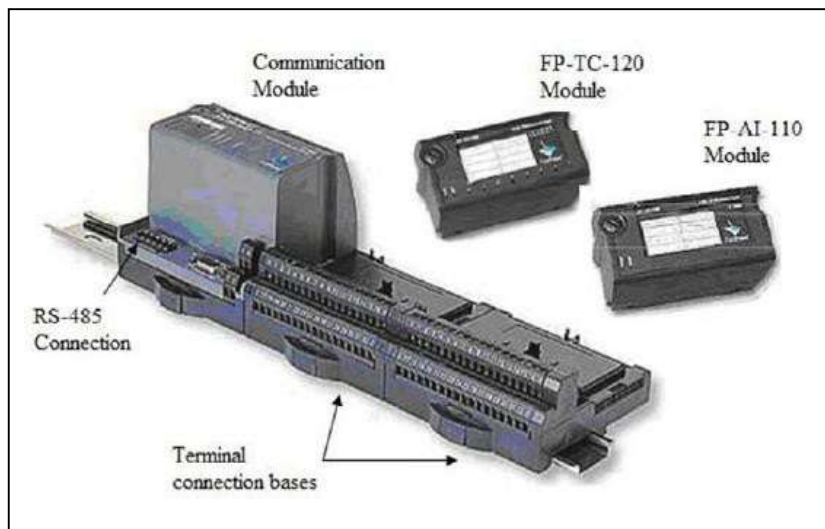


Figure 3-31. FieldPoint and its elements.

- Communication module: the communication module, model FP-1001, has the function of connecting the input-output module (I/O) through a high-speed local bus, integrated in the base of the terminals, with the computer and with other communication modules that form the net. The module communicates through a port RS485 (full duplex) to the computer. Each of these manage up to 9 forms I/O and a net of communication modules can be constituted for a maximum of 25 communication modules. Many applications can be communicated to the module through the set of commands Optomux Standard, as in the case of the program FireALL, or through an application client OPC (Open Process Control). Through a series of changers (commutators), situated in the superior part of the module, the speed of transmission

and the number of the port are assigned. Table 3-13 represents the characteristics of the communication model.

Table 3-13. Communication module technical data sheet.

Featrure	Description
Communications ports Transmission	RS-485
speed Communication parameter	Configurable up to a maximum of 115200 bps
Communications Protocol	1 bit of beginning, 8 bit of data, 1 bit of stop, without parity
Maximum distance from the computer	Optomux Standard
Alimentation	1200 m
Consume	1 W + 1,15W x I/O module
Work Temperature	-40 to 70 °C

- Terminals Bases: the terminal bases allow to connect the sensors to the modules I/O, as well as the power supply and communication with the net module. The I/O modules can be connected and disconnected from the base without interrupting the energy supply of the system. The high-speed local bus is made of these bases, in this way it is possible to connect the I/O modules with the communication modules. The terminals bases are of the type of FP-TB-1, enabling the use of every kind of I/O module. The bases have 36 terminals in total.

- Input Modules: this system allows to directly connect any sensor to several I/O modules, both analogic and digital, of high accuracy.

These modules filter, digitize, and calibrate the pure signal of the sensor. In addition, they incorporate systems of self-diagnosis, in order to identify such problems. Two kind of input modules are used:

- Thermocouple modules FP-TC-120;
- Analogic input modules FP-AI-100.

The modules FP-TC-120 are designed to measure temperatures by thermocouples. This kind of module can be calibrated for reading the temperature, supporting a wide range

of thermocouples standards, or for direct reading analogic signals in millivolts. Every form possesses 8 channels in input, separately configurable. This high-accuracy module, with a resolution of 16 bit, incorporates compensation of the cold union of the thermocouples (when work like a temperature measurement) and a filter to delete the noise of the input signal. The features of this module are shown in Table 3-14.

Table 3-14 Input module FP-TC-120 data sheet.

Featrure	Description
Model	FP-TC-120
Input channels Resolution Filter	8
Type of entry	16 bits, 50/60 Hz
Supported thermocouples Actualization of the signal speed Entry impedance	Thermocouple (temperature) Analogic (millivolts) , J, K, T, N, R, S, W, B  0.88 Hz (every channels)
Other	20 MΩ  Thermocouple signal open Optic isolation of the entry signal

The modules of analogic entry, FP-AI-110, have 8 channels of entry configurable for the voltage or current reading. The module has a resolution of 16 bits and it is possible to choose between 3 different noise filters, 50, 60 and 500 Hz. This provides a protection from overvoltage or tension excess (up to 40 V or 30 mA), isolating the entry signal. The characteristics of this module are shown in Table 3-15. This module is made to collect the pressure transducer and the radiometers data.

Table 3-15. Input module FP-AI-110 data sheet.

Feature	Description
Model	FP-AI-110
Input channels Resolution	8, 16 bits
Filter	50/60 Hz
Type of entry Range of entry	Analogic: Voltage or Current, $\pm 60$ mV, $\pm 300$ mV, $\pm 1$ V, from 0 to 5 V, from 0 to 10 V, From 0 to 20 mA, from 4 to 20 mA, $\pm 20$ mA
Actualization of the signal speed	From 5 to 0.66 Hz (every channels)
Entry impedance	100 M $\Omega$
Other	Optic isolation of the entry signal

### 3.6.3. PicoLog

PicoLog is a data acquisition software develop by PICO technology, which provides a visual, easy-to-use interface for users to quickly set up simple or complex acquisitions, record, view and analyse data, by the use of a TC-08 thermocouple data logger.

A scheme of the devices and of their connection with the software is presented in Figure 3-32.



Figure 3-32. Scheme of the thermocouples and their communications interfaces with PicoLog.

### 3.6.4. Optris PIXConnect

The IR analysis software Optris PIX Connect was used for the recording and the acquisition of the IR videos and images. The interface of this program shown in Figure 3-33 allows starting, monitoring and concluding the recording of the experiment in an easy way. Before initiating the experimental tests, the program permits to modify the



recording range temperature in order to omit all the unnecessary items for the analysis and focusing only on the temperature profile of the jet flame. Furthermore, the thermographic software is able to react immediately to temperature fluctuations and thus, supports several functions for automatic process and quality control procedures.

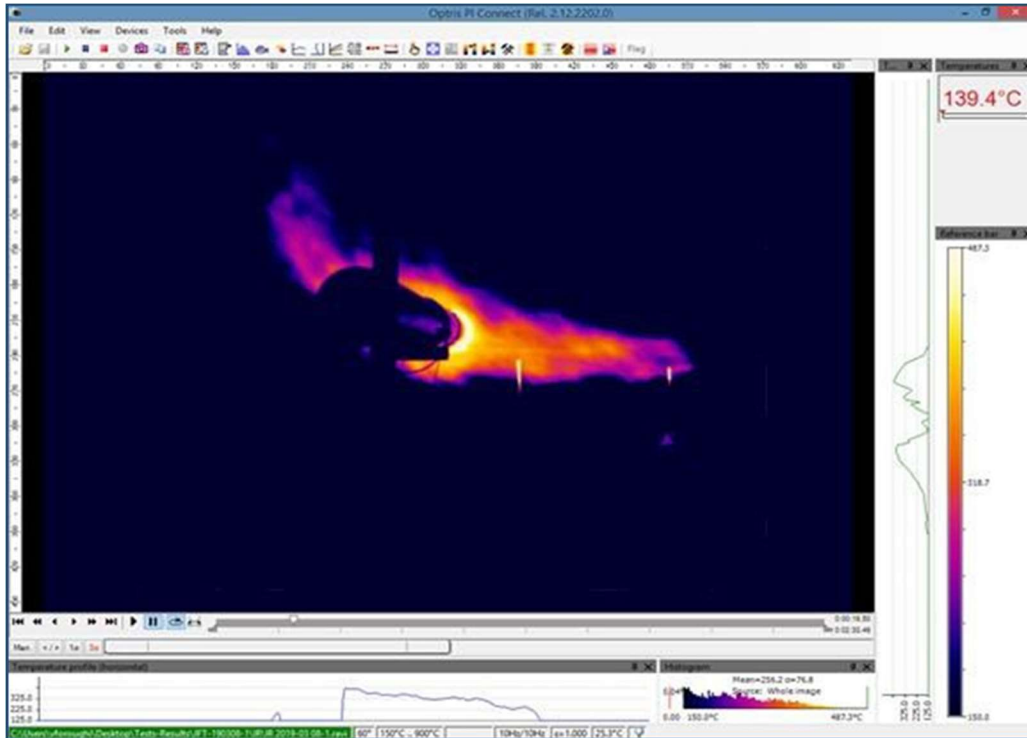


Figure 3-33. Interface of the software Optris PIX Connect.

In the lower row, and in the right column the horizontal and vertical temperature profile are shown. Moreover, thanks to this software it is possible to select a desired area for the temperature analysis. The IR camera is directly connected to the computer by an USB port as presented in Figure 3-34.



Figure 3-34. Scheme of the data acquisition system for the IR camera.

### 3.7. Data acquisition system elements arrangement

In this section, a scheme of the data acquisition system set-up is shown and described. For a better understanding, two different views, one from one side and one from the top of the experimental zone, associated with a legend of elements represented in Table 3-16, are shown in Figure 3-36 and Figure 3-37. In the top view, all the devices of measurement are arranged in order to easily understand their position in the laboratory room. In the side view, the cameras are used to allow focusing on the thermocouples and pressure transducer position in the set-up. The pressure transducer (PT-01) was installed at 12 cm before the exit of the nozzle. The thermocouple TCK-00 was positioned after the exit of the orifice, on the nozzle. Due to the turbulence of the jet, which could change the position of the thermocouple probe, this thermocouple was fixed to the facility. Before being located, the thermocouples used for the measurement of the temperature in the flame axis (TCB-01, TCB-02, and TCB-03) were settled on different masts. The thermocouples on the target pipe (TCK-01, TCK-02, TCK-03, and TCK-04) were positioned into drilled holes and hammered, and their positions in the pipe were fixed. During the experiments, these thermocouples were lined up with the central axis of the flame. The three heat flow sensors were located, in all the cases, perpendicularly to the flame, but a different distance from the jet flame that varied during the experiments. A general view of the experimental setup is shown in Figure 3-35.



Figure 3-35. Arrangement of the experimental setup.

Table 3-16. Legend of the devices.

Tag No.	Description
PT-01	Pressure transducer
TCK-00	Thermocouple (Type K)
TCK-01	Thermocouple (Type K)
TCK-02	Thermocouple (Type K)
TCK-03	Thermocouple (Type K)
TCK-04	Thermocouple (Type K)
TCB-01	Thermocouple (Type B)
TCB-02	Thermocouple (Type B)
TCB-03	Thermocouple (Type B)
IR-CAM-01	IR thermographic camera
VIS-CAM-01	Visible camera

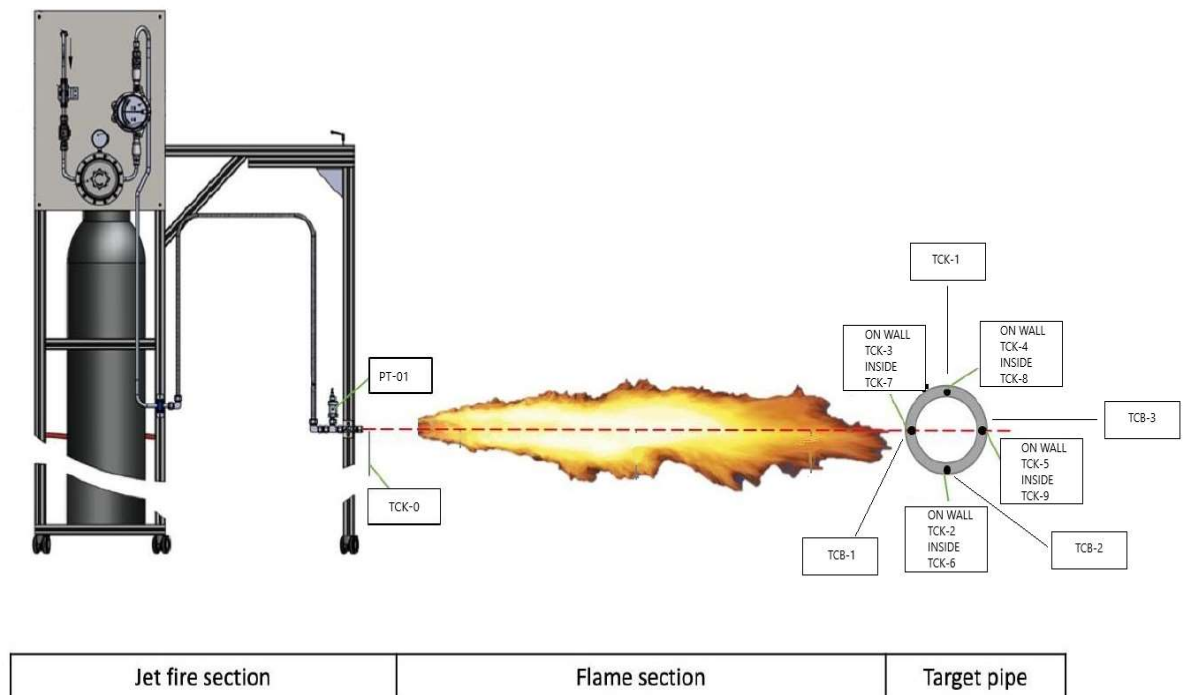


Figure 3-36. Side view of the measurement system elements arrangement.

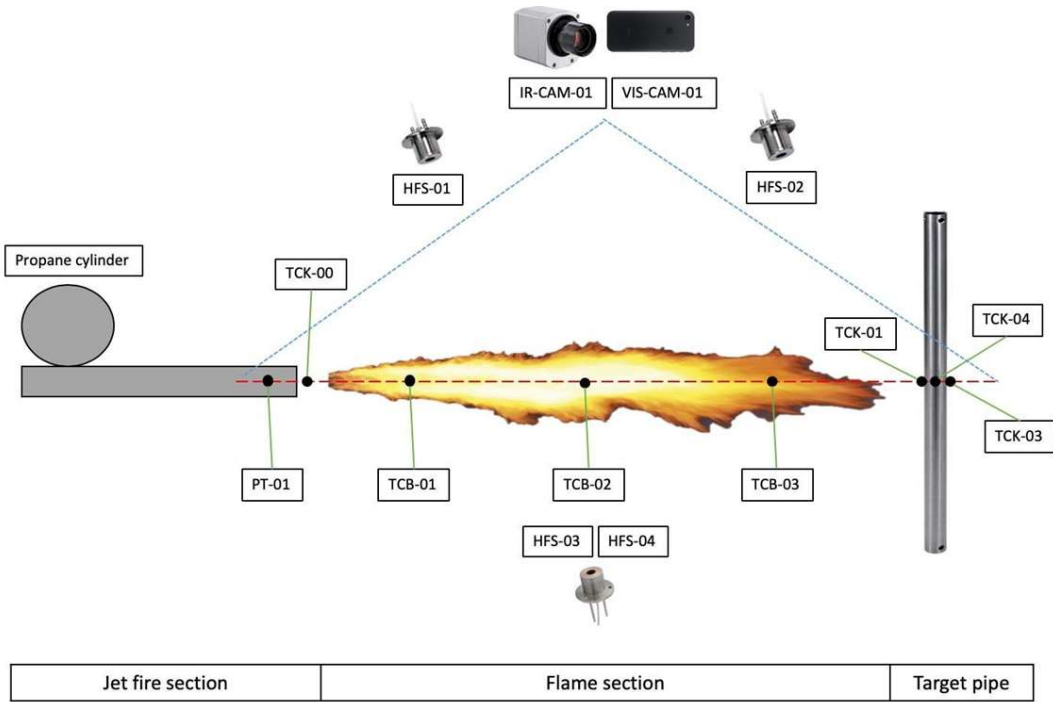


Figure 3-37. Side view of the measurement system elements arrangement.

### 3.8. Test procedure

Before starting the experimental campaign, an analysis of the steps that should be done before, during and after the tests was carried out.

The personnel needed to execute the operations and the attributions of the specific assignments of each member of the task team were determined, in order to reduce the operation time and to act with the maximum safety and simplicity.

The main steps conducted during the experimental tests are reported in Table 3-17.

Table 3-12. Test Procedure.

No.	Activity Description	Operator					
		A	B	C	D	E	F
1	Check for the availability and well condition of portable firefighting extinguisher.	█					█
2	Locate the setup facility in a fixed position and lock the wheels.	█	█	█			
3	Place the propane bottle and fasten the belt.	█	█	█			
4	Locate the target pipe in the wanted position.	█	█	█			
5	Locate the exit nozzle in the wanted height.	█	█	█			
6	Check for the fluid supply connections toward the target pipe.	█	█	█			
7	Locate the thermocouple masts along the jet axis/around the pipe and check for the wiring.	█			█		
8	Locate the heat flux sensors and check for the wiring.	█			█		
9	Connect the thermocouples, heat flux sensors, and pressure transducer to the FieldPoint.				█	█	
10	Turn on the Field Point power supply 13.8 Volts and open the FireAll software.				█	█	
11	Test the software FireAll.				█	█	
12	Locate the cameras (IR and VHS).	█	█	█			
13	Connect the IR camera to the PC and test the software PIX Connect.				█	█	
14	Connect the target pipe's thermocouples to the thermocouple data logger.				█	█	
15	Connect the thermocouple data logger to the PC and test the software PicoLog.				█	█	
16	Fill out the log sheet.	█			█		
17	Cover vulnerable objects with thermal insulation.	█	█	█			
18	Check for the ignition source.	█	█	█			
19	Ensure all the valves are closed and PCV-1 is in the minimum position.	█	█	█			
20	Prepare the mixture for the leakage test.	█	█	█			
21	Connect the hose (HS-01) to the propane bottle valve (VLV-00).	█	█	█			
22	Open the propane bottle valve (VLV-00) partially and perform a leakage test along the hose and connections up to VLV-01.	█	█	█			
23	Close the propane bottle valve (VLV-00).	█	█	█			
24	Turn on the air conditioning system.				█	█	
25	Start FireAll software.				█	█	
26	Define and check the channels for the thermocouples of the jet axis, heat flux sensors, and pressure transducer.				█	█	
27	Turn on the IR and VHS cameras.				█	█	
28	Start the PI Connect software.				█	█	
29	Start the PicoLog.				█	█	
30	Define and check the channels for the thermocouples on the target pipe.				█	█	
31	Run the fluid supply through the target pipe.	█	█	█			
32	Run simultaneously FireAll, PI Connect and PicoLog.				█	█	

Table 3-13. Test Procedure.

No.	Activity Description	Operator					
		A	B	C	D	E	F
33	Ensure PCV-01 is in the minimum position.	Green					
34	Turn on the power supply 24 V and open ESV-01.	Green		Yellow	Yellow		
35	Prepare the ignition tool and close it to the nozzle in the presence of a fireman.	Green					
36	Open the bottle valve VLV-00.	Green		Green			
37	Open manual needle valve VLV-01.	Green	Green				
38	Open PCV-01 gradually.	Green	Green				
39	Make ignition on the nozzle orifice.	Green					Blue
40	Regulate the flame condition through outlet pressure with PCV-01 by reading pressure values from PG-01 and PT-01 values.	Green	Green				Blue
41	Realization of the experimental test.	Green	Green	Green			Blue
42	Close gradually the valve on the bottle of propane VLV-00.	Green		Green			Blue
43	Turn off the power supply of the ESV-01 in order to close it.				Yellow	Yellow	Blue
44	Close the PCV-01 and the needle valve VLV-01.	Green	Green				Blue
45	Stop the software FireAll, PI Connect and PicoLog 6.				Yellow	Yellow	
46	Turn off the IR and VHS cameras.				Yellow	Yellow	
47	Turn off the air conditioning.				Yellow	Yellow	
48	Disassembly of the thermal insulations.	Green	Green	Green			
49	Disassembly of the measurement instruments.	Green	Green	Green			
50	Move the target pipe to the appropriate position.	Green	Green	Green			
51	Disconnected the hose HS-01 from the propane bottle.	Green	Green	Green			
52	Displace the propane bottle and move it to a safe place.	Green	Green	Green			
53	Move the setup facility to an appropriate position.	Green	Green	Green			

Important Notes:

- Operator A is the leader and should check the fire condition and make commands to others.
- A, B, C, and F operators should be present during all tests in the setup site.
- Operator F is a firefighter and should be present during all tests with a portable fire extinguisher somehow which can access all points of the lab.
- Before the ignition operator A is the main operator and operators B and C are checkers of all start-up activities.
- After the ignition, during the tests, operator A is the leader, operator B should stay beside the setup and control it, and Operator C should stay near the bottle and take care of its valve.
- Operators D and E should stay in the control room during all the tests and check for the software and turn off the power supply in an emergency conditions. Operator D is the leader and Operator E is the checker.

### 3.9. Safety measures

Throughout the duration of this specific experiment, the presence of substantial hazards posed by the potential jet fire and the handling of hazardous substances was recognized. In response to these risks, a meticulously implemented "Safety Plan" was put into effect, prioritizing the safety of all individuals involved.

The core focus of the protective measures revolved around mitigating the risk of thermal radiation on various crucial elements within the experimental facility. This encompassed safeguarding not only the facility itself but also the measuring instruments and the personnel participating in the tests. To achieve this, strategic measures were employed to minimize the impact of thermal radiation.

The protection of the facility and equipment involved the careful insulation of instruments, cables, and equipment located in close proximity to the jet flame. By effectively insulating these components, the risk of damage or compromised functionality due to excessive heat exposure was significantly reduced. This proactive approach aimed to maintain the integrity and functionality of the equipment throughout the experiment.

Additionally, to minimize exposure to radiation, video cameras and heat flux sensors were strategically positioned at a safe distance from the jet flames. This positioning allowed for the capture of essential data and observations without subjecting the equipment or personnel to harmful levels of thermal radiation. By maintaining a safe distance, the risk to both the sensitive instruments and the individuals involved in the experiment was effectively mitigated.

In summary, the "Safety Plan" implemented for this experiment focused on mitigating the risks associated with thermal radiation. Protective measures such as insulation and strategic positioning of video cameras and heat flux sensors were employed to safeguard the experimental facility, instruments, and personnel. By carefully addressing these potential hazards, the experiment could proceed with heightened safety measures, reducing the likelihood of damage, ensuring accurate data collection, and prioritizing the well-being of all individuals involved.

Additional protective measures were implemented throughout the course of the experimental tests, such as:

- Throughout all the tests, an individual was constantly stationed in the control room adjacent to the solenoid valve responsible for regulating the propane flow exit. In the event of an emergency, particularly when a blow-out phenomenon occurred, this valve could be promptly shut off to halt the fuel supply.
- A firefighter was positioned near the experimental setup facility, equipped with a portable fire extinguisher, ready to extinguish the fire and/or safeguard the individual who inadvertently ignited the fire.
- The individuals present in the experimental room were outfitted in firefighting attire, which included a heat-resistant jacket and protective goggles.

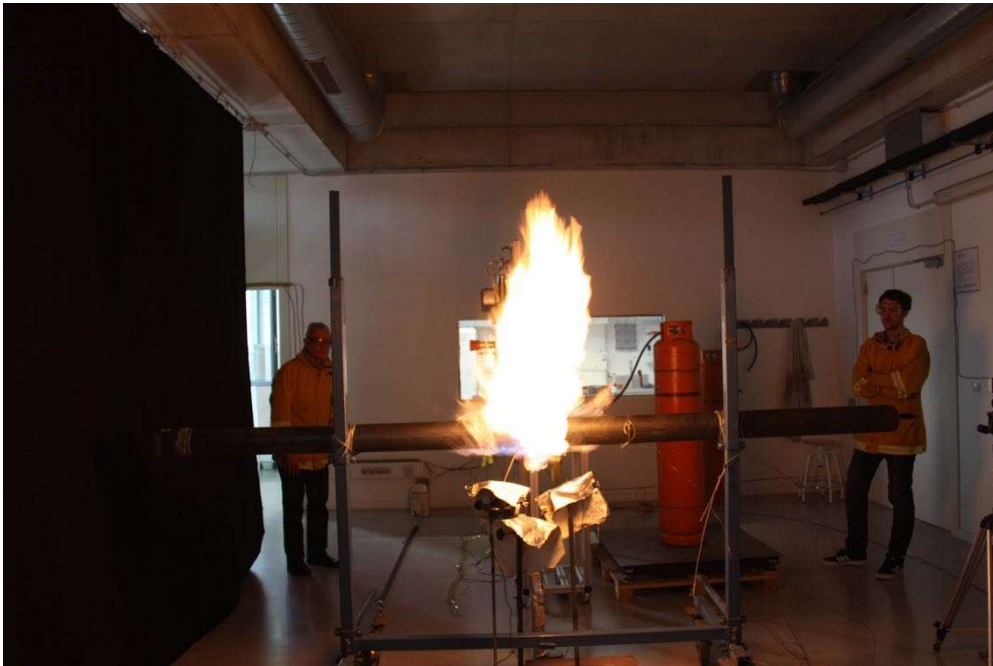


Figure 3-38. Front view of the experimental setup during an impingement test.



## 4. Geometric and thermal characteristics of horizontal jet fires

### 4.1. Introduction

This chapter investigates the physical characteristics of jet fires, focusing on flame length, flame temperature, and flame shape. These variables play a crucial role in understanding and mitigating the risks associated with jet fires. To provide a comprehensive overview, we define each variable and present a diagram illustrating the geometric aspects. Additionally, we discuss the three distinct regions of the flame: the flame front, the reaction zone, and the flame tail.

To establish the context for this research, the state of the art in analyzing the physical characteristics of jet fires was reviewed. The literature review encompasses various studies, including existing correlations, which delves into past efforts to quantify and analyze the properties of jet fires to predict this distance for the case of horizontal subsonic and sonic hydrocarbon jet fires, from both experimental data and the mathematical modelling of the main features of the flames. By examining these previous studies, we identify the existing gaps in knowledge that our research aims to address.

In this section, a general description of experimental methods employed to study the physical characteristics of jet fires. Furthermore, the image processing techniques applied to analyze the captured data, such as flame segmentation algorithms for identifying flame boundaries and temperature mapping algorithms for visualizing temperature distributions within the flame were discussed.

The present study unveils the outcomes of our experiments, presenting comprehensive results for each of the main variables. Following a systematic order, the quantitative measurements, graphical representations, and statistical analyses for flame length, flame temperature, and flame shape are sequentially presented. These findings contribute to an extensive comprehension of the physical characteristics exhibited by

jet fires, along with their variations under diverse experimental conditions.

Moreover, based on the experimental results, this research establishes new correlations that aim to unravel the intricate relationships among the variables of interest. These correlations facilitate a deeper understanding of the interdependencies and interactions that exist among flame length, flame temperature, and flame shape. Consequently, through the derivation of these correlations, valuable contributions are made to the existing body of knowledge, providing crucial insights for the domains of fire safety and risk management within industries where jet fires pose a significant concern.

In conclusion, this chapter provides an in-depth experimental analysis of the physical attributes manifested by jet fires. The study encompasses the identification of the variables of interest, an extensive review of the existing literature, a comprehensive outline of the employed experimental methods and image processing techniques, the reporting of experimental results for flame length, flame temperature, and flame shape, and the establishment of new correlations. Consequently, these endeavors enhance our comprehension of jet fire behavior and provide invaluable insights for enhancing fire safety and mitigating risks within relevant industries.

In the present thesis, a few relevant existing expressions are reviewed. Also, expressions to predict the reach of the possible impingement effects of sonic and subsonic propane jet fires, based on the experimental data and the modelling of the main geometrical features of the flames, are proposed. Mathematical expressions for estimating the size of the flames and reach as a function of several variables have been proposed and compared with previously suggested correlations. These expressions, together with the associated heat fluxes in the case of flame impingement, allow the prediction of the possible effects of a jet fire on a given area.

Predicting the main features of jet fires involves estimating key parameters that characterize the behaviour and characteristics of the flames. It is important to note that this prediction can be challenging due to the complex and dynamic nature of the flames. Experimental data, computational modelling, and empirical correlations are commonly used to develop predictive models allowing the estimation of these features. However, these predictions may have limitations and uncertainties, and it is essential to validate them with real-world measurements and observations whenever possible.

Jet fires studies focus on investigating the shape, size, and behavior of their flames, this being important for understanding their potential hazards. These studies utilize experimental setups, numerical simulations, and analytical models to analyze and quantify flame characteristics and related parameters. The findings contribute to improve safety practices, risk assessments, and fire protection strategies in various industries where jet fires can occur, such as oil and gas, chemical processing, as well as in the transportation of certain flammable fluids.

Here are some key aspects in jet fire flames studies:

- **Flames length:** This refers to the distance from the flames base to the flames tip. It is typically measured along the axis of the fuel jet. Flames length is influenced by factors such as fuel type, release rate, and ambient conditions. Predictive models based on empirical correlations or computational fluid dynamics (CFD) simulations can be used to estimate the flame length. Flame length can be correlated with the jet exit velocity and fuel properties, helping to estimate the potential reach and exposure zone of a jet fire.
- **Flame shape:** The shape of a jet fire can vary depending on factors such as the fuel type, the nozzle configuration, the jet exit direction, combustion features and surrounding environment (contact with some equipment). Predictive models or experimental correlations can provide insights into the typical flame shapes associated with different fuel types and release conditions. Jet fire flames can have various shapes, including cone-shaped, mushroom-shaped, or plume-like structures. Experimental studies analyze flame images or use mathematical modeling to characterize the flame shape and understand its behavior.

- Flame temperature: The temperature of a jet fire, together with its turbulence, is a crucial parameter for assessing its thermal effects and potential hazards for surrounding structures or equipment. Predictive models based on combustion theory and heat transfer mechanisms can estimate the flame temperature by considering factors such as fuel composition (gas or two-phase), combustion efficiency, and flame characteristics. Studies employ thermocouples, thermal imaging, or spectroscopic techniques to measure and analyze flame temperatures.

- Heat release rate: The heat release rate is a measure of the amount of energy released by the jet fire per unit time. It is an essential parameter for assessing potential fire hazards and designing safety measures. Predictive models can estimate the heat release rate based on fuel properties, release conditions, combustion characteristics and contact type with a given target.

- Radiative heat flux: The radiative heat flux is, together with the turbulent convection, a critical parameter for assessing the thermal impact on structures and personnel. Predictive models or empirical correlations can estimate the radiative heat flux based on flame characteristics, distance from the flame, and the geometry of the exposed surfaces. Jet fire flames emit significant thermal radiation, which can pose a threat to personnel and equipment in the vicinity. Studies quantify the radiative heat flux generated by the jet fire flames using heat flux sensors or radiometers. This data aids in assessing the potential thermal hazards and determining suitable protective measures.

- Flames contact: If there is impingement of the flames on a given object, the heat transfer rate to it will increase significantly due to the very important contribution of the convection. It will depend on the temperature and the turbulence of the flames.

- Flame stability: The stability of a jet flame refers to its ability to maintain a consistent shape and combustion process. Predictive models or empirical correlations can provide insights into the stability of jet flames by considering factors such as the velocity of the fuel jet, air entrainment, and turbulence effects. Researchers investigate the stability of jet fire flames, which can be affected by factors such as air entrainment, flame interaction with obstacles, and flames quenching. Jet fires can exhibit various types of instabilities, such as flickering, pulsation, or flapping of the flame, which can cause

fluctuations in flame shape, length, and intensity.

- Flame width: The flame width represents the lateral extent of the jet flames. It is typically measured perpendicular to the fuel jet's axis and indicates the flame's spread in the transverse direction. Flame width can vary along the flame length and is influenced by factors such as fuel type and velocity, turbulence, and confinement effects.

- Flame dynamics: Jet fire flame dynamics, including flame oscillations or instabilities, are of interest in studying their behavior. Researchers investigate the underlying mechanisms causing flame oscillations, their frequency, and the effect on flame geometry.

- Flame angle: The flame angle refers to the inclination or deviation of the flame from the vertical or horizontal axis. It indicates the direction in which the flame propagates or spreads. The flame angle can vary depending on fuel injection angle, combustion characteristics, and external influences such as wind or airflow.

- Flame base diameter: The flame base diameter represents the diameter of the flame at its lowermost point, where it emerges from the fuel source or nozzle.

- Flame front: The flame front represents the leading edge of the zone where the combustion process occurs. It is the region where the unburned fuel interacts with the oxidizer to sustain the flame. The shape and behavior of the flame front can vary depending on factors such as fuel composition, turbulence, and mixing patterns. The characteristics and dynamics of the flame front may differ based on variables including fuel composition, turbulence levels, and patterns of mixing.

#### **4.2. Literature review on the study of jet flame geometrical features**

Several authors have explored the geometry of jet flames using experimental and theoretical approaches. Hawthorne et al. (1949) conducted a study on turbulent vertical flames of various fuels, proposing an inverted circular cone shape to represent jet flames. This conical shape has been supported by subsequent researchers such as Odggard (1983), Turns (1991), Schefer et al. (2004), and Schefer et al. (2007). Baron (1954) suggested a shape resembling a vertical ellipse for turbulent vertical flames

without significant buoyant force. This elliptical shape was compared to a photograph of a small-scale city-gas flame by Whol et al. (1949), but it is important to note that the characteristics of this flame differed considerably from those of real accidental jet fires, which are typically larger and associated with supersonic exit velocities. The cylinder shape has also been proposed to define jet flames, supported by authors including Odggard (1983), Schuller et al. (1983), Sonju and Hustad (1984), Hustad and Sonju (1986), Bagster, and Schubach (1996), based on experimental and theoretical studies of subsonic jet fires. Another proposed shape is a frustum of a cone, suggested by Kalghatgi (1983), Chamberlain (1987), and Johnson et al. (1994). However, while this shape can describe certain types of flames, it does not accurately represent the contour of a real accidental vertical jet fire in still air.

Major number of Existing research primarily focuses on flares or subsonic jet fires, which have distinct conditions that differ considerably from accidental jet fires. Limited research exists on the shape of large-scale supersonic hydrocarbon jet fires, resulting in inadequate understanding. The width of a jet flame is influenced by factors such as mass flow rate, dimensionless heat release, stagnation pressure, and Froude number. However, most existing models describing flames based on centerline trajectory do not account for the width of the jet flame, and formulations for jet flame width primarily focus on hydrogen flames or subsonic jet fires. Various formulations have been suggested to estimate the trajectory, vertical displacement, and horizontal displacement of a jet flame in different scenarios, including horizontal jet flames, jet flames under crosswind conditions, and flares.

The literature survey also revealed the interest in working with LPG due to its involvement in a significant percentage of jet fire events recorded in European accident databases. Overall, the available studies have aimed to investigate the geometry of jet flames and develop methodologies to estimate flame size and shape, with particular attention given to LPG as a fuel in jet fire incidents.

This section of the thesis delves into three significant aspects pertaining to fire behavior, namely Jet fire lift-off correlations, Flame reach correlations, and Flames elevation. Jet fire lift-off correlations investigate the interdependencies between various characteristics of a jet fire, such as fuel properties and flow rate, and the specific height

at which the flame separates from the nozzle. By comprehending and analyzing these correlations, valuable insights into the behavior of jet fires can be gained, enabling the prediction of lift-off height under diverse conditions. Flame reach correlations concentrate on comprehending the intricate relationship between flame length and factors including fuel properties, release rate, and wind velocity. This knowledge serves to estimate the maximum distance over which a flame can propagate from its ignition source. Furthermore, Flames elevation encompasses the vertical extent to which a fire extends. This elevation is influenced by an array of factors, such as heat release rate, ventilation conditions, and fuel properties. Acquiring a comprehensive understanding of flames elevation is essential for evaluating fire hazards and formulating effective fire protection measures. By investigating these aspects, a deeper understanding of fire behavior is obtained, facilitating the development of robust fire safety strategies and risk management protocols in various domains.

#### **4.1.1. Jet Flame Lift-off correlations**

Previous studies have proposed various expressions for the lift-off distance in vertical and horizontal jet fires. However, these expressions tend to overestimate the lift-off values for horizontal jet flames, and the influence of fuel exit velocity on lift-off is found to be smaller in the present experimental data. Lift-off distance has been correlated by different authors for both vertical jet flames (Santos and Costa, 2005; Rokke , 1994) and horizontal jet flames (Wang ., 2019), considering normalized variables of fuel jet exit velocity and nozzle diameter.

Kalghatgi (1984) proposed an expression to predict vertical lift-off distances, which involved the Reynolds number and a dimensionless flow parameter. The reach of a jet flame refers to the horizontal distance covered by the flame from the nozzle and can vary based on factors such as fuel flow rate, burner design, fuel properties, and ambient conditions. The momentum of the fuel jet and its interaction with the surrounding air play a significant role in determining the flame reach. Increasing the fuel flow rate enhances the momentum of the jet, resulting in a longer flame reach.

To understand the flame reach distance, three correlations were reviewed. The first correlation, by Rokke (1994) and Sonju and Hustad (1984), examined the Froude

number, which relates inertia forces to gravitational forces acting on the flame. This dimensionless number helps assess the flame's horizontal propagation ability. The second correlation considered the  $Q^*$  dimensionless number, which incorporates heat release rate, flame height, and ambient conditions to estimate flame reach. It provides insights into the flame's behavior in different environments. Finally, the  $U^*$  dimensionless number was analyzed, combining wind velocity, characteristic length, and flame speed to determine flame reach. These studies on the Froude number,  $Q^*$  dimensionless number, and  $U^*$  dimensionless number contribute to our understanding of flame reach and assist in the development of effective fire safety strategies (Bradley et al., 2016).

### 4.3. Experimental tests

To thoroughly characterize the flame of the jet fire, two distinct sets of experiments were conducted, categorized as Test Group 3 and Test Group 4 in Chapter 3 of the study. The objective of Test Group 3 was to explore and analyze the temperature variations within the flames. Two specific tests were designed and executed, focusing on measuring and characterizing the temperature profile of the flames using nozzle diameters of 6 mm and 8 mm. These tests provided valuable insights into the thermal behavior of the flames under different nozzle configurations. On the other hand, Test Group 4 aimed to investigate the geometrical features of the flames, including size, shape, and area, and their dependency on release pressure and divergent gas flow rates. To comprehensively analyze these parameters, ten different experiments were carefully designed and conducted. The variations in release pressure and divergent gas flow rates allowed for a systematic assessment of their influence on the geometrical characteristics of the flames. It was crucial to conduct these tests separately from Test Group 3 because the presence of thermocouples during the measurement process could potentially impact the flame geometry. Therefore, isolating the experiments ensured accurate characterization of the flame's geometrical features. By conducting these separate sets of experiments, the study was able to effectively investigate both the thermal and geometrical aspects of the jet fire flame. This comprehensive approach provided valuable insights into the behavior and characteristics of the flame under different



nozzle configurations, release pressures, and gas flow rates. The findings from Test Group 3 and Test Group 4 significantly contribute to the understanding of jet fire dynamics and are pivotal in enhancing fire safety measures and risk management strategies in relevant industries.

#### 4.3.1. Flames temperature

The release conditions for temperature profile test are shown in Table 4-1.

Table 4-1. Flame temperature assessment tests: release conditions.

Experiment Title	Exit Nozzle Diameter (mm)	Release Regime	Gas release Pressure (barg)	Release mass flow rate (kg/s)
JFT-191114-2-T6	6	Subsonic	0,546	0.012
JFT-191114-2-T8	8	Sonic	0,790	0.016

Looking at a jet fire, three clearly distinct zones are identified inside the flame. These zones are characterized by different color, shape and behavior (Figure 4-4).

- Blue zone: it is the closest zone to the nozzle, it has a blue color, the shape is cylindrical and orientation is mostly horizontal (i.e., the same direction that the one of the exit jet), suggesting that this zone is dominated by momentum forces.
- Middle zone: color of the flame is orange and buoyancy forces start to smoothly change the shape and the orientation of the flame.
- Front Zone: it is the most distant from the nozzle, the color is bright yellow, higher buoyancy effects are present and shape is undefined.

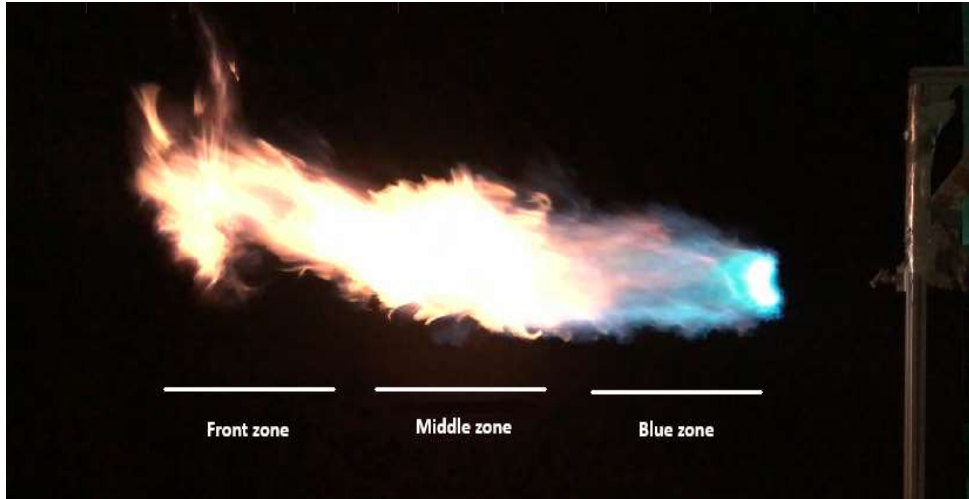


Figure 4-1. Horizontal jet fire blue zone, middle zone, and front zone (Foroughi, 2019).

#### 4.3.2. Flame geometry assessment

Horizontal jet fire geometry is assessed by defining diverse characteristic dimensions (Figure 4-2) the lift-off distance  $S$ , which concerns the flameless distance between the nozzle orifice and the base of the flame; the flame horizontal projection ( $R$ ); (related to the total length and reach), obtained summing the lift-off distance plus the horizontal projection; the flame vertical height ( $W$ ) and the projected flame area ( $A$ ), which represents the surface covered by the visible flame where the combustion reaction occurs (Palacios et al., 2020).

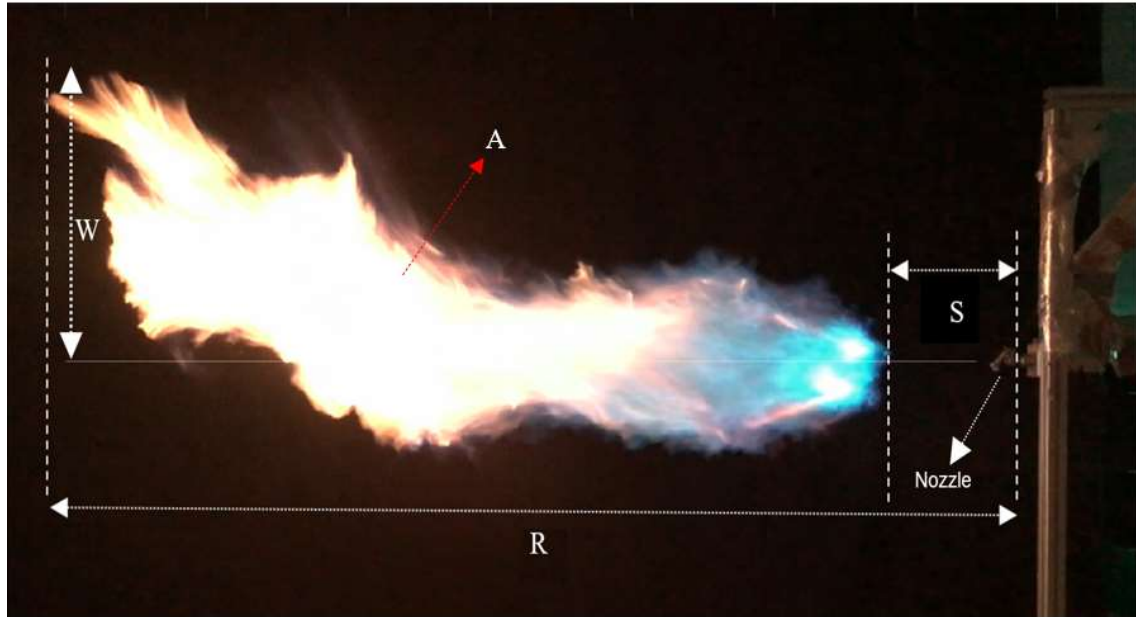


Figure 4-2. Horizontal jet fire geometrical parameters: image obtained by visible camera.

In order to measure these parameters several experiments were performed using an 8mm diameter nozzle at different operating pressures (Table 4-2), registering images with IR and visible camera positioned perpendicularly to jet flame axis.

A program developed by CERTEC is able to define flame contours analyzing IR images, giving as output the geometrical parameters of a flame. Hence, for each pressure, three frame per second for all the duration of the experiment, were used as input image of the CERTEC program; a sample of the type of images are collected and plotted in Figure 4-4.

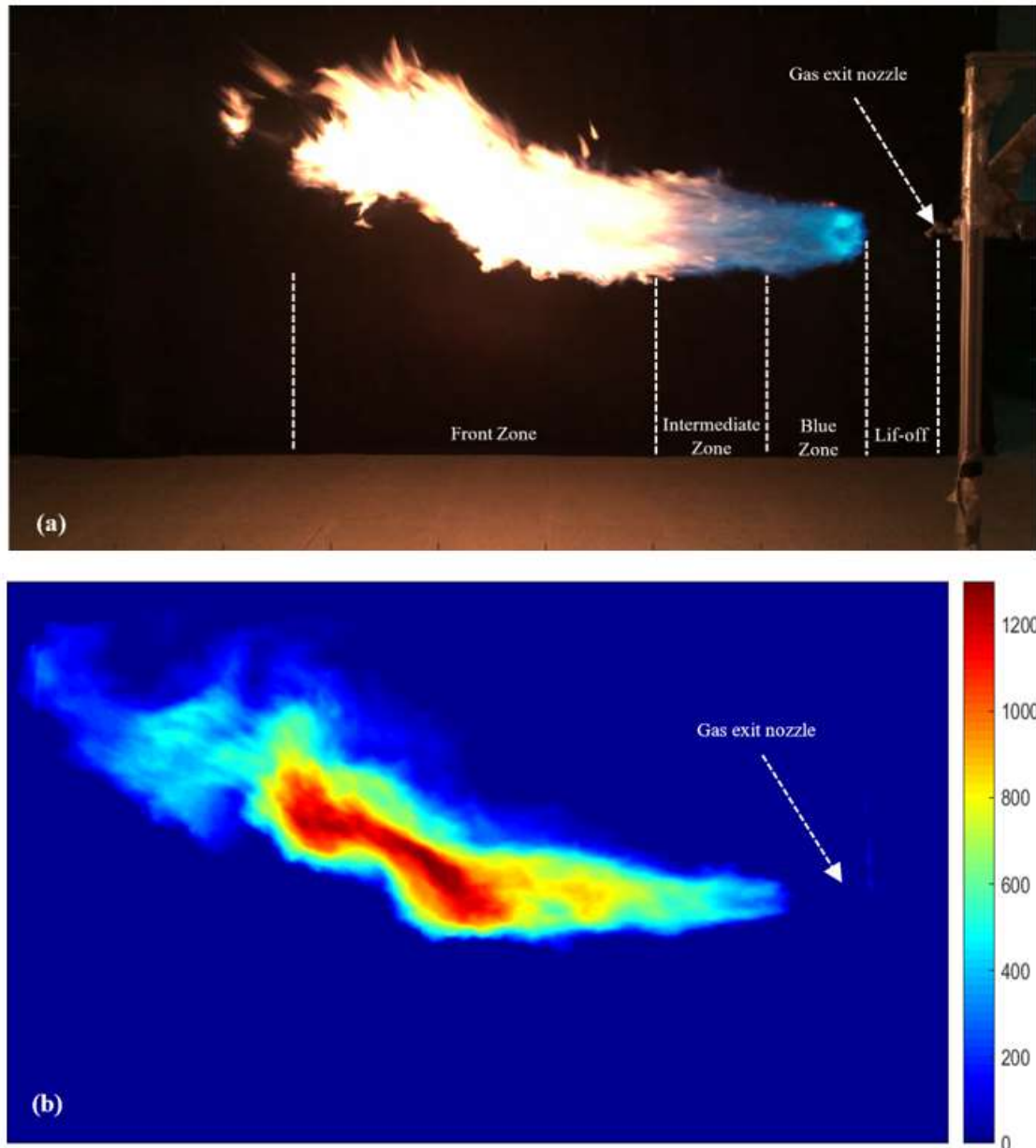


Figure 4-3. A free jet fire: (a) Visible image; (b) Infrared image (temperature in °C).

Figure 4-4 illustrates the relationship between time and two variables: gas release pressure (represented by the blue curve on the left side of the graph) and release mass flow rate of propane (represented by the orange curve on the right side of the graph). In these experimental tests, the data corresponds to the experimental conditions outlined in Table 4-1, which provides details about the tests conducted to assess flame geometry. Each experimental test has a duration of 60 seconds. Looking at the blue curve representing gas release pressure, we observe that as time progresses, the pressure of the released gas changes. The specific values of the gas release pressure are indicated on the left side of the graph. On the right side of the graph, the orange curve

represents the release mass flow rate. The release mass flow rate is the amount of gas that is released per unit of time. As the gas release pressure increases, the release mass flow rate also increases. This relationship implies that the mass flow rate is directly influenced by the released pressure.

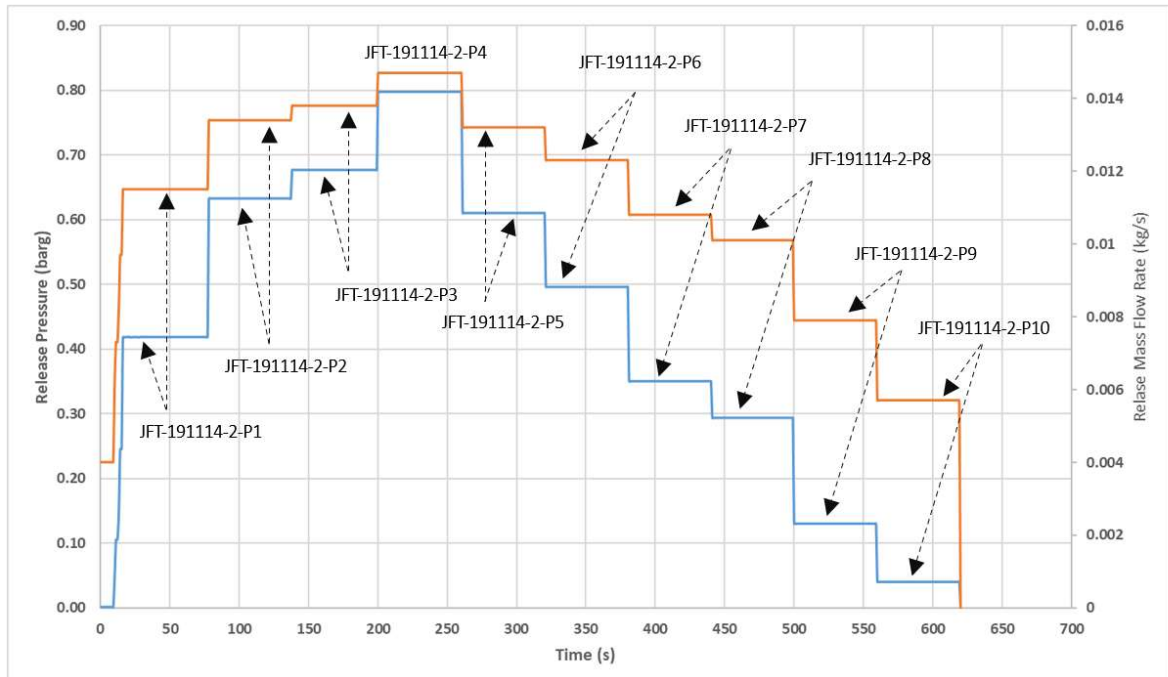


Figure 4-4. Release pressure/mass flow rate of propane during the tests for flame geometry assessment.

Looking at the blue curve representing gas release pressure, we observe that as time progresses, the pressure of the released gas changes. The specific values of the gas release pressure are indicated on the left side of the graph. On the right side of the graph, the orange curve represents the release mass flow rate. The release mass flow rate is the amount of gas that is released per unit of time. As the gas release pressure increases, the release mass flow rate also increases. This relationship implies that the mass flow rate is directly influenced by the released pressure.

As time progresses, the gas release pressure shows fluctuations, indicating variations in the pressure of the released gas. The corresponding values of the gas release pressure are clearly depicted on the left side of the graph. Simultaneously, the release mass flow rate, represented by the orange curve on the right side, demonstrates a direct correlation with the gas release pressure. As the gas release pressure increases, the

release mass flow rate also increases, suggesting a strong positive relationship between these two variables. This observation implies that the pressure at which the gas is released directly impacts the rate at which the gas flows out. The graph effectively visualizes these temporal changes in gas release pressure and release mass flow rate, emphasizing their interconnected nature.

In this experimental setup, it is important to note that the test labeled as JFT-191114-2-P4 corresponds to a sonic gas release, while the remaining experimental tests are classified as subsonic. This distinction is crucial as it indicates that the gas release in the JFT-191114-2-P4 test occurs at supersonic velocities. Therefore, the findings and trends observed in this particular test may differ from those observed in the subsonic tests.

Overall, the graph visually presents the temporal variation of both gas release pressure and release mass flow rate during the experimental tests, highlighting the direct relationship between the two variables.

Table 4-2. Experimental conditions of the tests for flame geometry assessment.

Nozzle diameter = 8 mm				
Experiment Title	Pressure [bar g]	Release mass flow rate [kg/s]	Duration of experiment [s]	Release Regime
JFT-191114-2-P1	0.42	0.0115	60	Subsonic
JFT-191114-2-P2	0.63	0.0134	60	Subsonic
JFT-191114-2-P3	0.68	0.0138	60	Subsonic
JFT-191114-2-P4	0.80	0.0147	60	Sonic
JFT-191114-2-P5	0.61	0.0132	60	Subsonic
JFT-191114-2-P6	0.50	0.0123	60	Subsonic
JFT-191114-2-P7	0.35	0.0108	60	Subsonic
JFT-191114-2-P8	0,29	0.0101	60	Subsonic
JFT-191114-2-P9	0.12	0.0079	60	Subsonic
JFT-191114-2-P10	0.04	0.0057	60	Subsonic

Table 4-3. Parameter range spanning the present experimental data.

Pressure Range [barg]	Average Stagnant Pressure [barg]	Exit Nozzle diameter [m]	V [m/s]	$\delta = v / SL$ [m]	$\nu$ (Nu) for Propane [m <sup>2</sup> /s]	Thermal diffusivity (m <sup>2</sup> /s)	$S_L$ for Propane [m/s]	$Re_D$	Fr
P1	0.42	8	202.64	3.42E-05	1.47E-05	5.7E-06	0.43	3.72E+05	5.23E+05
P2	0.63	8	235.56	3.42E-05	1.47E-05	5.7E-06	0.43	4.33E+05	7.07E+05
P3	0.68	8	242.27	3.42E-05	1.47E-05	5.7E-06	0.43	4.45E+05	7.48E+05
P4	0.79	8	250.75	3.42E-05	1.47E-05	5.7E-06	0.43	4.75E+05	8.01E+05
P5	0.61	8	233.25	3.42E-05	1.47E-05	5.7E-06	0.43	4.29E+05	6.93E+05
P6	0.50	8	215.44	3.42E-05	1.47E-05	5.7E-06	0.43	3.96E+05	5.91E+05
P7	0.34	8	189.33	3.42E-05	1.47E-05	5.7E-06	0.43	3.48E+05	4.57E+05
P8	0.29	8	179.56	3.42E-05	1.47E-05	5.7E-06	0.43	3.30E+05	4.11E+05
P9	0.13	8	139.61	3.42E-05	1.47E-05	5.7E-06	0.43	2.57E+05	2.48E+05
P10	0.04	8	134.55	3.42E-05	1.47E-05	5.7E-06	0.43	2.47E+05	2.31E+05

#### 4.4. Methodology of image processing

Image processing techniques can be employed to analyze and extract information about jet flame geometry from images or video footage of jet fires. The division of an image into meaningful structures using image segmentation is an essential step for the analysis of the flames. The segmentation of the flames areas of interest can be accomplished based on infrared imaging (IR) by applying different techniques. According to Acharya (2005) and Prakash (2018), Table 4-4 outlines of the steps involved in jet fire image processing for jet flames geometry analysis.

It is worth noting that the specific image processing algorithms and techniques utilized may vary depending on the characteristics of the images, the desired level of analysis, and the available software or programming tools. The complexity of the analysis can range from simple measurements to more sophisticated image processing and computer vision techniques. This methodology provides a general framework for infrared image processing of jet fires.

Table 4-4. Steps involved in jet fire image processing for jet flames geometry analysis.

Step	Description
Image Acquisition	Obtain high-quality images or video footage of the jet fire using suitable cameras or imaging devices. Ensure proper lighting conditions and capture the flame from different angles for comprehensive analysis.
Pre-processing	Pre-process the acquired images or frames to enhance the image quality and remove noise or artifacts. This may involve operations such as image denoising, contrast enhancement, and color correction to improve the visibility and clarity of the flame.
Segmentation	Apply segmentation techniques to separate the flame region from the background or other objects present in the image. This can be achieved using thresholding, edge detection, or region-based segmentation algorithms to create a binary mask representing the flame region.
Flame Contour Extraction	Extract the contour of the segmented flame region to represent its shape and boundary. This can be accomplished using algorithms like the Canny edge detection or active contour models to trace the boundary of the flame.
Flame Height Measurement	Determine the flame height by analyzing the vertical extent of the segmented flame region. This can be done by measuring the distance from the flame base to the flame tip or by using reference scales or markers in the image for calibration.
Flame Area Analysis	Calculate the area occupied by the flame by quantifying the number of pixels within the segmented flame region. This provides an estimation of the flame size or footprint.
Flame Shape Analysis	Analyze the extracted flame contour to derive geometric features such as flame width, flame aspect ratio, or flame curvature. This can help characterize the flame shape and its variations along different sections.
Quantitative Analysis	Perform quantitative analysis on the extracted flame geometry parameters to understand flame behavior, stability, and variations under different conditions. This may involve statistical analysis, trend analysis, or comparison with reference values or models.
Visualization and Presentation	Visualize the processed results, such as flame contours, height measurements, and shape analysis, in graphical or tabular form. Present the findings to facilitate understanding, comparison, and communication of the jet flame geometry characteristics.

In the field of fire imaging, the division of an image into meaningful structures using image segmentation is an essential step for early fire detection systems and flame analysis. The segmentation of specific flame areas of interest can be accomplished based



on infrared imaging (IR) through different techniques that vary depending on the features of the images.

In the present work, the methodology involved three main steps:

- 1) Creation of a segmentation mask
- 2) Calculation of discretization areas
- 3) Obtaining the main geometrical values

#### **4.4.1. Creation of a segmentation mask**

Segmentation of jet fire images plays a crucial role in studying the geometrical features of jet fires. It involves the process of separating the flame region from the background in the images, allowing for quantitative analysis and measurement of various flame parameters. Table 4-5 outlines an overview of the segmentation techniques commonly used for studying jet fire geometrical features.

After segmenting the flame region, various geometrical features can be extracted for quantitative analysis. These features may include flame area, flame length, flame width, flame perimeter, flame centroid, and flame shape parameters (e.g., circularity or elongation). These measurements provide valuable information for studying the geometrical characteristics of jet fires and understanding their behavior.

It is important to select an appropriate segmentation method based on the specific characteristics of the jet fire images, such as flame intensity, background complexity, and image quality. The choice of technique may also depend on the available computational resources and the accuracy requirements of the study. Researchers typically validate the segmentation results by comparing them with manual annotations or ground truth data. This helps ensure the accuracy and reliability of the segmentation process. It is also important to consider potential challenges, such as flame flickering, smoke interference, or low image resolution, which can impact the segmentation accuracy and require additional preprocessing or advanced techniques.

Table 4-5. Commonly techniques for used segmentation of jet fire geometrical features (Acharya (2005) and Prakash (2018)).

Step	Description
Thresholding	Thresholding is a basic image segmentation technique where a fixed threshold value is applied to the image to separate the flame region from the background. The choice of the threshold value depends on the characteristics of the image, such as flame intensity and background noise. Simple thresholding methods like global thresholding or adaptive thresholding can be used for flame segmentation.
Edge Detection	Edge detection techniques identify boundaries or edges between different regions in the image. In the context of jet fire segmentation, edge detection algorithms can be employed to extract the flame edges. Popular edge detection algorithms include the Canny edge detector, Sobel operator, or Laplacian of Gaussian (LoG) filter. Once the edges are detected, they can be connected to form closed contours representing the flame region
Region-based Segmentation	Region-based segmentation techniques divide the image into homogeneous regions based on intensity or color similarity. Methods like region growing, watershed segmentation, or mean-shift segmentation can be used to group pixels or regions with similar flame characteristics. These algorithms exploit the spatial coherence of flame pixels to separate the flame region from the background.
Machine Learning-based Segmentation	Machine learning approaches, particularly deep learning-based methods, have shown promising results in image segmentation tasks. Convolutional Neural Networks (CNNs) can be trained on annotated datasets to automatically segment jet fire images. U-Net, SegNet, and Mask R-CNN are popular architectures used for semantic segmentation tasks, including flame segmentation.
Hybrid Approaches	Hybrid segmentation techniques combine multiple methods to achieve better segmentation accuracy. For instance, combining thresholding with edge detection or region-based segmentation can help overcome the limitations of individual techniques and improve the segmentation results.

Creating a segmentation mask for infrared image processing of jet fires can be a challenging task due to the dynamic nature of the flames and potential variations in background conditions.

In this work, as a first step, a threshold temperature ( $T_h$ ) segmentation technique was used to separate the jet flame contour of the background area (Figure 4-5); any point  $(x,y)$  of the image, according to a threshold function such as  $f(x,y) > T_h$ , is called an

object point; otherwise, the point is called background point. So, by the global thresholding, the segmented image  $g(x,y)$ , is given by:

$$g(x,y) = 1, \text{ if } f(x,y) > Th, \text{ 0 if } f(x,y) \leq Th \quad (4-1)$$

Moreover, a normalization step was performed in the present algorithm; the  $Th$  value was used as a minimum value ( $T_{min}$ ), and a max value ( $T_{max}$ ) for each image was calculated using a maximization function to normalize the image according to  $T$ . In fact,  $I$  is an image that uses temperature values (K) as pixels. Then, every value of the image is normalized with Equation 4-2 obtaining the normalization matrix of the IR image  $T_{Norm}$ :

$$T_{min} = T$$

$$T_{max} = \max(I) \quad (4-2)$$

$$T_{Norm} = (I - T_{min}) / (T_{max} - T_{min})$$

It is important to remark that any point  $(x,y)$  of the image, according to a threshold function such as  $f(x,y) > Th$ , is called an object point; otherwise, the point is called background point. In other words, the segmented image  $g(x,y)$ , is given by:

$$g(x,y) = \begin{cases} 1, & \text{if } f(x,y) > Th \\ 0, & \text{if } f(x,y) \leq Th \end{cases} \quad (4-3)$$

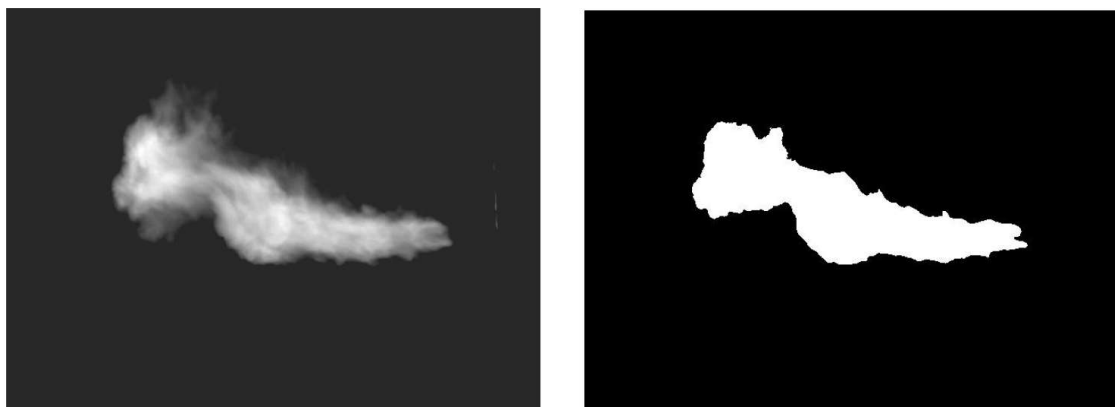


Figure 4-5. Flame contour of a current experimental horizontal jet flame obtained with the threshold segmentation technique.

The process given in Equation 4-1 is referred to as global thresholding. The term local or regional thresholding is sometimes used to denote variable thresholding in which the value of  $T_h$  at point  $(x,y)$  in an image  $(I)$  depends on the properties of neighborhood of  $(x,y)$ . Moreover, that point  $(x,y)$  corresponds to a temperature value of the matrix obtained from the IR image  $I$ . The most challenging part of using this segmentation technique is to obtain the accurate temperature threshold value for each test.

#### 4.4.2. Calculation of the discretization areas

Infrared image processing of jet fires typically involves discretizing the image into smaller areas or regions to facilitate analysis and extraction of relevant information. The choice of discretization areas depends on the specific objectives of the analysis and the characteristics of the images.

Table 4-6 illustrates a few common approaches for discretizing infrared images of jet fires. The selection of discretization areas should be guided by the specific analysis objectives and the nature of the jet fire images.

The next stage was to calculate the discretization of flames zones according to the thermal temperature ranges, considering the three temperature zones found in the jet fires (Foroughi et al., 2021): blue (beginning) zone, middle zone and flame front zone. Two steps were performed: quantize a thermal segmentation approach (Tyagi, 2018) and apply a Gaussian filter distribution (Thilagamani et al., 2014).

The present purpose was to segment the three internal flame zones with multiple threshold levels and values. Three quantization levels were specified in the matrix image to convert IR image to output-segmented image. Figure 4-6, Figure 4-7, and Figure 4-8 present measurements related to jet flame characteristics obtained through a discretization technique based on the applied methodology.

In Figure 4-6, the area of the jet flame is depicted, providing insights into the spatial extent of the flame. Figure 4-7 showcases the angle of the flame front in relation to a horizontal line originating from the nozzle, offering information about the orientation of the flame.

Lastly, Figure 4-8 illustrates distance measurements, including lift-off height (the distance from the nozzle to the point where the flame detaches from the nozzle), flame length (the extent of the flame along its axis), and flame elevation (the vertical distance from the nozzle to the highest point of the flame). These measurements are derived through the discretization technique and contribute to a comprehensive understanding of the jet flame's geometry and behavior.

Table 4-6. Common approaches for discretizing infrared images of jet fires (Acharya (2005) and Prakash (2018)).

Step	Description
Grid-based Discretization:	<ul style="list-style-type: none"> <li>- Divide the infrared image into a regular grid of equally-sized cells or regions.</li> <li>- The size of the grid cells can be adjusted based on the desired level of detail and computational resources.</li> <li>- Each grid cell represents a discrete area for further analysis, such as flame temperature measurement or flame area estimation.</li> <li>- Grid-based discretization enables systematic analysis of the entire image.</li> </ul>
Region-based Discretization:	<ul style="list-style-type: none"> <li>- Identify distinct regions or objects within the infrared image that are relevant to the jet fire analysis.</li> <li>- This can be done using segmentation techniques, as discussed earlier, to isolate the flame region or other areas of interest.</li> <li>- Each segmented region becomes a discrete area for subsequent analysis, such as flame shape characterization or temperature profiling.</li> <li>- Region-based discretization allows for focused analysis on specific areas of the image with meaningful information.</li> </ul>
Feature-based Discretization:	<ul style="list-style-type: none"> <li>- Identify key features or landmarks within the infrared image that are indicative of jet fire behavior or properties.</li> <li>- These features can include flame edges, flame tips, areas of high temperature gradients, or other salient characteristics.</li> <li>- Discretize the image by considering these features as discrete areas for further analysis and measurement.</li> <li>- Feature-based discretization provides a more selective approach to focus on specific aspects of the jet fire.</li> </ul>

Firstly, quantize an image is a technique that according to specified quantization levels and output values can segment region areas. In that case, the present purpose was to segment the three internal flame zones with multiple threshold levels and values. For this reason, three quantization levels specified in the matrix image to convert IR image into an output-segmented image were used.

Figure 4-1 shows the main geometrical features thus obtained from each jet flame image: the lift-off distance ( $S$ ), the total jet flames reach (horizontal projection,  $R$ ) and the jet flame elevation ( $W$ ). Due to the large quantity of similar individuals, a Gaussian variable or a Gaussian process, such as noise, heat, quantum etc., can approximate variety variables.

The Gaussian filter has the highest value in the centre of a standard deviation, decreasing rapidly in the area three times of standard deviation away from the centre. With these properties, a Gaussian filter was used as a low pass filter for smoothing or de-noising. Finally, an improved and efficient approach based on Gaussian and Gabor Filter (Thilagamani et al., 2014) reads the given input image and performed filtering and smoothing operations. The region occupied by the object was extracted from the image by performing various operations like bilateral filtering, Edge detection, Clustering, and Region growing.

In Figure 4-9 we can observe an example of the outcome achieved by employing the discretization technique based on region growing segmentation to measure the area of a horizontal jet fire in an IR image. The image has been segmented into three distinct regions representing the different areas of the jet flame. The blue zone corresponds to one region, the middle zone is depicted in yellow, and the flame front zone is highlighted in red. By discretizing the flame into these regions, we can quantitatively analyze and measure the individual areas, providing valuable information about the spatial distribution and characteristics of the jet fire. This approach enhances our understanding of the flame's behavior and enables more precise assessments for fire safety and risk management applications.

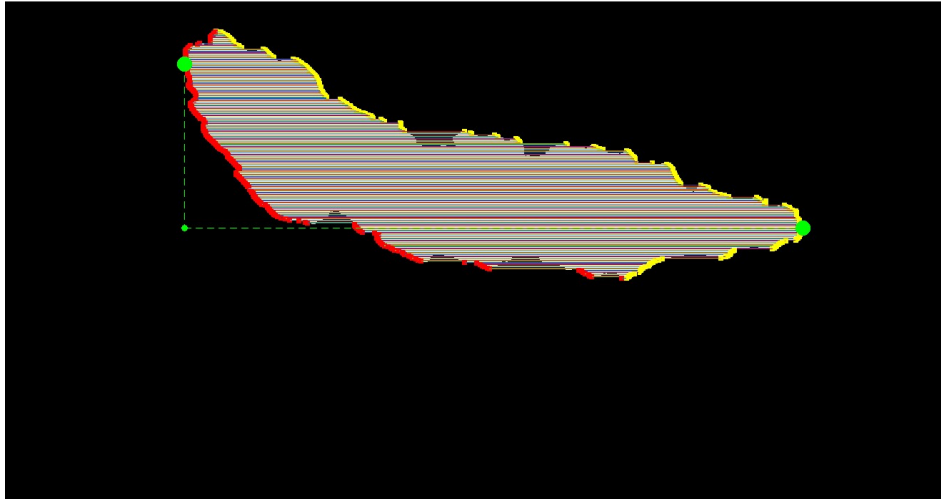


Figure 4-6. Area measurement from the discretization technique.

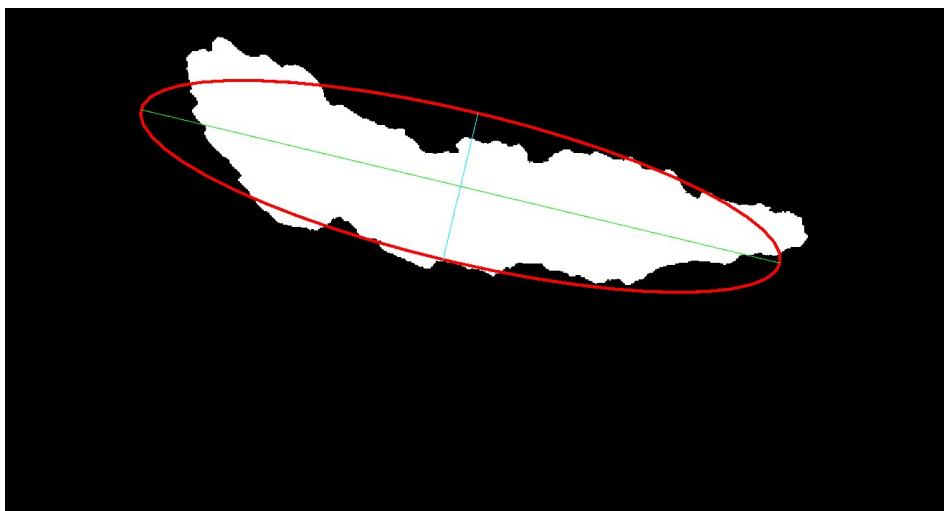


Figure 4-7. Angle measurement from the discretization technique.

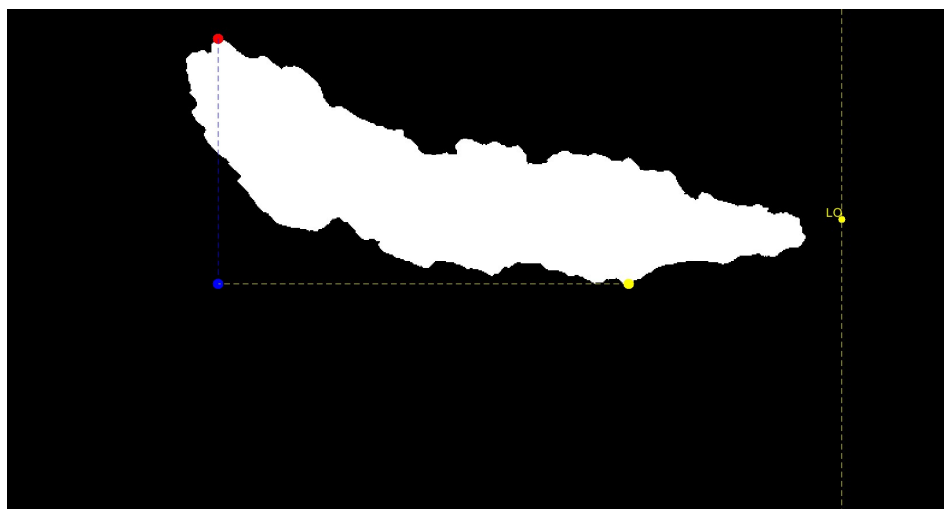


Figure 4-8. Distance measurement from the discretization technique.

Figure 4-9 represents an example of the original IR image with the temperature interval range. A second step was then performed applying a Gaussian filter, expressed as the normal distribution, which is the limiting distribution of the normalized sum of random variables. The Gaussian filter has the highest value in the center of a standard deviation, decreasing rapidly in the area three times of standard deviation away. A Gaussian filter was used as a low pass filter for smoothing or de-noising. Finally, an improved and efficient approach based on Gaussian and Gabor Filter (Thilagamani and Shanthi, 2014) read the given input image and performed filtering and smoothing operations. The region occupied by the object was extracted from the image by performing various operations like bilateral filtering, Edge detection, Clustering, and Region growing.

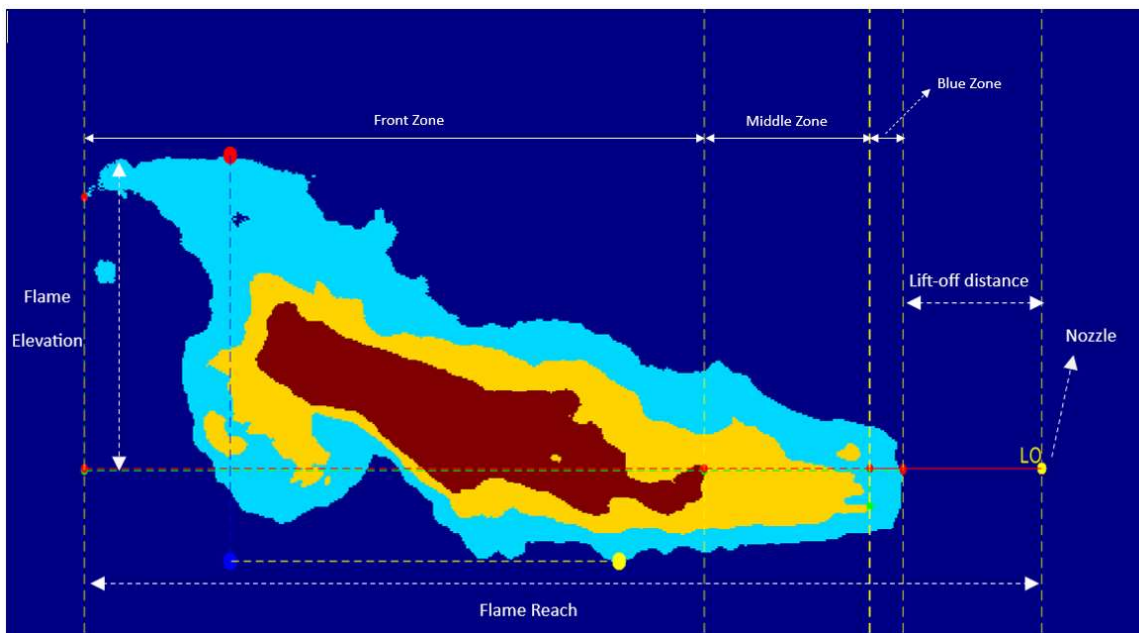


Figure 4-9. The three jet flame areas obtained from the discretization technique. The blue, middle and front zones of the flame are also indicated.

#### 4.4.3. Obtaining the main geometrical measurements

The main geometrical features that were obtained from each jet flame image through the discretization technique are shown in Figure 4-1: the total jet flame length in the horizontal projection ( $R$ ), the lift-off distance ( $S$ ), the flame elevation ( $W$ ), the flame area and angle of the flame.



## 4.5. Results and discussion

### 4.5.1. Results of flame temperatures experiments

Thermocouple temperatures (TCB) and release pressure (measured with pressure transmitter) (PT) during time are registered, and profiles are plotted as it is shown in Figure 4-10, Figure 4-11 and Figure 4-12 during the test JFT-191114-2- T8 in blue, middle and front zones of the flame.

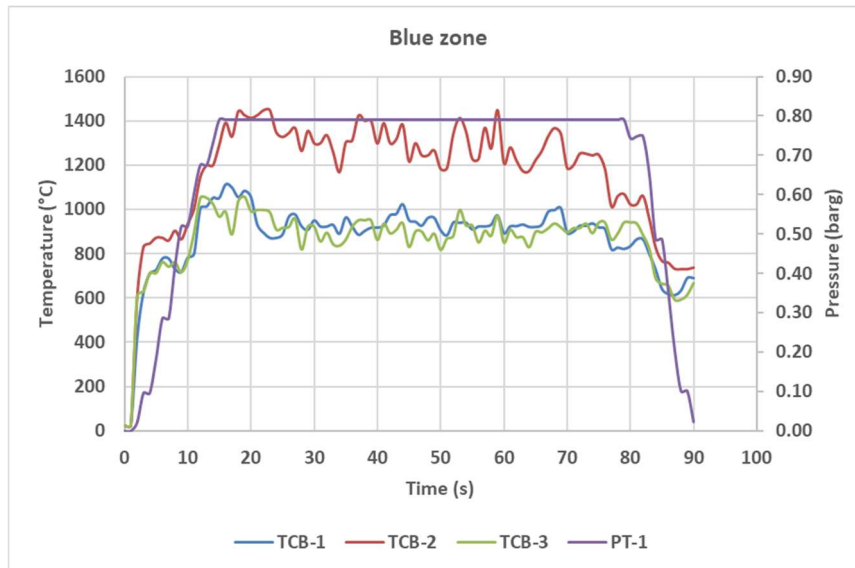


Figure 4-10. Plots of thermocouple temperatures (located in blue zone) and gas release pressure of JFT-191114-2- T8.

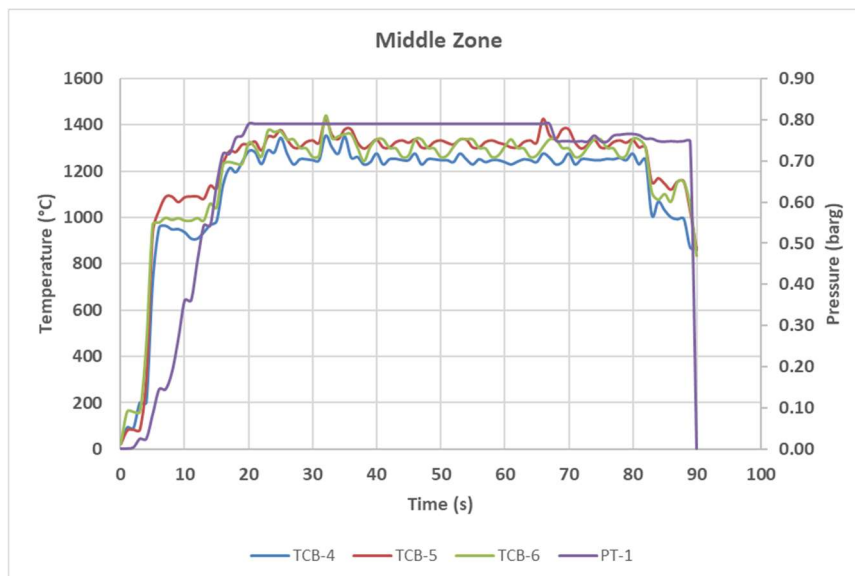


Figure 4-11. Plots of thermocouple temperatures (located in middle zone) and gas release pressure of JFT-191114-2- T8.

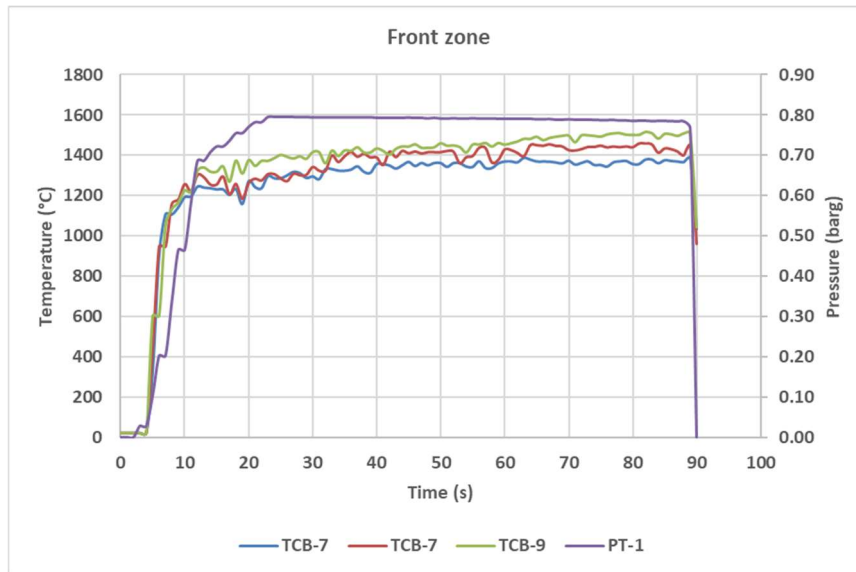


Figure 4-12. Plots of thermocouple temperatures (located in front zone) and gas release pressure of JFT-191114-2- T8.

Thermocouple temperatures (TCB) and release pressure (PT) during time are registered, and profiles are plotted as it is shown in Figure 4-13, Figure 4-14 and Figure 4-15 during the test JFT-191114-2- T8 in blue, middle and front zones of the flame.

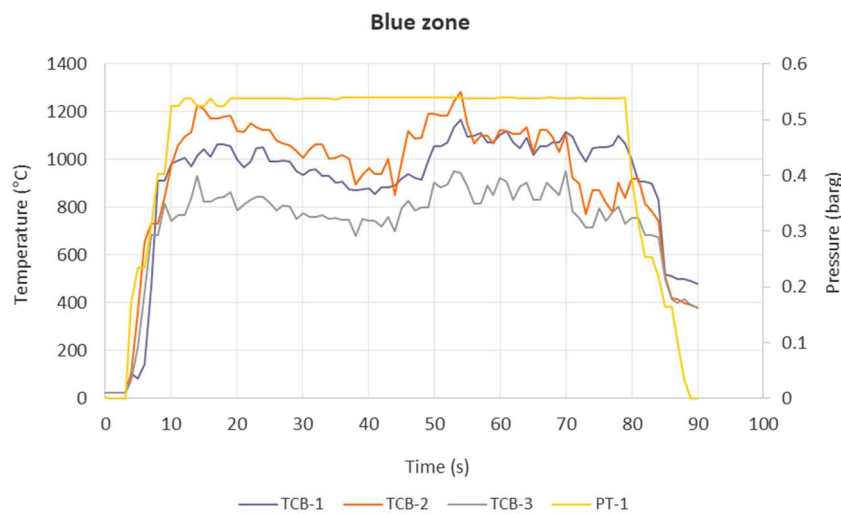


Figure 4-13. Plots of thermocouple temperatures (located in blue zone) and gas release pressure of JFT-191114-2- T6.

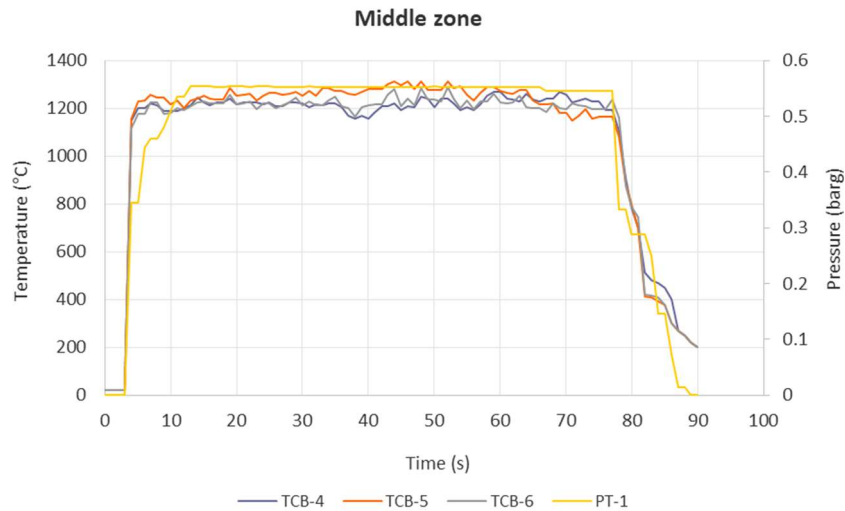


Figure 4-14. Plots of thermocouple temperatures (located in middle zone) and gas release pressure of JFT-191114-2- T6.

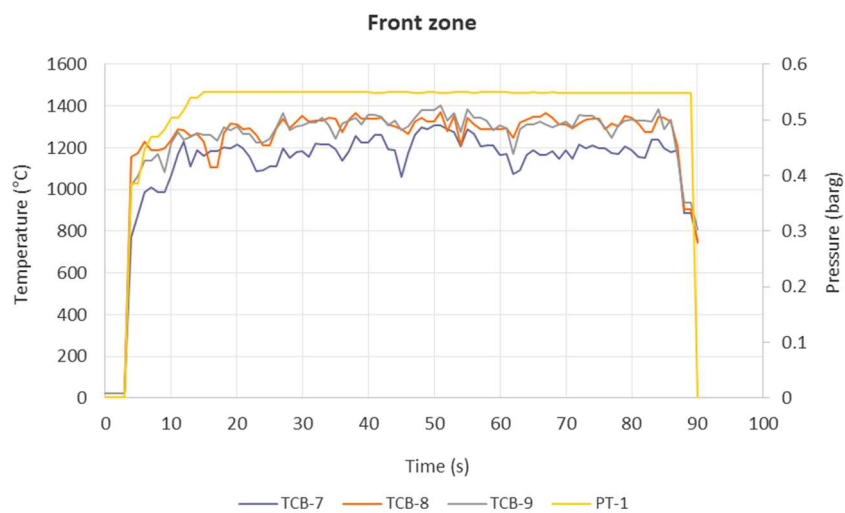


Figure 4-15. Plots of thermocouple temperatures (located in front zone) and gas release pressure of JFT-191114-2- T6.

The evolution with time of the temperature in each zone is also shown, more clearly, in Figure 4-10 to Figure 4-15. A certain quick oscillation of the value measured by the three thermocouples must be attributed to the high turbulence of the flames. It can be observed that there is a temperature significantly higher in one of the thermocouples in the blue zone.

As it can be seen in this figure, flame temperature is lower in the blue zone, sharply increases in the middle zone and varies smoothly in the front zone where it reaches the highest value. This behavior can be caused by the improvement in fuel/air mixing along

the jet fire axis, and by the progressive increase of gas temperature along the jet, since the fuel gas entering in the blue zone is colder than the gas entering in the middle and front zone (Gómez-Mares et al., 2009). The fuel/air mixing particularly affects the blue zone where high momentum forces are present. As it is shown in Figure 4-16, a presence of a visible “tunnel” inside the zone shows that probably no combustion is occurring especially in the jet axis; this observation is confirmed looking at temperature of blue zone TCB-3 thermocouple that shows lower values in both experiments. This phenomenon should be attributed to the fact that in this zone no enough air has been introduced yet to reach the lower flammability limit.



Figure 4-16. Presence of “tunnel” in the blue zone.

When pressure before the nozzle increases, flow rate increases as well and momentum forces become more dominant. As a consequence, flame length increases, flame height decreases, because momentum forces oppose buoyancy forces, and lift-off increases because higher exit velocity results in higher strain rate (Ab Aziz et al., 2020). These experimental results of flame geometry are consistent with those found in the literature.

#### 4.5.2. IR image measurement results

Table 4-7 displays the primary geometric characteristics extracted from each jet flame image using the discretization technique. The obtained measurements include the jet flame reach ( $R$ ), which represents the distance from the nozzle to the flame tip. Additionally, the lift-off distance ( $S$ ) is presented, indicating the distance between the nozzle and the base of the lifted flame. Furthermore, the flame elevation ( $W$ ) is

measured, representing the maximum vertical distance of the flame from a horizontal line originating from the nozzle center. These results correspond to the specific operating conditions outlined in Table 4-1, providing a comprehensive summary of the analyzed tests.

Table 4-7. The main geometrical features that were obtained from the IR image processing.

Pressure Range [barg]	Average Stagnant Pressure [barg]	Exit Nozzle diameter [m]	IR Flame Length [cm]	Elevation [cm]	Area [cm <sup>2</sup> ]	Angle [°]	Lift-off [cm]	Total Flame Length [cm]
P1	0.42	8	187	84	7989	21	21	208
P2	0.63	8	198	86	8964	22	25	223
P3	0.68	8	209	86	9058	22	24	234
P4	0.79	8	222	100	10071	21	30	252
P5	0.61	8	222	97	10464	24	24	245
P6	0.50	8	214	96	10667	25	21	236
P7	0.34	8	213	96	10927	23	20	233
P8	0.29	8	205	99	10053	27	20	225
P9	0.13	8	184	96	8044	34	18	202
P10	0.04	8	150	83	5967	32	16	166

According to Table 4-7, for a constant exit nozzle diameter, as fuel gas pressure increases its density increases as well and this implies logically a greater fuel flow rate feeding the fire. Therefore, the size of jet fire flames increases; this is clearly shown by the length of the flames and also by the length of the lift-off. As a result, the total flame reach (flames length plus lift-off) increases.

Table 4-8. Summary of parameter range spanning the present experimental data.

$P_i$ (bar abs)	$u$ (m/s)	$R$ (m)	$S$ (m)	$W$ (m)	$Fr$	$Re$
1.13 – 1.8	104 – 251	1.6 – 2.5	0.16 – 0.3	0.83 – 1	$1.3 \times 10^5$ – $8 \times 10^5$	$1.9 \times 10^5$ – $4.8 \times 10^5$

Table 4-7 and Table 4-8 presents the main geometrical features obtained from each jet flame image using the discretization technique. The measurements include the jet flame reach (R), lift-off distance (S), and flame elevation (W). The jet flame reach varies between 1.6 to 2.5 meters, while the lift-off distance ranges from 16 to 30 cm. Additionally, the flame elevation spans from 84 cm to 100 cm, representing the highest vertical distance of the flame from a horizontal line originating from the nozzle center.

These measurements were obtained under specific operating conditions, as summarized in Table 4-7 and Table 4-8. The release pressure of propane from the nozzle ranges from 1.04 to 1.8 bar, while the release velocity varies between 104 to 251 m/s. The Froude number ranges from  $1.3 \times 10^5$  to  $8 \times 10^5$ , and the Reynolds number ranges from  $1.9 \times 10^5$  to  $4.8 \times 10^5$ . These comprehensive measurements provide valuable insights into the geometric characteristics of the jet flames and their dependence on the operational parameters.

From the results obtained, a clear trend emerged indicating that an increase in pressure (and velocity) led to an increase in both the lift-off distance and the visible flame length. As the release pressure (and velocity) increased, the flames exhibited greater extension and reached higher distances from the nozzle. This observation suggests a direct relationship between the release conditions and the spatial characteristics of the flame, emphasizing the significant impact of pressure (and velocity) on the lift-off distance and the overall visible flame length.

These results were further utilized for comparison with existing correlations related to flame lift-off distance and flame reach. By comparing the obtained measurements with the established correlations, it was possible to assess the validity and accuracy of the existing models. This comparative analysis allowed for a deeper understanding of the relationship between the experimental results and the predictive capabilities of the current correlations. It provided valuable insights into the adequacy of the existing models in accurately predicting the lift-off distance and flame reach under the specific experimental conditions considered.

#### **4.6. Analyzing the prediction of lift-off, flame reach and elevation**

In this section of the thesis, three important aspects related to fire behavior were explored: Jet fire lift-off correlations, Flame reach correlations, and Flames elevation. Jet fire lift-off correlations investigate the relationship between the characteristics of a jet fire, such as fuel properties and flow rate, and the distance at which the flame detaches from the nozzle. By studying these correlations, we can gain insights into the behavior of jet fires and predict the lift-off length under different conditions. Flame reach correlations focus on understanding the relationship between flame length and factors such as fuel properties, release rate, and wind velocity. This knowledge helps estimate the distance that a flame can propagate from its source. Additionally, flames elevation refers to the vertical extent to which a fire extends. It is influenced by factors like heat release rate, ventilation conditions, and fuel properties. Understanding flames elevation is crucial for assessing fire hazards and developing effective fire protection measures. By examining these three aspects, we aim to contribute to a deeper understanding of fire behavior and enhance fire safety practices.

##### **4.6.1. Jet Flame Lift-off correlations**

Jet fire lift-off correlations refer to empirical relationships or models that estimate the distance at which a jet fire flame starts from the release point. The lift-off is established from an equilibrium between the speed of the jet after the exit from the nozzle (or the hole) and the speed at which the flame progresses through the flammable mixture fuel-air. It is influenced by factors such as jet velocity, fuel properties, release conditions, and ambient conditions.

Empirical correlations for jet fire lift-off are often developed based on experimental data and observations. These correlations may involve mathematical relationships or simplified equations that relate the lift-off to relevant parameters.

It can be seen that the expressions proposed previously by other authors for the lift-off of both vertical and horizontal jet fires overestimate the values of the present horizontal jet flames; the influence of the fuel exit velocity on the lift-off is also smaller in the present experimental data.

The lift-off distance has been correlated by several authors for vertical jet flames (Santos and Costa, 2005, Rokke et al., 1994) and horizontal jet flames (Wang et al., 2019) with the fuel jet exit velocity, both variables normalized by the nozzle diameter ( $S/D$ ,  $u/D$ ).

In the present study, the following expression has been found to correlate the lift-off of horizontal jet flames (Figure 4-17). The lift-off distance has been compared with previous suggested correlations. The results are shown in the following sections.

#### **Jet lift-off correlation:**

In the present study, the following expression has been found to correlate the lift-off of horizontal jet flames (Figure 4-17):

$$S/D = 0.12 (u/D)^{0.54} \quad (4-4)$$

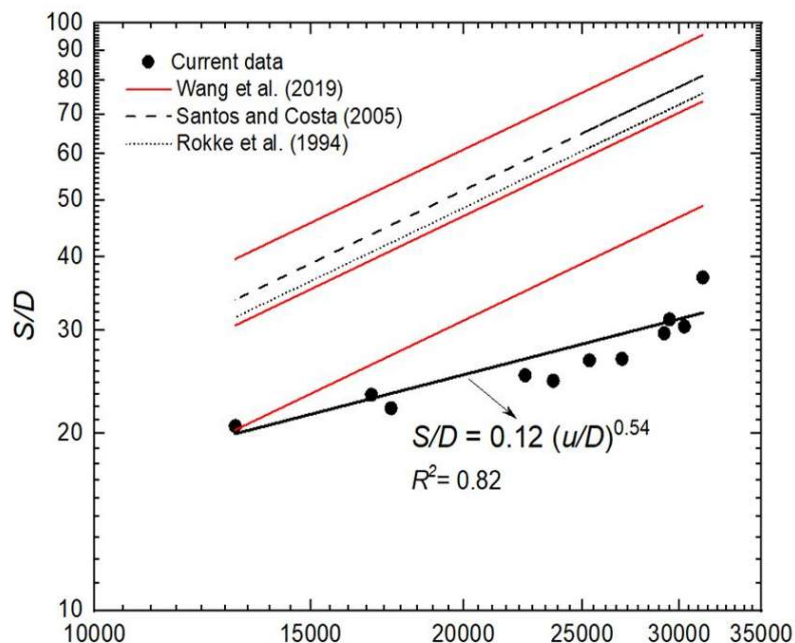


Figure 4-17. Variation in the normalized lift-off distance ( $S/D$ ) as a function of the normalized jet fuel exit velocity ( $u/D$ ,  $s^{-1}$ ): experimental results and previously suggested correlations.

From this figure it can be seen that the previous suggested expressions (Santos and Costa, 2005, Rokke et al., 1994) to predict the lift-off of vertical jet flames overestimate the lift-off values of the present horizontal jet flames. It should also be noted that this kind of correlation (Equation 4-4) is only suitable for subsonic flow; since once the sonic



flow has been achieved, the fluid velocity cannot be further increased and remains constant at the speed of sound in that gas. However, larger lift-off distances can still be obtained (using a specific nozzle) if the gas pressure inside the pipeline continues to be increased. Thus, Equation 4-4 is restricted to subsonic flow conditions and cannot be applied to sonic flow.

**Kalghatgi's correlation:**

Kalghatgi (1984) suggested an expression to predict vertical lift-off distances,  $L$ . The suggested expression involved: (i) a Reynolds number,  $LS_L/\nu_e$ , based on the maximum laminar burning velocity,  $S_L$ , with  $\nu_e$  the gas kinematic viscosity at the jet exit; and (ii) a dimensionless flow parameter  $(u_e/S_L)(\rho_e/\rho_a)$ , with  $u_e$  the fuel flow mean velocity at the exit plane of the pipe for subsonic flow, and  $(\rho_e/\rho_a)$  as the ratio of fuel density at the pressure of the ambient atmosphere, to that of the air at that pressure. Figure 4-18 shows the current experimental lift-off values expressed in terms of the dimensionless numbers suggested by Kalghatgi (Kalghatgi, 1984), together with other experimental data obtained by previous authors.

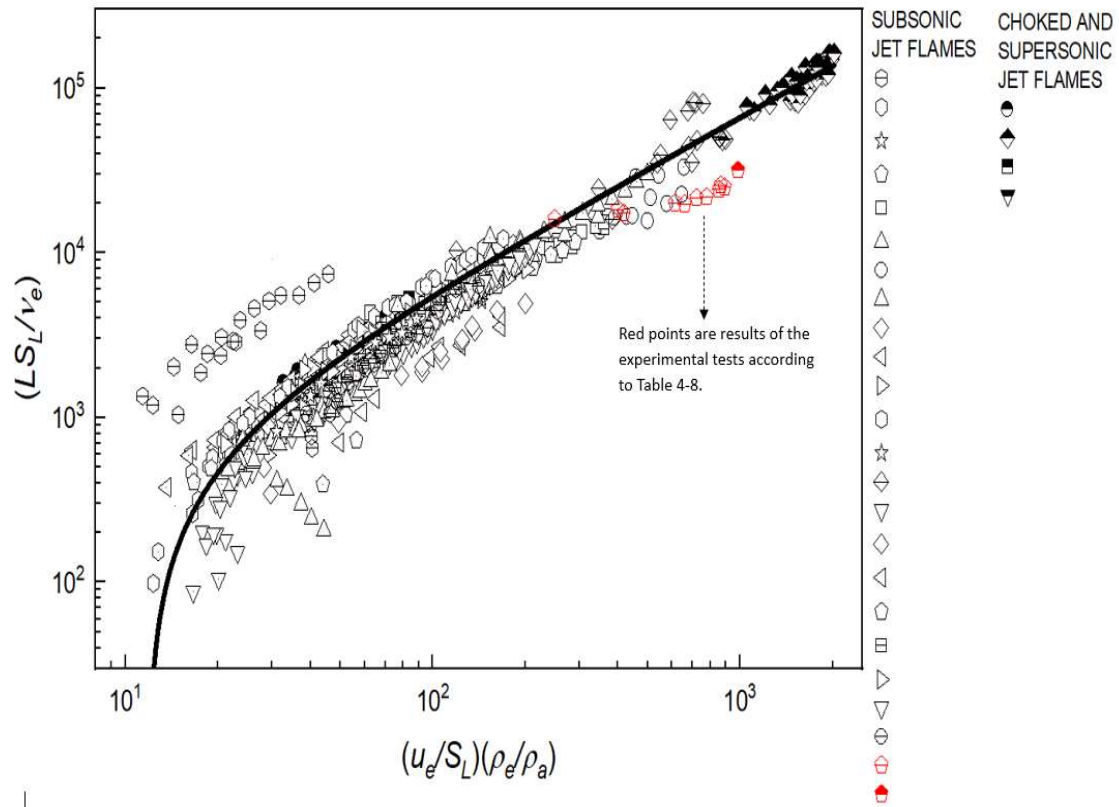


Figure 4-18. Normalised lift-off distance versus dimensionless flow, with data from the present study. Modified from Bradley et al. (2016).

From this figure it can be seen that although the present sonic and subsonic experimental data follow a similar trend as the other experimental works, they are overpredicted by the correlation suggested for vertical jet flames (Red points are results of the experimental tests according to Table 4-8).

#### 4.6.2. Flame reach correlations

The reach of a jet flame refers often to the horizontal distance covered by the flame from the nozzle (even though, as the flame experiences some elevation, the real reach is in fact higher). The reach can vary depending on several factors, including the fuel flow rate, burner design, fuel properties, and ambient conditions. The reach of a jet flame is influenced by the momentum of the fuel jet and its interaction with the surrounding air. As the fuel flow rate increases, the momentum of the jet increases, resulting in a longer flame reach. Similarly, a well-designed burner or nozzle that provides proper mixing and dispersion of the fuel can contribute to a longer flame reach. Other factors that can affect the reach of a jet flame include wind speed and direction, ambient temperature,

and the presence of obstacles or impingement surfaces. Wind can either enhance or reduce the reach of the flame depending on its direction and speed. Obstacles or impingement surfaces can disrupt the flow pattern and cause the flame to deviate or extinguish before reaching its maximum potential reach.

It is important to note that the reach of jet flames can vary significantly depending on the specific conditions and configuration. Empirical correlations and experimental data are often used to estimate or predict the flame reach for specific scenarios. However, due to the complexity and variability of jet flame behavior, it is recommended to conduct experiments or use advanced computational models for accurate predictions in real-world applications.

In the pursuit of understanding flame reach, three correlations were reviewed. The first correlation examined was based on the Froude number, which relates the inertia forces to the gravitational forces acting on the flame. This dimensionless number helps in assessing the flame's ability to propagate horizontally. The second correlation considered was related to the  $Q^*$  dimensionless number, which incorporates the heat release rate, flame height, and ambient conditions to estimate the flame reach. It provides valuable insights into the flame's behavior in different environments. Lastly, the  $U^*$  dimensionless number was analyzed, which combines the wind velocity, characteristic length, and flame speed to determine the flame reach. These studies on the Froude number,  $Q^*$  dimensionless number, and  $U^*$  dimensionless number contribute to our understanding of flame reach and aid in the development of effective fire safety strategies.

**The Froude number:**

The experimental values obtained for the total flame reach-horizontal projection ( $R$ ), of sonic and subsonic jet flames, have also been compared with the expressions previously proposed by Rokke et al. (1994) and Sonju and Hustad (1984); these authors correlated the jet flames reach  $R/D$  with the Froude number. Figure 4-19 shows their predictions, together with the present experimental data. The experimental values for the total flame horizontal reach,  $R$ , of sonic and subsonic jet flames have also been plotted against previous suggested correlations.

Furthermore, the analysis of the experimental values obtained has given the following equation:

$$R/D = 21 Fr^{0.2} \quad (4-5)$$

Fr being the Froude number:

$$Fr = \frac{u^2}{gD} \quad (4-6)$$

where  $u$  is the fuel exit velocity,  $g$  is the gravitational acceleration, and  $d$  is the pipe diameter. This expression is very similar to the one proposed previously by Sonju and Hustad (1984) and Rokke et al. (1994). The experimental data, together with Equation 4-5 and the correlations proposed by the aforementioned authors, have been plotted in Figure 4-19.

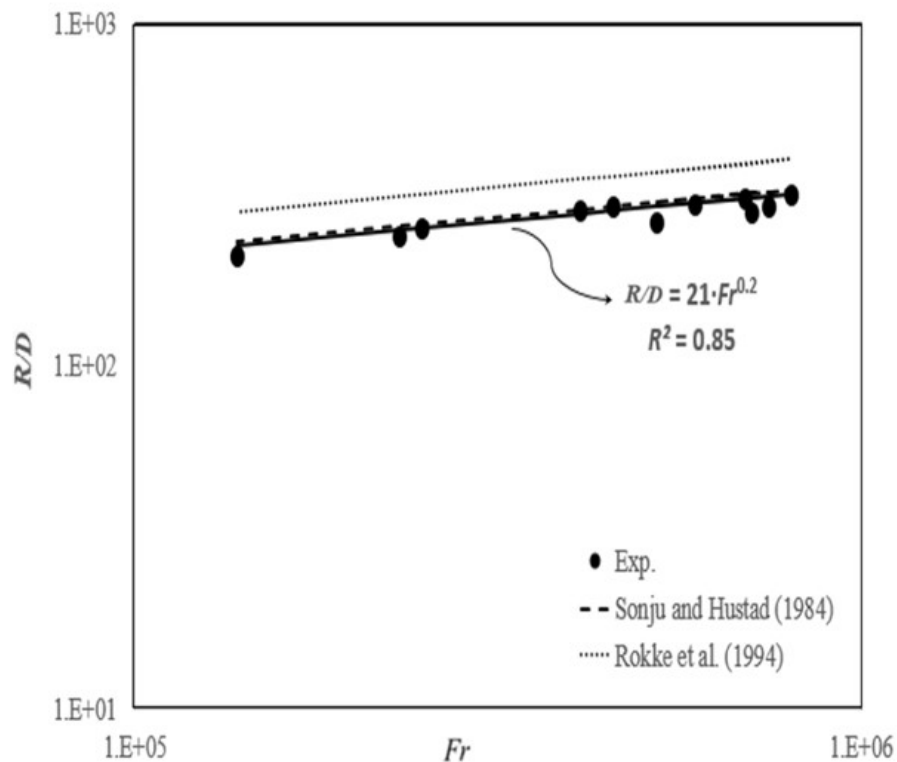


Figure 4-19. Variation normalized flame lengths ( $R/D$ ) as a function of the orifice's Froude number ( $Fr$ ). Previous suggested correlations are also plotted.

From Figure 4-19 it can be seen that the  $Fr$  is also elevated to the power of 0.2 for the present experimental data. This is in line with the previous studies developed with vertical jet fires of propane (Rokke, Hustad, Sonju, 1994, Palacios 2009). The suggested

equation proposed by Sonju and Hustad (1984) for vertical jet fires is similar to the one obtained in the present study for the horizontal jet flames. However, this expression is only suitable for subsonic flows (Palacios et al. 2009) since, as commented before, for a given value of Fr in the sonic regime and a nozzle value, larger flame heights are still possible if the gas pressure inside the pipeline continues to increase.

**The Q\* dimensionless number:**

The dimensionless Q\* group, is defined as:

$$Q^* = \dot{Q} \left( C_p T_\infty \rho_a g^{\frac{1}{2}} D^{\frac{5}{2}} \right)^{-1} \tag{4-7}$$

where  $\dot{Q}$  is the heat release rate,  $C_p$  is the specific heat of the ambient air,  $T_\infty$  is the air ambient temperature, and  $\rho_a$  is the air ambient density.

The expression found from the present experimental data (see Figure 4-20) is:

$$\frac{R}{D} = 3 \cdot Q^{*2/5} \tag{4-8}$$

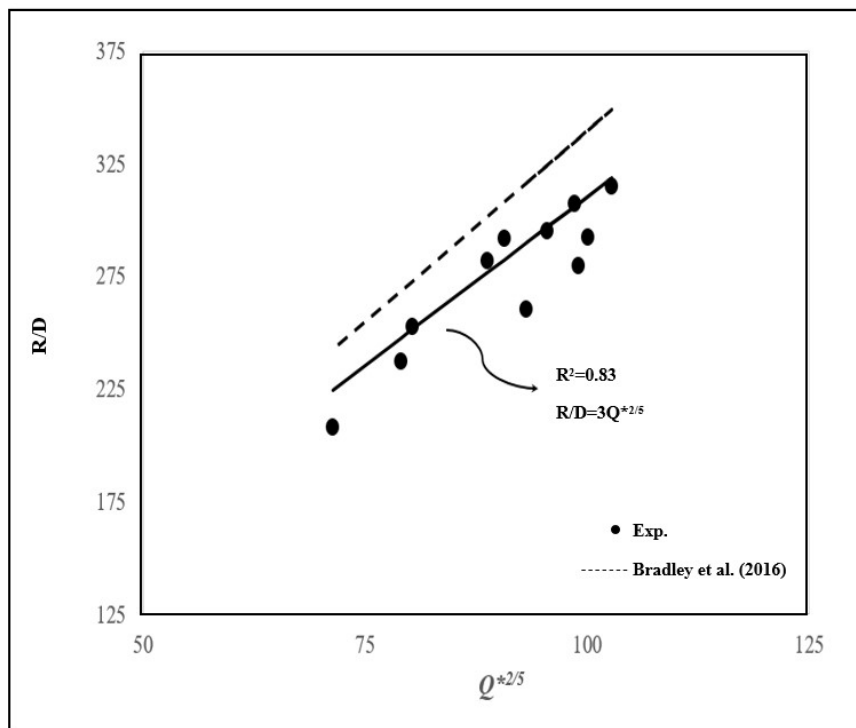


Figure 4-20. Variation of the normalized flame horizontal reach (R/D) as a function of the dimensionless number Q\*. A previous suggested correlation (Bradley et al., 2016) is also plotted.

This correlation had been already suggested by McCaffrey (1988) and Bradley et al. (2016); the expression from Bradley et al. has also been plotted in the figure. The dissimilarity observed between the correlation obtained and the proposed expression by Bradley et al. may be attributed to slight disparities in the experimental operating conditions.

**The U\* dimensionless number**

Flame reach each for vertical and horizontal jet flames of different fuel gases was analyzed by Bradley (2016). Bradley defined dimensionless flow number as:

$$U^* = (u/S_i)(v/D \cdot S_L)^{0.4}(P_i/P_a) \tag{4-9}$$

where  $u$  is the mean velocity at the pipe exit plane. The values of maximum burning velocity,  $S_L$ , and  $v$  are those for the ambient air conditions.  $P_i$  and  $P_a$  are the initial stagnation and atmospheric pressures, respectively. Figure 4-21 shows the dimensionless total flame height plotted against the dimensionless flow number,  $U^*$ . Previous suggested correlations proposed Bradley (2016) are also plotted in Figure 4-21.

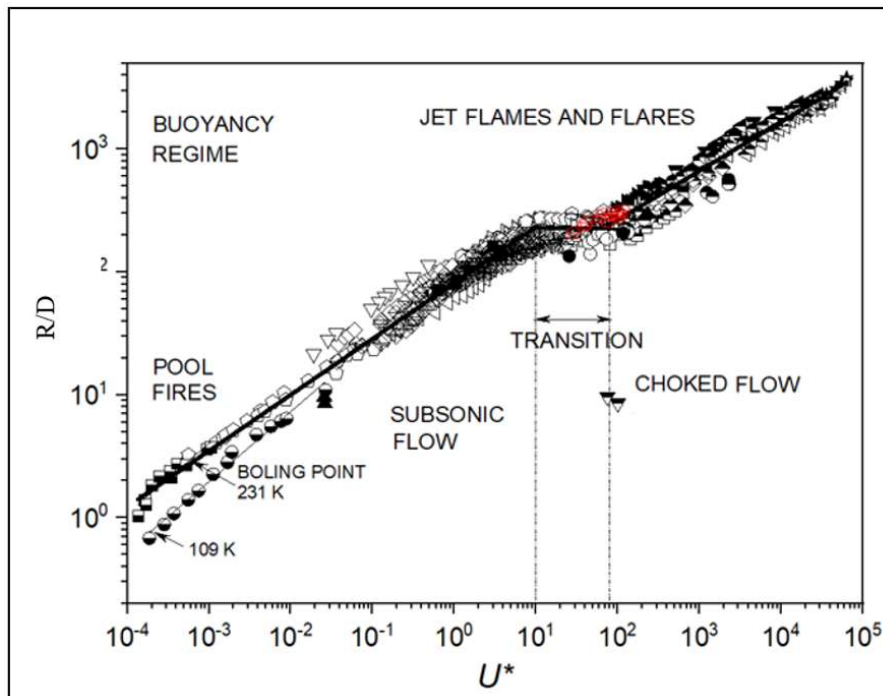


Figure 4-21. Variation normalized flame lengths ( $R/D$ ) as a function of the dimensionless flow number,  $U^*$ . Previous suggested correlation (Bradley et al., 2016] are also plotted. The vertical broken line indicates transition from subsonic to sonic flow.

From this figure it can be seen that the data are slightly underpredicted in average by Bradley et al., (2016). It should also be noted that most of the present experimental horizontal data seem to be part of the transition from subsonic to sonic regime. The average R/D value found for the present experimental horizontal jet flames of propane has been 270, with an average error of 9%.

#### 4.6.3. Flames elevation

The elevation of horizontal jet flames refers to the vertical distance between the nozzle or burner and the highest point of the flame above the horizontal plane. The elevation can vary depending on several factors, including the fuel flow rate, nozzle configuration, fuel properties, and ambient conditions. In general, as the fuel flow rate increases, the flame elevation tends to increase as well. This is because a higher fuel flow rate leads to greater momentum and buoyancy of the fuel jet, causing the flame to lift higher. The flame elevation can also be influenced by factors such as the angle of the nozzle, the presence of obstacles or impingement surfaces, and the air entrainment into the flame.

It is important to note that the flame elevation of horizontal jet flames can vary significantly depending on the specific circumstances. Empirical correlations and experimental data are often used to estimate or predict the flame elevation for a given set of conditions. However, due to the complexity and variability of jet flame behavior, it is recommended to conduct experiments or use advanced computational models for accurate predictions in specific scenarios. In the case of horizontal –or, better, not vertical- jet fires, the combined action of the floatability and the loss of the linear velocity due to the turbulent mixing with air and the combustion, originates a change in the flames shape, with an elevation of them; this does not happen in the case of vertical jet fires, even though their shape can also be modified if they undergo the influence of wind. The flames elevation in horizontal jet fires can be important from the point of view of their possible impingement on some equipment.

So, to predict the real possible reach of the flames of such jet fires both magnitudes, the reach horizontal projection and the flames elevation should be considered. Figures 4-22 and 4-23 depict the normalized maximum elevation ( $W/D$ ) of flames, represented as a ratio, with respect to the propane release mass flow rate and Froude number

correspondingly. By analyzing these figures, one can observe that the vertical position of the horizontal flames exhibits a progressive rise when considering a constant nozzle diameter. This upward trend in flame elevation is influenced by the release pressure of the gas and subsequently the jet exit velocity. The aforementioned figures provide valuable insights into the relationship between flame behavior and key parameters such as propane release mass flow rate and Froude number. The normalized maximum elevation ( $W/D$ ) serves as a measure of the height attained by the flames relative to the nozzle diameter ( $D$ ). The results indicate that as the propane release mass flow rate increases or the Froude number rises, the flames reach higher positions, suggesting a direct correlation between these factors and flame elevation.

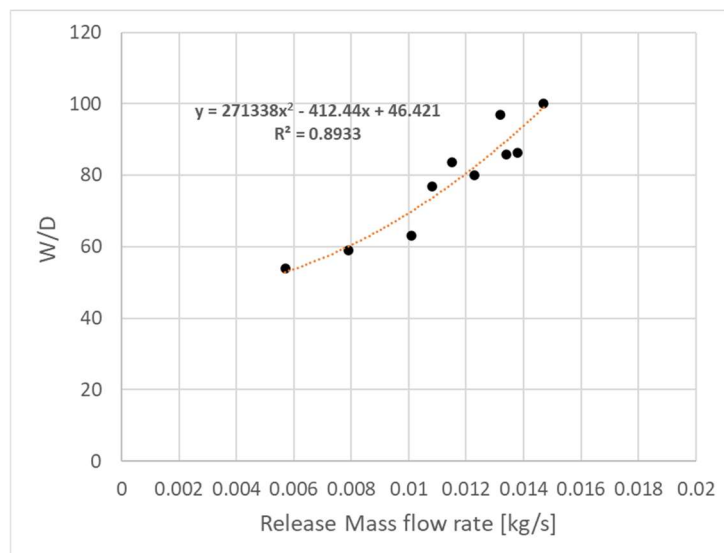


Figure 4-22. Variation of the normalized flame maximum elevation ( $W/D$ ) as a function of the propane release mass flow rate



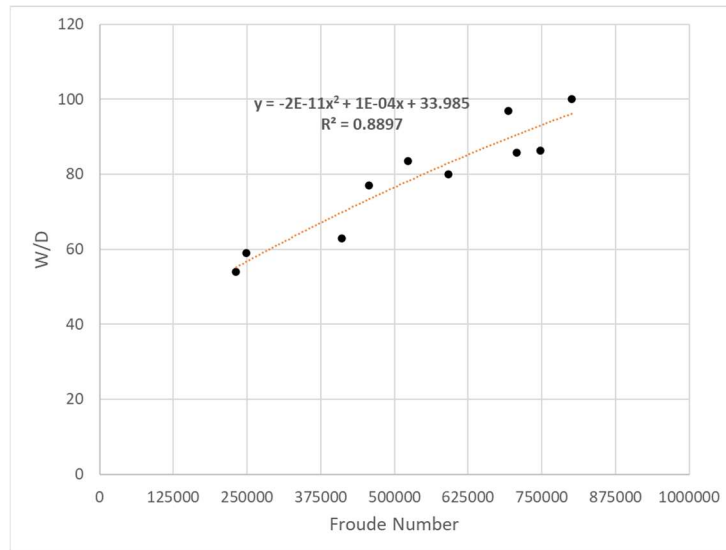


Figure 4-23. Variation of the normalized flame maximum elevation (W/D) as a function of the nozzle's Froude number.

#### 4.7. Final remarks

The experimental results and the associated data treatment have allowed obtaining expressions that can be used for the prediction of the probable lift-off distance and reach (horizontal projection) of horizontal sonic and subsonic jet fire flames.

These two magnitudes are important because, together with the flame's elevation, they will establish the distance over which there could be impingement –which is the worst situation concerning a possible domino effect, due to the extremely high heat fluxes that flames impingement can imply- on some equipment in the event of a jet fire.

The main findings can be summarized as follows:

- i) The values obtained for the flames lift-off (a distance which usually is much shorter than the flames themselves) of horizontal jet fires are smaller than those predicted by other authors for both horizontal and vertical jet fires
- ii) The experimental values of the flames horizontal reach (i. e. the projection of flames length on the horizontal axis of the nozzle plus the lift-off distance) are essentially the same as those obtained by other authors for the length of vertical jet fires.
- iii) However, in the case of horizontal jets there is a significant change in the jet fire shape, so the flames elevation must be also considered because they can have an influence on the zone possibly affected by flames impingement.

iv) This is something that should be taken into account when performing a risk analysis involving the possibility of jet flames impingement on an equipment, being therefore logical taking always a conservative approximation not limited to the expressions obtained from vertical jet fires.

## 5. Thermal Effects of Jet Fire Impingement on a Pipe

### 5.1. Introduction

This chapter presents the experimental study conducted to investigate the thermal effects of a jet fire impingement on a pipe. The objective was to assess the pipe's heat transfer characteristics and thermal response under different fire scenarios. The experiments were performed in a controlled laboratory setup (see Chapter 3), where a jet fire was directed toward a section of the pipe. Measurements of temperature distribution, heat flux, and thermal gradients along the pipe wall were recorded for different locations of the pipe in the jet flames zones.

The study considered different parameters, including fire intensity and the distance from the fire source. The results revealed significant thermal effects, including extremely high temperature rise of the pipe wall in certain cases, which can explain the very quick equipment failure observed in certain accidents occurred in the process industry and in transportation.

The findings provide valuable insights into the behavior of pipes –which could be extrapolated to other equipment– exposed to jet fires and contribute to the understanding of their thermal performance and structural integrity under such conditions. These experimental results could aid in the development of improved design guidelines and safety measures for industrial facilities where jet fire hazards are present.

### 5.2. Impingement tests

The jet flames impinged on a carbon steel pipe (API 5L X60, 11.5 cm outside diameter, 6 mm wall thickness, 3 m length) containing stagnant air or water (Figure 5-1). A set of K-type thermocouples located inside the pipe wall (4 mm inside pipe wall thickness) allowed the measurement of the wall temperature at different positions during the tests.

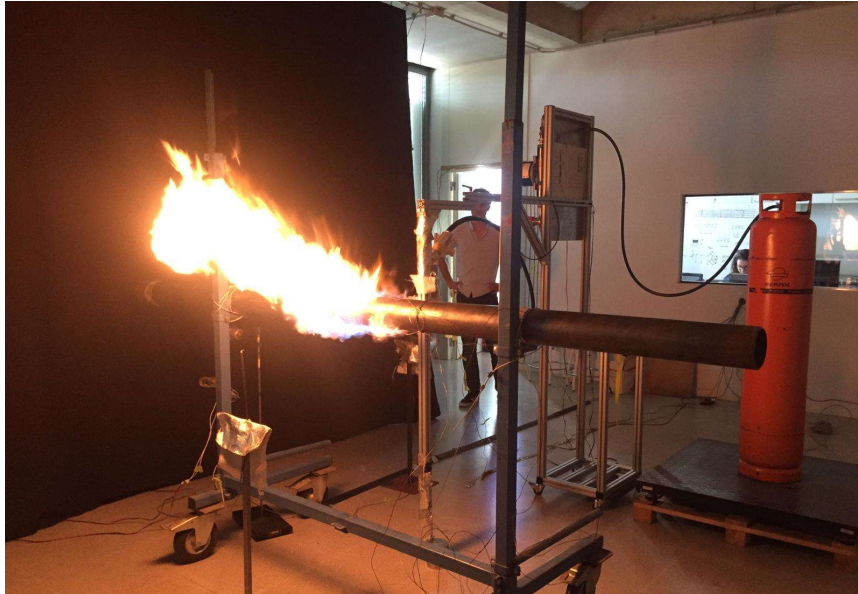


Figure 5-1. Arrangement of one of the configurations during an experimental test.

Additionally, as illustrated in Figure 5-2 and Figure 5-3, another set of four B-type thermocouples was located outside the pipe (at 1 cm distance from the pipe wall), to measure the flame temperature at the same above-mentioned positions.

With the purpose of analysing the heat loss during the experiment through the air temperature inside the pipe, four type K thermocouples were installed on a metal support. They were placed next to the thermocouples on the wall, at a distance not exceeding 3 cm. Looking at heat loss was useful to understand how long the heating of the pipe wall was effectively influenced only by a convective mechanism, and not by others.

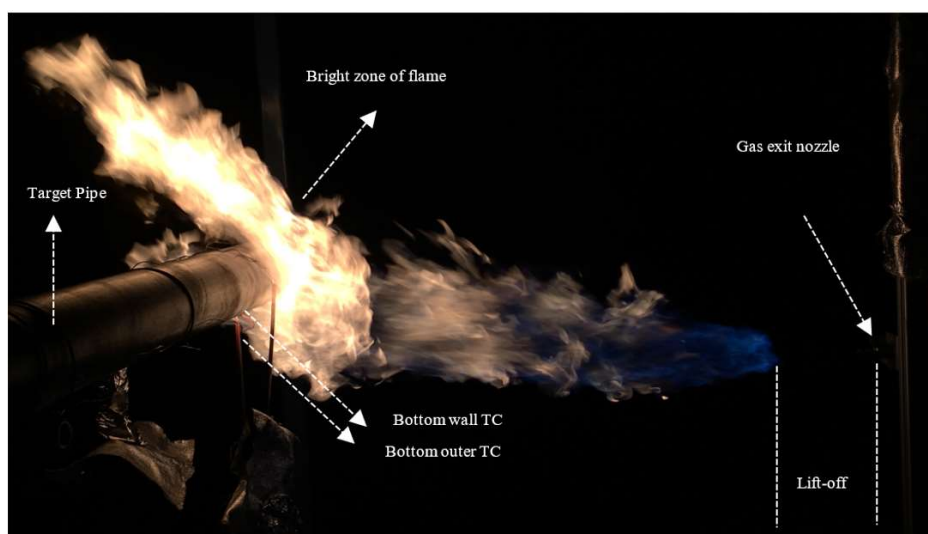


Figure 5-2. Visible image of jet fire impinging on the pipe and location of thermocouples.



Figure 5-3. The external B and the K type thermocouples inside/outside of the pipe wall.

The jet fires were filmed with both visible CCD and IR cameras to record the experiments, located orthogonally to the flames. From observations of visible and infrared images (Figure 5-4), the flame boundary was defined as that corresponding to a temperature of 800 K (Palacios and Casal, 2011) and an emissivity value of 0.35 was used (Palacios et al., 2012).

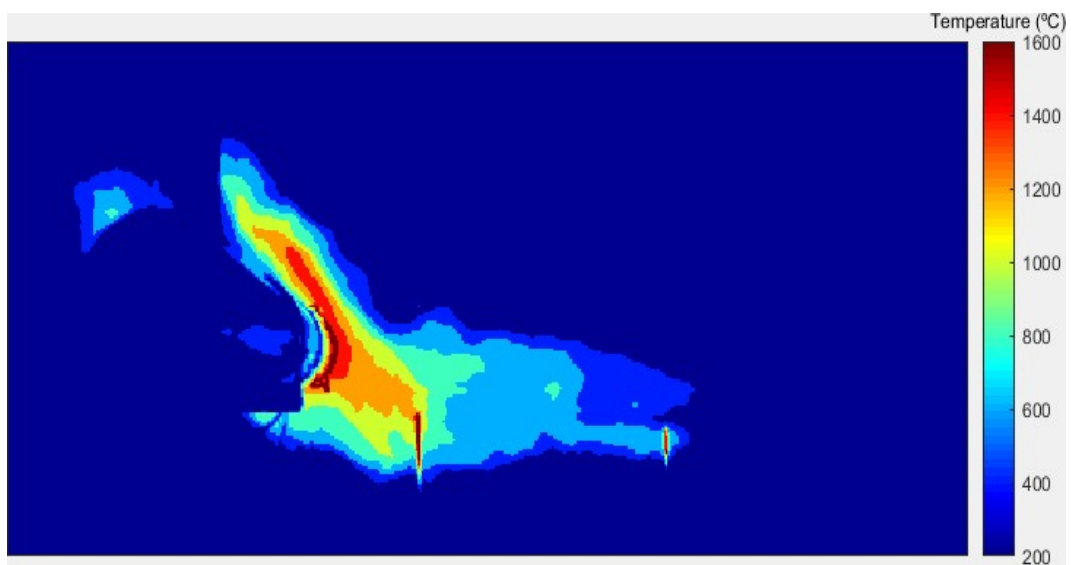


Figure 5-4. The IR image of the jet fire impinging on the pipe.

The condition of the pipe just after the flames impingement can be seen in Figure 5-5 (this image corresponds to a test in which inside the pipe there was air).

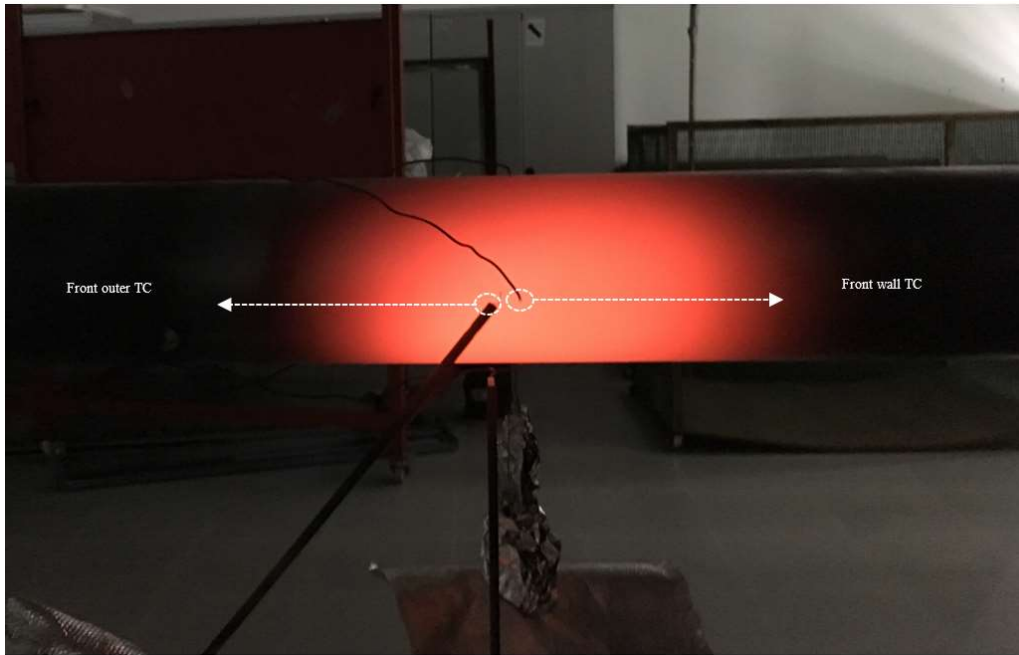


Figure 5-5. Impacted area of the target pipe just after impingement.

The values of pressure, temperature, and released mass flow rate of the fuel feeding the jet fire were continuously registered during the tests.

During the tests, the gas release nozzle was located at 105 cm (horizontal distance) from the target pipe centre, and the pipe centre line was elevated 115 cm from the ground level to take into account the elevation of the flames in the front zone. The position of the experimental test equipment is shown in Table 5-1.

Table 5-1. Position of experimental test equipment.

X: Horizontal distance from the nozzle to pipe centreline (cm)	Y: Elevation distance from level ground to pipe centre line (cm)	Location of thermocouples (cm)				
		Position	Front	Top	Back	Bottom
105	115	Wall TC	X: 100	X: 105	X: 110	X: 105
			Y: 115	Y: 120	Y: 115	Y: 110
		Flame TC	X: 99	X: 105	X: 111	X: 105
			Y: 115	Y: 121	Y: 115	Y: 109
		Internal TC	X: 101	X: 106	X: 109	X: 105
			Y: 115	Y: 119	Y: 115	Y: 108

In order to analyse the thermal impacts of a jet fire impingement on the pipe, two sets of experimental tests were designed and performed. The detailed description of the tests are discussed in Chapter 3, section 3.2 of (categorized as Test Group 1 and Test Group 2 respectively).

**Group 1- Thermal Impacts on Pipe Performance (Fluid Condition Study):** Study the thermal impacts of the pipe based on the operating fluid condition.

The objective of this set of tests was to allow the testing of different potential conditions that might happen during a pipeline impingement, originated from another parallel pipeline. Hence, three test conditions were defined, corresponding to the flow and the condition of the fluid inside the target pipe in three possible situations that can occur during the stationary operation of the pipe/pipeline or in the event of an emergency stop of the fluid flow:

- a) Continuous flow of liquid inside the pipe during the jet fire impingement.
- b) Stationary liquid: the liquid flow is stopped, and the liquid is blocked inside the pipe during the jet fire impingement.
- c) Continuous flow of gas: a continuous flow of gas inside the pipe during the jet fire impingement.

**Group 2- Thermal Impacts on Pipe Performance: Jet Flame Distance Study:** Study the thermal impacts of the pipe based on the distance from the release point of the jet flame.

The objective of this group of tests was to analyze the impact of distance from jet exit on the heat flux received by the pipe. Hence, three test conditions were defined depending on the distance of the pipe with the release point of the gas.

As mentioned already in Chapter 4, in a typical jet fire the flames can be divided into three distinct zones based on heat transfer characteristics and flame behavior.

These zones, here called blue, middle, and front zones respectively, have different effects in the case of impingement:

**Blue zone:** this section is the one that has the average flame temperature lower than the other two zones. Of course, when the flames enter in contact with the pipe the

associated turbulence improves the contact fuel-air and the flames colour and brightness change.

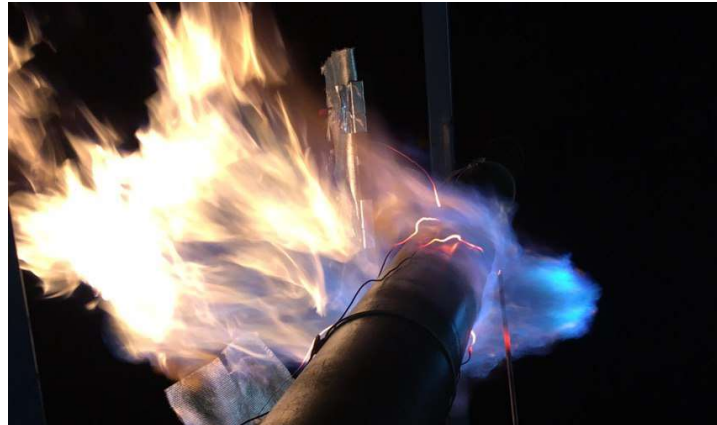


Figure 5-6. Example of impingement at the blue zone.

Middle zone: In this zone, the flame undergoes a mixing process with the entrained air, leading to enhanced combustion and turbulence (Fig. 5.8); its flames are bright and may exhibit fluctuations and turbulence due to the mixing process. The temperature here has an intermediate value between those of the other two zones.



Figure 5-7. Example of impingement at the middle zone.

Front zone: this is the outermost region of the jet fire, farthest from the fuel source.

This final part of the flame, the frontal zone, is the hottest zone among the three described and, in a horizontal configuration of the jet fire, it is the one that presents an elevation with respect to the reference plane.





Figure 5-8. Example of impingement at the front zone.

It is important to note that thermocouples' readings are affected by several factors, including the thermal radiation characteristics of the flame. During the experiments, it was seen that the recorded temperature in the blue zone is relatively lower than in the other zones. This could be explained by the basis of the thermocouple function. However, it is worth noting that thermocouples may register a lower temperature reading in the primary zone due to the heightened momentum resulting from fuel/air mixing in the blue zone. It is important to note that the boundaries between these zones are not sharply defined and can vary depending on factors such as fuel type, release velocity, and environmental conditions. The size and behavior of each zone can also change over time as the fire evolves. Understanding the characteristics of these zones is crucial for assessing the potential hazards, designing safety measures, and determining appropriate mitigation strategies in jet fire scenarios.

The length of the visible flames could be predicted with good accuracy —when there was no impingement— by the following expression proposed by Palacios and Casal (2011), although due to the high turbulence, it experienced an important oscillation:

$$L_{\text{flame}} = d \cdot \text{Re}^{0.4} \quad (5-1)$$

However, the existence of an obstacle —a pipe, a vessel— has a certain influence on both the shape of the flame and on its turbulence. The shape of the highly turbulent flames was of course somewhat disturbed by the presence of the target pipe in the impinging zone. Very light modifications in the respective positions of the flame and the pipe implied significant changes in the flame contact with the bottom, top and back

surfaces of the pipe wall, with the consequent influence on the heat transfer in those zones.

### 5.3. Results and Discussion of Group 1 Tests

The essential data concerning the operating conditions of these tests have been summarized in Table 5-2.

Table 5-2. Operating conditions of three tests in Group 1.

Experiment Title	Release diameter [mm]	Condition of the fluid inside the pipe	Release pressure [bar abs]	Flow Regime	Mass Flow rate [kg/s]	Exit Gas Velocity (m/s)	Distance Nozzle to pipe surface [cm]	Distance Nozzle to ground level [cm]
JFT-190308-1		stagnant air inside the pipe	1.74	Sonic	0.015	250.75	100	115
JFT-190311-1	6	stagnant liquid inside the pipe	1.73	Sonic	0.014	250.75	100	115
JFT-190311-2		stagnant liquid inside the pipe	1.04	Subsonic	0.0136	120.36	100	115

#### 5.3.1 Gas inside the pipe, sonic jet fire

The temperature of a pipe subjected to jet fire impingement increases quickly when it conveys or contains a gas. Figure 5-10 shows the temperature evolution registered by the four thermocouples (K- type) located inside the wall on top, bottom, front, and back, respectively, of a perimeter of the pipe (stagnant air inside) receiving the flames of the central section of a sonic jet fire.

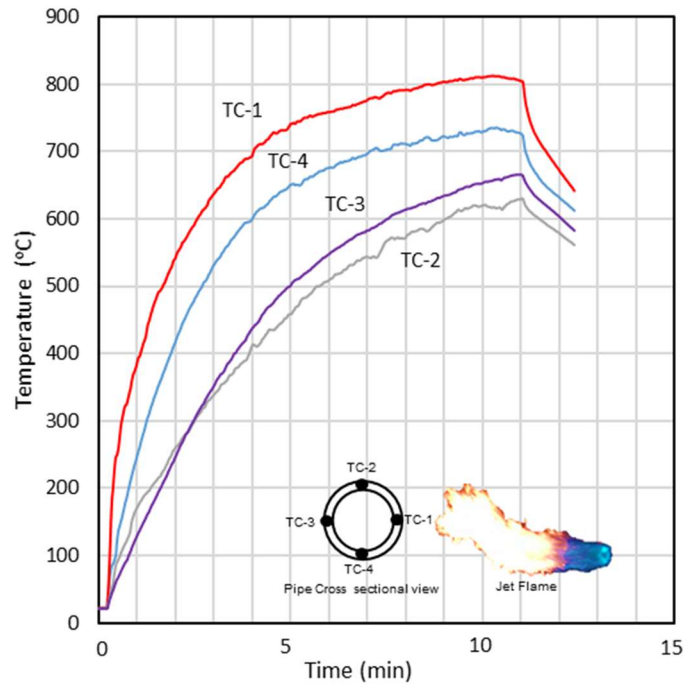


Figure 5-9. Evolution of pipe wall temperatures as a function of time (stagnant air inside the pipe, sonic jet impingement).

In the first step of the impingement, the heating rate of the pipe wall was very intense due to the high-temperature difference between it and the flames; for example, between the initial pipe temperature of 25 °C and 100 °C, the following heating rates were registered: 19.5 °C/s for front TC, 5.5 °C/s for the bottom TC, 3.7 °C/s for the top one and 2.2 °C/s for the back one. The front zone of the pipe wall (TC-1) underwent the highest heating, due to the higher turbulence and the more intense convective contribution.

The heating velocity decreased afterward gradually as the pipe wall temperature increased. Thus, the front zone of the pipe wall (TC-1) reached a temperature of 600 °C after 2.4 min from the start of the jet fire (this would correspond approximately to 50 % of the strength ratio of carbon steel at room temperature) and 750 °C (approximate steel strength ratio: 15 %) after 4.8 minutes. These very high heating rates are the reason why, in certain accidents, the failure of a pressurized pipe or vessel has occurred after a very short time from the start of the jet fire.

The thermocouple located in the bottom wall (TC-4) of the pipe registered somewhat lower —even though also very high— temperatures, reaching a maximum value of 737

°C. Lower temperatures were registered by the top and back wall thermocouples (TC-2, TC-3, respectively), even if the pipe wall was in contact with the flames. This should be attributed to a much lower contribution of the radiation on the back pipe surface originated by the flame features in this zone (see Figure 5-2), and to a significantly lower contribution of the convection mechanism in the top pipe surface due to the tangential contact of the flames. Additionally, four B-type thermocouples were located out of the pipe, in front of the thermocouples in the pipe wall, at 1 cm from the wall (see Figure 5-3 and Figure 5-5) to measure the flame temperature.

### 5.3.2 Liquid inside the pipe, sonic jet fire

If the pipe contains or conveys a liquid, the surface of the wall in contact with it (i.e., the section of the wall under the liquid level) will be cooled by the liquid, which after a short time will start boiling, and the wall temperature will reach much lower values than in the previous case due to the corresponding cooling effect. Figure 5-11 shows the temperature evolution of the different points of a pipe subjected to the impingement of a jet fire (with essentially the same features as those in Figure 5-10). In this case, stagnant water was contained in the pipe.

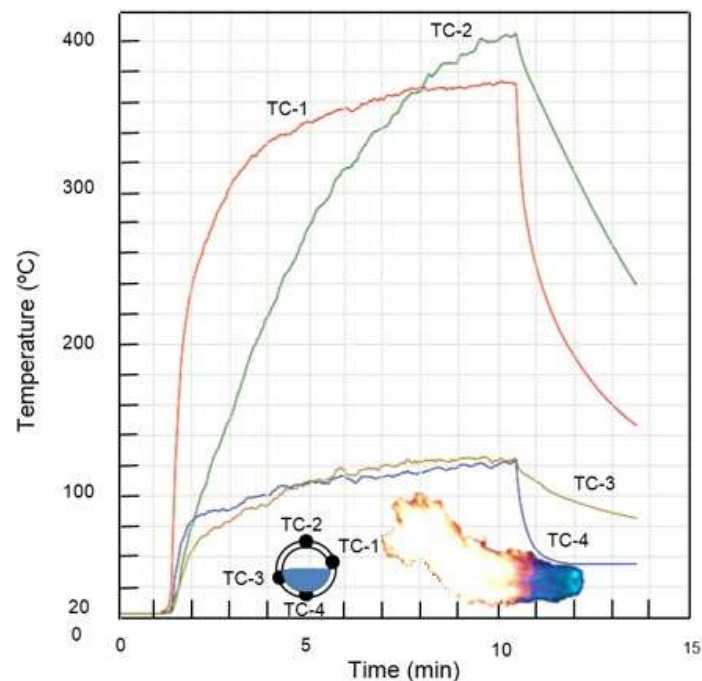


Figure 5-10. Evolution of pipe wall temperatures as a function of time (stagnant water inside the pipe, sonic jet impingement).

The temperatures registered by the thermocouples located at the front and top zones, TC-1 and TC-2, respectively, were relatively high (a maximum temperature of 375 °C for the front thermocouple was reached after 9 min of exposure, and 400 °C for the top one) but much lower than those found when the pipe contained air, due to the cooling action of the water droplets ejected by the boiling liquid; and the temperatures measured by the thermocouples located at the zones of the wall in contact with the water measured significantly lower values, lightly higher than the water boiling temperature. If water was flowing at a certain speed, the cooling effect would be higher. Similar results (to those from TC-2, TC-3 and TC-4) were obtained by Birk et al. (2006a) with longer exposure times, when studying the flames impingement on a vessel.

### **5.3.3 Liquid inside the pipe, subsonic jet fire**

If there is a low-velocity jet, for example, because the pressure in the source pipe has decreased significantly, then the turbulence in the jet and the entrainment of air will decrease; consequently, the combustion in the jet will be poor: the flame will be brighter due to the existence of soot particles, but its temperature will be lower. Therefore, the temperature increase at the pipe wall, even if it will increase quickly at the start of the impingement, will reach lower values than in the case of a sonic jet. Figure 5-12 shows the temperature evolution in the case of a subsonic jet ( $u = 40$  m/s) impinging on a pipe containing stagnant water. Thermocouples TC-4 (bottom) and TC-3 (back) were on the wall in contact with water, while TC-1 (front) and TC-2 (top) were located in the wall above water level.

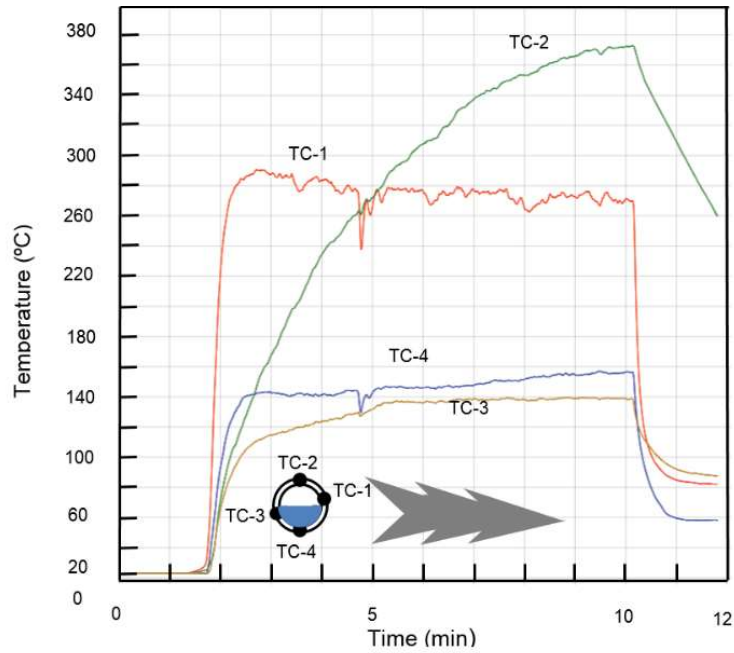


Figure 5-11. Evolution of pipe wall temperatures as a function of time (stagnant water in the pipe, subsonic jet impingement).

## 5.4. Results and Discussions of Group 2 Tests

### 5.4.1 Operating condition of tests

This series of tests were effectuated with larger jet fires, i.e. with two different exit nozzle diameters, 6 mm and 8 mm. The main data concerning the tests have been summarized in Table 5-3 to Table 5-6. Impingement at the three zones of the jet fire, blue, middle and front, has been analysed, as well as the evolution of the temperature at the different zones of the pipe wall and the corresponding heat fluxes.

Table 5-3. Test conditions of Three Zones Impingement Tests for 8 mm nozzle.




Experiment Title	Release diameter [mm]	Impingement Zone	Release pressure [bar abs]	Flow Regime	Mass Flow rate [kg/s]	Exit Gas Velocity (m/s)	Distance of Nozzle to pipe surface [cm]	Distance of Nozzle to ground level [cm]	Image
JFT-200225-1	8	Front Zone	1.83	Sonic	0.015	250.75	130	110	
JFT-200227-1			1.83	Sonic	0.015	250.75	130	110	
JFT-200226-1			1.66	Subsonic	0.0136	239.94	130	110	
JFT-200224-2	8	Middle Zone	1.81	Sonic	0.0148	250.75	100	114	
JFT-200227-2			1.62	Subsonic	0.0133	234.22	100	114	
JFT-200228-1			1.65	Subsonic	0.0135	238.52	100	114	
JFT-200207-1	8	Blue Zone	2.07	Sonic	0.0169	250.75	35	116	
JFT-200211-1			1.64	Subsonic	0.0134	237.10	35	116	

Table 5-4. Test conditions for 6 mm nozzle (pipe located in the front zone of the flame).


Experiment Title	Release diameter [mm]	Impingement Zone	Release pressure [bar abs]	Flow Regime	Mass Flow rate [kg/s]	Exit Gas Velocity (m/s)	Distance of Nozzle to pipe surface [cm]	Distance of Nozzle to ground level [cm]	Image
JFT-200221-1	6	Front Zone	1.75	Sonic	0.0081	250.75	100	110	
JFT-190409-1			1.74	Sonic	0.0081	250.75	100	110	
JFT-191203-3			1.70	Subsonic	0.0078	242.03	100	110	
JFT-200221-2			1.60	Subsonic	0.0074	231.31	100	110	
JFT-200224-1			1.40	Subsonic	0.0064	199.48	100	110	
JFT-191204-1			1.40	Subsonic	0.0064	199.48	100	110	
JFT-191204-2			1.20	Subsonic	0.0051	158.89	100	110	



Table 5-5. Test conditions for 6 mm nozzle (pipe located in the middle zone of the flame).


Experiment Title	Release diameter [mm]	Impingement Zone	Release pressure [bar abs]	Flow Regime	Mass Flow rate [kg/s]	Exit Gas Velocity (m/s)	Distance Nozzle to pipe surface [cm]	Distance Nozzle to ground level [cm]	Image
JFT-200130-2	6	Middle Zone	1.75	Sonic	0.0081	250.75	70	114	
JFT-200220-2			1.74	Sonic	0.0080	250.75	70	114	
JFT-200130-1			1.71	Subsonic	0.0079	244.13	70	114	
JFT-200130-3			1.60	Subsonic	0.0074	231.31	70	114	
JFT-200219-1			1.66	Subsonic	0.0077	239.94	70	114	
JFT-200219-2			1.59	Subsonic	0.0071	227.91	70	114	
JFT-200220-1			1.41	Subsonic	0.0066	201.45	70	114	
JFT-200129-1			1.30	Subsonic	0.0057	178.85	70	114	
JFT-200129-2			1.20	Subsonic	0.0051	158.89	70	114	

Table 5-6. Test conditions for 6 mm nozzle (pipe located in the blue zone of the flame).

Experiment Title	Release diameter [mm]	Impingement Zone	Release pressure [bar abs]	Flow Regime	Mass Flow rate [kg/s]	Exit Gas Velocity (m/s)	Distance of Nozzle to pipe surface [cm]	Distance of Nozzle to ground level [cm]
JFT-200206-2	6	Blue Zone	1.81	Sonic	0.0084	250.75	35	116
JFT-200206-1			1.77	Sonic	0.0081	250.75	35	116
JFT-200211-2			1.77	Sonic	0.0081	250.75	35	116
JFT-200214-1			1.71	Subsonic	0.0079	244.13	35	116
JFT-200218-1			1.63	Subsonic	0.0077	235.35	35	116
JFT-200205-1			1.60	Subsonic	0.0074	231.31	35	116
JFT-200218-2			1.59	Subsonic	0.0072	228.96	35	116
JFT-200205-2			1.42	Subsonic	0.0068	202.86	35	116
JFT-200218-3			1.41	Subsonic	0.0064	201.76	35	116
JFT-200204-1			1.20	Subsonic	0.0051	158.89	35	116



#### 5.4.2 Heat transfer fluxes and heat transfer coefficients

The analysis of both the pipe wall temperature and the jet flame temperature at any position of the pipe wall (i.e. front, bottom, back, and top) allowed to obtain the approximate values of the flame-to-wall heat transfer fluxes and heat transfer coefficients corresponding to each case (Figure 5-13, Figure 5-14, Figure 5-15 and Figure 5-16).

The heat fluxes reaching the pipe wall were calculated during the first step of the test (i.e. within the first 40 s, although the time-lapse varied with the pipe wall position), when the still relatively low temperature of the pipe (between 25 °C and 100 °C) implied negligible heat losses from it. In this condition, all the heat received through a given external surface area (i.e. for a given steel mass), during a certain time by both radiation and convection mechanisms, were invested in heating the pipe wall, as follows:

$$Q = \frac{m_p \cdot C_p}{A_p} \cdot \frac{dT_{\text{wall}}}{dt} \quad (5-2)$$

And the flames-to-wall heat transfer coefficient was estimated by:

$$Q = h \cdot A_p \cdot (T_{\text{flame}} - T_{\text{wall}}) \quad (5-3)$$

Due to the strong turbulence, in some cases the flame temperature underwent important oscillations, and an average value was taken. The flame-to-wall heat transfer coefficients were calculated from the value of the heat flux reaching the pipe wall, and by knowing both the pipe wall temperature at a given point and the flame temperature at that location (measured by the thermocouples located quite close to that wall point). This coefficient was associated to all the net heat flux reaching and entering the pipe wall, thus including the net contributions of both conductive and radiative phenomena. Afterward, as the pipe wall progressively increased and the temperature difference driving force decreased, the pipe heating rate decreased and the heat losses from it to the environment increased. Finally, an essentially constant temperature was reached when the heat received by the pipe was equal to the heat lost from it.

The values corresponding to each experimental test have been included in Table 5-7, Table 5-8, Table 5-9 and Table 5-10.

Table 5-7. Heat fluxes and heat transfer coefficients for a for 8 mm nozzle tests.

Experiment Title	Release diameter [mm]	Impinge. Zone	Release pressure [bar abs]	Mass Flow rate [kg/s]	h [kW/(°C*m <sup>2</sup> )]				Q [kW/m <sup>2</sup> ]			
					Bottom	Back	Front	Top	Bottom	Back	Front	Top
JFT-200225-1	8	Front Zone	1.83	0.015	0.115	0.18	0.189	0.115	136	140	210	95
JFT-200227-1			1.83	0.015	0.112	0.128	0.18	0.118	130	117	200	100
JFT-200226-1			1.66	0.0136	0.156	0.112	0.20	0.117	174	87.5	202	104
JFT-200224-2		Middle Zone	1.81	0.0148	0.14	0.162	0.213	0.13	145	148	193	118
JFT-200227-2			1.62	0.0133	0.118	0.103	0.174	0.142	126	100	181	112
JFT-200228-1			1.65	0.0135	0.113	0.116	0.168	0.151	117	103.5	173	111
JFT-200207-1		Blue Zone	2.07	0.0169	0.032	0.137	0.81	0.151	27.500	99	6	91.3
JFT-200211-1			1.64	0.0134	0.059	0.136	0.302	0.083	46.7	109	12.85	42.6

Table 5-8. Heat fluxes and heat transfer coefficients for 6 mm nozzle (pipe located in the front zone of the flame).

Experiment Title	Release diameter [mm]	Imping. Zone	Release pressure [bar abs]	Mass Flow rate [kg/s]	H [kW/(°C*m <sup>2</sup> )]				Q [kW/m <sup>2</sup> ]			
					Bottom	Back	Front	Top	Bottom	Back	Front	Top
JFT-200221-1			1.75	0.0081	0.112	0.114	0.16	0.125	126	90	17	95
JFT-191203-3			1.70	0.0078	0.157	0.152	0.175	0.16	125.6	138.2	190	122
JFT-200221-2			1.60	0.0074	0.095	0.087	0.157	0.1	100	70	165	73
JFT-200224-1	6	Front Zone	1.40	0.0064	0.081	0.047	0.143	0.092	73.5	24.8	155	56
JFT-191204-1			1.40	0.0064	0.198	0.108	0.075	NA	158	97	87.7	NA
JFT-191204-2			1.20	0.0051	0.067	0.098	0.056	NA	56	43.4	48	NA

Table 5-9. Heat fluxes and heat transfer coefficients for 6 mm nozzle (pipe located in the middle zone of the flame).

Experiment Title	Release diameter [mm]	Imping. Zone	Release pressure [bar abs]	Mass Flow rate [kg/s]	H [kW/(°C*m <sup>2</sup> )]				Q [kW/m <sup>2</sup> ]			
					Bottom	Back	Front	Top	Bottom	Back	Front	Top
JFT-200130-2	6	Middle Zone	1.75	0.0081	0.084	0.12	0.115	0.07	104	112	115	63
JFT-200220-2			1.74	0.0080	0.1	0.115	0.154	0.16	117	99	154	143
JFT-200130-1			1.71	0.0079	0.088	0.113	0.102	0.095	82	100	101.5	81
JFT-200130-3			1.60	0.0074	0.157	0.114	0.092	0.13	72	90	85	91
JFT-200219-1			1.66	0.0077	0.154	0.115	0.205	0.064	178	96-97	182	65
JFT-200219-2			1.59	0.0071	0.087	0.105	0.158	0.113	82	87	118	103
JFT-200220-1			1.41	0.0066	0.17	0.1	0.185	0.116	159	83	125	105
JFT-200129-1			1.30	0.0057	0.108	0.12	0.109	NA	97.6	103.8	94.9	NA
JFT-200129-2			1.20	0.0051	0.086	0.087	0.095	0.093	74.2	75.6	86	75

Table 5-10. Heat fluxes and heat transfer coefficients for 6 mm nozzle (pipe located in the blue zone of the flame).

Experiment Title	Release diameter [mm]	Imping. Zone	Release pressure [bar abs]	Mass Flow rate [kg/s]	H [kW/(°C*m <sup>2</sup> )]				Q [kW/m <sup>2</sup> ]			
					Bottom	Back	Front	Top	Bottom	Back	Front	Top
JFT-200206-2	6	Blue Zone	1.81	0.0084	0.030	0.113	0.103	0.134	31.7	101	54	94.9
JFT-200206-1			1.77	0.0081	0.024	0.120	0.20	0.096	25	95.8	41.2	70
JFT-200211-2			1.77	0.0081	0.047	0.120	0.127	0.1	49	96.5	21.9	96
JFT-200214-1			1.71	0.0079	0.061	0.128	0.175	0.073	55.1	105	25.4	56
JFT-200218-1			1.63	0.0077	0.067	0.117	0.185	0.098	53.7	94	33.0	56
JFT-200205-1			1.60	0.0074	0.048	0.130	0.212	0.112	41.2	96.3	34	60
JFT-200218-2			1.59	0.0072	0.061	0.118	0.160	0.07	50	98.5	31.8	55
JFT-200205-2			1.42	0.0068	0.078	0.116	0.205	0.072	51.6	82.3	30.8	46.8
JFT-200218-3			1.41	0.0064	0.069	0.103	0.172	0.049	54.5	89.4	29.7	44.5
JFT-200204-1			1.20	0.0051	0.065	0.118	0.135	0.069	42.500	90.5	38	56.1

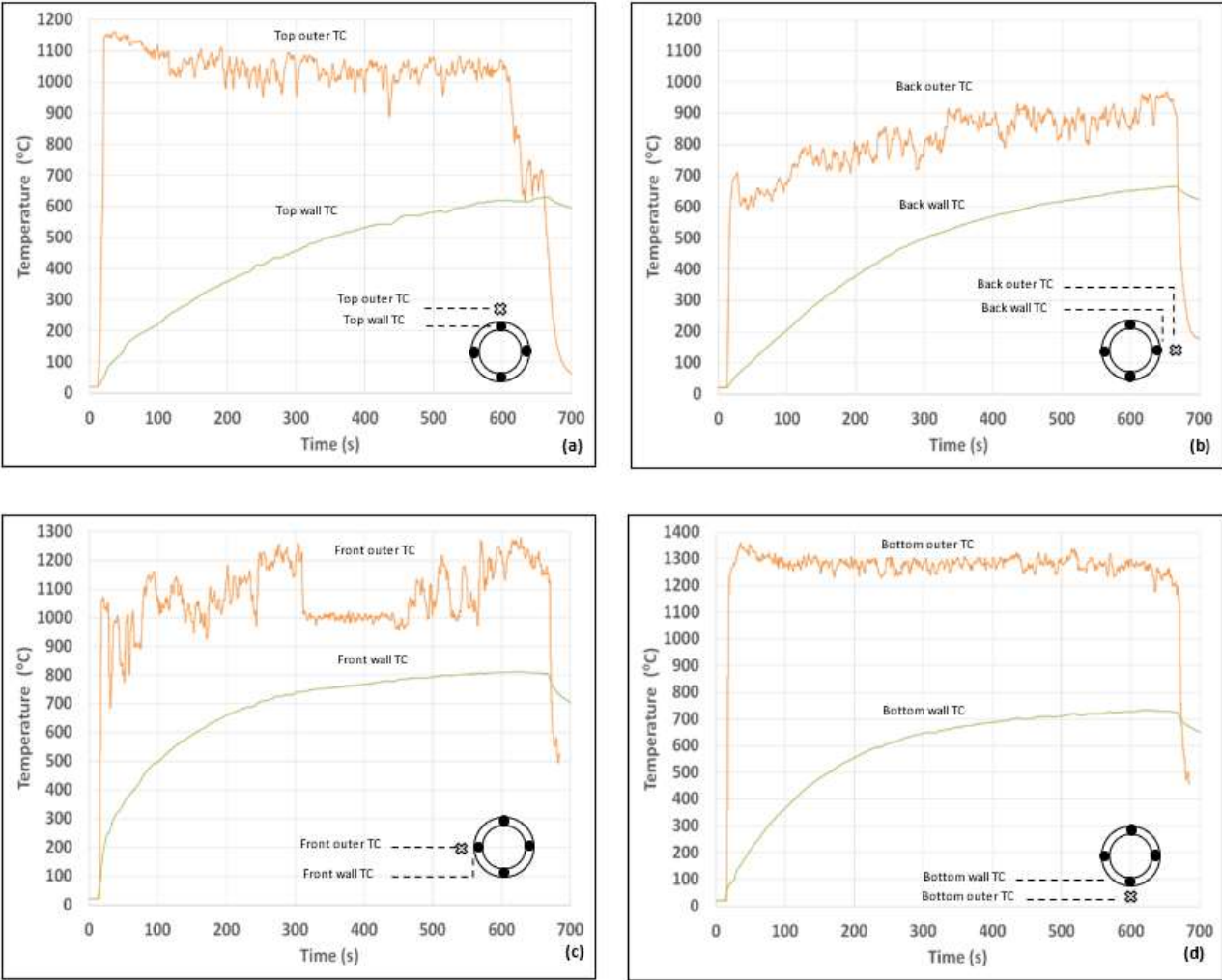


Figure 5-12. Evolution of flame and pipe wall temperature by a sonic flames impingement at the bright zone in (a) the top wall, (b) the back wall, (c) the front wall, and (d) the bottom wall. (Test ID: JFT-190409-1, Front Zone).



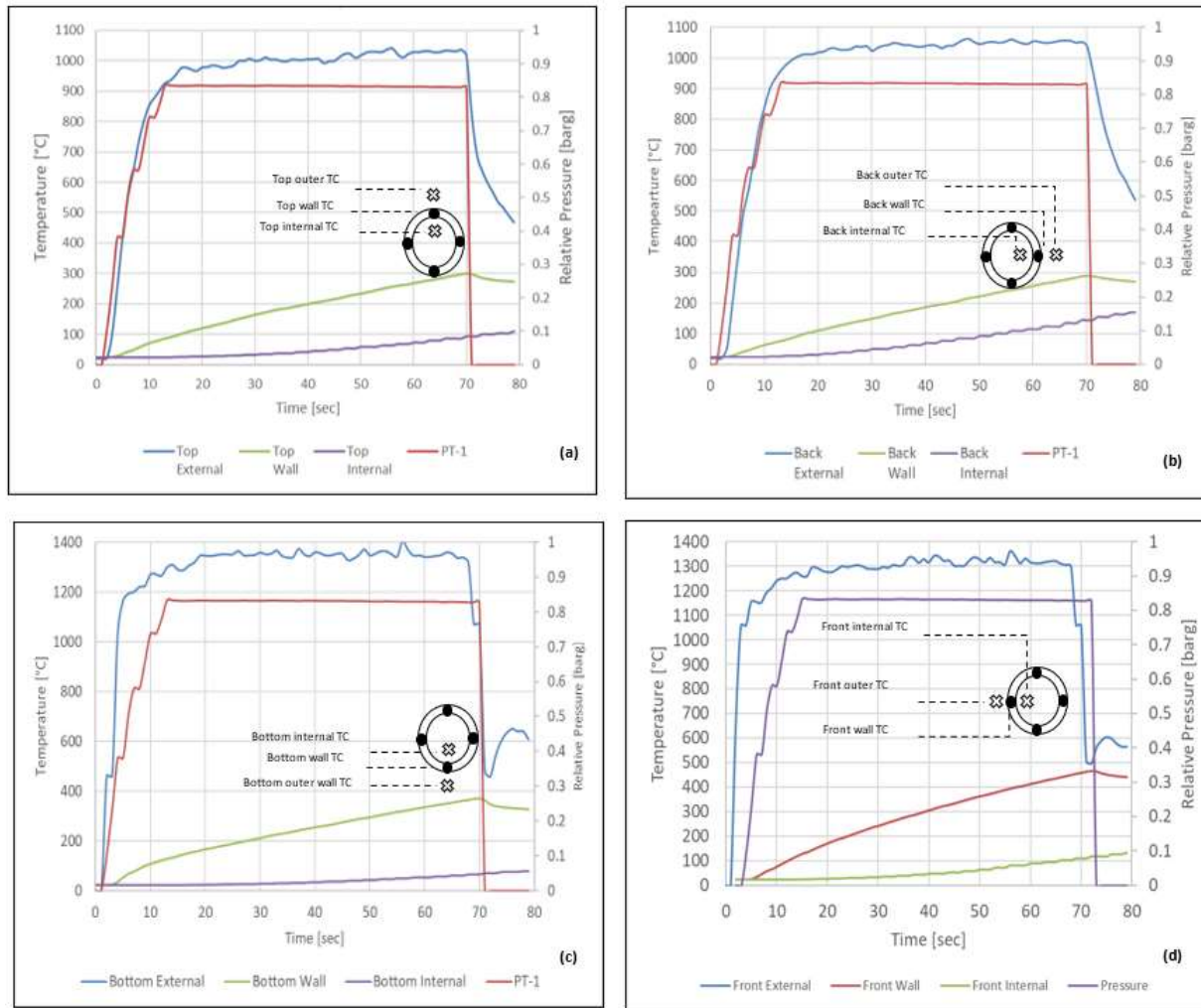


Figure 5-13. Evolution of flames temperature by a sonic flames impingement at the bright zone in (a) the top wall, (b) the back wall, (c) the front wall, and (d) the bottom wall. (Test ID: JFT-200227-1, Front zone).

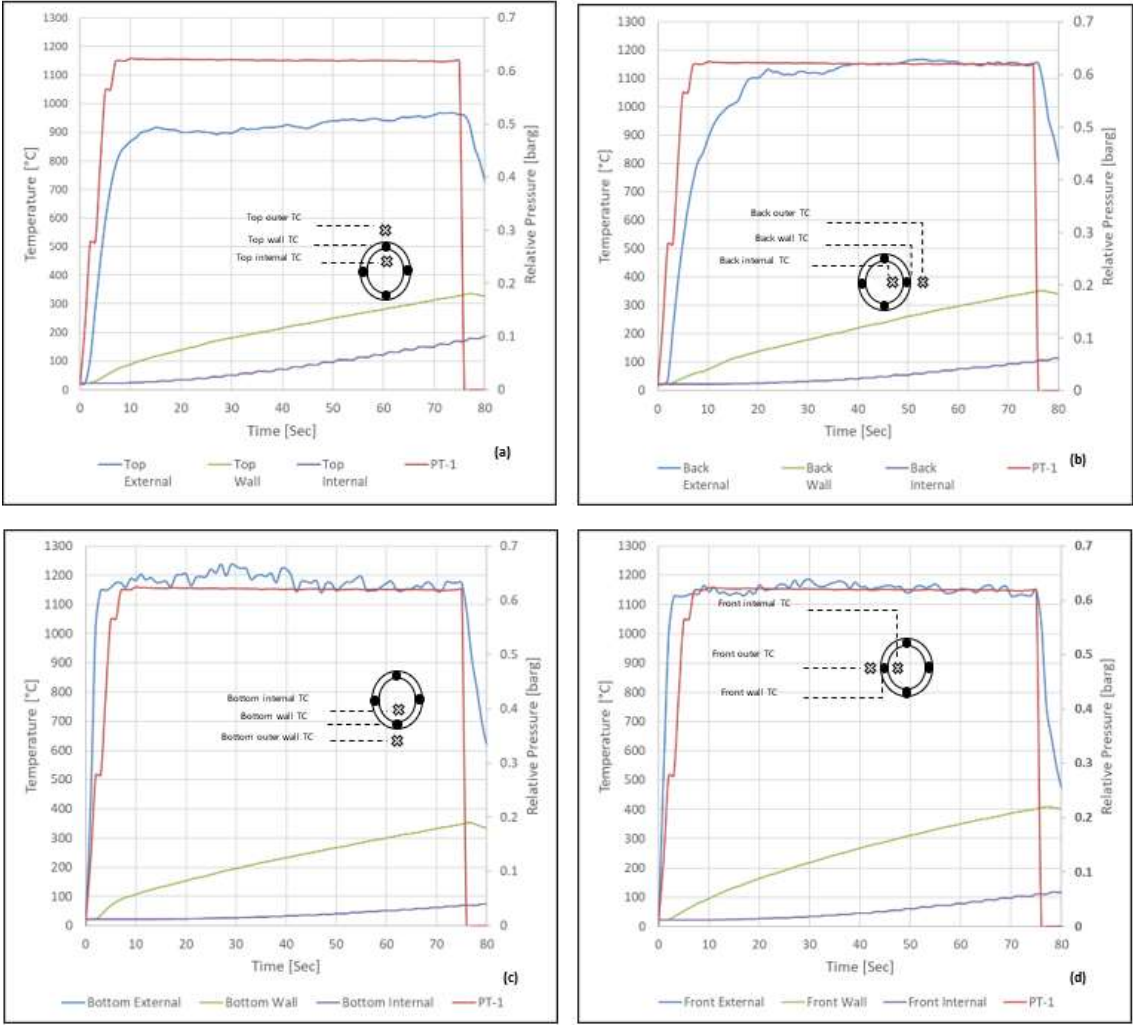


Figure 5-14. Evolution of flames temperature by a sonic flames impingement at the bright zone in (a) the top wall, (b) the back wall, (c) the front wall, and (d) the bottom wall. (Test ID: JFT-200227-2, middle zone).

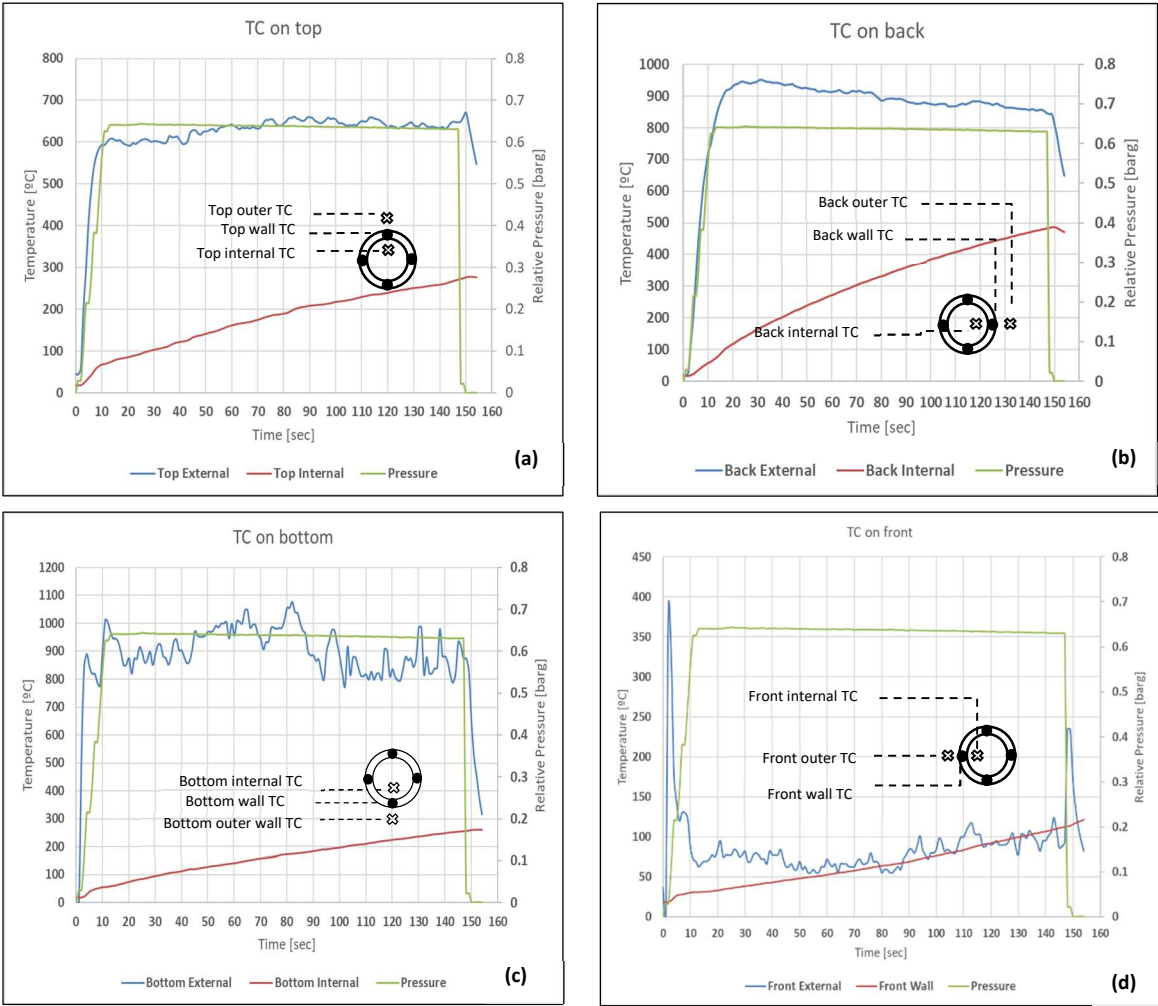


Figure 5-15. Evolution of flames temperature by a sonic flames impingement at the bright zone in (a) the top wall, (b) the back wall, (c) the front wall, and (d) the bottom wall. (Test ID: JFT-200211-1, blue zone).

## 5.5. Discussion

The analysis of the results obtained from the diverse tests and operating conditions have shown that the bright, fully developed zone of the jet fires (“front zone”) was the one (i.e. compared to the intermediate one and the blue one) which gave the highest heating rates. The evolution of the pipe wall temperatures in the four positions of the thermocouples (front, bottom, back, and top of the pipe) for this situation have been shown in Figure 5-13, Figure 5-14, Figure 5-15 and Figure 5-16 for a sonic jet fire.

The highest heat fluxes, reaching values of up to 275 kW/m<sup>2</sup>, were registered for the higher propane release pressures at the front position of the wall, where the flames impinged against the pipe wall with a very high turbulence and an intense convective contribution. These values were significantly higher than those measured by most of the other authors which also worked with propane jet fires (except for some tests by Wighus and Drangsholt, see Table 5-11). At the other positions (bottom, back and top), the heat fluxes were significantly lower due to the features of the flames-wall turbulent contact which significantly affected heat transfer by convection.

Table 5-11. Heat flux and convective heat transfer coefficient obtained by other authors.

Reference	Heat flux			Convective heat transfer coefficient (kW/m <sup>2</sup> ·°C <sup>-1</sup> )
	Total (kW/m <sup>2</sup> )	Radiative (kW/m <sup>2</sup> )	Convective (kW/m <sup>2</sup> )	
Bradley, 2017	50-250	NA	NA	NA
Virk, 2015	68-110	NA	NA	0.048 -0.094
Lowesmith et al., 2007	240	160	80	0.08
Persaud et al., 2001	180-200	NA	NA	NA
Wighus and Drangsholt, 1993	190-340	NA	NA	NA

Several authors have experimentally found that both radiation and convection parts can dominate the total heat flux in the case of flames impingement, depending on the circumstances (Kilham, 1948; Hustad and Sonju, 1991; Lowesmith et al., 2007). However, in the current experiments convection heat transfer was determined to be

always the more dominant part in the front wall of the pipe, followed by the back and bottom walls.

This could be explained as the consequence of direct contact with the highly turbulent jet flame for the front zone, the influence of the formation of jet fire wake (with the associated increase in the turbulence) on the pipe's back surface, and with the contribution of the flame buoyancy convection in the bottom zone. However, it was observed in the tests that slight differences in the position of the flames with respect to the pipe -which not always could be controlled- could have also a significant influence on the heat fluxes received by the bottom, back and top zones of the pipe wall. This should be attributed to the very high turbulence of the jet flames, which could also be significantly affected by the relative position and contact pipe-flames.

It is also interesting to note the possible influence of soot deposits on the pipe wall, a phenomenon that was detected in the diverse developed tests, which according to some authors (Patej and Durussel, 2007) could have a thermal insulating effect. Nevertheless, in the present tests the soot deposition was not important, being probably eroded by the jet action. The results obtained, with the very high heat fluxes that can be reached in the event of the impingement of a jet fire on a pipe or an equipment not thermally protected (or which thermal protection has been damaged or eroded), show the real danger that such a situation can imply and explain why, in accidents in which this situation occurs, the failure of the affected equipment can occur in times as short as just one minute or after a time of half an hour or more.

Although jet fire accidents are underrepresented in accident databases (probably because they are much less evident, visible or even spectacular than a pool fire), it is a fact that they have been the origin of important domino effect sequences.

In the specific case of parallel and close pipelines, if a loss of containment of a flammable gas or two-phase flow occurs through a hole or a flange —originated by corrosion, excavating machinery or other causes— and it gets ignited, the possibility of flames impingement on a secondary pipe can create a very dangerous situation even in the case of relatively small jet fires. The data obtained from an experimental setup, designed for performing indoor tests with small and medium size jet fires, have shown that impingement can imply very high heat fluxes (up to 275 kW/m<sup>2</sup> in the worst case),

originating extremely high temperatures in the pipe wall when there is a gas inside, if there is no fireproofing or it has been damaged. With stagnant gas inside the pipe, temperatures of the order of 600 °C were reached in 2-3 minutes (initial heating rates of up to 19.5 °C/s were registered), and of 750 °C in 5-6 min. When the pipe contained a liquid, the wall in contact with it was cooled and the situation much was less dangerous. These data emphasize the fact that safety distances must be considered essential in pipelines hallways, together with fire proofing and other safety measures.

## 6. CFD Simulation of Jet Fires

### 6.1. Introduction

Computational Fluid Dynamics (CFD) is a well-established tool within quantitative risk assessment due to its ability to describe complex three-dimensional geometries and environments, as well as reactive and non-reactive flow of compressible and/or incompressible fluids over time (Figure 6-1). One of the benefits from using Computational Fluid Dynamics (CFD) tools to study jet fires' impact is their ability to account for obstacles and site-specific factors. This chapter focuses on evaluating the effectiveness of the FLACS CFD code in simulating a horizontal jet fire involving propane. Experimental data obtained in this research is used to validate the code, with emphasis on the jet fire's geometric characteristics and flame temperature. Various numerical models provided by the FLACS code are compared to identify the most suitable ones for describing horizontal jet fires. The accuracy of the simulation results is assessed using statistical performance metrics.

Overall, the results demonstrate that the FLACS CFD code can effectively capture the phenomena associated with horizontal jet fires, although there is a slight tendency to overpredict the temperature compared to obtained results from experimental data. Building upon these findings, an initial investigation is conducted to explore the application of a proposed model for simulating the impingement of horizontal jet fires on a pipe, considering the possibility of utilizing the FDS CFD code.

In the context of dynamic risk assessment (which considers the transient evolution of accidents by taking into account factors such as obstacles, changes in meteorological conditions, and site-specific factors related to equipment layout), CFD modeling plays a crucial role in predicting the hazardous effects and consequences of jet fires. Therefore, one of the main objectives of this thesis is to evaluate the predictive capabilities of the FLACS CFD code in simulating a propane horizontal jet fire in a confined environment. This assessment serves as a foundation for studying impingement and domino effects.

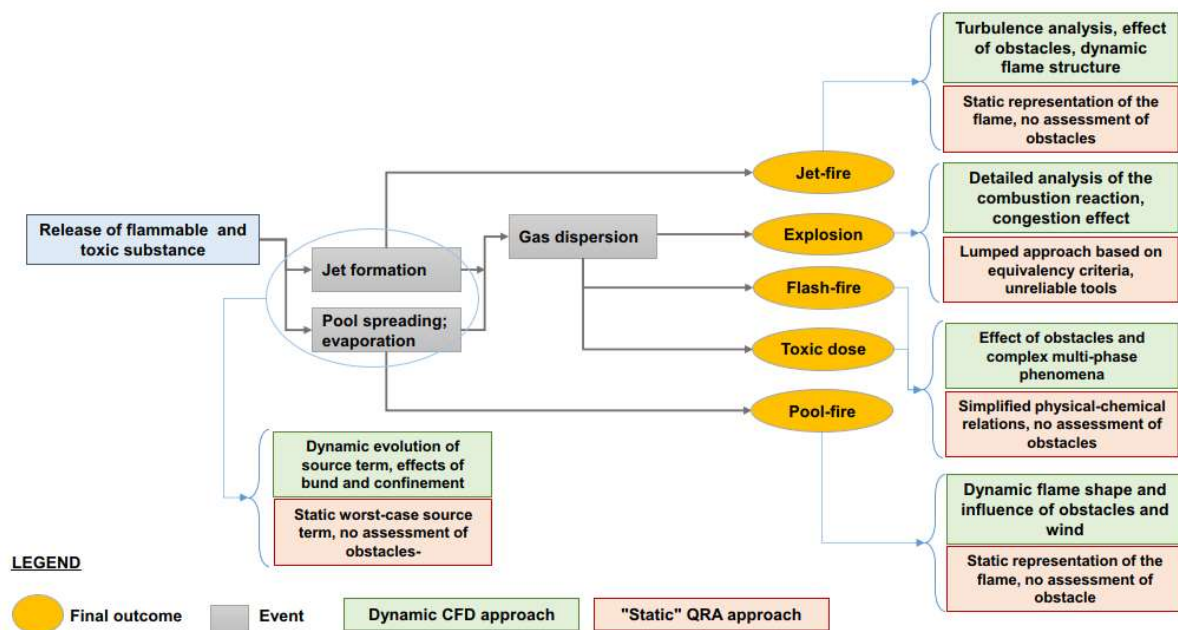


Figure 6-1. Schematic representation of the potentialities of computational fluid dynamics models in capturing dynamic accident scenarios and limitations of lumped parameters models implemented in quantitative risk assessment (Landucci et al., 2016b).

CFD modeling is a suitable approach for conducting an accurate risk assessment of jet fires in real-world scenarios, however, the complexity of CFD models presents certain challenges, such as the need for substantial person-hours and expertise to build the simulations, significant computational resources and time, and a comprehensive understanding of the input information. These factors can pose limitations to the widespread application of CFD modeling.

### 6.1.1. Computational Fluid Dynamics (CFD) modelling

A Computational Fluid Dynamics (CFD) model solves the conservation equations for mass, momentum, and energy in a three-dimensional space, resulting in a system of partial-differential (or integral-differential) equations. These equations are then approximated using a discretization method, most commonly the "finite volume method." This method involves dividing the geometric domain into a finite number of control volumes, known as a mesh, where the equations are applied. By assigning boundary and initial conditions, the program can solve these equations. Post-processing programs can be used to visualize the results in the form of plots, graphs, and 3D images. Figure 6-2, as illustrated by Landucci et al. (2016a), depicts a schematic representation of the approach used to conduct a CFD study to analyse an accidental scenario.



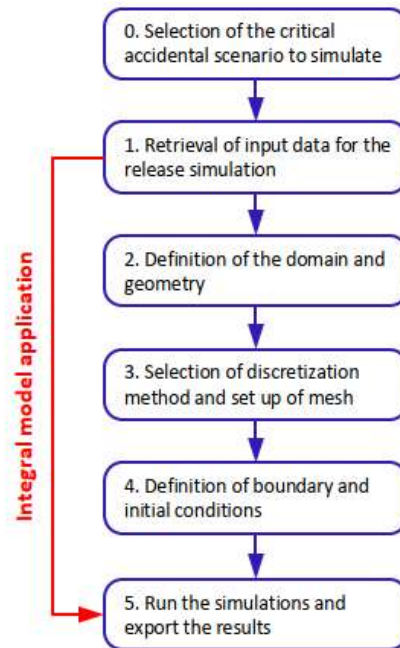


Figure 6-2 CFD (blue) and Integral approach (red) flowchart of the methodology (Landucci et al., 2016a).

Step 0 represents the initial stage of the process, where the scenario to be analyzed is determined, and an appropriate modeling strategy is selected to limit the number of cases that need to be assessed. This step is crucial for minimizing time and cost expenditures.

Moving on to Step 1, relevant input information regarding the release of substances is gathered. This data includes all the necessary parameters to accurately describe the phenomena. In conventional models, this step forms the basis for applying the integral approach, as indicated by the red line in Figure 6-2, where results are directly obtained.

In Step 2, the domain is defined, resulting in a three-dimensional representation of objects and the surrounding environment. Many programs employ a user-friendly graphical interface for this purpose.

Step 3 is a crucial stage, as it involves defining the computational grid. The accuracy of the results depends heavily on correctly assigning this parameter. Finer meshes yield more precise outcomes but also increase computational costs. Therefore, a sensitivity analysis is often conducted to assess the quality of the grid.

Before running the simulation, boundary and initial conditions are applied in Step 4 to complete the necessary information. Subsequently, results such as dynamic profiles of velocity, temperature, or concentration are obtained in Step 5.

### 6.1.2. CFD modeling of jet fire in literature

The primary application of CFD in jet fire simulation is primarily focused on modeling the consequences of such fires. By understanding the geometry of the jet fire and the dynamics of heat transfer, it becomes possible to take preventive measures to mitigate the occurrence of impingement phenomena.

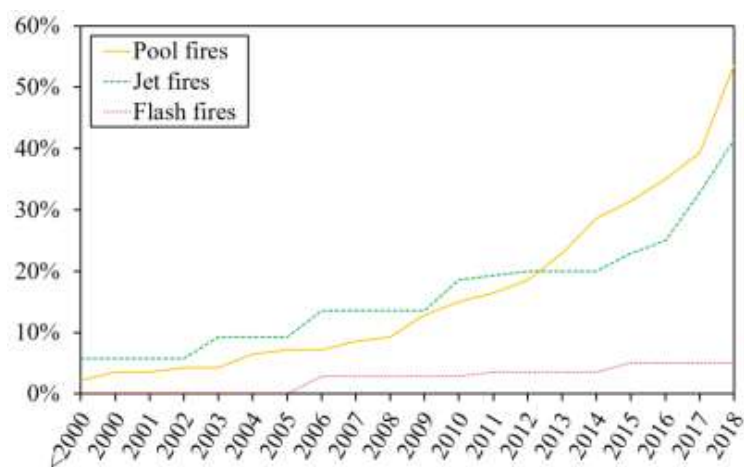


Figure 6-3. Publications frequency over the years. Flash fires (red), jet fires (green) and pool fires (yellow) trends is sharply increasing during the last years (Rengel, 2019).

In the study conducted by Rengel et al. (2019), which analyzed 62 publications on CFD fire simulations from the 1990s to 2018, jet fire modeling accounted for 40% of the total simulation studies. It was found to be the second most studied accident scenario after pool fires. The increased interest in jet fire simulations can be attributed to the growing number of accidents caused by these fires over the years, which has emphasized the need for a better understanding of their consequences. Figure 6-3 illustrates the frequency of publications related to CFD simulations of pool fires, jet fires, and flash fires over time. Various CFD codes have been used to simulate different scenarios involving jet fires. These codes can be either commercial, requiring costly licenses, or open-source and freely available, depending on the developer's interests and objectives. Recently used codes for jet fire simulation include ANSYS FLUENT, Fire Dynamics Simulator (FDS), Fire-FOAM, Kameleon FireEx KFX, and FLACS (Shen et al., 2020).

In this thesis, the FLACS CFD code, a commercial code developed by Gexcon AS, is employed to simulate a propane horizontal jet fire. Previous studies have been conducted on the application of FLACS for jet fire analysis, particularly for vertical (Rengel et al., 2020; Pedersen, 2012) and horizontal (Muthusamy et al., 2011) jet fires. However, further investigation, particularly regarding horizontal jet fires and the phenomenon of impingement on pipelines, is necessary to understand the capabilities of this software in accurately describing these phenomena and their consequences.

## **6.2. Step-by-step modelling of jet fires using FLACS**

In this section, we examine the simulation steps involved in replicating the jet fire experiments discussed in section. We provide a detailed analysis of the modeling procedure used in these simulations.

### **6.2.1 Geometry**

Geometry can be defined in FLACS by building complex objects by adding or subtracting several simple components from primitives (boxes, cylinders, etc.). Any geometry can consist of one or several objects, or assemblies of several objects. They are all managed and stored through a Database. To define the geometry, cylinders are created to represent the nozzles, with lengths of 50 centimeters and diameters of 6mm and 8mm. Additionally, a box measuring 7m (x) x 5m (y) x 0.5m (z) is generated to represent the ground. It is important to note that the purpose of the nozzle in this context is solely for spatial reference, as the specific leak characteristics will be specified in the LEAKS section within the scenario menu.

### **6.2.2 Computational grid**

Based on the experimental data, it is necessary to select a domain that encompasses the analyzed phenomena. In this regard, a core domain measuring 2m x 2m x 2m and a stretch domain of 4.5m x 3m x 5m are chosen.

Choosing an appropriate cell size is essential, considering three factors: computational resolution to achieve accurate results, computational cost to obtain timely results, and the applicability of models to avoid simulation errors.

To ensure these conditions are met, the characteristic diameter of the fire ( $D^*$ ) is taken into account as a starting point (Lin et al., 2010).

$$D^* = \left( \frac{\dot{Q}}{\rho_\infty c_p T_\infty \sqrt{g}} \right)^{\left(\frac{2}{5}\right)} \quad \text{with} \quad \dot{Q} = \dot{m}_{rel} \cdot \Delta H_c \quad (6-1)$$

Where  $\dot{Q}$  is the heat release rate of the fire that can be obtained multiplying the mass release rate  $\dot{m}_{rel}$  to the enthalpy of combustion  $\Delta H_c$ ,  $\rho_\infty$  is the ambient air density,  $c_p$  is the air specific heat,  $T_\infty$  is the ambient temperature and  $g$  is the gravitational acceleration.

Then, the non-dimensional parameter  $D^*/\delta_x$ , where  $\delta_x$  is the cell size, should be ranged between 4 (coarse cell size) and 16 (thin cell size) (Salley & Kassawara, 2007).

Choosing a cell size  $\delta_x=0.1$  m for all the experiments, the parameter  $D^*/\delta_x$  varies between 8 and 10 complying with the range, using the following data (Green & Perry, 2008):

$$\dot{m}_{rel} = 0.008 \div 0,016 \text{ kg/s}$$

$$\Delta H_c = 44333 \text{ kJ/kg}$$

$$\rho_\infty = 1.196 \text{ kg/m}^3$$

$$c_p = 1.006 \text{ kJ/(kg K)}$$

$$T_\infty = 295,15 \text{ K}$$

$$g = 9.81 \text{ m/s}^2$$

This value is implemented in the core domain, which corresponds to the region where the flame is expected. Consequently, the grid size of the stretch domain is automatically calculated, ensuring a stretch factor of 1.3.

However, it is necessary to refine the leak area to prevent ignition errors. Additionally, the manual suggests implementing grid refinement across the jet direction. During the refinement process, it is important to ensure that the minimum size is equal to the leak diameter. Furthermore, the maximum percentage difference should be kept below 40% (Gexcon AS, 2020). Following this procedure, a total of 125,000 cells are obtained, which requires approximately three days of computation.

The final results for simulations conducted with nozzle diameters of 6 mm and 8 mm are depicted in Figure 6-4.

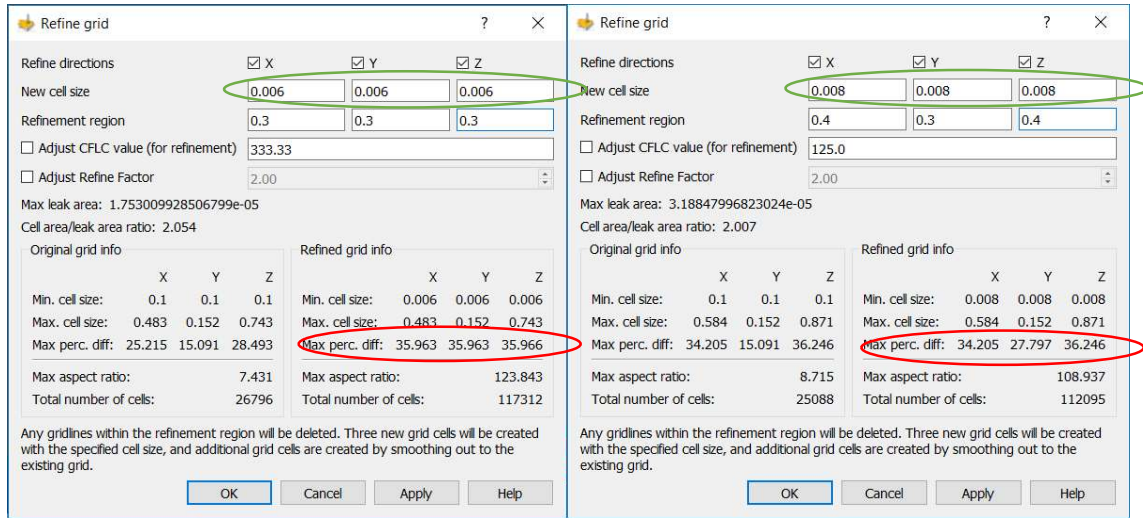


Figure 6-4. Grid refinement final results of 6 mm (left) and 8 mm (right) nozzle diameter simulations. Minimum cell size needs to be equal to the diameter of the leak (green circle) and the maximum percentage difference between minimum and maximum cell size needs to be lower than 40% (red circles).

### 6.2.3 Scenario

Gas phase horizontal release from an orifice is selected in the leak properties. The reservoir contains pure propane at experimental temperature and pressure conditions, and the volume is big enough to maintain a steady-state flow. The hole's diameter, time dependency, start time, and duration are selected in the release properties. The release starts at time zero and continues for the entire duration of the simulation. The discharge coefficient depends on the nozzle shape. Therefore, a value of 0.62 is chosen from the literature, considering a sharp-edged orifice (Casal, 2008). The Edwan-Moodie pseudo-source model is preferred because it shows better agreement with experiments (Gexcon AS, 2020), and an accurate velocity value is crucial for predicting flame shape. Finally, the atmospheric conditions are provided. The consistency of the values obtained from the leak wizard results for the JFT-191114-2-T6 simulation is verified by comparing them with the experimental data, as shown in Figure 6-6. Jet fire modeling assumptions are summarized in Table 6-1.

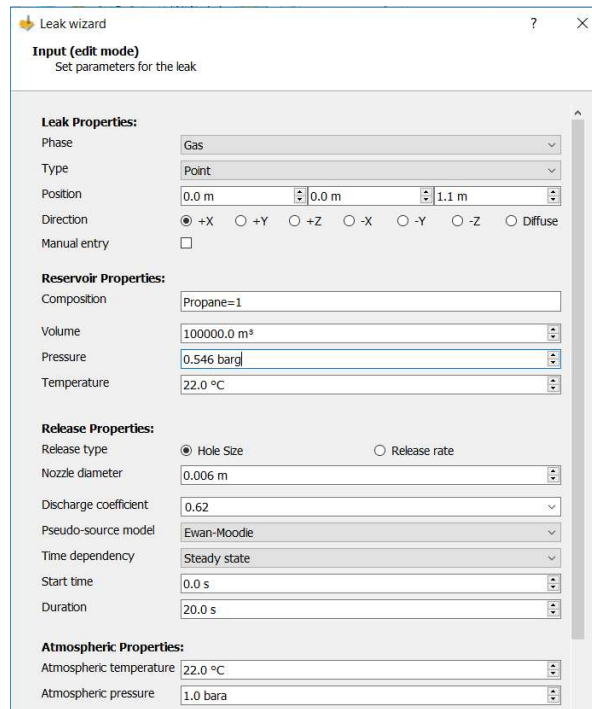


Figure 6-5. Leak wizard window, JFT-191114-2-T6 simulation data.

**Leak outlet**

Area	1.75301e-05 m <sup>2</sup>
Mass flow rate	0.00719173 kg/s
Velocity	217.584 m/s
Relative turbulence intensity	0.1
Turbulence length scale	0.00047244 m

Figure 6-6. JFT-191114-2-T6 simulation release properties results obtained by leak wizard tool.

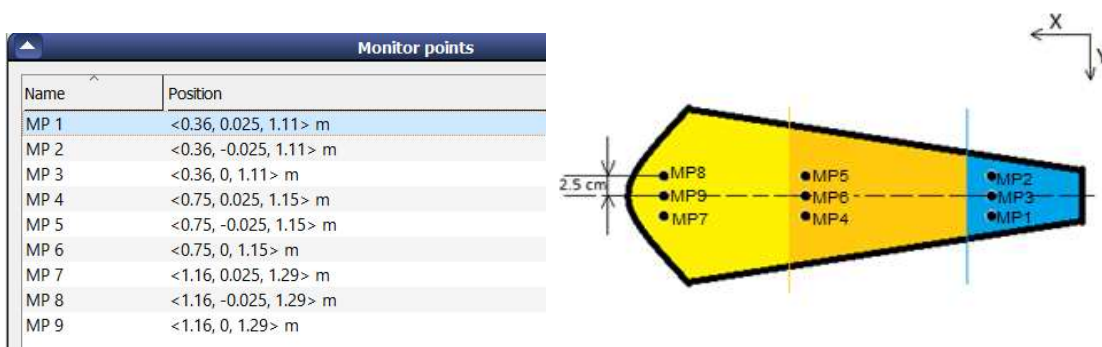


Figure 6-7. Monitor points positions in the domain  $\langle x, y, z \rangle$  (left), and inside the flame (right).

Table 6-1. Jet fire modeling scenarios and assumptions.

Parameter	Assumption
Scenario Setting	The simulation focuses on a jet fire scenario. To model the pseudo-source, the Leak-wizard tool was employed. Figure 6-5 displays the Leak-wizard panel for the JFT-191114-2-T6 test, where properties related to the leak, reservoir, and release are specified.
Leak Properties	The gas phase horizontal release from an orifice was configured in the simulation. The reservoir contains pure propane and was set to match the experimental temperature and pressure conditions. The release properties, such as the diameter of the hole, start time, and duration, are defined. The discharge coefficient was selected as 0.62, based on literature references for a sharp-edged orifice. (Casal, 2008).
Pseudo-Source Model	The Edwan-Moodie pseudo-source model was preferred due to its better agreement with experimental data (Gexcon AS, 2020). Accurate velocity values are crucial for predicting the shape of the flame.
Atmospheric Conditions	The relevant atmospheric conditions, such as temperature, pressure, and other relevant parameters, are provided to ensure a realistic simulation environment.
Monitor points	9 monitor points were defined to simulate the thermocouples. Positions tabulated Table 3-9 spaced by 2.5 cm are selected to reproduce experimental conditions (Figure 6-7), temperature and heat flux variables are registered.
Single field 3D output	Temperature, velocity vector, equivalent ratio, total, convective, and radiative heat flux, mass fraction of soot, product and fuel were selected as 3D parameter.
Simulation and output control	steady state condition was verified after 4 s simulation, for this reason this value was chosen for simulation duration. Data are registered every 0.1 s and CFLC = 20 and CFLV=2 are chosen as suggested by FLACS' manual for fire simulations.
Boundary condition	NOZZLE boundary condition was chosen as suggested by FLACS' manual for fire simulation.

Parameter	Assumption
Initial conditions	Ambient conditions were defined: T=22°C, P=1atm and no wind. Default values were not changed.
Gas composition and volume	No fuel was present in the domain before leak starts, and fuel composition was 100% propane.
Ignition	Time of ignition should be set with a short delay after the leak was started; for this reason, ignition time value equal to 0.2 s was chosen. It was recommended to use a large 3D ignition region to ensure that jet was ignited; all the domain was selected for this purpose.
Radiation	The impact of the radiation model on computational time was assessed. A simulation was conducted with and without the DTM radiation model, adjusting parameters such as frequency iteration period and domain size. The absorption coefficient model "DANISH-COUPLED-WSGGM" was selected, following the manual's recommendations.
Combustion	Eddy Dissipation Concept was chosen as combustion model due to the fact that flame shape accuracy was requested. The model was indeed more precise in the analysis of combustion rate, taking into account turbulence effects.
Smoke/Soot	A comparison between CFM and FOX was performed to analyze the effects of soot model. Soot yield equal to 0.09 was selected for propane according to several trials.
Conduction	Conduction was switched off, reducing computational time, because it was not necessary to the calculation. In addition, conduction model is under validation by FLACS' developer for this reason it is not suggested to use it.



For each test, the data described above are used to simulate the experiments. The characteristic experiment parameters that are changed for each test include the leak hole diameter and the release pressure.

### **6.3. Jet fire results**

To assess the flame geometry and temperatures, a 2D Cut plane function is utilized. This function creates a cross-section of the domain, specifically an XZ cross-section parallel to the flame axis at  $Y = 0$ , where the nozzle is located. The temperature variable is selected, and a temperature threshold of 800 K is applied to visualize the flame contours, following the approach by Palacios and Casal (2011). Thermocouple temperatures are obtained using Scalar time plots. The Temperature variable is selected for each monitor point, and the temperatures are recorded at the end of the simulations when steady-state conditions are achieved. Qualitative checks are also performed using 3D plots to validate the results.

#### **6.3.1. Radiation model**

Flame geometry and temperature are evaluated with and without the radiation model. By comparing the flame contours, it is observed that the flame shape remains similar, indicating that the presence or absence of the radiation model has minimal impact on the geometry of the fire. However, in the absence of a radiation model, there is an overprediction of flame temperatures compared to the obtained data from experimental tests, as shown in Figure 6-8. This observation aligns with previous findings in the literature by Pedersen (2012).

#### **6.3.2. Soot model**

Based on Figure 6-9, it can be observed that the flame geometry is minimally affected by the inclusion of the soot model. However, the CFM model has an impact on temperature values and the temperature profile of the flame. Specifically, the CFM model leads to lower temperatures and a smaller hottest area within the flame. This can be attributed to the higher soot concentration when the CFM model is applied, which affects the radiated energy. In conclusion, the results indicate that the radiation model is crucial for accurately describing flame temperatures, but it has limited influence on assessing flame geometry. Similar effects are observed when different soot models are

used. As a result, for simulations focused on flame geometry assessment, the combination of the DTM model with the FOX model is selected, using a smaller domain to save computational time. On the other hand, for simulations aimed at assessing flame temperatures, a larger DTM domain is used to improve accuracy, and a comparison between the CFM and FOX models is conducted.

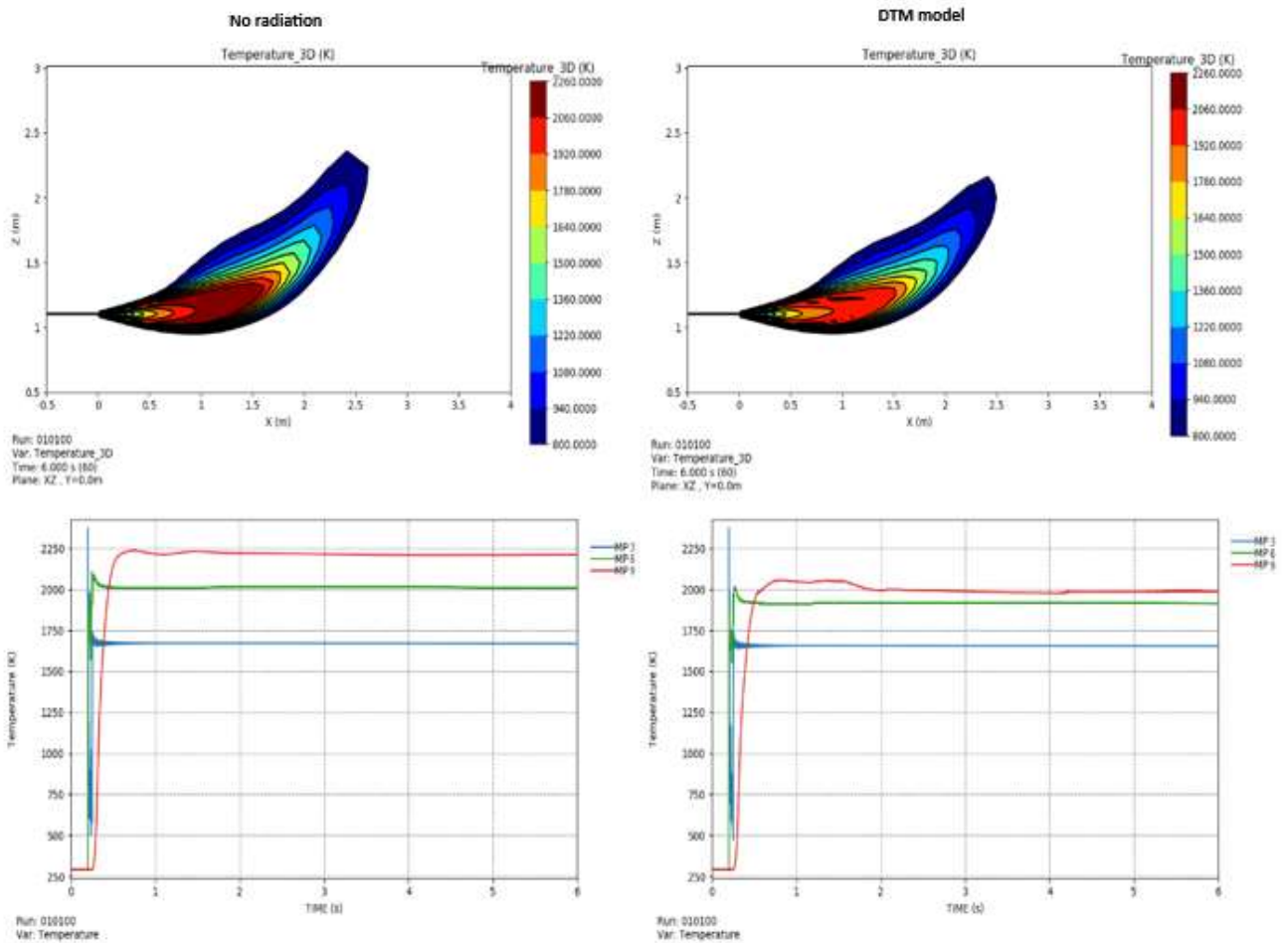


Figure 6-8 XZ plane of flame temperature and scalar plot of temperature over time comparison without (left) and with (right) DTM radiation model. Lower temperatures were detected when DTM model is used.

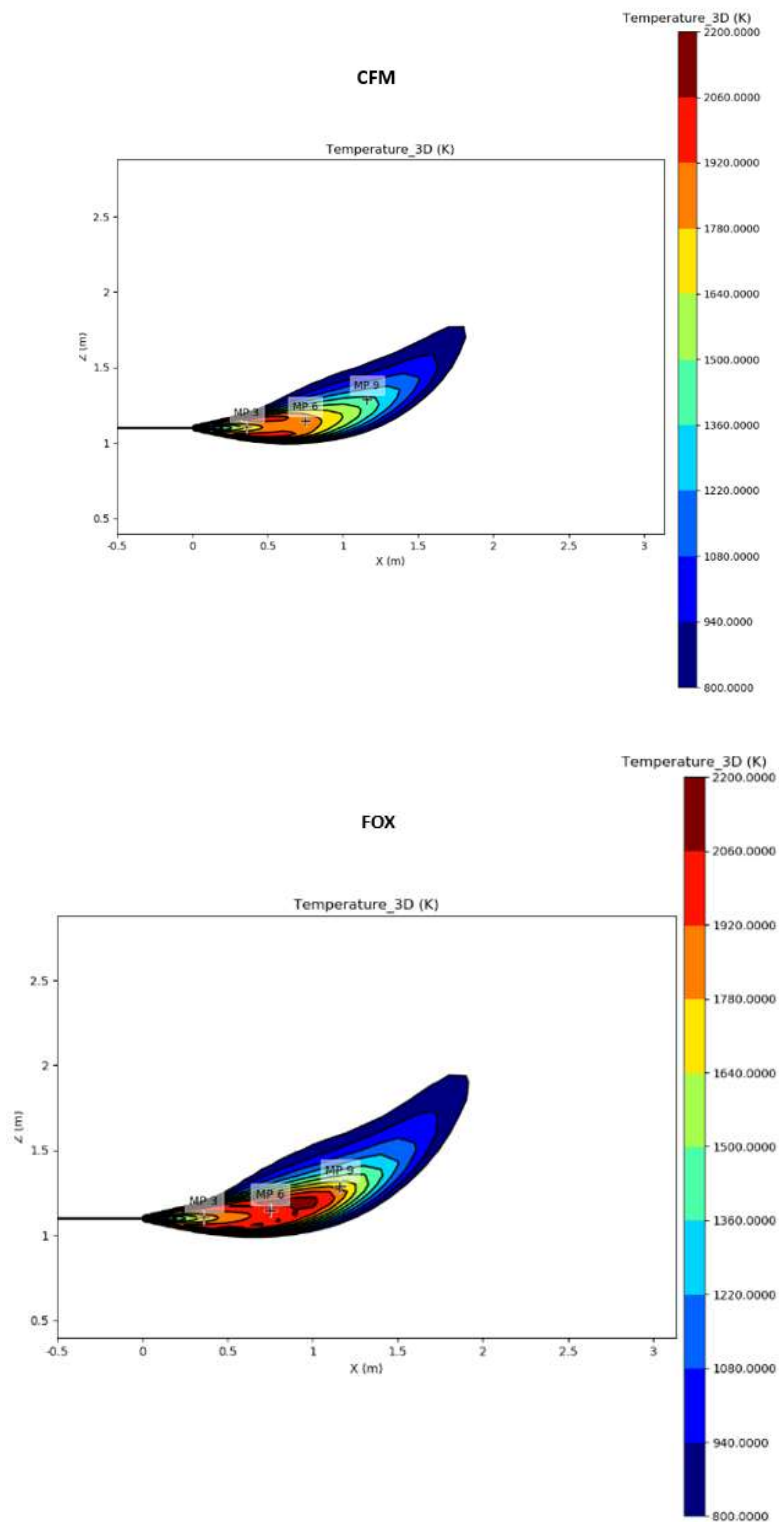


Figure 6-9 Comparison between CFM and FOX model; lower temperatures were detected when CFM model is used.

### 6.3.3. Flame geometry

After selecting a temperature threshold of 800 K and defining the flame contours (

Figure 6-10), the various flame characteristics can be plotted including flame length, lift-off distance, and height. Additionally, the flame area is calculated using the open-source software ImageJ (Rasband & National Institutes of Health USA). The pixel area of the plotted results is evaluated, and then converted into real dimensions using the actual nozzle area as a reference measure. The results of the geometric parameters are presented in Table 6-2.

Table 6-2. Flame geometry parameter results: flame length ( $X_f$ ), height ( $Z_f$ ), lift-off ( $S_f$ ) total length ( $L_t$ ) and area ( $A_f$ ).

		$X_f$ [cm]	$Z_f$ [cm]	$S_f$ [cm]	$L_t$ [cm]	$A_f$ [cm <sup>2</sup> ]
P1	Experimental	186.65	83.54	21.34	208.00	7989.43
	Simulated	224.05	124.00	0.95	225.00	11169.00
P2	Experimental	198.32	85.83	25.08	223.40	8964.08
	Simulated	238.04	118.00	0.96	239.00	13567.00

P4	Experimental	222.01	100.02	29.55	251.56	10071.21
	Simulated	248.03	121.00	0.97	249.00	13718.00
P6	Experimental	214.39	95.82	21.47	235.86	10666.74
	Simulated	229.07	124.00	0.93	230.00	11504.00
P8	Experimental	204.99	98.57	20.13	225.11	10052.51
	Simulated	206.10	130.00	0.90	207.00	6765.00
P10	Experimental	171.07	92.99	18.64	189.71	7297.62
	Simulated	173.10	132.00	0.90	174.00	6906.00

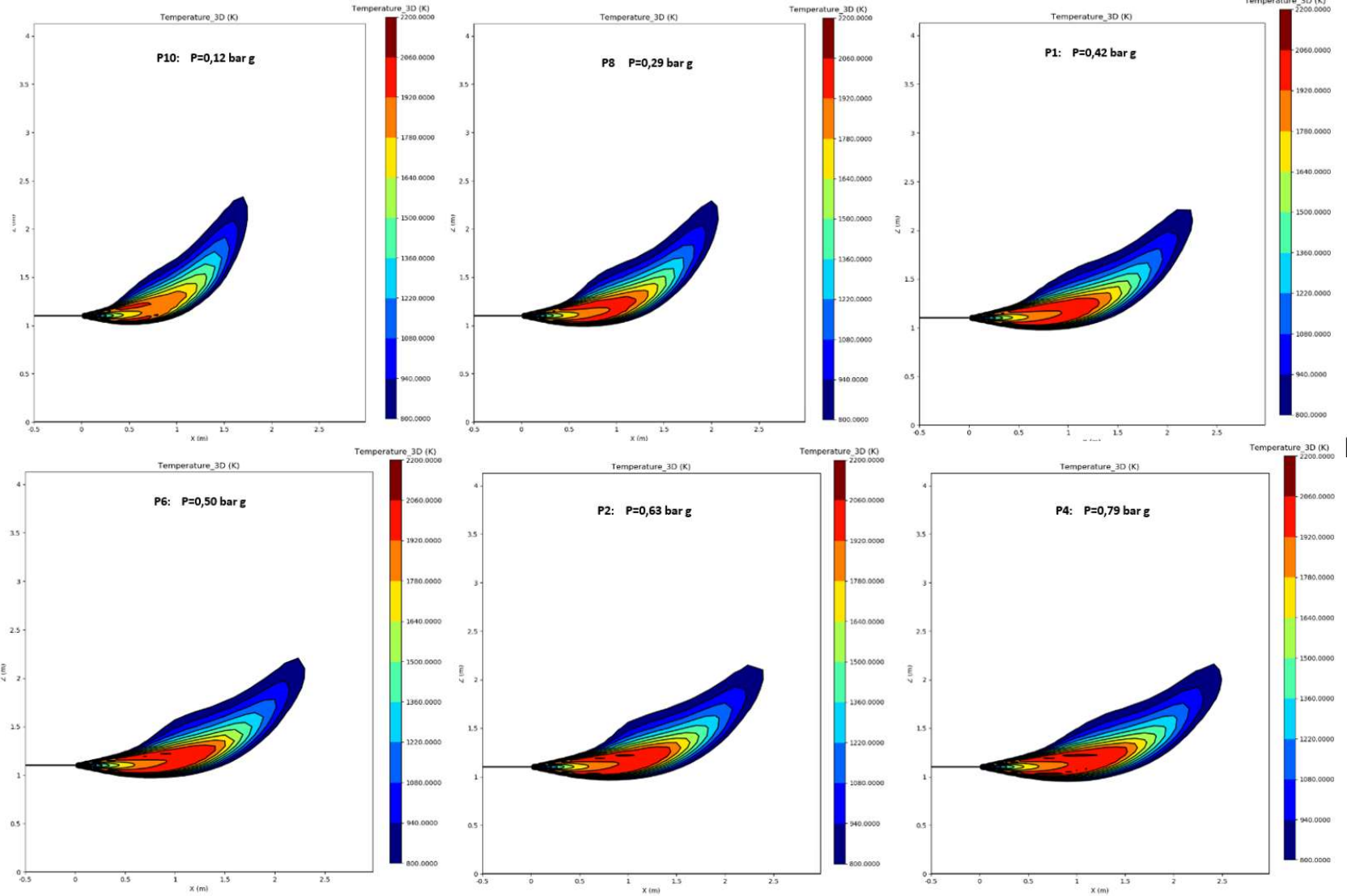


Figure 6-10. XZ plane 2D temperature plots results of simulations of jet fire geometry assessment.

### 6.3.4. Flame temperature

The temperatures at monitor points for the JFT-191114-2-T6 and JFT-191114-2-T8 experiments are obtained using the FLACS Flowvis postprocessor module. Scalar line plots illustrating the temperature profiles are displayed in Figure 6-11, and the corresponding tabulated results are provided in Table 6-3.

Table 6-3. JFT-191114-2-T6 and JFT-191114-2-T8 simulation results; temperature of monitor points using CFM and FOX soot formation model, and experimental values of corresponding thermocouple (EXP).

	JFT-191114-2-T6			JFT-191114-2-T8		
	Exp [°C]	CFM [°C]	FOX [°C]	Exp [°C]	CFM [°C]	FOX [°C]
MP1	1010	1530	1537	937	1450	1466
MP2	1022	1530	1537	1281	1450	1466
MP3	804	1414	1430	913	1371	1386
MP4	1218	1576	1742	1263	1617	1662
MP5	1264	1576	1742	1330	1617	1662
MP6	1222	1584	1716	1314	1603	1643
MP7	1191	1113	1474	1347	1228	1702
MP8	1303	1113	1474	1396	1228	1702
MP9	1307	1126	1511	1452	1237	1712

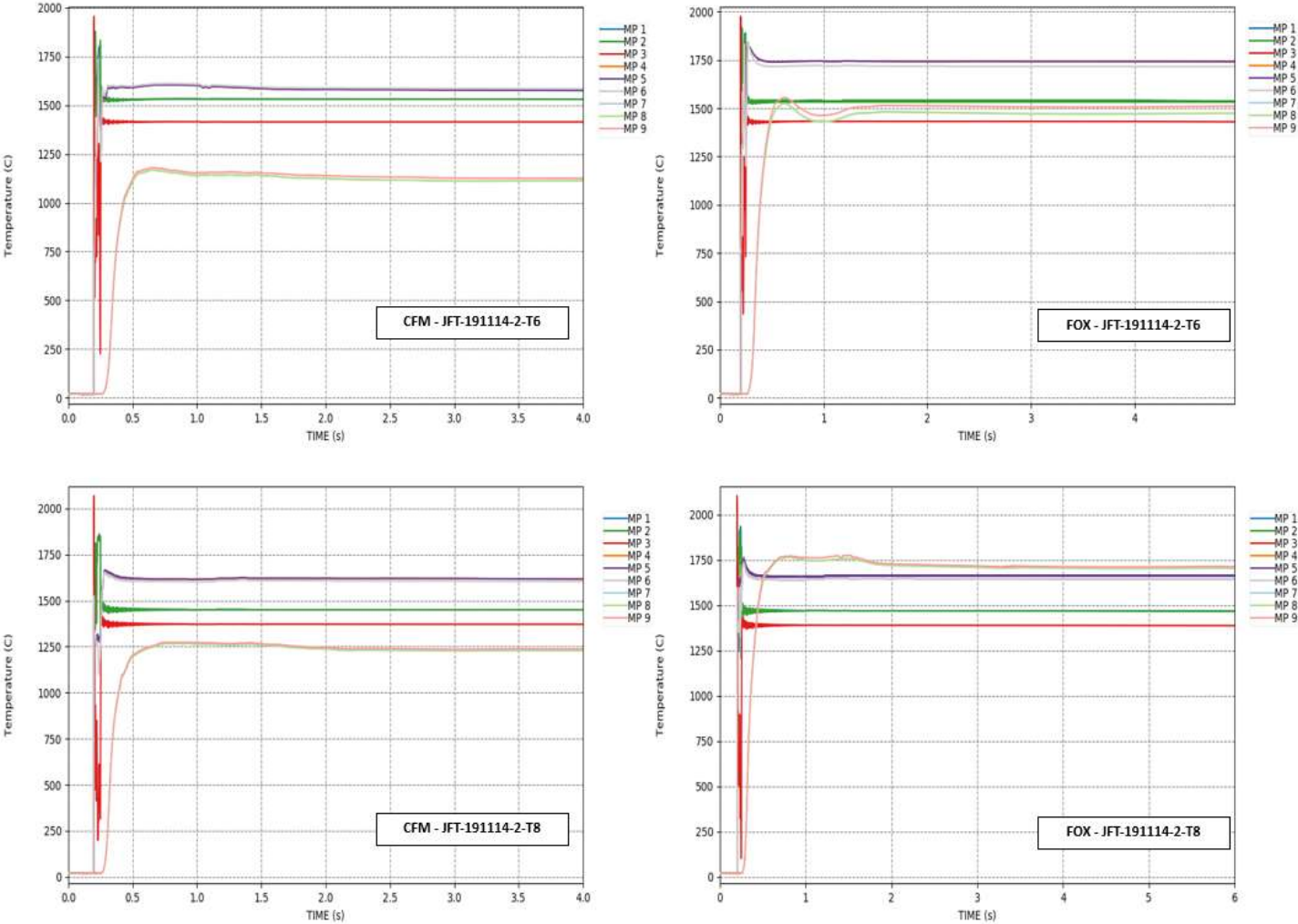


Figure 6-11. Temperature-time plots of experiment JFT-191114-2-T6 and JFT-191114-2-T8 simulations, using CFM and FOX soot formation model.



## 6.4. Discussion

The assessment of the accuracy and acceptability of the results is carried out by evaluating parameters that measure the performance of the simulations. Subsequently, the findings regarding the jet fire geometry and flame temperatures are analyzed and discussed.

### 6.4.1. Performance parameters

The accuracy of the results obtained from the FLACS-CFD code is evaluated both quantitatively and qualitatively using performance metric parameters provided by Gexcon AS (2020). The FAC2 parameter is utilized to assess the performance of the simulations graphically. In this evaluation, simulation values that fall within a factor of two of the observed values are considered acceptable.

$$0,5 X_0 \leq X_p \leq 2 X_0 \quad (6-2)$$

Subsequently, scatter plots are generated to visually depict the simulated data, with a solid line representing perfect agreement with the experimental values and dotted lines indicating the  $\pm 50\%$  error range. Acceptable values should fall within the region delimited by the dotted lines.

Quantitative analysis is conducted using the fractional bias (FB) (Equation 6-3) and the normalized mean square error (NMSE) (Equation 6-4). In these equations, "n" represents the total number of experiments, "X<sub>0</sub>" denotes the experimental mean value, and "X<sub>p</sub>" represents the predicted value. Ideally, a perfect model would yield FB and NMSE values of zero. A negative FB value indicates an overprediction. As performance criteria, NMSE values below 0.5 and FB values within the range of  $\pm 30\%$  are considered acceptable, as specified by Hanna. (2004).

$$-0,3 \leq FB = \frac{1}{n} \sum_{i=1}^n 2 \frac{X_0 - X_p}{X_0 + X_p} \leq 0,3 \quad (6-3)$$

$$NMSE = \frac{1}{n} \sum_{i=1}^n \frac{(X_0 - X_p)^2}{X_0 X_p} \leq 0,5 \quad (6-4)$$

### 6.4.2. Flame geometry

Performance parameters are calculated to evaluate the accuracy of the flame geometry results.

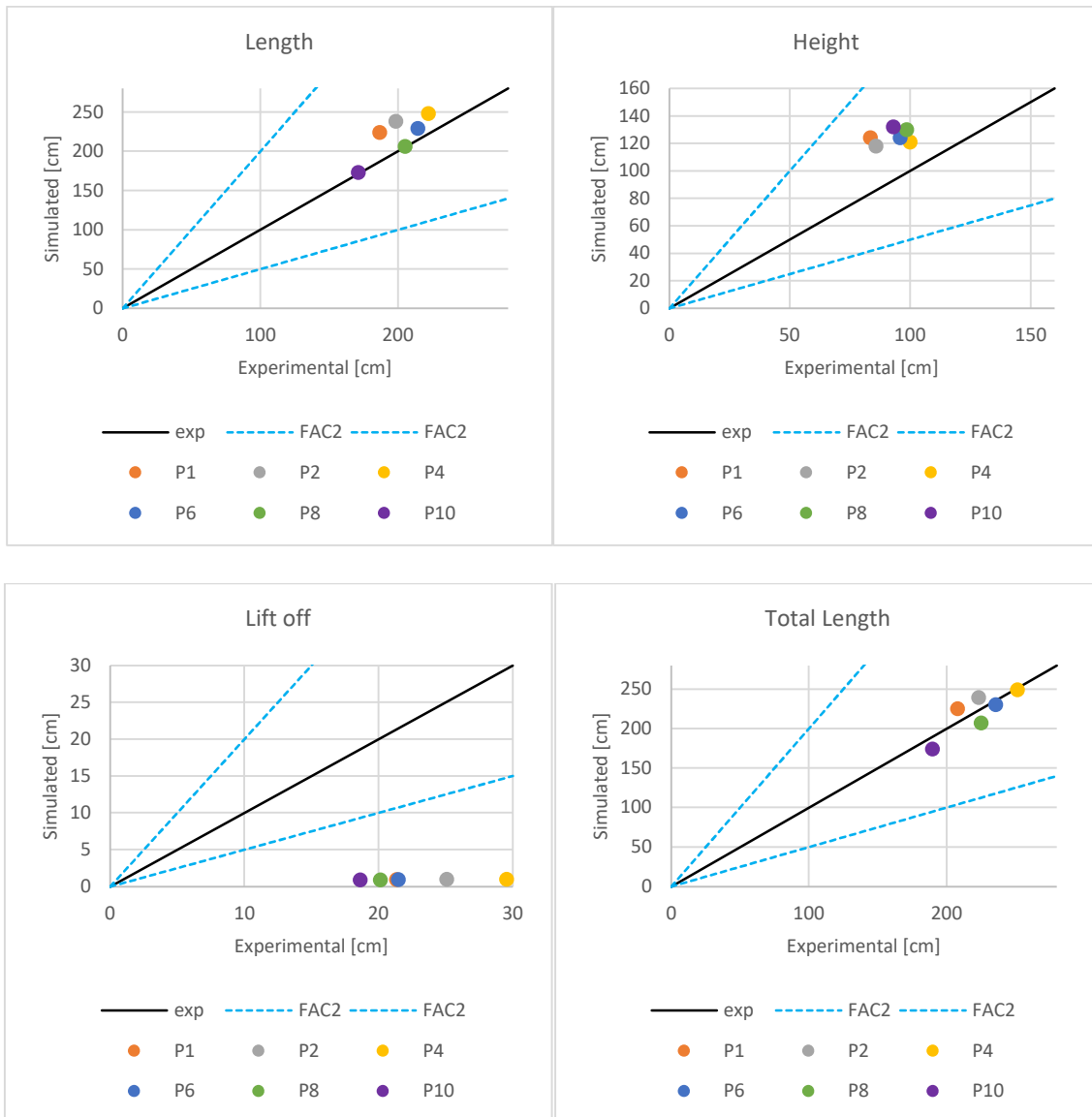


Figure 6-12. Qualitative analysis of flame geometry parameter results of experiment P1, P2, P4, P6, P8 and P10 using FAC2 criteria; straight black line represents a perfect agreement with experimental data. Values are acceptable if they are within the zone delimited by the blue dot-line.

Based on the qualitative analysis (Figure 6-12), it is observed that all the parameters, except for the lift-off distance, fall within the acceptable range. This observation is further supported by the quantitative analysis presented in Table 6-4. However, it is important to note that the underprediction of the lift-off distance in jet fires is a known issue that is acknowledged in all versions of FLACS-Fire, as documented in the manual (Gexcon AS, 2020). Further investigations are required to address this issue.

Table 6-4. Quantitative analysis of flame geometry parameter results using FB and NMSE criteria; in red the values that are out of the acceptable range.

	<b>Xf</b>	<b>Zf</b>	<b>Sf</b>	<b>Lt</b>	<b>Af</b>
FB	-0.093	-0.296	1.839	0.010	-0.113
NMSE	0.014	0.094	22.245	0.004	0.092

Specifically, the results indicate that the flame length, height, and area are slightly overpredicted, while the total length of the flame is nearly accurately predicted by the model. Considering the limitations of the FLACS-Fire code, it can be concluded that the model used is capable of describing the shape of the jet fire.

Qualitative analysis shows that model used are acceptable, taking into account the FAC2 criteria (Figure 6-13). In addition, according to the quantitative study, predictions obtained with CFM model are closer to experiments value (Table 6-5). In conclusion, an overall overprediction of flame temperature is detected, especially when FOX soot model is used.

The qualitative analysis indicates that the models used in the study meet the acceptance criteria based on FAC2 (Figure 6-13). Furthermore, the quantitative analysis demonstrates that the predictions obtained with the CFM model align more closely with the experimental values (Table 6-5). In conclusion, there is an overall tendency to overpredict the flame temperature, particularly when the FOX soot model is employed.

### 6.4.3. Flame temperature

Performance parameters were calculated to evaluate the accuracy of the flame temperature results, as depicted in Figure 6-13.

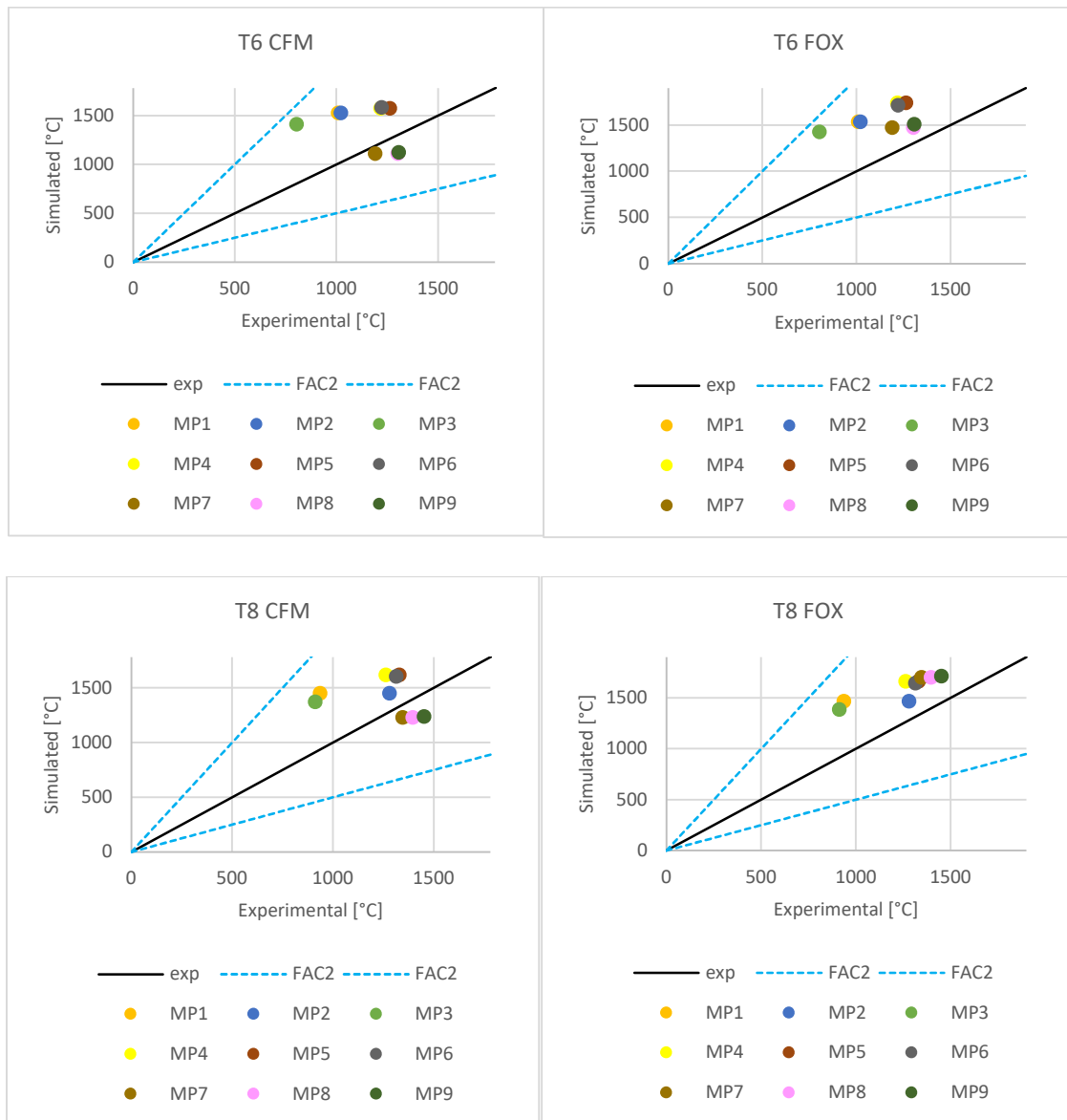
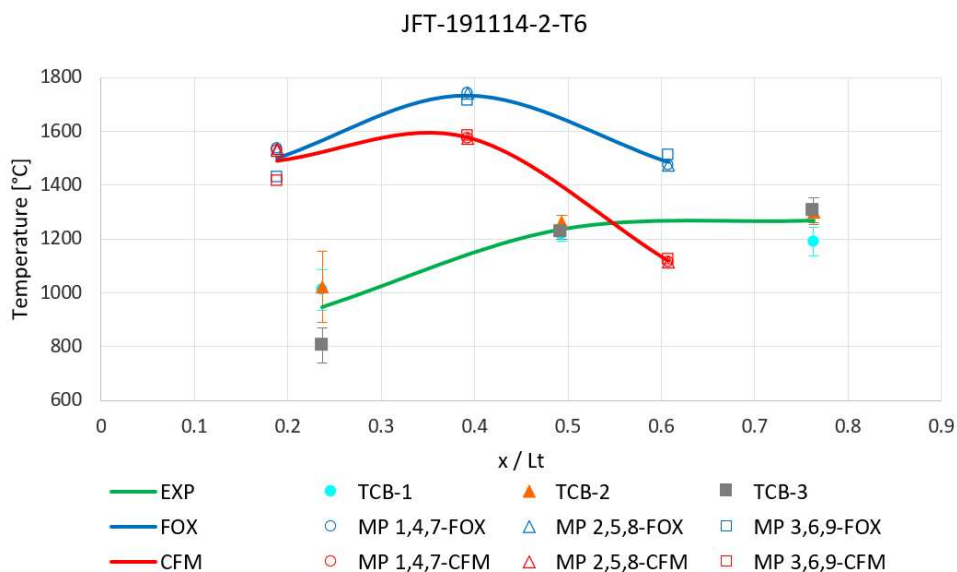


Figure 6-13. Qualitative analysis of flame temperature results of JFT-191114-2-T6 and JFT-191114-2-T8 experiments coupled with CFM and FOX model, using FAC2 criteria; straight black line represents a perfect agreement with experimental data. Values are acceptable if they are within the zone delimited by the blue dot-lines.

Table 6-5 Quantitative analysis of flame temperature results of JFT-191114-2-T6 and JFT-191114-2-T8 experiments coupled with CFM and FOX model using FB and NMSE criteria.

		CFM	FOX
JFT-191114-2-T6	FB	-0.191	-0.318
	NMSE	0.100	0.124
JFT-191114-2-T8	FB	-0.135	-0.255
	NMSE	0.063	0.077

The heat transfer resulting from the impingement of a jet flame undergoes changes in accordance with the temperature distribution. Therefore, an assessment of the temperature is performed by analyzing the temperature profiles (Figure 6-14). In the case of the JFT-191114-2-T6 simulations, both CFM and FOX models predict temperature profiles that reach a peak at around 30-40% of the flame length, which differs from the experimental data where the maximum temperature is reached at 75%. Similar conclusions are drawn when analyzing the JFT-191114-2-T8 simulation using the CFM model. However, interesting results are obtained when employing the FOX model. In this case, the temperature profile closely mirrors the experimental data, albeit with an overprediction of temperature. In summary, the CFM model yields better results in terms of temperature values, whereas the FOX model provides a more accurate description of the temperature profile, particularly when sonic conditions are met.



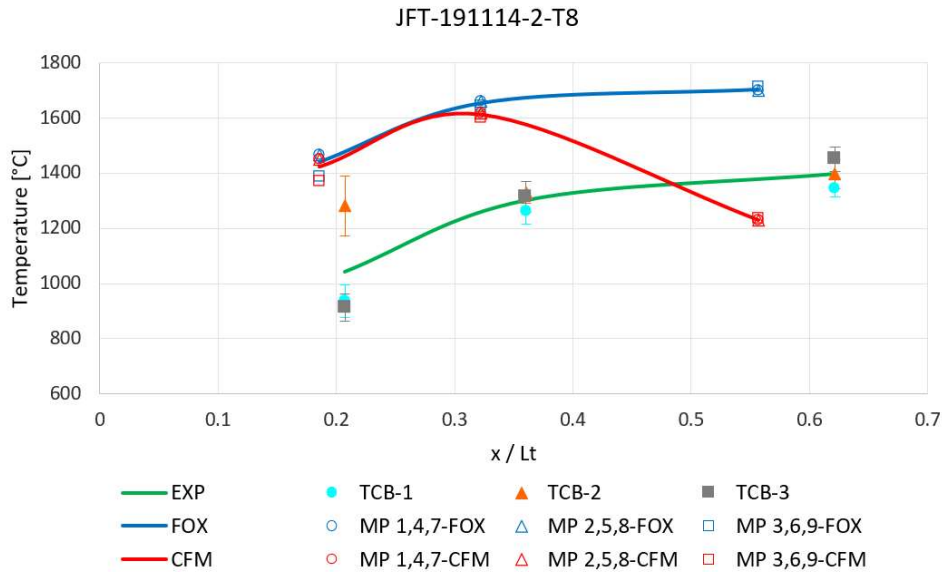


Figure 6-14. Temperature profile for JFT-191114-2-T6 and JFT-191114-2-T8 nozzle diameter. CFM model (red) and FOX model (blue) simulations and experimental data (green). Profiles are obtained interpolating data of averaged thermocouple temperatures.

## 6.5. Further studies: Jet Fire Impingement

In this section, we present the first study conducted on the impingement of a horizontal jet fire on a pipe using the FLACS CFD code. The implemented models from the previous sections of this work are utilized in these simulations. The primary objective of this study is to examine the impact of impingement phenomena on the external flame temperature of the pipe and assess the capability of FLACS to accurately simulate such scenarios. The simulations are validated against the impingement experiments obtained in Chapter 5.

### 6.5.1. Experimental set up and impingement experiments

The experimental setup described in Chapter 3 was employed to generate horizontal propane jet fires with various release conditions. These jet fires were directed towards a pipe with dimensions of 3 meters in length, 4 inches in external diameter, and 6 mm in thickness. Thermocouples of type-B were positioned at four different locations relative to the pipe, namely the front, top, bottom, and back, each situated 1 cm away from the external wall of the pipe. The temperatures of the flame were recorded using these thermocouples. Three pipe impingements were tested within different zones of the flame, specifically the blue zone (IB8), middle zone (IM8), and front zone (IF8), under

sonic release conditions. Table 6-6 provides a summary of the experimental conditions and the positions of the instrumentation.

Table 6-6. Experimental conditions and instrumentation position.

Experiment name	IB8	IM8	IF8
Impingement zone	Blue	Middle	Front
Nozzle diameter [mm]	8	8	8
Release pressure [bar g]	1.06	0.8	0.83
Release Condition	Sonic	Sonic	Sonic
Nozzle position [cm]	$X_N=0; Z_N=110$	$X_N=0; Z_N=110$	$X_N=0; Z_N=110$
Pipe position [cm]	$X_P=40.08;$ $Z_P=110$	$X_P=105.08;$ $Z_P=112$	$X_P=135.08;$ $Z_P=115$

### 6.5.2. CFD modeling and results

The modeling procedure is conducted by simulating the experiment JFT-191114-2-T8 described in this study. This choice is made due to the similarity in scenario conditions and the agreement of results with the experimental data. Therefore, the same simulation parameters used for the JFT-191114-2-T8 FLACS simulation are utilized unless otherwise specified, with the addition of elements necessary to accurately depict the impingement phenomena. Based on the geometry of the JFT-191114-2-T8 simulation, a separate cylinder is generated with a length of 3 m and a diameter of 4 inches to serve as a representation of the pipe. The position of this cylinder is adjusted based on the provided data.

To configure the computational grid, the same procedure as described in section 6.2 is followed. Additionally, a refinement near the pipe is implemented to improve the accuracy of results in the specific area of interest. The release pressures are adjusted based on the data presented in section 6.5, and the FOX soot formation model is chosen due to the temperature profile depicted in Figure 6-14, which demonstrates that the simulated data aligns with the experimental data when the FOX model is employed. Furthermore, the existing monitor points used for evaluating flame temperature are removed and replaced with four new monitor points positioned around the pipe to

simulate the thermocouples TC1, TC2, TC3, and TC4. The results are qualitatively evaluated by examining the 3D plots of temperature (Figure 6-15).

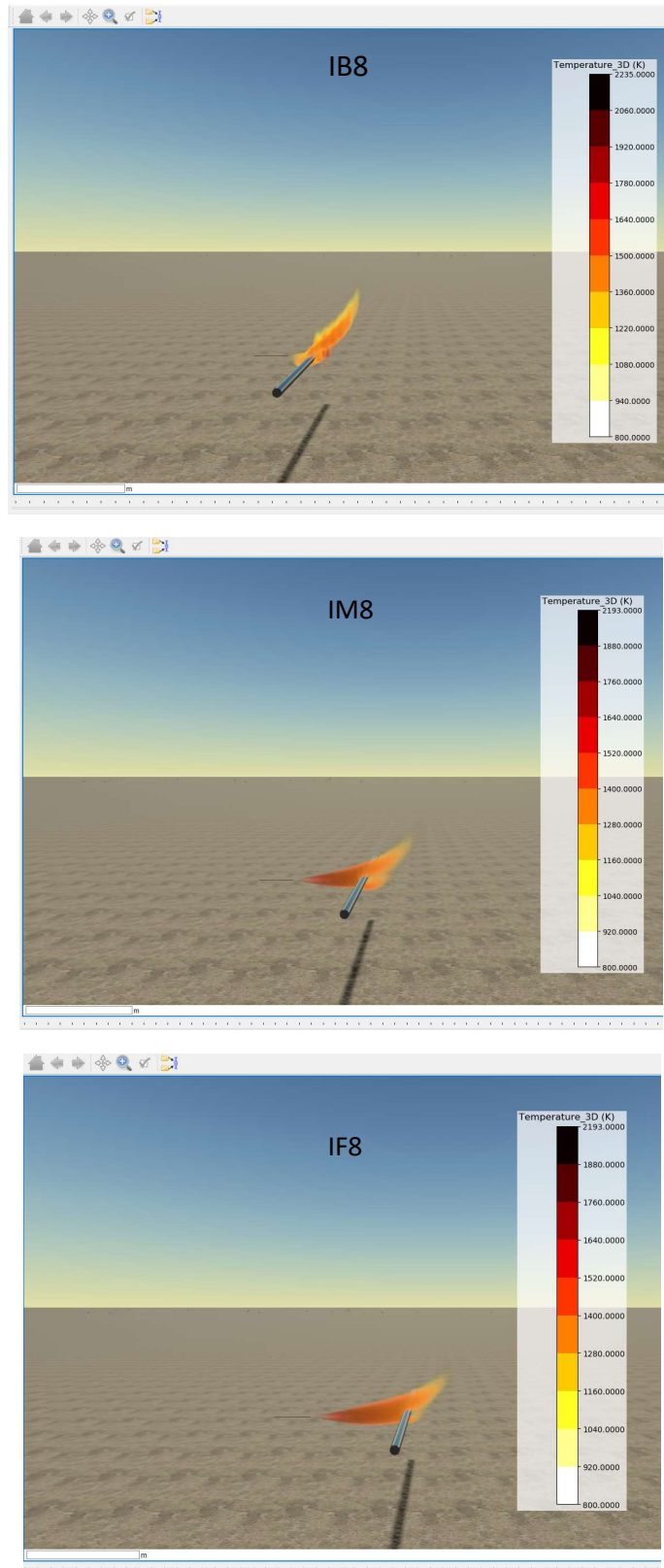


Figure 6-15. 3D plots of temperature of simulated experiments IB8, IM8 and IF8, flame contours are obtained applying the temperature threshold equal to 800 K.



The temperature of the monitor points is extracted using the Flowvis post-processor FLACS module to create temperature-time plots, and the values are displayed in Figure 6-16.

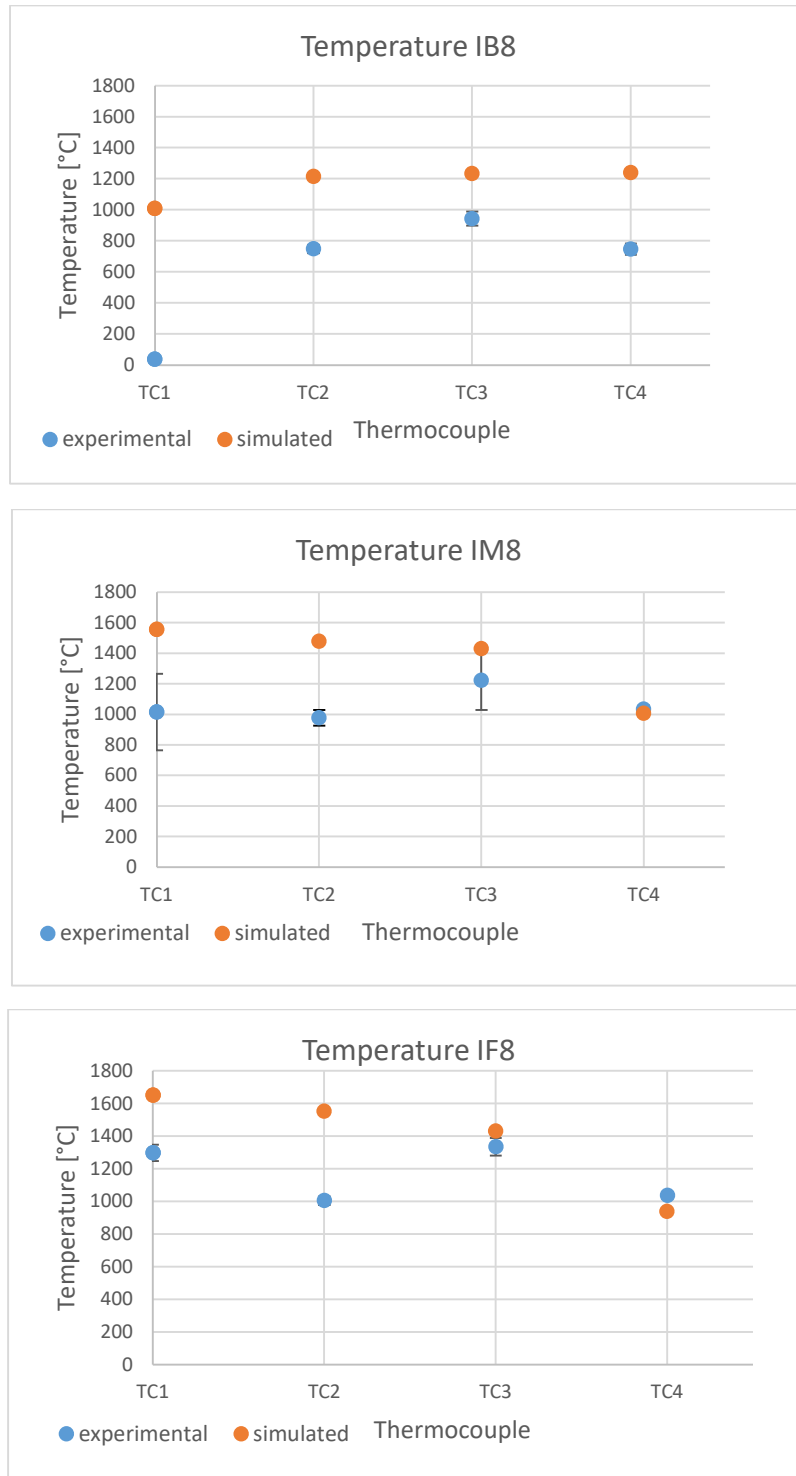


Figure 6-16. Simulated and experimental average temperature values of simulations IB8, IM8 and IF8.

### 6.6. Discussion

The qualitative analysis, depicted in Figure 6-17 using the FAC2 parameter, indicates an overall overprediction of temperatures.

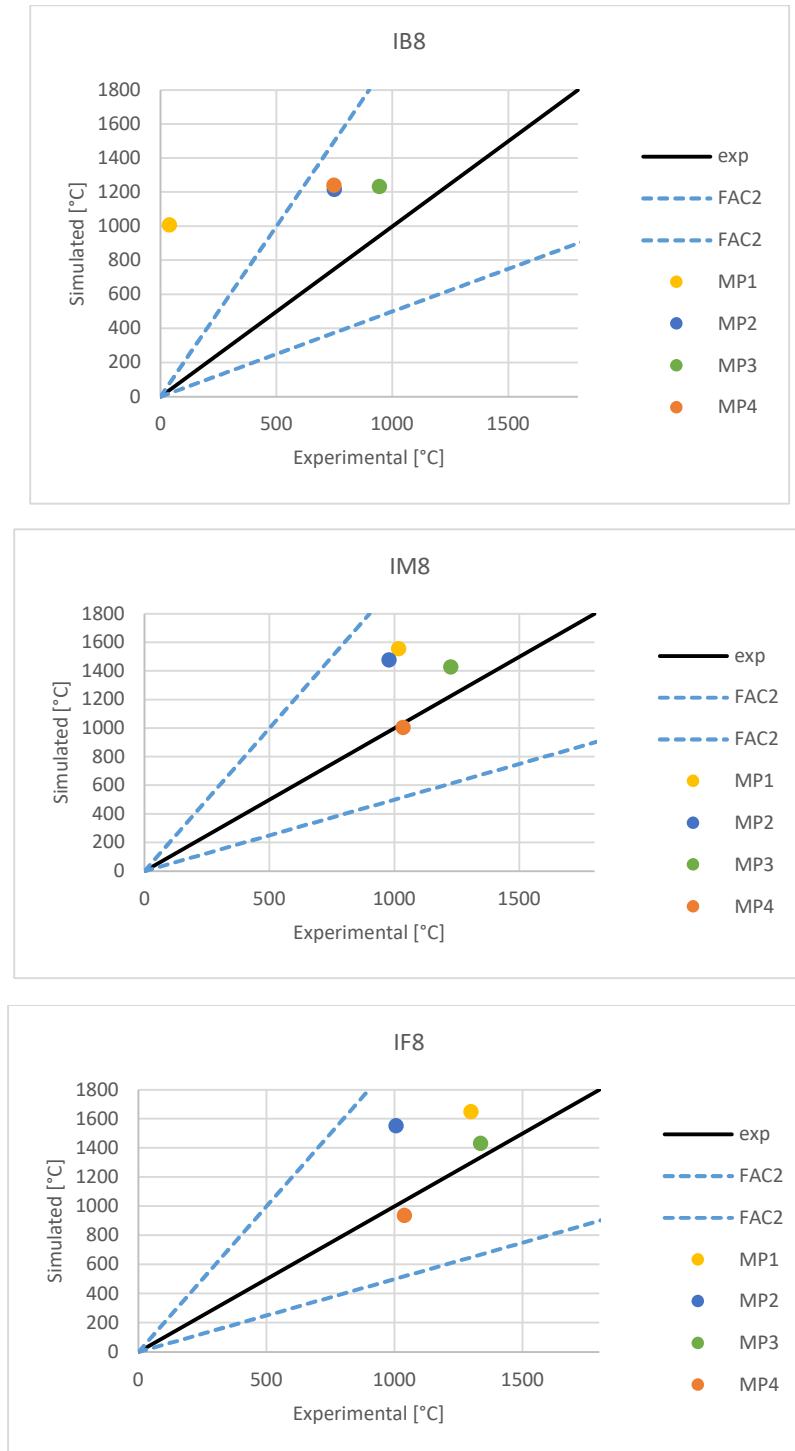


Figure 6-17. Qualitative analysis of temperature results of experiment IB8, IM8 and IF8 using FAC2 criteria; straight black line represents a perfect agreement with experimental data. Values are acceptable if they are within the zone delimited by the blue dot-line.

However, the implemented models appear to be capable of describing the impingement phenomena. In particular, the quantitative analysis using the FB and NMSE parameters (Figure 6-2) reveals that the simulation results for the IM8 and IF8 experiments are in good agreement with the experimental data. On the other hand, the results of the IB8 simulation are deemed unacceptable. When examining the experimental value of thermocouple TC1 in the IB8 experiment, the observed low temperature can be attributed to the presence of the hole depicted in Figure 6-17 where no combustion occurs. As mentioned in the jet fire analysis, FLACS is unable to accurately depict the unburnt phenomena at the base of the flame. Therefore, this could be a contributing factor to the model's poor performance when analyzing impingement in the blue zone.

According to these results, it must be considered proved that radiation model and soot model are necessary to assess flame temperature, while flame geometry is not particularly affected by them. Flame geometry parameters are described by the implemented models with a good accuracy, despite being slightly overpredicted, and especially total flame length is simulated with almost perfect agreement with experimental data. On the other hand, the FLACS code is intrinsically not able to describe lift-off distance that is clearly underpredicted.

Table 6-7. Quantitative analysis of IB8, IM8 and IF8 simulation results using FB and NMSE criteria.

	IB8	IM8	IF8
FB	-0.77	-0.24	-0.16
NMSE	6.28	0.1	0.07

In relation to flame temperature measurements, the utilization of the DTM radiation model in conjunction with the CFM soot model demonstrates the highest level of conformity with experimental data. However, it should be noted that the FOX soot model exhibits a more accurate representation of the temperature distribution in the jet flame under conditions of supersonic release. Consequently, it is imperative to clearly define the objectives of the study in order to select the most suitable model. For example, in scenarios involving impingement, the precision of the temperature distribution is crucial for accurately evaluating the impact of the incident on the pipeline.

Conversely, when assessing the temperature of an object in close proximity to the fire source, the absolute temperature values assume a pivotal role, as they are directly associated with radiative energy. Nevertheless, both aforementioned models effectively capture the phenomena of the jet fire, albeit with a tendency to overestimate the results, while maintaining a satisfactory level of agreement with experimental observations.

Thus, it can be concluded that the FLACS CFD simulator is a reliable tool for conducting conservative risk assessments of jet fires. Furthermore, the implemented model has been successfully tested to simulate impingement phenomena using experimental data, specifically involving a pipe positioned in the blue, middle, and front zones of the flame. The results highlight the limitations of the code in accurately reproducing phenomena at the base of the flame, preventing the description of impingement in the blue zone. However, impingement in the middle and front zones is depicted with high accuracy.

Given these findings, several recommendations for future research are provided as follows:

- Validate the proposed model using various release conditions and fuels to enhance its applicability and broaden its scope.
- Conduct further investigations to examine the impact of release conditions on the temperature profile and geometry of jet fires, thus deepening the understanding of these phenomena.
- Perform a comparative analysis by utilizing different computational fluid dynamics (CFD) simulators to assess the consistency and robustness of the obtained results.
- Explore additional studies focusing on validating the FLACS CFD code specifically for assessing jet fire impingement, thereby expanding its validation portfolio and strengthening its reliability.

## 7. Conclusions

The investigation carried out in this thesis has led to the following conclusions:

1. The historical analyses of accidents occurred in process plants and in the transportation of flammable materials have shown that jet fires have been, with a high frequency, the first step in domino effect sequences resulting in major accidents involving further fires or explosions. Nevertheless, their serious effects when impinging on equipment such as vessels or pipes —or, more specifically, in the case of a jet fire from a pipeline impinging on another pipeline in the same corridor— have been rather scarcely studied. A lack of information in this field was clearly identified.

2. When observing a sonic or subsonic jet fire, three distinct zones have been clearly identified within the flames, with variations in temperature, color, shape, and behavior. The first one, called here the blue one, is located closest to the nozzle, follows the same direction than the exit fuel jet and is predominantly influenced by momentum forces, showing at its center a tubular region with almost no combustion. The middle zone, with higher temperatures than the blue one, manifests an orange flame color and buoyancy forces gradually begin to influence on the shape and orientation of the flames. Finally, the front zone, with the highest temperatures and located farthest from the nozzle, exhibits a bright yellow color and experiences stronger buoyancy effects, resulting in an undefined shape.

3. The lift-off increases with the fuel exit velocity and the exit diameter, being smaller than that corresponding to vertical jet fires. For horizontal subsonic jet fires the following expression has been obtained:

$$S/D=0.12 (u/D)^{0.54}$$

4. The experimental data have shown that for both subsonic and sonic jet fires the size, i.e. the length and width of the jet flames, as well as their elevation (from the center of

the nozzle), increase with the fuel mass flow rate. As for the flames reach horizontal projection, the following expressions has been obtained for horizontal jet fires:

$$R/D = 21 Fr^{0.2}$$

The treatment of the experimental data has also allowed to obtain another expression which allows a good prediction of the flames elevation:

$$W/D = 271338 \cdot m_{rel}^2 - 412 \cdot m_{rel} + 46.4$$

These expressions allow to establish the maximum distance zone at which there could be flames impingement on an equipment, as it depends on both the reach and the elevation of flames.

5. With flames impingement of sonic jet fires very high heat fluxes were obtained. The highest values, up to 275 kW/m<sup>2</sup>, were registered for the higher propane release flow rate at the front position of the wall, where the flames impinged against the pipe wall with a very high turbulence and an intense convective contribution. With subsonic jet fires, the heat fluxes were lower, of the order of around 150 kW/m<sup>2</sup>.

6. These high heat fluxes originate extremely high temperatures at the pipe wall in very short times when there is a gas inside; if there is no fireproofing (or it has been damaged) temperatures of the order of 600 °C were reached in 2-3 minutes (initial heating rates of up to 19.5 °C/s were registered), and of 750 °C in 5-6 min. These values show that in the event of flames impingement, the failure of a pipe or a vessel could occur after a very short time. With a liquid inside, temperatures somewhat above its boiling temperature were reached in the wall in contact with it.

7. The simulation of horizontal jet fires using propane under various release conditions has been validated. The models accurately determined flame temperature but slightly overpredicted flame geometry. The FLACS code had limitations in predicting lift-off distance. The DTM radiation model with the CFM soot model best matched experimental data for flame temperature. Both models provided satisfactory representations of jet fire phenomena. The FLACS CFD simulator is valuable for conservative risk assessments of jet fires.

8. Furthermore, the implemented models (CFM and FOX) were evaluated for its ability to simulate impingement phenomena using experimental data obtained from the

experiments involving a pipe located within the blue, middle, and front zones of the flame. The findings indicate that the CFD code's limitations in reproducing the phenomena at the base of the flame hinder its capability to describe impingement in the blue zone accurately. However, the model effectively captures impingement within the middle and front zones with high accuracy.

9. The findings from this research enhance our comprehension of jet fires, enabling improved predictions of their dimensions, geometry, and thermal effects when impinging on other equipment. However, given the limited availability of data in this area, it would be beneficial to verify these results through large-scale field tests involving different fuels and larger orifice diameters.





## Nomenclature

$A_p$	surface area of the pipe wall taken for the heat flux calculation ( $m^2$ )
$A_f$	flames total area, $m^2$
$C_p$	specific heat of ambient air, $kJ\ kg^{-1}\ K^{-1}$
$D, d$	nozzle diameter, m
$D^*$	characteristic diameter of a fire, m
$dt$	duration of initial heating measurement (s)
$dT_{wall}$	temperature increase in the pipe wall ( $^{\circ}C$ )
$f$	frequency of occurrence ( $year^{-1}$ )
$Fr$	nozzle Froude number, $u^2/(gD)$
$f(x,y)$	threshold function, -
$g$	acceleration of gravity, $m\ s^{-2}$
$g(x,y)$	threshold function, -
$H$	total flames length horizontal projection, m
$\Delta H_c$	enthalpy of combustion, $kJ/kg$
$h$	flames to wall heat transfer coefficient, $kW\ ^{\circ}C^{-1}\ m^{-2}$
$I$	image using temperature values (K) as pixels
$L$	length of a vertical jet fire, m
$L$	length of the surface or pipe (m or mm)
$L_{flame}$	length of the jet flame (m)
$L_{bv}$	vertical length of an inclined jet fire, m
$L_t$	total flames length horizontal projection, m

$m_p$	mass of the pipe wall taken for the heat flux calculation (kg)
$m_{rel}$	mass release rate, kg/s
OD	outer diameter of pipeline (in, cm or mm)
P	probability of occurrence (-)
$\bar{P}$	probability of occurrence of the complementary event (-)
$P_a$	atmospheric pressure, Pa
$P_i$	pressure inside vessel or pipe, Pa
$P_{in}$	stagnant pressure inside the pipe or the vessel (Pa)
$P_{out}$	pressure downstream the outlet orifice (Pa)
Q	flames to wall total heat flux, kW
Q'	heat release rate of the jet fire, kW
R	flame reach (horizontal projection), m
Re	Reynolds number, $Du/\nu$
S, $S_F$	lift-off distance, m
$S_L$	maximum laminar burning velocity of the fuel-air mixture, m/s
T	temperature, K
TC	thermocouple
$T_f$	Flash point temperature
$T_\infty$	ambient temperature, K
$T_{flame}$	average temperature of flame at a given location ( $^{\circ}C$ )
$T_h$	threshold temperature, K
$T_{wall}$	temperature of pipe wall at a given location ( $^{\circ}C$ )
$U^*$	dimensionless flow number, -
u	fuel exit velocity, m/s
$u_e$	fuel flow mean velocity, m/s

$u_w$	wind velocity, m/s
$X$	thermocouple distances from the nozzle, m
$X$	horizontal distance from nozzle to pipe centre line (cm)
$X_F$	flames horizontal projection, m
$Y$	thermocouple distances from the ground level, m
$Y$	elevation distance from level ground to pipe centre line (cm)
$W$	flame elevation from the nozzle centreline, m
$Z_F$	flames vertical height (elevation), m

### Greek

$\alpha_a$	angle of an inclined jet fire, °
$\delta_x$	cell diameter, m
$g$	ratio of specific heats, -
$\nu$	kinematic viscosity, $\text{m}^2 \text{s}^{-1}$
$\mu$	dynamic viscosity, $\text{kg m}^{-1} \text{s}^{-1}$
$\rho$	density, $\text{kg m}^{-3}$
$\rho_\infty$	density of ambient air, $\text{kg m}^{-3}$

### Subscripts

a	ambient, air
e	fuel isentropically expanded to atmospheric pressure
f	fuel
min	minimum value
max	maximum value
Norm	normalized

## Acronyms

BLEVE	boiling liquid expanding vapor explosion
CCD	charged-coupled device
CFD	computational fluid dynamics
ESV	electro solenoid valve
FB	fractional bias
FPS	frames per second
FM	flowmeter
IB8	impingement test blue zone with 8mm nozzle
IF8	impingement test front zone with 8mm nozzle
IM8	impingement test middle zone with 8mm nozzle
I/O	input-output module
IR	infrared
JFT	jet fire test
LPG	liquefied petroleum gas
NA	not available
NG	natural gas
NMSE	normalized mean square error
NZ	nozzle
PCV	pressure control valve
PG	pressure gauge

PT	pressure transmitter
TC	thermocouple
TCB	thermocouple B Type
TCK	thermocouple K Type
VCE	vapor cloud explosion
VLV	valve
IR-CAM	infrared thermographic camera (Optris PI 640®)
VIS-CAM	visible camera



## References

- Ab Aziz, N. S., Kasmani, R. M., Samsudin, M. D. M., & Ahmad, A. (2020). Main geometrical features of horizontal buoyant jet fire and associated radiative fraction. *Process Safety Progress*, 39 (S1), 2–10.
- Abdolhamidzadeh, B., Abbasi, T., Rashtchian, D., & Abbasi, S. A. (2010). A new method for assessing domino effect in chemical process industry. *Journal of Hazardous Materials*, 182 (1-3), 416-426.
- Abdolhamidzadeh, B., Abbasi, T., Rashtchian, D., & Abbasi, S. A. (2011). Domino effect in process-industry accidents e an inventory of past events and identification of some patterns. *Journal of Loss Prevention in the Process Industries*, 24 (5), 575-593.
- Acharya, T., and Ray, A. K. (2005). *Image Processing: Principles and Applications*. John Wiley & Sons.
- ARIA (Analysis, Research and Information on Accidents). (2012). French Ministry of Ecology, sustainable development and energy. Available from: [www.aria.developpement-durable.gouv.fr](http://www.aria.developpement-durable.gouv.fr) Accessed 10.4.13.
- Badri, N., Rad, A., Kareshki, H., Abdolhamidzadeh, B., Parivizedghy, R., Rashtchian, D. (2013). A risk-based decision making approach to determine fireproofing requirements against jet fires, *Journal of Loss Prevention in the Process Industries* (26) 771-778.
- Bagster, D. F., Pitblado, R. (1991). The estimation of domino incident frequencies. An approach. *Process Safety and Environmental Protection* (69) 195-199.
- Baukal, C.E., Gebhart, B. (1995). A review of flame impingement heat transfer studies. Part 1: experimental conditions. *Combustion Science and Technology* (104) 339-357.
- Bennett, J.F., Cowley, LT., Davenport J.N., Rowson, J.J., 1991. Large scale natural gas and LPG jet fires. Final report to the CEC, TNER.91.022. Shell Research Limited.
- Birch, A. D., Brown, D. R., Dodson, M. G., & Swaffield, F. (1984). The structure and concentration Decay of high pressure jets of natural gas. *Combustion Science and Technology* (36) 249–261.

Birk, A. M., Poirier, D., Davison, C. J. (2006). On the response of 500 gal propane tanks to 25% engulfing fire. *Journal of Loss Prevention in the Process Industries* (19) 527-541.

Birk, A. M., Poirier, D., Davison, J. (2006). On the thermal rupture of 1.9 m<sup>3</sup> propane pressure vessels with defects in their thermal protection system. *Journal of Loss Prevention in the Process Industries* (19) 582–597.

Birk, A. M., VanderSteen, J. D. J. (2006). The effect of pressure relief valve blowdown and fire conditions on the thermo-hydraulics within a pressure vessel. *Journal of Pressure Vessel Technology* (128) 467-475.

Birk, A. M., Davison, C., Cunningham, M. Blast overpressures from medium scale BLEVE tests. *Journal of Loss Prevention in the Process Industries* (20) 194-206).

Bradley, D., Gaskell, P.H., Gu, X.J., Palacios, A. (2016). Jet flame heights, lift-off distances, and mean flame surface density for extensive ranges of fuels and flow rates. *Combustion and Flame* (164) 400–409.

Bradley, I. (2017). A review of the applicability of the jet fire resistance test method to severe release scenarios. Health and Safety Executive. Report RR1120.

Bubbico, R., Carbone, F., Ramírez-Camacho, J. G., Pastor, E., Casal, J. (2016). Conditional probabilities of post-release events for hazardous materials pipelines. *Process Safety and Environmental Protection* (104) 95–110.

Casal J. (2018). Evaluation of the effects and consequences of major accidents in industrial plants. Elsevier, Amsterdam.

Casal J., Gómez-Mares M., Muñoz M., Palacios A. (2012). Jet Fires: ¿a "Minor" Fire Hazard? *Chemical Engineering Transactions* (26) 13-20.

Council Directive 96/82/EC on the control of major-accident hazards involving dangerous substances. OJ No. 10, 14 January 1997.

Chemical Safety Board (2012). Available from: [www.csb.gov](http://www.csb.gov). Accessed 10-4-2020.

Darbra, R. M., Palacios, A., & Casal, J. (2010). Domino effect in chemical accidents: main features and accident sequences. *Journal of Hazardous Materials* (183) 565-573.



Delvosalle, C. Domino effect phenomena: definition, overview and classification. First European Seminar on Domino Effect. Leuven, 1996.

Droste, B., Schoen, W. (1998). Full scale fires test with unprotected and thermal insulated LPG storage tanks. *Journal of Hazardous Materials* (20) 41-53.

EGIG (2015). Report of the European Gas Pipeline Incident Data Group. Document number EGIG 14.R.0403.

Failure and Accidents Technical information System (FACTS) (2010). TNO industrial and external safety. Available from: [www.factsonline.nl](http://www.factsonline.nl). Accessed 10.4.2019.

Foroughi, V., Palacios, A., Barraza, C., Àgueda, A., Pastor, E., Casal, J. (2021). Thermal effects of a sonic jet fire impingement on a pipe. *Journal of Loss Prevention in the Process Industries* (71) 1-10.

Foroughi V., Cavini, A., Palacios, A., Albó, K., Àgueda, A., Pastor, E., Casal, J. (2019). Domino effect by jet fire impingement in pipelines. *Chemical Engineering Transactions* (77) 931-936.

Gexcon A.S. (2020). FLACS-CFD 20.1 User's Manual.

Gómez-Mares, M., Muñoz, M., & Casal, J. (2009). Axial temperature distribution in vertical jet fires. *Journal of Hazardous Materials* (172) 54–60.

Gómez-Mares, M., Zárata, L., Casal, J. (2008). Jet fires and the domino effect. *Fire Safety Journal* (43) 583-588.

Gopaldaswami, N., Liu, Y., Laboureur, D. M., Zhang, B., Mannan, M. S. (2016). Experimental study on propane jet fire hazards: comparison of main geometrical features with empirical models. *Journal of Loss Prevention in the Process Industries* (41) 365-375.

Green, D. W., Perry, R. H. (2008). *Perry's Chemical Engineers' Handbook*, 8th ed. McGraw-Hill.

Hanna, S. R., Hansen, O. R., Dharmavaram, S. (2004). FLACS CFD air quality model performance evaluation with Kit Fox, MUST, Prairie Grass, and EMU observations. *Atmospheric Environment* (38) 4675–4687.

Hassan, F., Ahmed, F. (2007). Metallurgical analysis of high pressure gas pipelines rupture, *Pakistan Journal of Engineering and Applied Sciences* (1) 14-23.

Hassan, F., Iqbal, J., (2006). Consequential rupture of gas pipeline. *Engineering Failure Analysis* (12) 127–135.

Hemmatian, B., Abdolhamizadeh, B., Darbra, R.M., Casal, J., (2014). The significance of domino effect in chemical accidents, *Journal of Loss Prevention in the Process Industries* (29) 30–38.

Hemmatian, B., Planas, E., Casal, J. (2015). Fire as a primary event of accident domino sequences: the case of BLEVE. *Reliability Engineering & System Safety* (139) 141–148.

<https://www.bst-tsb.gc.ca/eng/enquetes-investigations/pipeline/2014/p14h0011/p14h0011.html> (consulted 9/2020).

<https://www.bst-tsb.gc.ca/eng/rapports-reports/pipeline/1995/p95h0036/p95h0036.html> (consulted 9/2020).

<https://www.bst-tsb.gc.ca/eng/rapports-reports/pipeline/2012/p12h0105/p12h0105.html> (consulted 9/2020).

<https://www.tsb.gc.ca/eng/rapports-reports/pipeline/2011/p11h0011/p11h0011.html> (consulted 9/2020).

Hustad, J. E., Sonju, O. K. (1986). Radiation and size scaling of large gas and gas/oil diffusion flames. *Dynamic of reactive systems Part I: Flames and configurations*. AIAA Progress in Astronautics and Aeronautics. New York (105) 365-387.

Hustad, J. E., Sonju, O. K. (1991). Heat transfer to pipes submerged in turbulent jet diffusion flames. In: Da Graça Carvalho M., Lockwood F. C., Taine J. (eds). *Heat Transfer in Radiating and Combusting Systems*. EURO THERM Seminars, (17) 474-490. Springer, Berlin, Heidelberg.

Kalghatgi G. T. (1984) Lift-off heights and visible lengths of vertical turbulent jet diffusion flames in still air. *Combustion Science and Technology* (41) 17-29.

Kilham J. K. (1948). Energy transfer from flame gases to solids. *Combustion Flame and Explosion Phenomena* (3) 733-740.

Kourniotis, S. P., Kiranoudis, C. T., Markatos, N. C. (2000). Statistical analysis of domino chemical accidents. *Journal of Hazardous Materials* (71) 1-3.

Kozanoglu, B., Zárate, M. Gómez-Mares, L., Casal, J. (2011). Convective heat transfer around vertical jet fires: an experimental study *Journal of Hazardous Materials* (197) 104–108.

Kreder, R. A., Berwanger, P. C. (1995). Making safety data safe. *Chemical Engineering* (102) 131-138.

Kuntikana, P., Prabhu, S.V. (2018). Heat transfer investigations on methane-air premixed flame jet exiting from a circular nozzle and impinging over semi-cylindrical surfaces. *International Journal of Thermal Sciences* (128) 105–123.

Landucci, G., Cozzani, V., Birk, M. (2013). Heat radiation effects. In G. Reniers and V. Cozzani eds. *Domino Effects in the Process Industries: modelling, prevention and managing*, 70-115. Elsevir, Amsterdam.

Landucci, G., Pontiggia, M., Paltrinieri, N., Cozzani, V. (2016a). Computational fluid dynamics modelling: tutorial and examples. In *Dynamic Risk Analysis in the Chemical and Petroleum Industry: evolution and interaction with parallel disciplines in the perspective of industrial application*. Elsevier, Amsterdam.

Landucci, G., Pontiggia, M., Paltrinieri, N., & Cozzani, V. (2016b). Dynamic consequence analysis through computational fluid dynamics modelling. In *Dynamic Risk Analysis in the Chemical and Petroleum Industry: evolution and interaction with parallel disciplines in the perspective of industrial application*. Elsevier, Amsterdam.

Launder, B. E., Spalding, D. B. (1974). The numerical computation of turbulent flows. *Computer Methods in Applied Mechanics and Engineering* (3) 269–289.

Lin, C. H., Ferng, Y. M., Hsu, W. S., Pei, B. S. (2010). Investigations on the characteristics of radiative heat transfer in liquid pool fires. *Fire Technology* (46) 321–345.

Lowesmith, B. J., Hankinson, G., Acton, M. R., Chamberlain, G. (2007). An overview of the nature of hydrocarbon jet fire hazards in the oil and gas industry and a simplified approach to assessing the hazards. *Process Safety and Environmental Protection*. (85) 207-220.

- Majid, Z. A., Mohsin, R. (2013). Multiple failures of API 5L X42 natural gas pipeline. *Engineering Failure Analysis* (31) 421–429.
- Majid Z. A., Mohsin, R., (2012). Failure investigation of natural gas pipeline. *Arabian Journal of Science and Engineering* (37) 1083–1088.
- Majid Z. A., Mohsin, R., Yusof, M. Z. (2011). Erosive wear of natural gas pipes due to high velocity jet impact: computer simulation study, *Journal of Teknologi* (56) 27–52.
- Majid Z. A., Mohsin, R., Yusof, M. Z. (2012). Experimental and computational failure analysis of natural gas pipe. *Engineering Failure Analysis* (19) 32–42.
- Majid Z. A., Mohsin, R., Yusof, M. Z. (2013). Multiple failures of API 5L X42 natural gas pipe: experimental and computational analysis. *Engineering Failure Analysis* (34) 10–23.
- Majid, Z. A., Mohsin, R., Yaacob, Z., Hassan, Z. (2010). Failure analysis of natural gas pipes, *Engineering Failure Analysis* (17) 818–837.
- Majid, Z. A., Mohsin, R., Yusof, M. Z. (2011). Erosive wear of natural gas pipes due to high velocity jet impact: physical examination and experimental study, *Journal of Teknologi* (56) 1–25.
- Major Accident Reporting System (MARS) (2012). Major Accident and Hazards Bureau (MAHB). Available from: [www.emars.jrc.ec.europa.eu](http://www.emars.jrc.ec.europa.eu) Accessed 10.4.13.
- Major Hazardous Incident Data Service (MHIDAS) (2007). In AEA Technology, London. HSE-Health and Safety Executive (UK).
- Malikov, G. K., Lobanov, D. L., Malikov, K. Y., Lisienko, V. G., Viskanta, R., Federov, A. G., (2001). Direct flame impingement heating for rapid thermal materials processing. *International Journal of Heat and Mass Transfer* (44) 1751-1758.
- Mazzola, J. (2006). Thermal interaction analysis in pipeline systems: a case study, *Journal of Loss Prevention in the Process Industries* (12) 495–505.
- McCaffrey, B. Flame height. In P. J. DiNenno (ed.) (1988): *SFPE Fire Protection Handbook*, 298-305. National Fire Protection Association. Quincy, MA, 02269.

McGrattan, K., Hostikka, S., Floyd, J., McDermott, R., Vanella, M. (2006). Fire dynamics simulator validation guide. NIST Special Publication 1018 (3).

McGrattan, K., Hostikka, S., McDermott, R., Floyd, J., Weinschenk, C., Overhold, K. (2020). Fire Dynamics Simulator User 's Guide (FDS), 6<sup>th</sup> ed. NIST Special Publication 1019 (6).

MHIDAS (Major Hazardous Incident Data Service) (2007). AEA Technology, London. HSE-Health and Safety Executive (UK).

Mohsin R., Majid Z. A., Tan F. L., (2015). Numerical analysis of wall shear patterns on the external wall of an API 5L X42 natural gas pipe. *Engineering Failure Analysis* (48) 30–40.

Mohsin, R., Majid, Z. A., Yusof, M. Z., (2014). Safety distance between underground natural gas and water pipeline facilities. *Reliability Engineering & System Safety* (131) 53–60.

Morad, M. R., Momeni, A., Fordoei, E., Ashjaee, M. (2016). Experimental and numerical study on heat transfer characteristics for methane/air flame impinging on a flat surface. *International Journal of Thermal Sciences* (110) 229-240.

Muthusamy, D., Hansen, O. R., Middha, P., Royle, M. (2011). Modelling of hydrogen jet fires using CFD. 4th International Conference on Hydrogen Safety, 5892. NTSB. (2012). Available from: [www.nts.gov](http://www.nts.gov). Accessed 10.04.19.

Palacios, A. Study of jet fires geometry and radiative features. Doctoral thesis. UPC, 2011.

Palacios, A., Muñoz, M., Darbra, R. M., Casal, J. (2012). Thermal radiation from vertical jet fires. *Fire Safety Journal* (51) 93-101.

Palacios, A., Bradley, D. (2017). Generalised correlations of blow-off and flame quenching for sub-sonic and choked jet flames. *Combustion and Flame* (185) 309-318.

Palacios, A., Muñoz, M., Casal, J. (2011). Assessment of the shape of vertical jet fires. *Fuel* (90) 824-833.

Palacios, A., Rengel, B. (2020). Computational analysis of vertical and horizontal jet fires. *Journal of Loss Prevention in the Process Industries* (65) 104096.

Palacios, A., Casal, J. (2011). Assessment of the shape of vertical jet fires. *Fuel* (90) 824-833.

Palacios, A., García, W., Rengel, B. (2020). Flame shapes and thermal fluxes for an extensive range of horizontal jet flames. *Fuel* (279) 118328.

Palacios, A., Muñoz, M., Casal, J. (2009). Jet fires: an experimental study of the main geometrical features of the flame in subsonic and sonic regimes. *AIChE Journal* (55) 256–263.

Prakash, O., and Saini, R. (2018). "Survey on Image Processing Techniques for Infrared Images." *International Journal of Image, Graphics and Signal Processing*, 10(8), 38-47.

Patej, S., Durussel, T. (2007). Domino effect: thermal impact of jet fires on industrial pipes. *ICHEME Symposium Series no. 153*, 1-6.

Pedersen, N. (2012). Modelling of jet and pool fires and validation of the fire model in the CFD code FLACS. Thesis report. University of Bergen

Persaud, M. A., Butler, C. J., Roberts, T. A., Shirvill, L. C., Wright, S. (2001). Heat-up and failure of liquefied petroleum gas storage vessels exposed to a jet fire. *Proceedings of the 10th International Symposium (2001) 1069-1106*. Stockholm, Sweden.

PHMSA, Pipeline and Hazardous Materials Safety Administration (2014). *All Reported Pipeline Incidents*

Planas E., Montiel H., Casal J. (1997). A survey of the origin, type and consequences of fire accidents in process plants and in transportation of hazardous materials, *Transactions Icheme* (75) Part B (3), 3-8.

Planas. E., Pastor, E., Casal, J., Bollina, J. M. (2015). Analysis of the boiling liquid expanding vapor explosion (BLEVE) of a liquefied natural gas road tanker: The Zarzalico accident. *Journal of Loss Prevention in the Process Industries* (34) 127–138.

Planas, E., Casal, J., Lancia, A., Bordignon, L. (1996). Protection of equipment engulfed in a pool fire. *Journal of Loss Prevention in the Process Industries* (9) 231-240.

Ramírez-Camacho, J. G., Carbone, F., Pastor, E., Bubbico, R., Casal, J. (2017). Assessing the consequences of pipeline accidents to support land-use planning. *Safety Science* (97) 34-42.

- Ramírez-Camacho, J. G., Pastor, E., Amaya-Gómez, R., Mata, C., Muñoz, F., Casal, J. (2019). Analysis of crater formation in buried NG pipelines: a survey based on past accidents and evaluation of domino effect. *Journal of Loss Prevention in the Process Industries* (58) 124-140.
- Ramírez-Camacho, J. G., Pastor, E., Casal, J., Amaya-Gómez, R., Muñoz-Giraldo, F. (2015). Analysis of domino effect in pipelines. *Journal of Hazardous Materials* (298) 210-220.
- Rasband, W. National Institutes of Health USA. Image J. <http://imagej.nih.gov/ij>
- Rengel, B. (2019). Validation of CFD codes for risk analysis of accidental hydrocarbon fires. Doctoral thesis. Universitat Politècnica de Catalunya.
- Rengel, B., Àgueda, A., Pastor, E., Casal, J., Planas, E., Hu, L., Palacios, A. (2020). Experimental and computational analysis of vertical jet fires of methane in normal and sub-atmospheric pressures. *Fuel* (265) 116878.
- Reniers, G. (2010). An external domino effects investment approach to improve cross-plant safety within chemical clusters. *Journal of Hazardous Materials* (177) 167-174.
- Reniers, G., Cozzani, V. (Eds.). (2013). *Domino Effects in the Process Industries. Modelling, prevention and managing*. Elsevier, Amsterdam.
- Rokke, N. A., Hustad, J. E., Sonju, O. K. (1994). A study of partially premixed unconfined propane flames. *Combustion and Flame* (97) 88-106.
- Ronza, A., Félez, S., Darbra, R. M., Carol, S., Vílchez, J. A., Casal, J. (2003). Predicting the frequency of accidents in port areas by developing event trees from historical analysis. *Journal of Loss Prevention in the Process Industries* (16) 551- 560.
- Salley, M. H., Kassawara, R. P. (2007). *FDS (NUREG-1824, Volume 7) - Verification and Validation of Selected Fire Models for Nuclear Power Plant Applications*.
- Santos, A., Costa, M. (2005). Reexamination of the scaling laws for NO<sub>x</sub> emissions from hydrocarbon turbulent jet diffusion flames. *Combustion and Flame* (142) 160-169.
- Scarponi, G. E., Landucci, G., Birk, A. M., Cozzani, V. (2018). LPG vessels exposed to fire: scale effects on pressure build-up. *Journal of Loss Prevention in the Process Industries* (56) 342-358.

- Shen, R., Jiao, Z., Parker, T., Sun, Y., Wang, Q. (2020). Recent application of Computational Fluid Dynamics (CFD) in process safety and loss prevention: A review. *Journal of Loss Prevention in the Process Industries* (67) 104252.
- Sonju, O.K., Hustad, J. (1984). An Experimental Study of Turbulent Jet Diffusion Flames. *Norwegian Maritime Research* (4) 2–11.
- Sonju, O.K., Hustad, J. E. (1984). An experimental study of turbulent jet diffusion flames and react systems. *AIAA Progress in Astronautics and Aeronautics* (95) 320-339.
- Team, N. (2018). Notepad++ (v7.5.9). <https://notepad-plus-plus.org/>
- Tennekes, H., Lumley, J. (2018). *A First Course in Turbulence*. MIT Press.
- Thilagamani, S., Shanthi, N. (2014). Gaussian and Gabor filter approach for object segmentation. *ASME Journal of Computing and Information Science in Engineering* (JCISE), 14 (2), 021006.
- Thunderhead Engineering Consultants. (2002). PyroSim (2020.4.0902). <https://www.thunderheadeng.com/>
- Townsend, W., Anderson, C., Zook, J., Cowgill, G. (1974). Comparison of thermally coated an uninsulated rail tank filled with LPG subjected to a fire environment. Report No. FRA-OR&D 75-32. US Department of Transportation Federal Railroad Administration. Office of Research Development and Demonstrations.
- TSB, Transportation Safety Board of Canada. Commodity Pipeline Occurrence Report P95H0036. Natural gas pipeline ruptures. Rapid City, Manitoba, Canada, July 29, 1995.
- TSBC, Transportation Safety Board of Canada. Commodity Pipeline Occurrence Report P95H0036, Natural gas pipeline ruptures. Near Beardmore, Ontario, Canada, February 19, 2011.
- TSBC, Transportation Safety Board of Canada. Commodity Pipeline Occurrence Report P95H0036, Natural gas pipeline ruptures, TSB. Near Buick, British Columbia, Canada, June 28, 2012.
- TSBC. Transportation Safety Board of Canada. Commodity Pipeline Occurrence Report P95H0036, Natural gas pipeline ruptures, TSB. Near Otterburne, Manitoba, Canada, January 25, 2014.



- Tyagi, V. (2018). *Understanding Digital Image Processing* (1st ed.). CRC Press.
- USDI, US Department of the Interior Minerals Management Service. Gulf of Mexico OCS Region. OCS Report Investigation of March 19, 1989, Fire South Pass Block 60 Platform B, Lease OCS-G 1608, <https://www.bsee.gov/sites/bsee.gov/files/incident-statisticssummaries-fire-explosions/reports/90-0016-pdf.pdf> (consulted 09/2020).
- USDT. Department of Transportation, Pipeline and Hazardous Materials Safety Administration, Natural gas pipeline ruptures, Marengo County, Alabama, US, December 3, 2011.
- Vílchez, J. A., Espejo, V., Casal, J. (2011) Generic event trees and probabilities for the release of different types of hazardous materials. *Journal of Loss Prevention in the Process Industries* (24) 281-287.
- Vílchez, J. A., Sevilla, S., Montiel, H., Casal, J. (1995). Historical analysis of accidents in chemical plants an in the transportation of hazardous materials. *Journal of Loss Prevention in the Process Industries*, 8, 87-96.
- Virk, A. S. (2015). *Heat Transfer Characterization in Jet Flames Impinging on Flat Plates*. Thesis submitted to the faculty of the Virginia Polytechnic Institute and State University in partial fulfilment.
- Wang Z., Zhou K., Liu M., Wang Y., Qin X., Jiang J. (2019). Lift-off behavior of horizontal subsonic jet flames impinging on a cylindrical surface. *Proceedings of the 9th International Seminar on Fire and Explosion Hazards (ISFEH9)*, 831-842.
- Wighus, R., Drangsholt, G. (1993). *Impinging jet fire experiments - propane 14 MW laboratory tests*. SINTEF NBL – Norwegian Fire Research Laboratory. Report STF25 A92026.
- Yeoh, G. H., Yuen, K. K. (2009). Field modelling approach. In *Computational Fluid Dynamics in Fire Engineering* (pp. 29–133). <https://doi.org/10.1016/b978-0-7506-8589-4.00002-8>
- Wang, Z., Fu, Z., Zou, Y., Liu, L., Liu, H. (2011). Study on risk assessment of urban gas pipeline based on domino effect. *International Conference on Pipelines Trenchless Technol.* 1720–1727.

Zhang, B., Liu, Y., Laboureur, D., Mannan, S. (2015). Experimental study of propane jet fire hazards: thermal radiation. *Industrial & Engineering Chemistry Research* (54) 9251-9256.

## A. FLACS-Fire CFD

### A.1. Modeling approach

FLACS-CFD is a commercial code produced by Gexcon AS a world-leading company in the field of safety and risk management. It is a specialized computational fluid dynamics tool, developed especially to address process safety applications such as dispersion of flammable or toxic gas, gas and dust explosions, propagation of blast and shock waves, pool and jet fires. In addition, The FLACS-Fire module adds some features to the program, focusing on jet and pool fire simulations.

In this chapter a brief introduction of modeling approach is provided reporting the main models implemented in FLACS. More details can be found in the FLACS-CFD manual (Gexcon AS, 2020).

The code solves compressible fundamental conservation equations (i.e. mass, momentum, energy) in a 3D cartesian grid using a finite volume method. The method consists in dividing the domain in a finite number of cells, wherein the fundamentals conservation equations are solved and the results are stored at their center. Rectangular shape face cells are used by FLACS. In order to solve the equations, interpolation between center cell values is needed. The accuracy of FLACS solver is of 2nd order, that means that interpolations are performed linearly.

First/second order interpolation in time is controlled by the Courant-Friederichs-Lewy (CFL) condition, which places restriction on the time step to maintain physically feasible conditions. In particular, the CFL restrictions are based on sound velocity (CFLC) and fluid flow velocity (CFLV) that means that each time step length is chosen so that sound waves, in the first case, or fluid, in the second case, may propagate only for a limited distance, which is the average control volume length multiplied by the value of CFLC and CFLV respectively.

### **A.1.1. Turbulence**

A focus on the turbulent flows physics is necessary to better understand the jet fire phenomena and its modeling. According to Tennekes and Lumley (Tennekes & Lumley, 1976) the characteristics of turbulent flows are:

- Irregular: the quantification of characteristics of turbulence can be performed only statistically
- Diffusivity: diffusivity of turbulence increases the rates of momentum, heat and mass transfer
- Large Reynolds Number: the inertia forces are much higher than the friction forces.
- 3D Vorticity Fluctuations: turbulent flow clearly reveals the presence of rotational three-dimensional flow structures, called turbulent eddies. The dynamics of these structures play an important role in the description of the phenomena.
- Dissipation: Turbulent flows are always dissipative. Viscous shear stresses increase the internal energy of the fluid dissipating the kinetic energy. This means that a continuous supply of energy is needed to compensate viscous losses.
- Continuum: turbulence is a continuum phenomenon; thus it is governed by the equations of fluid mechanics.

In light of what is discussed above, in order to describe the complex structure of the jet fire phenomena, fundamental conservation equations are coupled with additional sub-models. These models take into account the effects of turbulence on different physical aspects i.e. flow regime, combustion and radiation.

### **A1.2. Turbulence flow model**

Nowadays, two main approaches are used to find a simplified solution of Navier-Stokes equations capable of describing turbulent flows: the Large Eddy Simulations (LES) and the Reynolds-Averaged Navier-Stokes (RANS). In both cases, only the important small-scale processes are considered, neglecting the very small effects but the first one is more

accurate despite it requires more expensive computer calculation. FLACS software uses the RANS approach.

Considering RANS approach, the fluid property  $\phi$  is decomposed in an averaged velocity  $\bar{\phi}$  and their fluctuations  $\phi'$ , as it is shown in Figure A-1 and described by the Equation A-1 (Yeoh & Yuen, 2009).

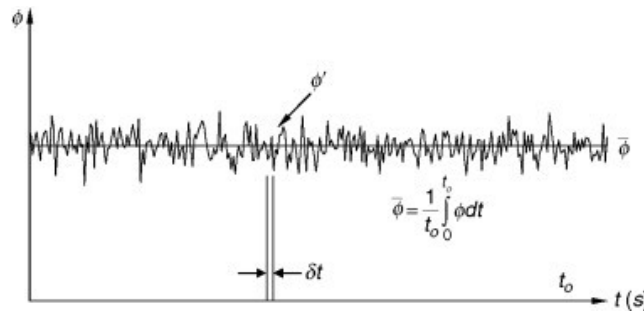


Figure A-1 Fluid property decomposition (Yeoh & Yuen, 2009).

$$\phi = \bar{\phi} + \phi' \quad \text{with} \quad \bar{\phi} = \frac{1}{t_0} \int_0^{t_0} \phi dt \quad (\text{A-1})$$

In particular, FLACS uses Favre-averaging where the flow variables are decomposed in density weighted averaged value and fluctuations. This decomposition is suggested when high changes in density are expected, for example when compressible flows are involved. Hence, due to the presence of the fluctuation term, the modified Navier-Stokes set of equations is an open system that needs what is called a “turbulence model”, in order to be closed.

For this purpose,  $k - \varepsilon$  two-equation eddy viscosity model (Launder & Spalding, 1974) is used by FLACS. The model introduces the turbulent kinetic energy ( $k$ ) and the turbulent kinetic energy dissipation rate ( $\varepsilon$ ) conservation equations, coupled with experimental constants, to filter out the unresolvable turbulence terms.

### A1.3. Combustion model

The presence of eddies during turbulent condition, strongly changes the interaction between fuel and oxidizer, affecting the combustion process. For this reason, the knowledge of whether the process is governed by chemical kinetics or turbulent mixing, determines the appropriate selection of a suitable model. Mix Is Burnt (MIB) and Eddy Dissipation Concept (EDC) are the two models implemented in FLACS.

MIB model considers that the chemistry is rapid enough for chemical equilibrium to always exist at the molecular level. That means that the combustion reaction occurs immediately when fuel and air are available in a cell. On the other hand EDC considers that the rate of combustion is assumed to be determined by the rate of intermixing on a molecular scale of fuel and oxygen eddies, which is presented by the rate of dissipation of eddies. It is evident that the second method is more accurate, but also more complex and for this reason it needs higher computational costs.

#### **A1.4. Radiation model**

In order to solve the enthalpy conservation equation, a description of the radiative source term is required. The governing equation for describing radiation intensity field in absorbing, emitting and scattering medium is the Radiative Transfer Equation (RTE) (Siegel & Howell, 2001) which is an integral-differential equation. The analysis of the radiative term through this equation is extremely difficult and computationally expensive, hence it requires the formulation of models.

Six-flux and Discrete Transfer Method (DTM) radiation models are used by FLACS. In both case, the approach is based on spatial discretization of the RTE through a finite number of solid angles and the solution of radiative heat transfer equation along pre-specified directions. Due to its simplicity, Six-flux method is computationally cheap, but it presents many limitations. On the other hand, DTM is very accurate but CPU-intensive.

#### **A1.5. Soot formation model**

Production of soot during combustion severely affects the heat transfer by radiation. The phenomena is difficult to study especially due to the lack of knowledge about the topic. FLACS uses two approaches for the modelling of soot: the Conversion Factor Model (CFM) and the Formation-Oxidation model (FOX).

In the first model (CFM), a certain amount of fuel carbon is directly converted to soot. The conversion in this case depends only on fuel composition, and soot yield of different fuels are tabulated (Table A-1).

The FOX approach instead, solves a transport equation for soot, taking into account in the source term not only the process of formation, but also the oxidation (combustion)

of the soot. The upper limit for the mass fraction of soot is given by the soot yield tabulated.

Table A-1 Soot yield conversion data, FLACS manual (Gexcon AS, 2020).

Species	Soot yield
Methane	0,7%
Ethane	2,0%
Propane	9,0%
Butane	10,0%

### A1.6. Leak model

Considering a pressurized reservoir, when a leak occurs, gas condition at exit needs to be calculated in order to analyze jet fire phenomena. Sub-sonic, sonic or supersonic condition can be reached outside the nozzle, depending on pressure inside the reservoir. What is called a pseudo-source model is used to calculate the status of an under-expanded jet in terms of temperature, velocity, diameter and density at the position where the jet pressure reaches atmospheric condition. Two different approaches are implemented in FLACS to compute the expanded jet properties: Single planar shock (Birch model), and Edwan-Moodie model.

In the first case, it is assumed that the jet passes through a single planar shock and atmospheric pressure is imposed at pseudo-source; on the other hand, the second model is based on energy conservation, considering equal nozzle temperature and sonic velocity at pseudo source. The second approach results in higher jet velocities and thus greater CPU time compared to the first one.

### A2. FLACS-CFD interfaces

Usually CFD simulators adopt a pre-processor, in order to create the input file that will be used by the processor to run the simulation, and a post-processor to analyze results obtained. These programs are user-friendly and they permit to communicate with the processor without knowing the codes languages. The majority of the functions implemented in a processor can be selected directly using these additional programs but some of them have to be invoked directly by the code. For this reason, a deeply understanding of the processor and the pre/post-processor programs is needed to

correctly use this tool. CASD pre-processor, Flowvis post-processor and RunManager processor interface are used by FLACS-CFD to perform simulations.

### A2.1. CASD pre-processor

CASD is an acronym for Computer Aided Scenario Design and it is used to create the input data, called job data that comprise information about geometry, computational grid, porosities (blocking of each grid cell by the geometry elements in the cell) and scenario description. Main window of CASD is shown in Figure A-2.

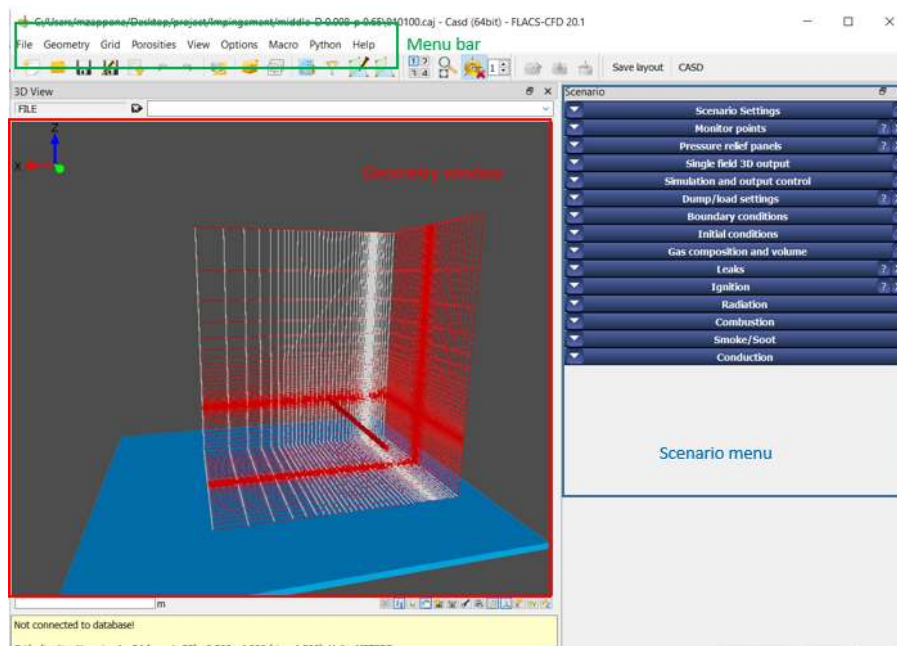


Figure A-2 Main CASD windows: menu bar (green), geometry window (red) and scenario menu (blue).

### Geometry

Geometry is selected in the menu bar. A database containing primitive objects i.e. box, cylinders, ellipsoids is created. Dimensions and orientations are specified and color is assigned in the material tabs (Note material properties are not specified in this tab). When the database is completed, objects are inserted in the domain specifying their position (Figure A-3).



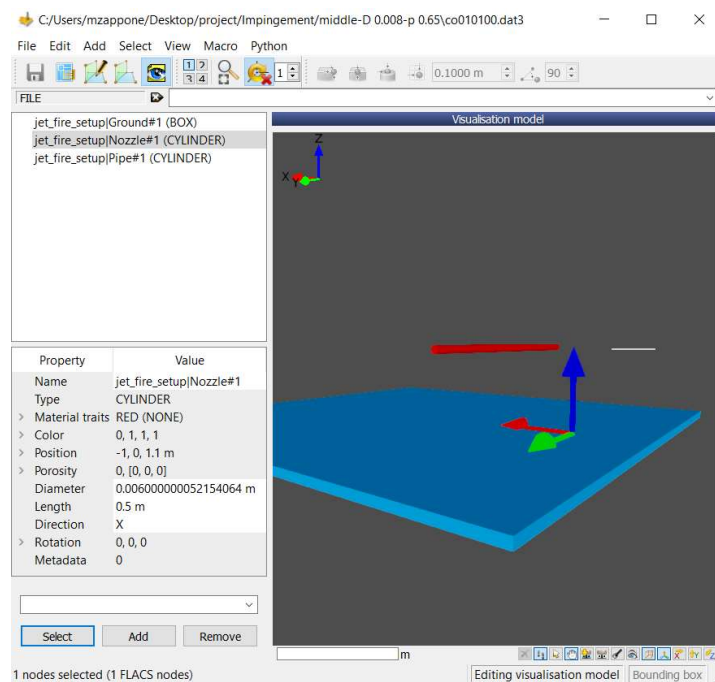


Figure A-3 Geometry window: primitive objects are inserted in the domain specifying position.

### Computational grid

Grid is selected in menu bar. “Quick grid” option (Figure A-4) permits to decide the dimensions of the domain and the size of the cells. The “core domain” is where the studied phenomena is expected, and it is characterized by small dimensions and finer cell size. Instead, the “stretch domain” is the entire domain that is analyzed, where bulk condition are supposed to verify, and coarser grid size are present. Concerning to specific zone of the domain, i.e. leaks region, additional refinements of computational domain can be specified in other sections, in order to have better results.

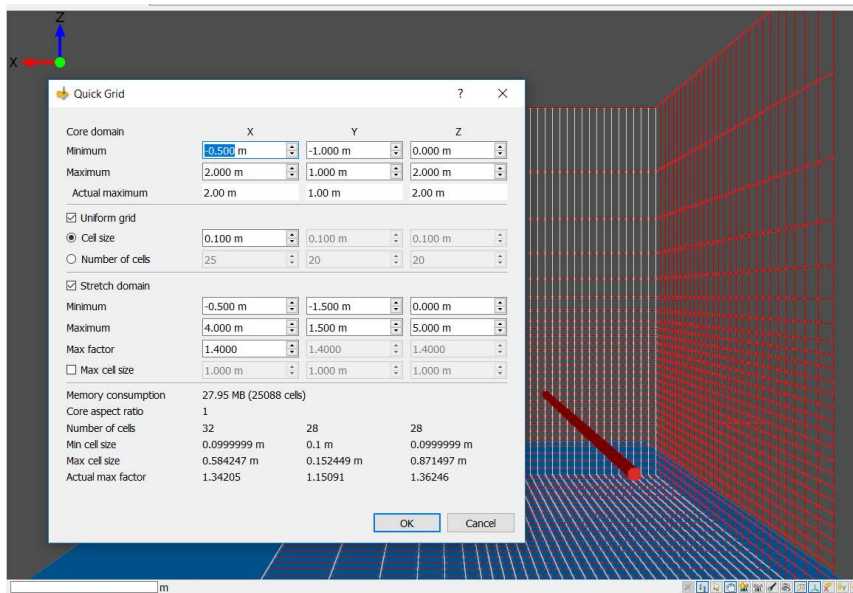


Figure A-4 “Quick grid” values; a grid is created and visualized in the geometry window.

## Scenario

Scenario menu is composed by different sections where all input data are specified. A brief description of the sections is provided:

- Scenario setting: simulation type is selected i.e. fire, dispersion and ventilation, gas explosion, and wizard command can be selected to set up the wind or leak conditions.
- Monitor points: user-defined locations in the simulation domain where one or more variables are monitored during the simulation. Position of monitor points and variables monitored during simulation are selected in this section.
- Pressure relief panels: used only in case of explosion
- Single field 3D output: 3D output variables are selected and registered during simulation
- Simulation and output control: Duration of simulation, CFLC, CFLV and data registration frequency are selected.
- Dump/load settings: additional simulation settings are visualized in this panel.
- Boundary condition: boundary conditions for the outer boundaries of the simulation domains are specified.
- Initial conditions: Initial conditions of simulation are selected i.e. ambient temperature and pressure, air composition, presence of wind, gravity direction.
- Gas composition and volume: fuel composition and volume are specified.

- Leaks: leak characteristics created during the “leak wizard” are shown and position and direction are defined. In this section is also possible to refine the grid near the leak area.
- Ignition: here it is specified where the flame is expected (ignition region) and the when the ignition occurs (ignition time).
- Radiation: radiation model parameters are selected
- Combustion: combustion model parameters are selected
- Smoke/Soot: soot model parameters are selected
- Conduction: conduction calculations are switched on/off

### A2.2. FLACS-CFD RunManager

RunManager is a graphical interface to start and monitor simulations. Figure A-5 shows its main windows: commands, simulation window, log file and plot.

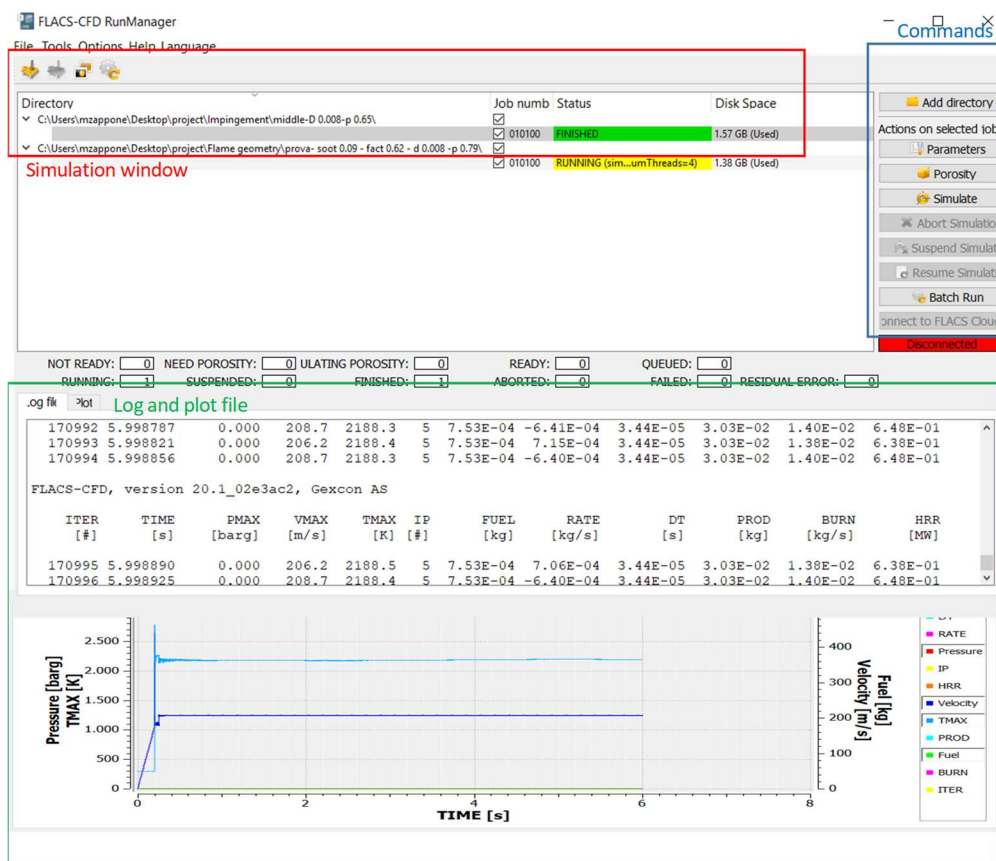


Figure A-5 RunManager main windows: simulation window (red), commands (blue), log and plot file (green).

## Simulation window

Directory, name, status and disk space of job loaded can be visualized in the directory window. The status can be: NOT READY, when the CASD project is not completed and calculation of porosities have not been performed yet; READY, when the simulation is ready to start; RUNNING, when the simulation is running; SUSPENDED, when the simulation is suspended; ABORTED, when the simulation is aborted or programming errors do not allow to perform the calculations and FINISHED, when simulation is finished.

## Commands

With the add directory function, a folder containing job data is selected. Then, different actions can be performed on the selected job. The command Parameters is used to add specification of job loaded for example to modify the duration of the simulation, adding a so-called cc-file and writing a code line to stop the simulation at specific time (Figure A-6).

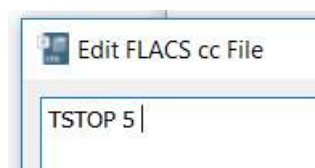


Figure A-6 Example of code line to stop the simulation at time equal to 5 seconds.

This tool is particularly useful when, for instance, the simulation has reached a stationary phase and it is necessary to stop the simulation while the program is running. The added parameters can be visualized in the dump/load settings in CASD interface. Through Parameters command is also possible to start parallel run selecting the number of threads that are the number of CPU cores used by FLACS; selecting more cores, simulation time is reduced.

Calculation of porosities is started by the Porosity command, and it is a necessary step before starting the simulation. When the simulation is in the RUNNING state, it is possible to press on the Abort or the Suspend command. The simulation results can be compromised using the Abort command, for this reason, to stop a simulation or modify it before the end time, it is preferred the Suspend command. The Parameters command

is available only when simulation is in the SUSPENDED status. The Resume command is used to restart the simulation after a suspension and the Batch run command can be used to run simultaneously two or more different jobs.

### Log file and plot

Updated real time simulation data and errors are visualized in log file window. It is necessary to look at this window to understand if simulation is correctly performed and no errors occurred. In plot window, a graphical representation of log file is shown; this tool is particularly useful to understand if simulation has reached a convergence and calculations are successfully completed.

### A2.3. Flowvis post-processor

Flowvis post-processor of FLACS-CFD allows to visualize results from simulations through 1D, 2D and 3D plots as it is shown in the main window of the program (Figure A-7).

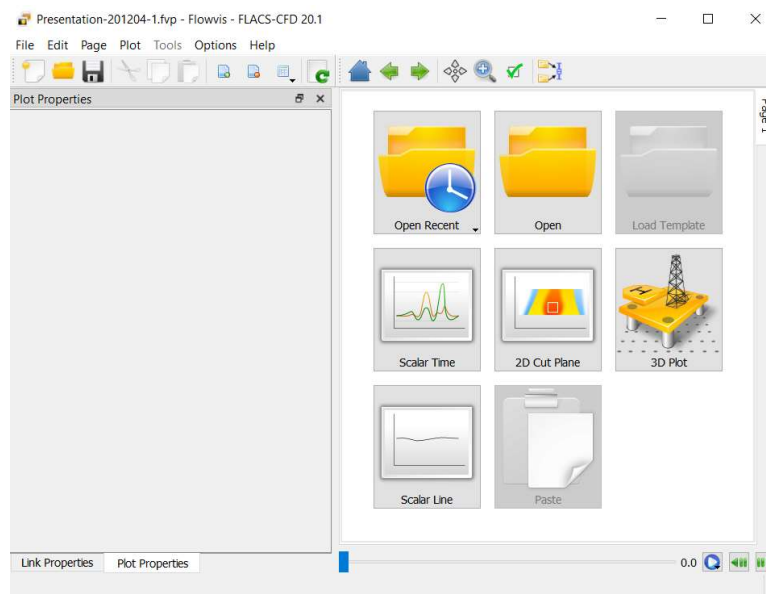


Figure A-7 Flowvis main page.

Open command permits to open a saved presentation job. Scalar time and Scalar line generate one-dimensional plot of scalar variable over time and space respectively. 2D Cut plane creates a two-dimensional cross section of domain, parallel to a grid plane, reporting values for scalar and vector quantities over time. In conclusion, 3D plot command generates three-dimensional representation of the geometry together with

the simulation results. Four visualization typologies are available for the scalar variable: Volume, Surface, Isosurface and 2D slice, while three modes are provided for vector variables: Glyphs, Streamlines and 2D Slices.